Study on Laser Beam Micro-Machining with Different Assisted Medium

Thesis submitted by

NILANJAN ROY

DOCTOR OF PHILOSOPHY (Engineering)

DEPARTMENT OF PRODUCTION ENGINEERING

FACULTY COUNCIL OF ENGINEERING & TECHNOLOGY

JADAVPUR UNIVERSITY

KOLKATA-700032 INDIA

2018

JADAVPUR UNIVERSITY
KOLKATA-700032

Index No. 242/11/Engg.

TITLE OF THE Ph.D. (Engg.) THESIS:

Study on Laser Beam Micro-Machining with Different Assisted Medium

NAME, INSTITUTE & DESIGNATIONS OF THE SUPERVISORS:

(i) Prof (Dr.) Arunanshu Shekhar Kuar
Professor, Department of Production Engineering,
Jadavpur University,
Kolkata – 700032, West Bengal, INDIA.

(ii) Prof (Dr.) Souren Mitra
Professor, Department of Production Engineering,
Jadavpur University,
Kolkata – 700032, West Bengal, INDIA.

List of Publication

International Journal

1. "Multi-objective Optimization of Nanosecond Pulsed Laser Microgrooving of Hydroxyapetite Bioceramic", Materials Today: Proceedings. Vol.18- 7, Pp-5540-5549..
2. "Mathematical Modelling of the Nd:YAG Laser Microdrilling of Aluminium 5052 for Process Optimization and Analysis of Sensitivity", International Journal of Laser Science: Fundamental Theory and Analytical Methods, (2018), Vol.1 (2), pp. 91-108.
3. "Submerged Pulsed Nd:YAG Laser Beam Cutting of Inconel 625 Superalloy: Experimental Investigation", Lasers in Engineering,(2016), Vol.35 (1-4), pp. 151-171.

National Journal

Nil

Book chapter

1. "Sensitivity analysis of submerged Laser beam cutting on Inconel 625 superalloy", Application of Lasers in Manufacturing; Lecture Notes on Multidisciplinary Industrial Engineering, Eds: Dixit U., Joshi S., Davim J., Springer, Singapore, pp. 231-253. DOI: https://doi.org/10.1007/978-981-13-0556-6_10.
2. "Underwater pulsed laser beam cutting with a case study", Microfabrication and Precision Engineering; Research and Development, Ed: J. Paulo Davim, Mechanical Engineering Series; Woodhead Publishing, 2017, pp. 189-212, ISBN 9780857094858, DOI: https://doi.org/10.1016/B978-0-85709-485-8.00007-3.
3. "Laser Beam Micro-cutting", Non-traditional Micromachining Processes; Fundamentals and Applications, Series of Materials Forming, Machining and Tribology; Springer international Publishing AG 2017, G.Kibria et.al. (eds.), pp. 253-274. ISBN 978-3-319-52009-4-7. DOI: https://doi.org/10.1007/978-3-319-52009-4_7.
4. "Nd:YAG Laser Microdrilling of SiC-30BN Nanocomposite: Experimental Study and Process Optimization", Lasers Based Manufacturing. Topics in Mining, Metallurgy and Materials Engineering, 2015, Springer, Joshi S., Dixit U. (eds.), pp. 317-341, ISBN: 978-81-322-2351-1, DOI: https://doi.org/10.1007/978-81-322-2352-8_17.

International Conference

1. "Experimental Investigation of Submerged Laser Beam Cutting on Inconel 625 Super Alloy", Proceedings of the 3rd International Conference on Laser and Plasma Application in Materials Science (LAPAMS), on 15-17 January 2015 KOLKATA, West Bengal., INDIA, pp. 159-163.
2. "Study of cut width deviation during laser beam cutting of Inconel 625 superalloy at submerged condition" E- Proceedings of the 20th International Conference on Advances in Materials & Processing Technologies (AMPT), on December 11-14, 2017 at VIT University – Chennai campus, INDIA.
3. "Comparative study on quality characteristic of laser beam cutting of Inconel 625 superalloy at Different Environment by Sensitivity Analysis" Abstract proceedings of 40th International MATADOR Conference on Advanced Manufacturing, on July 8-11, 2019, Hangzhou, CHINA, page 139.
4. "Multiobjective optimization of laser microdrilling of SiC-30BN nanocomposite based on grey relational analysis" Proceedings of the 4th International and 25thAll India Manufacturing Technology, Design and Research (AIMTDR) Conference, on December 14-16, 2012 at Production Engineering Department, Jadavpur University.
5. "Optimized laser microdrilling of SiC-30BN nanocomposite using grey relational analysis", Proceedings of the International Conference on PRECISION, MESO, MICRO AND NANO ENGINEERING (COPEN-8: 2013), December 13-15, 2013, NIT Calicut, Kerala, India, Vol. II, pp.
6. "Nd:YAG laser microdrilling of SiC-30BN nanocomposite: Experimental study and process optimization", Proceedings of the 5^{th} International and 26^{th} All India Manufacturing Technology, Design and Research (AIMTDR) Conference, December 12-14, 2014, Mechanical Engineering Department, IIT Guwahati, Guwahati, India, pp. 224 (1-6).
7. "Parametric study of submerged Laser beam cutting on Inconel 625 superalloy", Proceedings of the International Conference on PRECISION, MESO, MICRO AND

NANO ENGINEERING (COPEN-9: 2015), December 10-12, 2015, IIT-Bombay, Powai, Mumbai, pp. 212(1-6).

8. "Sensitivity analysis of submerged Laser beam cutting on Inconel 625 superalloy" Proceedings of the 6th International and 27thAll India Manufacturing Technology, Design and Research (AIMTDR) Conference, on December 16-18, 2016 at Department of Production Engineering and Industrial Management, College of Engineering, Pune. Maharashtra, India, pp. 402-404, ISBN: 978-93-86256-27-0.
9. "Sensitivity Analysis of Process Parameters in Submerged Laser beam Cutting on Inconel 625 Superalloy", Proceedings of the 10th International Conference on PRECISION, MESO, MICRO AND NANO ENGINEERING (COPEN-10: 2017), December 7-9, 2017, IIT-Chennai, India, pp. 247-250, ISBN: 978-93-80689-28-9.
10. "Multi-objective Optimization of Nanosecond Pulsed Laser Microgrooving of Hydroxyapetite Bioceramic" Abstract proceedings of 9th International conference of Materials Processing and Characterization (ICMPC 2019), March 8-10, 2019, GRIET Hyderabad, India. Page 187.

National Conference

1. "Parametric Optimization of Laser Microdrilling of SIC30BN Nanocomposite", Proceedings of the National Conference on Recent Trends in Manufacturing Science and Technology (RTMST-2013), April 18-19, 2013, Department of Mechanical Engineering, NITTTR, Kolkata, India, pp. 227-235.

Patent

Nil

JADAVPUR UNIVERSITY
FACULTY OF ENGINEERING AND TECHNOLOGY
DEPARTMENT OF PRODUCTION ENGINEERING

CERTIFICATE FROM THE SUPERVISORS

This is to certify that the thesis entitled "**Study on Laser Beam Micro-Machining with Different Assisted Medium**" *submitted by Shri. Nilanjan Roy, who got his name registered on 8th December 2011 for the award of Ph.D. (Engg.) degree of Jadavpur University is absolutely based upon his own work under the supervision of Prof. Arunanshu Shekhar Kuar and Prof. Souren Mitra and that neither this thesis nor any part of the thesis has been submitted for any degree/diploma or any other academic award anywhere before.*

---------- ----------

(Signature of the Supervisor and date with official seal)

(Signature of the Supervisor and date with official seal)

Preface

Laser is a device that emits electromagnetic radiation through the process of stimulated emission, is an invaluable tool for mankind for it's diverse application in the field of science, technology, entertainment and art. In laser beam machining process, laser beam incident on workpiece which helps to convert the laser energy into thermal energy at irradiate zone by means of lattice vibration and free electron movement. This thermal energy heats up the irradiate zone locally followed by melting and vaporization. Debris in molten or vapor form, removed from the machining zone either by any assist gas flown co-axially or by hydrodynamic nature of melt pool/ vapor. Absence of mechanical damages in/around the machining zone and tool wear due to processing of work substrate in macro/micro domain by thermal energy make this process a suitable one to machine a wide range of engineering materials with high precision at very minimum time and any kind of complicated or normal shape.

A very few investigations have been documented on laser processing of hard to machine advance materials in different environment. Experimental investigation is needed to understand the feasibility of laser machining of these kinds of advance materials at different environment. Keeping in view the aforesaid laser beam micromachining characteristics for material processing in micro domain at different machining environment, the present research work has been planned and designed to investigate and optimize the laser beam micromachining quality characteristics during micromachining in terms of microdrilling and microcutting of different advance engineering materials.

1) To study the mechanism of material removal in laser machining in submerged condition.
2) To understand the CNC supported nanosecond pulsed Nd:YAG laser system for carrying out the experiments at different assisted medium.
3) To design and fabricate the jigs and fixture for holding the job sample during machining at different machining conditions.
4) To set the design space from the observations of trial experiments, for carry out the final experiments based on different methodology along with different assist medium in terms of different compressed air or inert argon gas for microdrilling process and compressed air and underwater condition for microcutting process.

5) To carry out the laser microdrilling process on Aluminum 5052 alloy and Silicon Carbide 30% Boron Nitride nano-composite and material and laser microcutting operation on Hydroxyapetite in its pure form and Inconel 625 superalloy to investigate the most influencing parameters including the assist medium for desired machining characteristics with the aid of some statistical method like sensitivity analysis.

6) To make comparative analysis of micromachining performance for laser with different assist medium.

7) To determine the optimal combinations of pulsed laser machining parameters along with assisted medium.

In depth study of laser beam microdrilling of aluminum alloy & Silicon Carbide 30% Boron Nitride (ceramic based nanocomposite material) and microcutting of Hydroxyapatite in it's pure form & Inconel 625 (Nickel based superalloy) has been done in this present research work with aid of a 75 watts nanosecond pulsed Nd:YAG laser (highest laser power obtained during the study is 45 watts) with wavelength in near infrared region (1064 nanometer) to investigate the feasibility of laser processing of aforesaid materials in single pass at different environment/ assist medium. It is also try to observe and analyze effects of various process variables on machining responses during the machining and find out the optimum parametric condition to achieve the desired machining characteristics. In this present research activity main emphasis is given to compare the effect of different assist medium during laser processing of nanocomposite material and nickel based superalloy.

The thesis is prepared in well-organized manner into seven chapters. A brief summary of each chapter is provided as below:

A brief overview of micromachining consists of need for micromachining, history of micromachining, characterization of micromachining, various kind of micromachining along with their advantages and disadvantages are outlined in chapter 1. Various kinds of laser systems applied for micromachining operations are discussed in this chapter. Chapter 1 concludes with the justification of more suitability of thermal machining process in terms of laser beam machining over other nonconventional micromachining processes in micro domain. Brief overview of assisted medium on laser beam micromachining has been discussed on the chapter 2

followed by detailed description of laser matter interaction in dry and wet medium elaborately. Effect of assisted medium to overcome the adverse effect of laser beam micromachining has been discussed here in brief. Specific applications of laser beam micromachining are also discussed in this chapter. Chapter 3 consists of literature review of past research works which helps to outline the research objectives by elimination of knowledge gaps find during literature review. Details of Laser beam machining set up along with assist gas supply unit and development of a workpiece holding unit for underwater laser beam machining has been documented in the Chapter 4. Different kind of methodologies which applied not only for design the experiments but also for analysis and optimization of experimental observations are also discussed in this chapter. In chapter 5 experimental investigations of laser percussion microdrilling of highly reflective Aluminum alloy Al 5052 and SiC30BN nanocomposite material has been performed to study the influence of process variables on machining responses during making a through hole on thin sheet. A second order polynomial model is developed during laser beam microdrilling by response surface methodology (RSM) to establish the correlation between input and output of the process. Emphasis is given here to find out sensitivity of responses towards the process variables during laser microdrilling of Aluminum alloy Al 5052. Different Optimization technique is used to find out optimum parametric condition for two different work substrates and get the desired output within the chosen design space. In this chapter main emphasis is given on the comparative study of different assist medium, i.e., compressed air and argon gas flow co-axially with the laser beam on machining response during laser percussion microdrilling of SiC30BN. Chapter 6 demonstrates about laser beam blind microcutting of Hydroxyapatite bio ceramic and Inconel 625 superalloy in different environment where compressed air is used an assist medium for both the work substrate, machining at submerged condition is also performed on later one. This chapter starts with experimental study of feasibility to make a groove on the surface of Hydroxyapetite in it's pure form by laser beam and thereafter optimized the process after the first one is justified. Here also an empirical model is developed by response surface methodology (RSM) from experimental results to establish the correlation between input and output variables. Surface plots, contour plots help to analyze the experimental observations and helps to find out the feasible region of responses within the selected design space. In this chapter also emphasis is given to demonstrate the effect on different assist medium on machining responses and compare it elaborately from

experimental results and pictorial observations. Chapter 5 & 6 have also contains a outcome after each experimental study. Chapter 7 consists of overall concluding remarks on laser beam micromachining in terms drilling of hard to machine material from metal alloy to ceramic based nanocomposite and cutting of bioceramic to metallic superalloy on the basis of experimental results and discussion.

The main outcomes of the study are the feasibility of laser processing of newly developed nanocomposite material in different gaseous environment and laser processing of Inconel 625 superalloy in underwater as well as under flow of compressed air condition. Effect of the assisted medium is well in discussion in this study. Compatibility of different assisted medium during laser based processing of hard to machine materials with very low power laser system is discussed here which is indicates at the novelty of the study. The findings of the current research work indicates at the feasibility of local processing in terms of low power laser processing of the said superalloy as the superalloy is used in marine and chemical industries. Thus it may be said that the observations of the experimental investigation not only used in laboratory research purpose but also have an chance of application in industry which establish the justification of the current research work.

Acknowledgement

First and foremost, I would like to express my deepest gratitude and wholehearted appreciation to my supervisor Professor Arunanshu Shekhar Kuar, Production Engineering Department, Jadavpur University, Kolkata for his enthusiastic guidance, valuable suggestions and persistent supervision which are indispensable for the completion of this research work. I am indebted to him for his constant encouragement and undeniable support through the inevitable ups and downs of this research and for always keeping me focused and giving me sound advice in all aspects of my studentship.

I would also like to express my sincere thanks and heartily gratitude to my co-supervisor Professor Souren Mitra, Production Engineering Department, Jadavpur University, Kolkata for his guidance, valuable advice and association throughout the research.

I would also like to express my heartiest appreciation to Professor Soumya Sarkar for his encouragement, precious suggestions, support and association all the way through development of the present research work.

I would cordially like to articulate my deepest admiration to Professor Siddhartha Ray, Professor Jyotirmoy Saha, Professor Dipankar Bose, Professor Subir Kr. Sanyal and Professor Ajoy Kumar Dutta for their incessant encouragement and valuable advice at every aspect and in any form during the research period.

I would also cordially like to express my sincerest admiration to Professor Bijoy Bhattacharyya for his valuable advice and support as a coordinator of the Centre of Advanced Study (CAS) – Phase IV Programme of the University Grants Commission (UGC), New Delhi at Production Engineering Department, Jadavpur University, Kolkata for technical support throughout the current research work.

I am extremely grateful to all the faculty members of Production Engineering Department for their co-operation during the research work. I am greatly thankful to Biswanath Das Lab Assistant (currently retired) of Production Engineering Department, Jadavpur University, for his kind support during this research work tenure.

My heartiest gratitude to my ***parents*** for their moral support, ceaseless encouragement, tolerance, understanding and inspiration during the inevitable ups and downs of this research. I would like to express great appreciation to Mainak Roy my nephew, Subhamita Mandal my niece and all other family members for their moral support. I would like to express my heartily appreciation to my friends Gourav Howlader, Tamal Bhattacharyya, Koushik Mukherjee, Tirupati Banerjee for their moral encouragement, unwavering support and motivation.

I wish to express my deep sense of gratitude to all my fellow colleagues Dr. Bappa Acherjee, Debal Pramanick, Kingshuk Mandal, Abhishek Sen, Subham Biswas, Somnath Das, Nabin Sardar, Arka Mandal and K. Paramasivan for their academic guidance, motivation and untiring support to successfully complete the research work.. I would also like to acknowledge Arani Das and Shreyashi Mahanty, undergraduate students of Production Engineering Department, Jadavpur University for their co-operation during this research work. I also want to extend my heartily gratitude to Debasish Dey, service manager of Sahajanand Laser Technology for his continuous technical support to Nd:YAG laser machine manufactured by the same company.

I also extend my deep gratitude to Dr. (Prof.) Suman Kr. Roy for his enormous encouragement during this research tenure.

VITA

The author, Nilanjan Roy, son of Mr. Indu Bhushan Roy and Mrs. Madhuri Roy, was born on 8th day of June 1983 in Titagarh, 24 Parganas (north), West Bengal. He Passed Secondary Examination under West Bengal Board of Secondary Education from Ramakrishna Vivekananda Mission High School, Barrackpore in 1999 and Higher Secondary under West Bengal Council of Higher secondary Education from Barrackpore Government High School in 2001.

The author completed his graduation in Mechanical Engineering in 2006 from Birbhum Institute of Engineering and Technology under West Bengal University of Technology with first class. Author received his Post Graduation degree in Manufacturing Technology in 2009 from National Institute of Technical Teachers Training and Research, Kolkata under West Bengal University of Technology with first class. Then he joined in IMPS College of Engineering & Technology as Assistant Professor in March 2009. After that he Joined in Production Engineering Department, Jadavpur University as a Research Fellow under, "DST-PURSE phase II" in June 2011 and later as a National Fellow under, "Rajiv Gandhi National Fellowship Programme 2014" in April 2015. He has done his research work in the area of laser beam micromachining of various hard to machine engineering materials with the assistance of different environment during entire period. Author has published 5 research papers in international referred journals and also presented 14 research papers in reputed national and international conferences related to laser beam micromachining in INDIA and abroad. Author also published 5 research articles as book chapter in various books on laser based manufacturing and non-conventional machining.

Dedicated to my Parents
My foundation of strength and source of motivation
For their love, inspiration and boundless support

Table of contents

TITLE SHEET I

LIST OF PUBLICATIONS OUT OF THE RESEARCH WORK V

CERTIFICATE FROM THE SUPERVISORS IX

PREFACE XI

ACKNOWLEDGEMENT XV

VITA XVII

DEDICATION XIX

TABLE OF CONTENTS XXI

1. Introduction 1
   - 1.1 Need for micromachining 1
   - 1.2 Different types of micromachining 3
   - 1.3 Laser beam micromachining 5
   - 1.4 Application of laser in micromachining and microfabrication 9
2. Laser beam micromachining with different assisted medium 11
   - 2.1 Laser matter interaction in dry condition 11
     - 2.1.1 Absorptivity of laser irradiate zone 11
     - 2.1.2 Phase change and plasma formation 13
     - 2.1.3 Evaporation & ablation 14
   - 2.2 Laser beam micromachining with aid of assist gas 14
   - 2.3 Underwater laser beam micromachining 15
   - 2.4 Material removal mechanism of nanosecond pulsed laser beam cutting at submerged condition 16
3. Literature review and objectives of present research 19
   - 3.1 Review of past research work 19
   - 3.2 The objective and scope of the present research work 33
4. Machining Setup 35
   - 4.1 Laser generation Unit 35
   - 4.2 Beam delivery unit 39

4.3 Cooling unit 41
4.4 CNC controlled workstation 42
4.5 Fixtures for Laser micromachining 43
4.6 Assist gas supply unit 44
4.7 Development of underwater workpiece holding unit 45
4.8 Methodology used for experimental planning and analysis 46
4.6.1 Taguchi methodology 46
4.6.2 Taguchi based Grey relation analysis 48
4.6.3 Response surface methodology 51
4.6.4 Sensitivity analysis 53
5. Experimental studies on laser beam microdrilling 55
5.1 Parametric study on laser beam microdrilling of Aluminium 5052 alloy with compressed air as an assist medium 56
5.1.1 Material Specification 56
5.1.2 Design of experiments 57
5.1.3 Results and discussion 58
5.1.4 Sensitivity analysis of machining responses 69
5.1.5 Determination of optimal process parameter settings 78
5.1.6 Outcome of the study 81
5.2 Laser beam microdrilling of SiC30BN Nanocomposite material 82
5.2.1 Parametric study on laser beam microdrilling of SiC30BN nanocomposite material with compressed air as an assist medium 83
5.2.1.1 Experimental Planning 83
5.2.1.2 Results and discussion 85
5.2.1.3 Determination of optimal parameter settings 92
5.2.1.3.1 Single objective optimization 92
5.2.1.3.2 Taguchi based Grey relation analysis for multi objective optimization 93
5.2.2 Parametric study on laser beam microdrilling of SiC30BN nanocomposite material with argon gas as an assist medium 96
5.2.2.1 Experimental planning 97

5.2.2.2 Results and discussion 97
5.2.2.3 Determination of optimal parameter settings 105
5.2.2.3.1 Single objective optimization 105
5.2.2.3.2 Taguchi based Grey relation analysis for multi objective optimization 106
5.2.2.4 Outcome of the study 108
5.2.3 Comparative study of the effect of different assist medium on laser micro-drilling of SiC30BN 109
6. Experimental studies on laser beam microcutting 119
6.1 Parametric study on laser microgrooving of Hydroxyapatite bioceramic with compressed air as an assist medium 120
6.1.1 Experimental details 121
6.1.2 Experimental observations and discussion 122
6.1.3 Determination of optimal parameter settings 126
6.1.3.1 Single objective optimization 126
6.1.3.2 Taguchi based Grey relation analysis for multi objective optimization 127
6.1.4 Outcome of the study 130
6.2 Laser beam microcutting of Inconel 625 superalloy 131
6.2.1 Parametric study on laser beam microcutting of Inconel 625 superalloy with compressed air as an assist medium 132
6.2.1.1 Experimental details 132
6.2.1.2 Results and discussion 133
6.2.1.3 Sensitivity analysis 148
6.2.1.4 Determination of optimal process parameter settings 160
6.2.2 Parametric study on laser beam microcutting of Inconel 625 superalloy at submerged condition in water 163
6.2.2.1 Experimental setup 163
6.2.2.2 Experimental results and discussion 165
6.2.2.3 Sensitivity analysis 180
6.2.2.4 Determination of optimal process Parameter settings 192
6.2.2.5 Outcome of the study 195

6.2.3 Comparative study of the effect of different assist medium on laser microcutting of Inconel 625 196
7. General conclusion and future scope of work 201
7.1 General conclusion 201
7.2 Future scope of work 204
Bibliography 205

Chapter 1

1. Introduction

Ever since the beginning of civilization, the materials have been processed into meaningful components or tools, by modifying their physical properties like size, shape, texture, mechanical and metallurgical properties. Tools for drilling and cutting of metals are known to have been used in ancient Egypt about 4000 BC. By the 17th century instruments for machining are widespread. More sophisticated tools for machining powered by water, steam, and electricity are emerged over the 18th and 19th centuries. Various parts of wristwatch are the said to be micro products and manufactured around hundred years back. The idea of miniature machines is often first attributed to Richard Feynman, who gave an influential presentation on the topic in 1959 [1]. Machining processes and their associated machine tools have continued to benefit from the notable achievements made in terms of precision machining of complex shapes and their measurement in the electronics and computer industries (1980s to 1990s). Increasing demands for components of dimensions on the order of micrometers (μm) are witnessed in 1990s. Microengineered products are required in microelectronics and optical industries where components have to be produced to ever-decreasing size or to finer accuracies, as example micro gear, small bearings in watch. Manufacturing of micro parts which capable to deal with atomic and molecular dimensions is increasing significantly.

1.1 Need for micromachining

Micromanufacturing is a set of processes or techniques used to machine microcomponents or microsystems, or to create microfeatures on macro/ micro parts. In today's high tech engineering industries, the objective of miniaturization is either to create small parts with better capabilities or to create small features on a large component to enhance its functionality. Miniaturization of products have merits, such as, less amount of material and energy consumption during manufacturing, portability, lightness, cost/ performance advantages and exploitation of new effects through the breakdown of continuum theory in the micro domain. Micro fabrication considers the miniature parts/ products/ structures which are not easily observed by naked eye and have dimensions in the range of 1 micron to 999 micron. Microelectronics, aerospace,

automobile and medical industries are at the forefront in the application of microproducts. These industries are keen on introducing microcircuit manufacturing techniques to produce microsensors, cooling holes in turbine blade, complex fuel injection systems, safety devices, micromotors, microactuators and bio compatible microfluidic devices in their existing and new products.

Generally, microfabrication of products is achieved either by material deposition or by material removal where the later one is known as micromachining technique. The unit removal of material in micromachining operations is in micro/nano scale. Identification and minimization of influencing factors is very important in micromachining operations as it is considered as precision technology. Influence of machine tool deformation, inaccuracy along with chip removal, material properties, thermal deformation, surface integrity, vibration, and temperature in machining zone are the significant consideration in the micromachining domain. Furthermore, inspection and measurement of micro parts are very difficult by conventional probes and gauges, because of the small dimensions of the products. Non contact type 3D optical systems are generally used for measurement of micro products. Online measurement is becoming a prerequisite for micromachining operations.

In micromachining volume or size of material removed by the unit removal phenomenon (UR) must be very small, generally known as top down approach. In terms of precision, identification and minimization of error generation factors is very important [1]. The relative magnitude of different forces changes with the variation in size of a system. At very large scales, physical problems are handled using relativity whereas in small scales, those problems are handled using quantum mechanics [2]. Even a small change in scale, from ordinary macroscopic object to microscopic objects, can have a great effect. While the physical forces are the same, the relative importance changes considerably from macro to micro scale machining operations. Prediction of system behavior in micromachining operations are generally governed by scaling law. Micromechanical devices can withstand larger accelerations without breaking than macroscopic mechanical systems. The electrostatic force is independent of scaling when the voltage is kept at constant. The response time decreases as the system is miniaturized. The power consumed per unit volume is a very important factor in machining performed in micro scale. The temperature of miniature devices to reach equilibrium very quickly, for that reason device's heat capacity is proportional to its volume, while the rate of heat transfer is proportional to its surface area. The

relative importance of surface forces increases as the volume to surface area ratio changes with miniaturization of device.

1.2 Different types of micromachining

The term, 'processing unit' is introduced by N.Taniguchi to distinguish between material removal phenomenon for micro and macro machining techniques. Various micromachining applications can be classified as mechanical micromachining, thermo-electrical micromachining, chemical/electrochemical micromachining and hybrid micromachining.

1.2.1 Mechanical micromachining

Micromachining is the most basic technology for the production of miniaturized parts and components. In conventional micromachining operations material removal or processing have some resembles with macro/meso scale operations, i.e, drilling, cutting, turning milling, grinding etc. In micromachining, the goal is to produce mini and micro systems (typically 1 or less cm in size) with micro components (typically 1 to 100 μm in size) with sufficient tolerances to achieve required functionality and repeatability. During this process, precise microtool/abrasive particle interact with work substrate with very high kinetic energy and remove the material either by shear deformation (for ductile workpiece) or by brittle fracture (for brittle workpiece) in the form of micro/nano chip to form desired shape. Abrasive waterjet micromachining, Ultrasonic micromachining are the examples of mechanical micromachining. Machining force may influence machining accuracy and elastic deformations of microtools are the main two constrain for mechanical micromachining [1]. The adverse effects of this micromachining technique are high tool wear and generation of heat at the tool–work interface in conventional micromachining, poor control over shape generation in abrasive micromachining, dynamics of the equipment, low MRR and vibration of tool holding device in ultrasonic micromachining.

1.2.2 Thermo-electrical micromachining

In this micromachining process material removal mechanism is governed either by melting and vaporization or only by vaporization, skipping the phase of melting. Thermal and optical properties of workpiece are more influencing over mechanical properties in this micromachining process. Adjustment of the electrical parameters may help to control over pulse energy which is the most influencing process input in this micromachining technique. Absence of mechanical forces due to non contact in nature makes it more suitable over the other micromachining processes for a wide range of materials in different kind of environments. Sometimes the

quantum energy of the machine tool (Ion beam) exceeds the binding energy of the work substrate which leads to removal of material by decomposition of molecules into atom. These aforesaid mechanism of micromachining helps to get micro features with high precision. Laser beam micromachining, Electro discharge micromachining, Electron beam micro machining, Ion beam micromachining are examples of thermo-electrical micromachining. Heat affected zone (HAZ) is the main drawback for various thermo-electrical micromachining technique along with precise control over process parameters and resolidification in electro discharge micromachining, laser beam machining, ion beam micromachining [1].

1.2.3 Chemical/electrochemical micromachining

The principal of electrochemical dissolution in liquid is steered the material removal mechanism in this micromachining process. Ionic reaction based material removal mechanism leads to unit removal in the perpendicular direction to the surface makes this process suitable to produce3D profile. Controlling of current density may effects the accuracy of machining. Type of electrolyte, flow pattern, temperature of electrolyte and gap between tool and workpiece are the main influencing process variables which may influence the dimensional precision of micro product [1]. As the material removal mechanisms is involvement of a number of reaction and sequences, it is very difficult to control process along with precise control over electrode and workpiece during machining and very hard to machining of chemically resistant materials, low cost effectiveness are the limitations of chemical and electrochemical micromachining.

1.3.4 Hybrid micromachining

Micro-components/products are already been found across the broad spectrum of application areas especially in sectors such as automotive, aerospace, photonics, renewable energy and medical instruments. These micro-components/products are usually made of multi-materials (may include hard-to-machine materials) with complex shaped micro-structures. Combination of more than one micromachining technique may be used simultaneously to process these complex shaped micro parts precisely. Integration of various micromachining processes simultaneously, to get improved machinability, geometrical accuracy, tool life, surface integrity, machining rate and reducing the process forces are known as hybrid micromachining. Hybrid micro-machining processes are classified into two major categories namely, assisted and combined hybrid micro-machining techniques [3]. Some of the hybrid micromachining processes include Electro

chemical spark micromachining, Laser assisted electrochemical micromachining, Electrolytic Inprocess Dressing, Electro Discharge Grinding etc.

From the above study it may conclude that in various conventional or non-conventional micromachining, thermal micromachining have some advantages over other micromachining processes. Absence of mechanical deformation, specialized microtool, proper maintaining of gap between microtool and workpiece, coordinate shift in tool handling, post processing operations along with very fast machining time makes thermal machining process a very suitable alternative for processing of wide range of materials. This process not only use for micromachining by subtraction but also by addition with help of some additional attachment facility. Though thermal damages are present in this machining process (except ion beam machining) but proper selection/adjustment of process variables, may nullify the adverse effect of thermal damages. In various kind of thermal machining processes, laser micromachining with certain drawbacks like, heat effected zone, high capital cost, thickness of material etc, is most suitable for micromachining in addition of some preventive approach during the process. Laser micromachining can apply for processing of vast range of advanced engineering material processing with various types of straight or complicated shape due to it's noncontact type nature, high flexibility which affects the machining response as well as machining efficiency by absence of post machining operations, tool vibration as the energy transfer from machine tool to workpiece by radiation, dependence of material properties, i.e., brittleness, toughness, hardness.

1.3 Laser Beam Micromachining

1.3.1 Laser beam as micromachining tool

In late 20^{th} century, optical energy is emerges as a more versatile energy source due to additional "knobs to turn," facility. Laser beam machining is the machining processes involving a laser beam as a machine tool. Laser can be considered as one of most useful non-conventional micromachining tool because of advantages like,

a) Lack of tool wear and tear
b) Precision of operation,
c) Minimal wastage of material,
d) Absence of finishing operations,
e) Localized processing,
f) Flexibility

g) High speed of operation.

It is a thermal process where laser beam is used as a heat source to remove materials without mechanical engagement with workpiece material. The main properties of laser radiation are high spatial and temporal coherence along with high collimation, high monochromaticity, high brightness and minimal divergence which results in to produce very high intensity laser beam. A wide range of materials can be processed by laser due to its large irradiances (up to 10^{21} W/cm^2) at the surface, for the high focusability which is enough to evaporate any material or even to start a nuclear fusion reaction [4]. In laser beam machining process, material removal isn't dependent on mechanical, physical or electrical properties of workpiece but on thermo-optical properties of the material [5].

The beam wavelength has a great impact on absorptivity of laser light on workpiece surface for which it is relatively important for laser material processing. A discrete spatial profile termed as transverse electromagnetic mode is exhibit by cross section of laser beam. Generally fundamental TEM_{00} is used for laser beam machining operation, has Gaussian spatial distribution. The output of laser can either be constant amplitude or periodic, commonly known as continuous wave (CW) mode, and pulsed beam mode respectively. Normal pulsing, Q-switching, and mode locking are the various pulsing way during pulsed laser operation. A high energy density is achieved in short pulse duration during pulsed laser operation after threshold energy is reached. Pulse duration and pulse repetition rate are the most influencing parameters for pulsed laser machining [6]. During laser beam machining two geometrics are generally used, either a moving target or a moving beam.

1.3.2 Laser Beam-Machining Systems used for Micromachining

CO_2 laser, Nd:YAG, DPSS, free-electron laser and Excimer are generally used for micromachining because of their characteristics. Characteristics of various laser systems used for micromachining are given below,

a) CO_2 Laser

The laser device consists of three main parts: a gain or laser medium CO_2, an optical resonator or cavity with two mirrors (mirror 1 and 2, placed at opposite ends), and an energizing or pumping source that supplies energy to the gain medium to activate CO_2 into amplifying state [7]. The chemical species in the gain medium (composition, bond energy, band gap, etc.) determines the wavelength of the optical output. Between the two mirrors, one is a fully

reflecting and the other is partially reflecting one. The emitted radiation is coherent with the stimulating source so that the wavelength, phase and polarization between the two mirrors are identical. Stimulated emission of radiation in gain medium is governed by the principal of quantum mechanism. The pumping source helps to create more photons via population inversion which moves to and forth along the optical axis after reflected by the resonator mirrors to interact with other excited atoms, thus get amplified. A percentage of these photons come out through the partially transmitting mirror as laser beam, in each of these cycles. Finally, the laser beam interacts with the workpiece through beam delivery system.

b) Semiconductor or Diode Lasers semiconductor

lasers are now becoming increasingly popular both as a pump source for solid-state laser and in materials processing because of their unique features like small size, low weight, high efficiency, and reliability. More frequently used diodes are based on double hetero-junction using ternary compounds such as AlGaAs (p) and GaAs/GaAlAs. Recombination of electrons in the conduction band with holes in the valence band is the reason behind stimulated emission in this type of laser. The amount of emitted radiation is increased by mounting of more than one diode bars into the multi-channel heat sinks which are stacked on one over of each other [8].

c) Solid state laser (Nd:YAG laser)

Neodymium doped yttrium aluminum garnet (Nd:YAG) is one of the most commonly used solid-state lasers. Neodymium atom in its trivalent state is doped in the yttrium aluminum garnet crystal ($Y_3Al_5O_{12}$orYAG). A flash and arc lamp is used here as an exciter. Wavelength in near infrared region (1.06 μm) and optical fiber based laser radiation delivery makes it more advantageous over CO_2 laser in industry. The output power is in the range of a few watts up to a few kW can be achieved during continuous wave operation. The output energies for pulsed lasers range is from a few mJ to a few tens of Joules. Attempts are being made to develop sensitizer atom contained new active material to enhance the total efficiency. In micro domain Nd:YAG laser is mainly used for materials processing (cutting, drilling, welding, marking, surface engineering) applications in pulsed mode [9].

d) Free Electron Laser

Electron beam propagating through a periodic magnetic field, called a wiggler or undulator which combined with radiation to act as a lasing medium in free electron laser. The free-electron laser is continuously tunable to produce high average power up to several kilowatts and peak

power up to a giga-watt at a wide variety of pulse formats. Free-electron laser is mainly configured with an oscillator driven by a radiofrequency linear accelerator [10].

e) Excimer Laser

Use of unstable molecules such as Ar, Kr, Xe with halogen atoms like, F, Cl, Br, as the active material that is formed within the same electrical discharge used for the excitation in Excimer laser. These lasers are used for spectroscopy and photochemistry experiments in the ultraviolet range and for many applications related to surface treatment [11].

Table 1: Most common lasers used for material processing. [12]

Laser Type	**Wavelength (nm)**	**Power (Watts)**	**Pulse Energy (mJ)**	**Fluence (J/cm^2)**	**Pulse Duration (seconds)**	**Repetition Rate (kHz)**
Q-Switched Nd:YAG	1064	1-35	8	-	5-100 ns	1-400
	532	0.5-20	5	-	5-70 ns	1-300
	355	0.2-10	3	-	5-50 ns	15-300
	256	0.5-3	< 1	-	5-30 ns	15-300
Ti:sapphire	800 (Central)	0.5-2	0.25-0.9	-	100-150 fs	1-5
	700- 980	-	-	-	-	-
Excimer	-	-	-	-	10-20 ns	5-10 Hz
XeF	351	-	-	1.8-9.1	-	-
XeCl	308	-	-	1.2-9.8	-	-
KrF	248	-	-	0.9-9.8	-	-
ArF	193	-	-	0.7-4.0	-	

1.3.3 Different techniques of Laser beam micromachining

In the modern technologies, miniaturization is an important trend to fabricate microparts for biotechnological, microelectronics, telecommunication, MEMS, and medical applications. Laser beam micromachining is utilized for the generation of microproducts with better flexibility in the dimensional design. Photothermal or photochemical ablation is the mechanism behind the material removal in micron or in sub-micron range during laser beam micromachining operation. Laser beam with wavelength in the range in near infrared (1.06μm) to deep Ultraviolet (150nm) is commonly used in micromachining operation. Photon energy increases with shorter wavelength enhance the material removal, results in less thermal damages like melting, charring of adjacent unirradiate material. Thermal diffusitivity, thermal relaxation time and absorption coefficient have a great effect on ablation process [13]. Efficiency of ablation increases by lower

value of thermal diffusitivity whereas the pulse duration shorter than thermal relaxation time facilitates restriction of temperature distribution on the surrounding material. Shorter pulse width (<100 nanosecond to few femtosecond) is preferably utilized for micromachining application due to high peak intensity (> 10^{15} W/cm^2) to get précised dimensional accuracy with substantially low thermal damages [14]. Direct writing, mask projection, and interference are the important techniques of micromachining. In direct writing technique laser beam is directly focused on work substrate to produce the desired pattern either by moving the laser beam in respect to work substrate (Galvo system) or by translating the substrate in respect to stationary laser beam (CNC based work-table) [15]. Hole drilling, cutting, scribing, and marking are the extensively used micromachining application of this technique.

1.4 Application of laser beam micromachining

In manufacturing industry from automotive to medical, laser beam micromachining is used to process a wide range of materials with a precision and in a cost effective way. Laser processing in micro domain not only restricted to conventional industries like medical, aerospace, automotive, MEMS but also in jewellery industry for cutting diamonds, gemstones etc., in packaging industries for marking on the box with minimal material removal as well as marking in gold ornaments also. Typical examples for the usage of laser technology for cutting in textile industries are filters, upholstery, heat protection fabrics, textile components in the automotive industry or sails. Gradually laser micro machining in terms of cutting and drilling is also applied in woodcraft industries to produce complicated 3D shape on wood.

Table 2.2 Application Laser microdrilling and microcutting

Industry	**Applications of Laser micromachining**	
	Laser beam microdrilling	**Laser beam microcutting**
Micro-Electronics	Array of microhole on the nozzle of inkjet printer, Interconnects of PCB, Optical switching, Electric insulators, thru micro hole on SiC wafers for transistor structure and microhole on atom chips to load cold atoms	Cutting of printed circuit board (PCB), NanoSD card, cutting of Membrane key boards, matrix lead frames and Key board foils.
Medical & Biomedical Industry	Aerosol spray atomizer, Lab on a chip, Catheter sensors, DNA sampling.	Cutting of high-grade coronary & Gastrointestinal Stents, Surgical equipments, Precision tubes, Cutting of Human Tissue & Skin.

Industry	Applications of Laser micromachining	
	Laser beam microdrilling	**Laser beam microcutting**
Aerospace	Microhole in Turbine engines for cooling, Microhole in wings and tailsd to reduce drag force, microholles on turbine blades, combustors, vanes, and afterburners.	Cutting of combustor liners and cans, fabrication of aircraft component.
Automotive	Drilling of vent holes in various machine parts for cooling purpose, injection nozzles,	Cutting of carriage components, Cutting of 3D shaped hydroformed parts, airbag
Renewable energy System	Fuel cell particulate filters	Cutting of thin-film Solar cells and silicon.

From the above study it may conclude that laser as a machine tool for micromachining operation is greatly acceptable in the various field of engineering. Various research works have been performed to study the feasibility of laser as an instrument for machining in the micro domain to find out the advantages and disadvantages of laser micromachining system. Till date lots of research is carried out to get desired machining characteristics either by changing the characteristics of laser beam or adding some subsystem with the machining setup which are documented in the next section of the research work as laser beam micromachining at different assisted medium.

Chapter 2

2. Laser beam micromachining with different assisted medium

Sometimes laser beam machining process has performed at various atmospheric conditions, i.e., with compressed air or inert gas as assist gas or submerged condition or in preheated condition or in vacuum or sometime mixture of various conditions to get desired quality characteristics in micro domain.

2.1 Laser matter interaction in dry condition

The phenomenon of electromagnetic radiation Laser-matter interaction is generally a coupled of electronic and thermal events which regardless starts with an electronic excitation followed by local heating due to photon-electron interactions.

2.1.1 Absorptivity of laser at irradiate zone

Reflection, refraction, absorption, scattering and transmission are the physical phenomena that take place when the electromagnetic wave (laser beam) interacts with workpiece surface. Linear and non-linear absorption are the most important phenomenon of the laser matter interaction. Figure 2 shows a schematic of interaction of laser beam with work material.

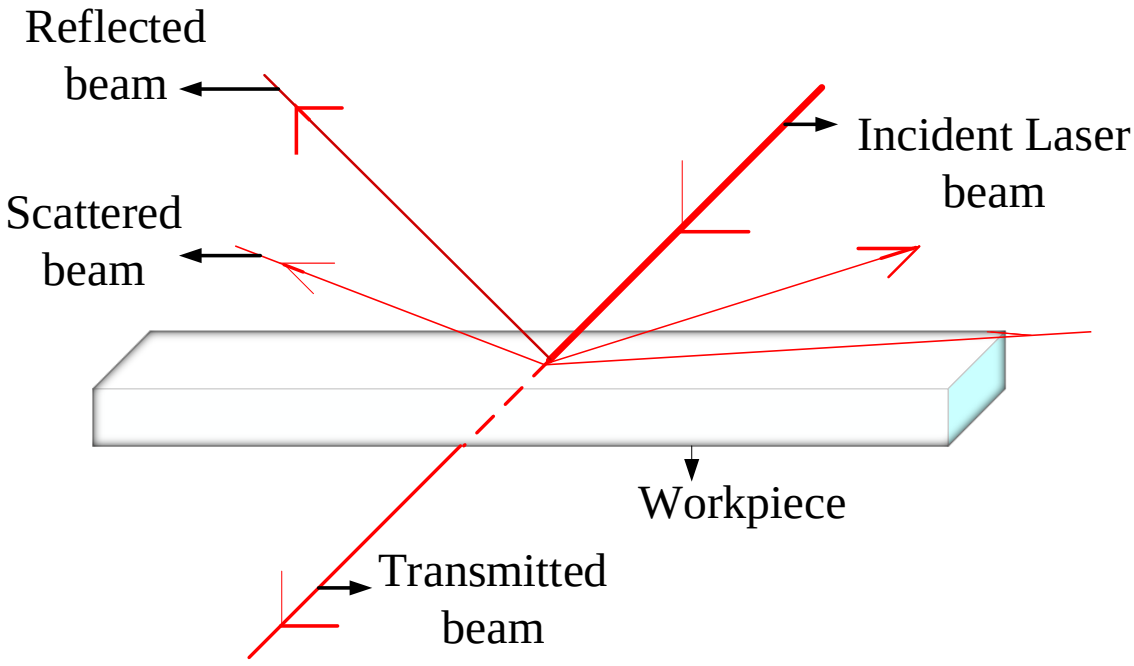

Fig. 2 Interaction of laser beam with workpiece material [16]

Absorption at irradiate surface are not only depend on the wavelength of the laser radiation, but also on other factors such as incident angle, surface roughness, and temperature of the solid. The absorption coefficient of material proportional to electrical resistivity whereas increases with decrease in wavelength. Probability of nonlinear absorption increases strongly with growing laser intensity is the reason behind multiphoton excitation processes at constant laser fluence with a shorter laser-material interaction time. Absorption of laser energy can be described as interaction between electrons and nuclei lattice of target material. A force is exerts by opto-electric field of incident electromagnetic radiation by which the nuclei lattice and electrons get vibrational motion. The absorbed radiation, thus, results in the excess energy of the electrons such as kinetic energy of the free electrons, excitation energy of the bound electrons [17]. Excess energy of the electrons are damped by collision with vibrating lattice of nuclei and some incident laser energy transferred to the lattice leads to generation of heat. By Beer-Lambert law [18], the absorption of laser radiation in the target substrate is generally expressed,

$$I(Z) = I_0 e^{\mu z} \qquad 2.1$$

Where, where I_0 is the incident intensity, $I(z)$ is the intensity at depth z, and m is the absorption coefficient. The intensity of the laser radiation gets faded along with the depth inside the material. The length over which the significant reduction of intensity of the laser radiation takes place is known as attenuation length (L) and expressed as reciprocal of the absorption coefficient (μ) of target substrate [19],

$$L = \frac{1}{\mu} \qquad 2.2$$

Generally for opaque material, the absorptivity can be defined as fraction of incident radiation, absorbed at normal incidence which can be expressed [20] as,

$$A = 1 - R \qquad 2.3$$

Where, A is absorptivity of irradiate substrate and R is the reflectivity of irradiate substrate.

Various physical effects in the material include heating, melting, and vaporization of the substrate is occurred, depending on the temperature distributions in the material. Thermal energy transported through the substrate by thermal conduction and convection and radiation from the surface of the substrate.

2.1.2 Phase change and Plasma formation

Phase transformations such as surface melting and evaporation are takes place by sufficiently high laser intensity which is generally referred as melting (I_m) and vaporization (I_v) threshold intensity. During laser irradiation, the melting starts at a certain temperature when laser intensity reaches at melting threshold energy and creates a solid liquid interface at the surface. Solid liquid interface moves away from the surface along the depth with increase in laser energy density and a melt pool was formed. The depth of melting is decreased during pulsed off time and vice versa [21]. To and fro movement of solid liquid interface at a very high velocity (≤30 meter/second) is the reason behind surface melting and subsequent resolidification at the machining zone in pulse duration [22]. The depth of melting (Z max) reaches at maximum when the laser irradiates surface temperature reaches at boiling point. Evaporation takes place with further increase in laser power density or pulse on time, results in material removal from irradiate region. The liquid vapour interface to move inside the material with continuous laser irradiation after the vaporization is initiated. Depth of vaporization [18], mass of material removed per unit time and velocity of the liquid–vapour interface can be calculated by

$$\dot{m} = V_s \rho \qquad 2.4$$

Where $\dot{m}$ the mass of material removed per unit time, Vs is the velocity of the liquid–vapour interface and ρ is the density.

$$d = V_s t_p \qquad 2.5$$

Where, t_p is the pulse time and d is the depth of vaporization.

$$V_s = \frac{H}{\rho\left(cT_b + L_v\right)} \qquad 2.6$$

Where, H is the absorbed laser power, T_b is the boiling temperature at surface and Lv is the latent heat of vaporization. Evaporation induced recoil pressure exceeds the highest possible value of surface tension pressure during laser beam processing, i.e. drilling, cutting, marking, welding, cladding etc. during materials processing, recoil pressure plays an important role in melt expulsion from machining zone [18]. At high laser irradiance (I≥109 W/cm^2) the vapour or the ambient gas becomes ionized due to the interactions between the resulting vapour and the

incident laser beam, termed as plasma. Plasma is formed after around 10^{-12}s (picosecond). Plasma plume forms a shield over the machining area and reduces the energy available to the workpiece. Emission of the plasma is governed by shockwave and has been occurred in timescales from the picoseconds regime to beyond the millisecond [23].

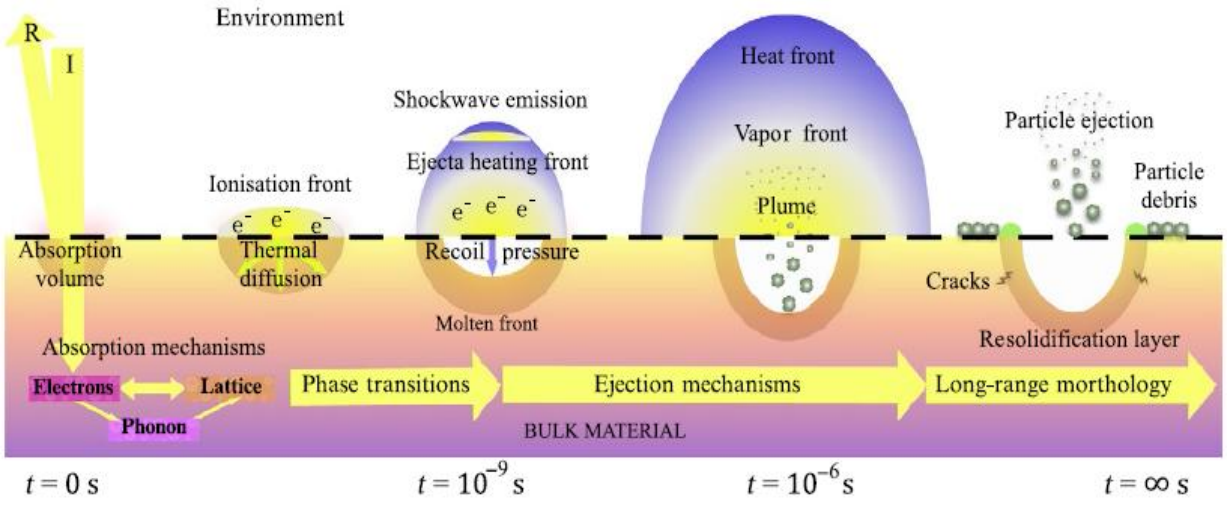

Fig. 2.1 Laser-matter interaction mechanisms and range of time scales [24].

2.1.3 Evaporation & ablation

Rapid vaporization starts when the incident laser energy on the target surface is sufficiently large to exceed the boiling temperature. The vapour particle size decreases with decreasing pressure and evaporation rate [25]. Plasma is generated at high laser irradiance ($I \geq 109$ W/cm^2) where the vapour or the ambient gas becomes ionized due to the interactions between the incident laser beam and the produced vapour. Less laser energy is available on machining zone due to shielding effect of plasma plume. In photo-thermal ablation process material is removed by thermal stresses and surface vaporization. Whereas in photo-chemical ablation material removal takes place by molecular fragmentation without significant thermal damage by the high energy photon causes the direct bond breaking of the molecular chains in the organic materials [26].

2.2 Laser beam micromachining with aid of assist gas

Application of assist gas flown along with the same delivery nozzle of laser beam not only helps to cool down the zone of irradiation but also assist to remove the formed melt pool or gaseous debris from the machining zone. Variation in properties of aided gas sometimes helps to add

some more energy in the machining zone by mean of exothermic reaction which aggravates the formation of melt pool. Change in pressure of assist gas, generally helps to quick removal of molten or gaseous debris from the machining zone which restrict the heat affected zone at the neighborhood of machining zone. Sometimes application of reactive gases as an assist medium makes adverse effects on the machining response, either by forming oxide layer over the melt pool or by presence of oxide/ nitride on the surface of irradiation. On the other hand sometimes presence of reactive gas as assist medium helps to increase the absorptivity of irradiate surface and by reducing the viscosity in melt pool, enhance the material removal. From previous research works it is also observed that high assist gas pressure sometimes change the refractive index on the interface of environment-liquid due to formation of density gradient fields which adversely affects the machining process by defocusing the laser beam irradiation spot. Generally compressed air, helium, argon, oxygen and nitrogen in its pure or industrial form used as assist gases [27].

2.3 Underwater laser beam micromachining

Undesired quality aspects, i.e., dross formation, heat affected zone, recast layer, difficulties in debris removal and desired surface morphology during laser micromachining sometimes removed or partially corrected by irradiate the workpiece material at submerged condition. Reduction in heat affected zone, risk of atmosphere contamination along with increase in absorptivity by work substrate and enhancement of debris removal by hydrodynamic force generates due to bubble dynamics make the underwater laser beam machining process more suitable than other laser beam micromachining or laser assisted micromachining techniques. Along with the absorption, heating, melting/vaporization and ablation, some other phenomenon also occurred during nanosecond pulsed laser beam micromachining at submerged condition. High drag force and low settling velocity in liquid helps quick removal of debris from machining zone. Generally, fluid in flowing condition is recommended to avoid scattering and absorption of laser light by debris. Liquids molecules may be excited, ionized, and dissociated by laser-induced plasma temperatures and plasma UV /IR radiation and thus become chemically active [28] Restriction of plasma expansion in confined condition enhances the action of laser irradiation. Dissolution of workpiece and debris takes place in supercritical water generated by high intensity laser beam. Collapse of the vapour bubbles generates mechanical impact of microjets results in easy removal of debris from machining zone [29]. Now a day's research on

different types of liquid assisted laser beam machining, i.e. laser ablation in submerged condition, underwater waterjet guided laser beam machining, underwater gas assisted laser beam machining, chemical assisted laser beam machining is carried out by researcher. Some researchers have find that laser beam cutting in chemical solution get better surface quality than processing in pure water [30]. Electrochemical dissolution / localized breakdown is enhanced by laser beam in neutral salt solution Optical absorptivity of workpiece substrate increased in water due to higher refractive index of water [31].

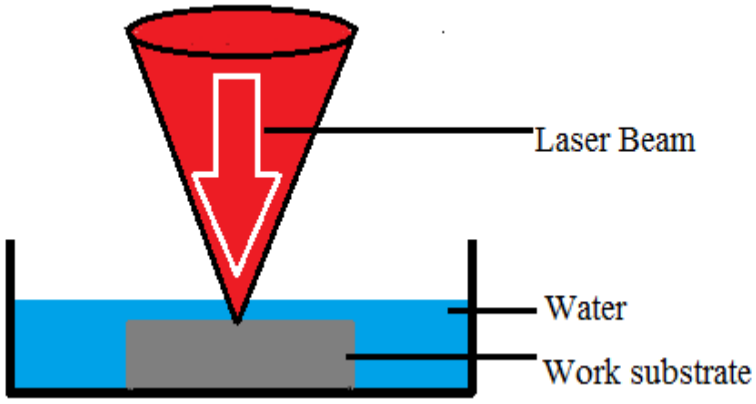

Fig. 5. Underwater laser ablation process [32].

2.4 Material removal mechanism of nanosecond pulsed laser beam cutting at submerged condition

Along with the absorption, heating, melting/vaporization and ablation, some other phenomenon also occurred during nanosecond pulsed laser beam cutting at submerged condition.

High drag force and low settling velocity in liquid helps quick removal of debris from machining zone. Formation of bubble and thermal gradient generated by laser induced heat causes convection in liquid. Fluid in flowing condition is recommended to avoid scattering and absorption of laser light by debris. Liquids molecules may be excited, ionized, and dissociated by laser-induced plasma temperatures and plasma UV /IR radiation and thus become chemically active. Restriction of plasma expansion in confined condition enhances the action of laser irradiation. Dissolution of workpiece and debris takes place in supercritical water generated by high intensity laser beam. Collapse of the vapour bubbles generates mechanical impact of microjets results in easy removal of debris from machining zone [33].

From the above study it may concluded that assist media has a great impact on laser based thermal machining in macro/micro domain. The assist medium not only helps to restrict the degradation of the undesired quality characteristics but also helps to enhance the efficiency of the said thermal process. Reason of the above said phenomenon has been enlightened through the elaborate discussion of laser matter interaction in different assisted medium. Lots of analytic as well as experimental research has been implemented to get desired machining outcome either by adding some different environment/ subsystem with the machining setup or by manipulate with the process variable of the existing laser systems which are documented in the next section of the thesis as literature review.

Chapter 3

3. Literature review and objectives of the present research work

3.1 Review of Past Research Works

After invention of LASER on may 16, 1960 by Dr. Teodore Maiman in the laboratories of the Hughes Aircraft company, in Malibu, California, researchers from various fields try to develop laser systems to apply it in manufacturing for fabrication.

Laser beam intensity distribution and laser matter interaction has been considered for establish a theoretical model to predict machining depth during laser machining with 50 ns pulse tripled Nd:YAG laser. Estimation of kerf/slot along with shape of transverse section has been made with the developed model. This model also helps to calculate the threshold radius of laser beam propagation along the thickness of job sample. An experimental analysis also performed to investigate the influence of focal spot on depth of cut. During experiments it is observed that diameter from material is removed is lesser than the spot diameter. It has been concluded that depth of cut is maximum when the focal spot is adjusted 1~2 mm below the top surface [34].

To study the influence of the fluid flow and heat transfer in the transient development of a laser drilled hole in a turbine airfoil, a direct computer simulation technique is developed by Ganesh R.K. To develop the model, most factors are considered, i.e. the material removal mechanism is governed by vaporization and melts ejection. Coupled conduction heat transfer in the solid and advection-diffusion heat transfer in the liquid metal, fluid dynamics of melt expulsion and tracking of interface, such as vapour-liquid, liquid-solid are mathematically modeled for the 2D axisymmetric case. All thermo-physical properties including latent heat of vaporization, gravity, and surface tension driving forces are taken into account to solve the problem by volume of fluid approach based donor–acceptor cell method. The developed model is used to simulate drilling for a number of spatially and temporally varying laser intensity profiles. Comparison of the simulated results indicates that material removal per joule of absorbed energy is inversely proportional to the square root of the peak beam intensity whereas rate of drilling is proportional to the square root of the surface pressure. It has been also observed that recast is formed during pulse interval which has some great significance on hole geometry [35].

The effect of the laser parameters and the material properties on the hole quality has been examined by Yilbas B.S. Factorial design technique is employed to test the significance level of the factors that affect the hole quality. stainless steel, nickel and titanium, are considered as workpiece to carry out the laser drilling process. From the experimental study is found that first order interaction of pulse-thickness of workpiece and pulse length-Focus settings is the most dominant process variables whereas second order interaction of pulse length-focus-thickness is the significant factor. For titanium reduction in pulse length results in reduction in resolidification whereas change in pulse length reduces the mean hole diameter, inlet cone and taper for nickel. Increase in focus setting above the surface helps to enhance the hole quality for all the materials. It is also found from the study that taper increases with increase in thickness and overall quality decreases with increase in pulse energy [36].

An investigation on laser drilling of SiC fibres in a borosilicate glass matrix has been performed by Tuersley I.P. with a view to identifying the influence of the various laser pulse parameters on maximum rate of material removal and the material removal efficiency, and also improving the processed surface quality (minimizing the induced damage). A 400 watts pulsed Nd:YAG Laser has been employed to carry out the drilling. During experimentation it has been observed that the incident peak power and the pulse energy have a more influence upon penetration of the beam than the pulse duration. The geometry of the drilled holes is generally low quality but of remarkably consistent. Redeposited matrix material to be found adhered to the process surface along with traces of matrix recrystallization at a distance of approximately 150 mm from the processed surface has also been observed [37].

Machining characteristics in terms of hole diameter and depth of hole govern by different process variable has been studied by D.sciti and A. Ballosi during laser processing of silicon carbide. Pulsed CO_2 laser is used here to make a blind drill on silicon carbide surface. Range of the process variables are chosen as 0.5 and 1 kW of average laser power, pulse duration of 0.5 to 2 μs and focal length of 31.8 mm, 63.5 mm and 95.3 mm with different lenses. Compressed air of 10 Psi is also used in some experiments for proper removal of molten material and damage prevention of protecting glass from sputtering of debris. Closely spaced array of blind holes with diameter ranging from 100-200 μm and depth upto 400 μm with center to center distance of 200 μm are achieved with 1kW power laser system. SEM analysis indicates at heat affected zone and

formation of microcrack along the edge of holes. Machining with 0.5kW power and 1 µs indicates lower value of hole diameter with undesired characteristics [38].

An experimental investigation on laser beam microdrilling has been conducted by Tunna. L. et.al. Diode pumped solid state laser with normal (1064 nm), doubled (532 nm) and tripled (355 nm) frequency laser is used to perform the laser microdrilling on 0.25 mm thick 99% pure copper sheet. A detailed study of physical characteristics of drilled hole and recast layer as a function of change in wavelength and intensity has been carried out. Highest etch rate is observed with second harmonic wavelength. The directionality of shielding gas assist the melt flow at the top surface to produce unique flow structure when the copper is processed with NIR wavelength at all the selected intensities [39].

Effects of process variable on machining characteristics has been studied by Ng.G.K.L and Li. L during laser percussion drilling on 2 mm thick EN3 mild steel plate by 400 watts Nd:YAG fibre laser. Experimental data along with SEM image analysis demonstrate that melt ejection behavior, governed by pulse width and peak power have an great impact on repeatability which affects the hole geometry. Combination of higher peak power with lower pulse width, produce higher vapour recoil pressure which helps to melt ejection in shorter duration to produce great repeatability of drilled hole with smaller spatter thickness and vice versa. The circularity of the entrance hole (defined as the ratio between the minimum and maximum diameters of the hole) ranges from 0.94 to 0.87, has a correlation with repeatability. A relationship has been established between the percentage standard deviation (PSD) of entrance hole diameter, hole circularity and the operating parameters. 3.5–7 kW peak power, and 1–3 ms pulse width help to generate PSD of entrance hole diameter ranges between 1.47% and 4.78% [40].

To control hole taper, a statistical model is developed by Li.L. et.al. A six factorial fractional CCD technique is used to carry out multi pulse laser drilling of 2.36 mm thick Nimonic 263 alloy with aid of oxygen assisted Nd:YAG laser. Experimental data indicates that laser power, hole wall erosion and non uniform melt ejection during beam propagation in the direction of thickness, is the governing factor of hole taper formation. Peak power, pulse width, position of focal plane and number of pulse are the most sensitive factors as per statistical model. a new approach of laser drilling has been demonstrate with variable pulses (inter-pulse shaping) rather than identical pulses which eases elimination of taper formation as well as form negative taper sometimes [41].

Principal and phenomenon behind laser beam cutting of thick job sample is much more different than cutting of thin sample. Laser beam cutting of thick ceramic substrate by controlled fracture technique is investigated by Tsai, C.H. and Chen. H.W. Application of Nd:YAG and CO_2 laser synchronously make a scribe groove on the top surface followed by formation of fracture by thermal stress along the edge of groove, results in controllably separation of substrate along the path of laser movement. 60 watts Nd:YAG and CO_2 laser is used to cut 10 mm thick alumina ceramic substrate. Analysis of experimental results along of SEM image for Microstucrtural study indicates that fracture growth in transverse direction due to tensile stress at groove crack edge is stable whereas unstable along the direction of thickness and the fracture region isn't uniform throughout the thickness for higher cutting speed [42].

An analytical model is developed by Ho.C.Y. and Lu. J.K. to study the laser drilling of silicon nitride and alumina. a TEM_{00} 10 ns pulse Nd:YAG laser is used to perform the laser drilling process Material is removed only by evaporation and thermal properties and material density does not change with temperature rise after irradiation are the assumptions are taken to develop the one dimensional thermal model. The model is solved with the aid of Laplace transformation method and results indicates that plasma absorption have an great impact on drilled hole depth per pulse. Increase in plasma absorption at higher power density have an adverse effect on hole depth per pulse for both the silicon nitride and alumina. Optical properties of workpiece also have some effects on erosion depth per pulse [43].

Laser cutting on mullite alumina has been carried out by Quintero F. to investigate the characteristics of heat affected zone (HAZ) as a function of average laser power, pulse frequency, cutting speed, and assist gas pressure. Analytical image processing of dimensional magnitudes which is easily identified from optical images is used for quantitative analysis of the HAZ characteristics. A 500watts pulsed Nd:YAG laser with 500 µm spot diameter has been used to carry out the process. Argon is used here as assist gas. From the investigation it is evident that laser in pulse mode have an great influence on the extension and intensity of the HAZ whereas effect of cutting speed at higher value and assist gas pressure are negligible [44].

Diode pumped solid state (DPSS) Nd:YAG laser with different wavelengths 1064 nm, 532 nm and 355 nm is employed to find limitations during percussion micro drilling on aluminum. Geometric analysis of machining response has been carried out by interferometric and optical methods to investigate the effect of laser fluence and wavelengths on response, in terms of

precision. During investigation it has been observed that etch depth per pulse and machining depth is greatly influenced by wavelength and laser fluence due effect on melt pool and plasma formation. From the interferometric analysis it has been observed that micro holes are tapered in nature due to intensity profile of laser and it has been also observed that with increase in wavelength, etch depth per pulse drastically reduced to 10 µm at 1064 nm wavelength from 50 µm at 355nm with aid of processing fluence of 4000J/cm^2 [45].

Laser processing of WC-Co hard metal has been theoretically studied and experimentally analyzed by G.Dumitru et. al.. A detailed study on thermal properties of WC-Co after laser process with nanosecond and high fluence femtosecond has performed. EDX analysis of the processed sample indicates at the presence of very thin (<3µm) modified zone at the neighborhood of the machined zone due to collateral influence of laser beam. From the analysis, it is also observed that reason behind the formation of modified is different for different pulsing time where secondary rediposition is the main reason for modified region during laser processing femtosecond pulse, recrystallization of WC grain is the reason behind formation of modified region during nanosecond pulsed laser processing [46].

CNC pulsed Nd:YAG laser micro-drilling of zirconium oxide (ZrO_2) have been carried out by Kuar A.S. et. al. to experimentally investigate the HAZ thickness and phenomenon of hole taper. Response Surface Methodology-based optimal parametric analysis has been performed to determine the optimal setting of process parameters such as pulse frequency and pulse width, lamp current, assist air pressure for achieving minimum HAZ thickness and taper of the micro-hole. From experimental results, it has been observed that 0.0675 mm HAZ thickness can be achieved when the lamp current, pulse frequency, assisted air pressure and pulse width are selected as 17 amp, 2.0 kHz, 2.0 kg/cm^2 and 2% of the duty cycle, respectively. It is also observed that taper formation increases with the increase in pulse width at lower value of lamp current but becomes insignificant during higher value [47].

A one dimensional analytical model has been employed by Ng G.K.L. et.al. which incorporates the effects of the enthalpy of oxidation due to use of oxygen as assist gas during laser beam drilling to study the effect of pulse width variation, pressure variation, formation of recoil pressure and hole depth. The modified model indicates that cooling effect of oxygen as an assist gas is negligible inspite of which it provides additional energy to the system, which increase the temperature of melt surface temperature. Prediction from analytical model and experimental

results are envisioned that increase in drilling velocity and melt ejection velocities when oxygen is used as an assist gas [48].

Nd:YAG laser with 1064 nm wavelength has been used to carry out drilling operation on two most widely used bio-ceramics bioglass-ceramic (BGC) and hydroxyapatite (HAP) by Huang J.X. and Huang Y.X. to evaluate the effect of laser parameter and machining parameters on machining quality. From evaluation it is found that HAP has a much greater absorption coefficient (12 cm^{-1}) at the laser wavelength of 1064 nm than that of BGC (0.2–0.3 cm^{-1}) which enhances the machining efficiency of HAP. HAP also smaller thermal conductivity which helps lo localized the adverse effect of thermal damage into a narrow zone adjacent to irradiate spot [49].

Ablation treatment of a sintered hydroxyapatite ($Ca_{10}(PO_4)_6(OH)_2$) sample has been studied by Nakata K. et. al. during irradiation by the Excimer laser in air at one atmospheric pressure for the micro machining treatment. Three different Excimer lasers of ArF, KrF and XeF with wavelengths of 193 nm, 248 nm and 351 nm, respectively have been used to examine the effect of wavelength on the ablation rate and the surface morphology of the ablated area. During experimentation it has been observed that Photochemical ablation is governed the material removal during ablation by ArF and KrF Excimer laser whereas Photothermal ablation occurred in the case of XeF laser due to a long wavelength. Experimental results indicates that the ablation rate is much more incase of XeF than other two Excimer laser, on the contrary ablated surface was rough and not flat [50].

Investigation of laser rapid manufacturing for Inconel 625 superalloy has been carried out by Paul C.P. et. al. A high-power continuous wave (CW) CO_2 laser system, integrated with a co-axial powder-feeding system and a three-axis workstation is used to perform the process. In depth study on the effect of process parameters on deposition rate is also performed by employing the L_9 array of Taguchi technique. Experimental results indicates that the powder feed rate is the most dominant process variable followed by scan speed and laser power. Results of non destructive testing, like (like—ultrasonic testing, dye-penetrate testing), tensile testing, impact testing, metallographic examinations and micro-hardness measurement revels that material deposition is defect free along with improved mechanical strength without sacrificing the ductility [51].

Laser micromachining of barium titanate ($BaTiO_3$)-polymer nanocomposite and sol-gel thin films has been conducted by Das R.N. et. al. with the help of frequency-tripled Nd:YAG laser operating at a wavelength of 355 nm to produce thin film capacitors over large surface areas, having high capacitance density and low loss. Surface topography of laser ablated polymer nanocomposite has been performed by optical imaging, SEM and AFM. From the image analysis it has been observed that the thickness of the capacitors decreases with an increasing number of laser pulses. The surface smoothness of the ablated areas that define the laser micro machined capacitors depends upon the uniformity of the spatial energy distribution of the laser beam. SEM images indicate at noticeable conversion from a smooth surface to wavy cavity structure of laser processed as-deposited $BaTiO_3$ film. Sharp micro machined $BaTiO_3$ edge at the glass surface has been observed from atomic force microscope (AFM) image which is very useful for micro fabricating membranes for MEMS applications [52].

Parametric study of laser machining of aluminum nitride has been done by Gilbert.T. et.al. through laser-machined lines and single-layer pockets on the surface of workpiece with an ultra-violet (UV) and near-infrared (NIR) laser. Three laser systems, i.e. frequency tripled Nd:YAG laser producing ultra-violet (UV) radiation at a wavelength of 355 nm, 70 watts Nd:YAG laser producing near infrared (NIR) radiation at a wavelength of 1064 nm and 250 watts CO_2 laser producing far-infrared radiation with a wavelength of 10,600 nm are used to carry out the experiments. Analysis based on experimental results along with SEM image and surface profile demonstrates that different laser system can produce different machining characteristics. NIR laser can remove more material than UV laser whereas in terms of micro features UV system is much preferable. Pulse overlap has a linear relationship with surface roughness and produce lower value of surface roughness with smaller pulse overlap [53].

Limitations of pulsed laser drilling process are investigated by Salonitis K. et.al. To investigate the limitations, a theoretical model is developed assuming that a finite volume of material is melted and removed during each laser pulse whereas no vaporization takes place. Experimental test data and predictions of analytical model indicate that formation of melt pool depends on pulse frequency whereas drill depth is a function of laser power density which affects, HAZ, formation of tensile residual stresses, generation of cracks, excess oxidation, etc [54].

Three different ceramic material, viz. silicon carbide (SiC), silicon nitride (Si_3N_4) and alumina (Al_2O_3) has processed with 1064 nm wavelength based pulsed YAG laser with a 0.72 mJ/pulse

with a 500 Hz incident frequency to investigate geometrical characteristics of box shaped hole by Kurita. T et.al.. Suitable machining conditions in terms of laser spot size, scanning path, scanning speed and scan times are investigated also. In depth comparison study also performed of nano and femtosecond laser processed surface with the help of SEM analysis, electron probe microanalysis (EPMA), micro-hardness testing, tensile and compression stress analysis. During observation, it has been found that machined surface as well as debris is varied with change in different laser system and also for workpiece. It also observed that change in micro hardness and tensile stress value on the neighboring zone of machined area with nano second pulsed laser which is vanished when machine with femtosecond pulsed laser [55].

Effect of multiple reflections on the amount of laser energy absorbed, the thermal effects for melting the material, vapor pressure effect for expelling out the molten material, material losses due to evaporation, the inverse effect of surface tension on the expelled depth and transient effect of laser beam de-focusing due to change in machined depth as a function of expelled material during machining for precise estimation of the melted depth during each pulse are incorporated in a hydrodynamic computational model to predict desired depth of cut and corresponding value of thermal energy during pulsed Nd:YAG laser based one dimensional machining of alumina with 1064 nm wavelength [56].

A hybrid method based on combined Taguchi methodology and response surface methodology (TMRSM) for the multi-response optimization has been applied by Dubey A.K. and Jadava V. to study the performance characteristics during laser beam cutting of thin sheet silicon alloy. In this approach, Taguchi quality loss function is used at first to find the optimum level of controllable variables such as assist gas pressure, pulse width, pulse frequency and cutting speed which later used as the central values in the response surface method to develop and optimize the second-order response model. Considerable improvement in both different nature quality characteristics, i.e. smaller-the-better type kerf width and higher the better type material removal rate (MRR) have been observed from experimental results [57].

Laser consolidation (LC) of IN-625 has been evaluated at both room temperature and elevated temperature (650 ◦C) to study the fatigue behavior by Theriault A. et. al. Fatigue behavior of LC Inconel 625 superalloy has been examined properly and the outcome indicates that the LC IN-625 has a fatigue resistance higher than the cast material but lower than the wrought material.

Tensile and fatigue test results along with the examination of microstructures and crack initiation sites are also presented [58].

Direct metal deposition technology has been successfully applied by Dinda G.P. to fabricate a series of samples of the Ni-based superalloy Inconel 625. High power CO_2 laser was used to create a molten pool on the Inconel 625 substrate into which an Inconel 625 powder stream was delivered to create a 3D object which is later examined by optical and scanning electron microscopy, X-ray diffraction and microhardness testing to investigate the microstructure and properties of the 3D object formed. Investigation result indicates that microstructure is columnar dendritic in nature which grew epitaxially from the substrate. Thermal stability test of the dendritic morphology has been carried out in in the temperature range 800–1200◦C which demonstrate that all the machined samples are free from relevant defects such as cracks, bonding error and porosity [59].

Physical phenomena governs the material removal process during machining the structural ceramics, i.e. alumina (Al_2O_3), silicon carbide (SiC), silicon nitride (Si_3N_4) and magnesia (MgO), by a JK 701 pulsed Nd:YAG laser (1064 nm wavelength) has been investigate by Samanta A.N. and Dahotre N.B.. Discrimination and incorporation of governing physical processes, i.e., dissociation, melting and vaporization into a hydrodynamic machining model has been conducted to predict time required to get desired depth of cut and subsequent thermal energy. Details of the governing physical processes and computational results associated with laser machining of each individual ceramic material are separately described [60].

Parametric study of laser drilling of thick ceramic plate has been studied by Kacar.E. et.al. Effects of process variables, i.e., pulse duration and peak power on hole characteristics has investigates during pulsed Nd:YAG laser drilling of 10 mm thick alumina ceramic plate. Experimental results establish a linear relationship between hole characteristics and peak power and pulse duration. Diameter of 1mm to 50 micron is drilled via percussion drilling though barreling around the hole neck is observed due to resolidification of molten debris at entrance of hole. Difficulties in material removal through the thick section is the reason behind negative taper formation with large exit hole diameter than entrance hole diameter [61].

Samanta A.N. et.al. has developed a theoretical model for laser through hole drilling to predict hole depth incorporating various physical phenomenon, i.e., decomposition, surface tension in expelling molten part of the decomposed species, evaporation-induced recoil pressure, loss in

energy due to dissociation and cooling of the surface due to evaporation. A 300 Watts pulsed Nd:YAG laser system is used to drill 2mm &3mm thick silicon carbide plate. During experiment, it has been observed that aforesaid laser system takes 0.5 sec to make a through hole in 2mm thick plate whereas takes 2.5 min to drill 3mm plate with pulse duration of 0.5 ms, and repetition rate of 50 Hz. Computational model based on developed theoretical model indicates that 21 pulses and 103 pulses can make through hole in 2mm and 3mm thick plates respectively. Ejection of melt pool from machining zone by evaporation induced recoil pressure of 3.73×10^5 Pa (max.) has been found during analysis [62].

A 355 nm X-Avia laser is used o carry out the drilling of single crystalline silicon carbide wafer of 350 μm at different medium, i.e. in ambient air, under water (stagnant and flowing stream), and under methanol. Influence of laser fluence and thickness of liquid films (500 mm, 1 mm, and1.5mm) on machining output also studied. Discussion of possible material removal mechanism during laser drilling at assisted medium also documented here. During investigation it is found that liquid work as cooling medium and rediposition on the side wall of drilled hole is reduced. Melt expulsion, formation of bubbles at superheated liquid adjacent to melt pool are the governing phenomenon for laser ablation of SiC in liquid environment. Results of microstructural analysis and images by EDX and SEM respectively, indicates that solvent assisted laser machining produces improved hole quality than machining at ambient air or under water condition in terms of reduction in drilled hole imperfection, i.e. minimum thermal damages and microcrack formation nearer to hole periphery. Volatility of solvent helps to faster removal of ejected particles from irradiate zone and produce a cleaner ablation effect with a deeper hole [63].

A comprehensive modeling and optimization of the laser micro-drilling of gamma-titanium aluminide has been carried out. by Biswas R. et.al.. Central composite design (CCD) technique based on response surface methodology (RSM) is employed to study the effect of process variable, i.e. Lamp current, pulse frequency, air pressure and thickness of the job on hole circularity at exit and the hole taper of the drilled hole. From experimental study it has been found that desired value of hole circularity can be achieved at lower values of lamp current, higher value of thickness and moderate values of air pressure and pulse frequency whereas optimum value of hole taper has been found out at lower value of lamp current, lower value of air pressure, higher value of pulse frequency and at higher thickness [64].

Pulsed laser microdrilling on Titanium nitride-alumina is a ceramic composite has been carried out by Biswas R. et. al. to investigate geometrical aspect of drilled microhole, i.e., hole taper, hole circularity at entry and exit. Effects of controllable process variable such that lamp current, pulse frequency, pulse width, assist air pressure and focal length on machining responses are studied in depth. ANOVA results based on developed polynomial model indicate at the adequacy of the process. The optimum value of hole circularity at entry has been found out at negative focal length, lower value of lamp current, moderate value of pulse frequency and air pressure, and at higher value of pulse width. The optimum value of hole circularity at exit has been found out at lower value of pulse width, at moderate value of pulse frequency, at higher value of lamp current and air pressure and at positive focal length. Moderate values of lamp current, air pressure, lower value of pulse width, higher value of pulse frequency, and positive focal length gives optimum value of hole taper [65].

Experimental study on straight cut and curved cut profile has been performed by Sharma A. et. al. during pulsed laser beam cutting of nickel based superalloy thin sheet. The kerf quality characteristics, such as kerf width, kerf taper and kerf deviation are measured through Tool Makers Microscope. From the experimental results it has been observed that oxygen pressure, pulse width, pulse frequency and cutting speed are the most influencing process variable. Taguchi quality design concept based L_{27} orthogonal array has been used for conducting the experiments for both straight and curved cut profiles. The results indicated that the optimum input parameter levels suggested for curved cut profiles are entirely different from straight cut profiles except kerf width [66].

The effects of cutting parameters on thermal characteristics for the net shaping during the laser cutting of Inconel 718 super-alloy sheet by using a high power CW Nd:YAG laser has been investigate by Ahn D.G. et. al. three-dimensional quasi-steady heat transfer analysis is carried out to examine the influence of the process parameters on the temperature distribution in Inconel 718 sheets. The empirical data helps to determine the relationship between process parameters and the kerf width. The critical power of the laser has been predicted from empirical formulation which is needed to restrain the delayed cutting phenomenon. The results of Experimental run and empirical formulation assists to obtain optimal cutting conditions to get minimum kerf width at critical cutting speed [67].

An analytical model has been established by Ahmed N. to simulate an extended laser beam during laser melting of Inconel 625 superalloy. Melt depth and melt pool profile and progression have been predicted by modeling, which are compared with experimental results from melting of Inconel 625. Result of analytical modeling is very helpful to determine the optimized value of overlapping required in laser surface treatment. It has been also observed that the model is more successful where the Marangoni effect is minimal, i.e. either there is no melt pool or the shape of the melt pool is look like a hat. Experimental results indicate that absorptivity value of 0.35 (35%) is suitable for Inconel 625 irradiated with a 940nm wavelength laser beam [68].

Fatigue crack growth and fracture toughness characteristics of laser rapid manufactured (LRM) compact tension specimens of Inconel 625 superalloy with thickness 12 and 25 mm are investigated by Ganesh P. et. al. fatigue crack propagation which is characterized by steady crack growth (Paris'regime) in the investigated stress intensity range (ΔK) of 14–38MPa$\sqrt{}$ m. Stage-II crack growth with nearly same slopes of log-log plot of da/dN versus ΔK has been observed in both of the specimens and slip on predominantly (1 1 1) planes is associated with transgranular fatigue crack propagation in LRM specimens. Fractograhy results indicate that increase in ΔK helps to narrowed down the difference between FCGRs in LRM and wrought specimens. J-integral test results exhibits stable crack growth without pop-in behavior [69].

Characteristics of crater geometry of a nanosecond pulsed high intensity laser processed aluminum 5052 has been experimentally studied by M.H. Mahdieh. Experiments are performed with aid of second harmonic of pulse Nd:YAG laser with single and variable pulse trains at two different environment, i.e. dry and underwater condition. The outcome of the study has established the enhancement of material removal, results in greater depth and wider crater when laser processing is performed in ambient water [70].

Experimental investigation into pulsed Nd:YAG laser microdrilling of alumina has been carried out by Kuar A.S. et. al. to get desired micro hole characteristics, such as minimum hole taper and HAZ width which may produce high quality microdrills. Taguchi based Grey analysis has been employed to simultaneous optimization of both the quality characteristics. Experimental results indicate at the validity of proposed multi-objective optimization. The optimization procedure is simplified by the conversion of multiple quality characteristics to a single performance characteristic called grey relational grade [71].

A two-dimension (2D) axisymmetric finite element (FE) model for simulation of temperature field and proceeding of hole formation during percussion drilling has been developed by Yan Y. et. al. to study the laser percussion drilling numerically followed by experimental study. The effects of laser peak power, pulse duty cycle and pulse repetition rate on hole diameter and spatter deposition has been investigated by the developed models and verified by experimental results. Experimental observation indicates, that the size and temperature of the melt front significantly affects formation of hole diameter and spatter deposition during laser percussion drilling whereas melt pool characteristic has mainly determined by the laser peak power, pulse repetition rate and pulse duty cycle. Combined study helps to find optimum parametric settings to get desired hole with minimum taper and spatter deposition. A microstructural analysis is also performed to study HAZ characteristics near the machining zone [72].

Coupled methodology of Finite Element Method (FEM) and Artificial Neural Network (ANN) has been used by S. Mishra & V.Jadava to develop a prediction model for Laser Beam Percussion Drilling (LBPD). Thermo-optical properties and phase change phenomenon has been considered for FEM based 2D axisymmetric thermal model during laser percussion drilling of aluminum. Grey relation analysis (GRA) coupled with principal component analysis (PCA) has been successfully utilized here for multi-objective optimization. The developed predicted model by feed forward ANN technique indicates that pulse width is the most dominated factor for hole taper and material removal rate whereas heat affected zone is mainly governed by pulse frequency. Outcomes of multi-objective optimization demonstrate increase in MRR with decrease in hole taper and HAZ width at optimal parametric settings [73].

To eliminate the disturbance in simple underwater laser ablation by bubble formation and non uniform water thickness due to vaporization, a new underwater machining procedure is proposed and developed by Duangaws N. et al. Overflow assisted underwater approach is applied for machining of titanium alloy. Main aim of the model is to marginalize the effect of uneven and non uniform water surface created by vaporization of water by laser beam having wavelength in infrared region and plasma formation during laser ablation. As the system pumps the water into the system regularly, the debris and bubbles are taken away from the machining zone which helps to generate uniform and even water thickness at machining region. From the experimental results it is observed that no oxide layer is formed during laser ablation in overflow assisted underwater condition. a clean cut with minimal rediposition is achieved with the aid of the

proposed non-complicated method, thus justified the feasibility of the overflow assisted underwater laser ablation in industry [74].

A new kind of rediposition dominant underwater laser micro machining technique is discovered by Alhamari A.M. et.al. Effect of rediposition on the machined microchannels has been studied in details during laser micromachining of Inconel 718 superalloys in static submerged condition. Experimental results indicate that two sub-channels are formed instead of one microchannel due to pile up of rediposited debris in the middle of the microchannel which enhances the productivity. From the study it is also found that scanning speed is the most dominant process variable followed by pulse repetition rate around 34 kHz to obtain desired maximum depth and width with minimum taper of channel's side wall [75].

An analytical model is developed to investigate the energy loss mechanism in water jet assisted underwater laser cutting process. The model is developed by considering various laser–material–water interaction phenomena, different loss mechanisms and shear force provided by the water-jet which later applied to predict quality characteristics like cut front, cut front temperature, maximum cutting speed, loss of laser power as a function of water jet speed and laser power. Experimental results are compared with predicted values of kerf width, cut front temperature. It is also observed that loss of laser power by scattering is the most dominant loss mechanism (40%- 50%) which can be minimized by conduct the process at high laser power with low cutting speed. Dynamics of water vapour layer and plasma formation at laser-workpiece-water interaction zone by laser in continuous wave mode has been found to be an cyclic process which is occurred in a time span of 3 micro-second under the defined parametric settings. It is also observed during experimental procedure that laser cutting efficiency is comparatively more in pulsed mode than CW mode due to prevention of excessive vapour plasma formation by shorter pulse on time and minimize the scattering of laser beam by proper removing of vapour plasma from zone of interaction during longer pulse off time [76].

3.2 The objective and scope of the present research work

From the documented research literature it is evident that different kind of lasers are applied as a means to process various types of engineering materials, like ceramics, composite, superalloys with précised shape and size. Several research works are done to find out the reasons behind these undesired machining responses and try to partially or totally elimination of these undesired machining responses. But still some research works have to be done on machining responses like HAZ, taper formation and high aspect ratio cut/ hole, nano-finished surface inside the machining zone etc. Few past researchers use different assist medium which some time enhance the machining characteristics or degrade it. Fewer of them also used combination of two different kind assist medium to get further better result whenever a single environmental change around the machining zone give a better machining response. In some past literature it has been found that researcher try to model laser beam machining in different assisted medium with lots of assumptions. From this above mentioned fact, it may be concluded that further in depth study is required to find proper technological knowledge of laser beam machining of various hard to machine developed engineering materials with different assisted medium along with different kind of laser power source.

Keeping in view the aforesaid laser beam micromachining characteristics for material processing in micro domain, the objective of the present research work are as follows:

1) To study the mechanism of material removal in laser machining in submerged condition.
2) To understand the CNC supported nanosecond pulsed Nd:YAG laser system for carrying out the experiments at different assisted medium.
3) To design and fabricate the jigs and fixture for holding the job sample during machining at different machining conditions.
4) To set the design space from the observations of trial experiments, for carry out the final experiments based on different methodology along with different assist medium in terms of different compressed air or inert argon gas for microdrilling process and compressed air and underwater condition for microcutting process.
5) To carry out the laser microdrilling process on Aluminum 5052 alloy and Silicon Carbide 30% Boron Nitride nano-composite and material and laser microcutting operation on Hydroxyapetite in its pure form and Inconel 625 superalloy to investigate the most

influencing parameters including the assist medium for desired machining characteristics with the aid of some statistical method like sensitivity analysis.

6) To make comparative analysis of micromachining performance for laser with different assist medium.
7) To determine the optimal combinations of pulsed laser machining parameters along with assisted medium.

The stated research objectives are accomplished through several scientific investigations described in the subsequent chapters of the thesis.

Chapter 4

4. Machining Setup

A CNC pulsed Nd:YAG laser machining system manufactured by M/s Sahajanand Laser Technology, India, is used for the experimental study. The CNC Nd:YAG laser machining system consists of the various subsystems such as; Laser generation unit, Beam delivery unit, Power supply unit, cooling unit and CNC controlled workstation. Specification of Nd:YAG laser is documented in table 4.11 and image of the system is given in fig 4.1.

Table 4.1. Specification details of Nd:YAG laser machining setup.

Specification	Description
Laser Type	Nd:YAG Laser
Wave Length	1064 nm (Fixed)
Mode of operation	Pulsed (by RF-Q switch)
Type of Q switch	Acousto-optic Q switch
Mode of Laser beam	Fundamental mode TEM00 (Fixed)
Mirror Reflectivity	Rear mirror 100%, Front mirror 80%
Beam Diameter(1/e2)	1 mm (by default)
Laser beam Spot diameter	100 µm
Average Power	75 Watts
Pulse Width	120 ns to 150 ns

4.1 Laser generation unit

Laser generation unit consists of laser head, resonator, intra-cavity aperture and intra-cavity ape safety shutter. A brief description of laser generation unit given below with pictorial image of Nd:YAG laser machining set up along with assist air supply unit.

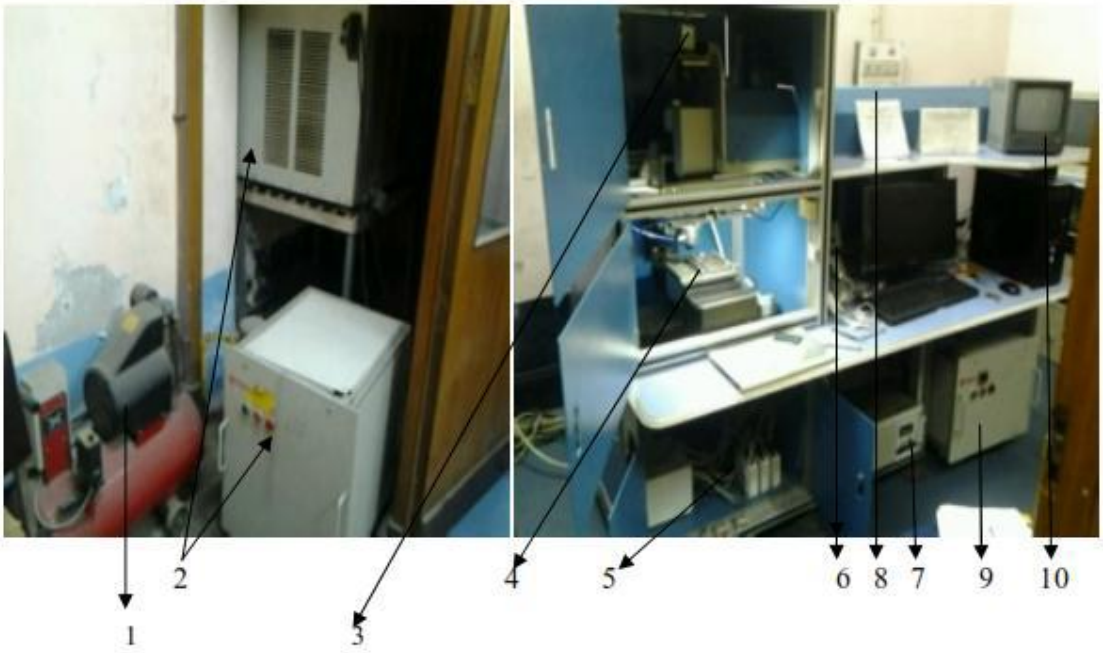

Fig.4.1 Pictorial image of Nd:YAG laser machining system with subsystems, (1. Air compressor, 2. Outer water cooler unit & Heat exchanger unit, 3. Z axis mounted CCD camera, 4. CNC controlled machining table, 5. CNC controller unit. 6. RF Q-switch driver unit, 7. Lamp current controller unit. 8. Laser head. 9. Inner chiller unit, 10. Monitor.)

4.1.1 Laser Head

In Nd:YAG Laser, Neodymium (Nd^{3+}) ion (lasing media) are embedded in an Yttrium Aluminum Garnet (YAG) crystal host. Concentration of neodymium in YAG crystal is only 1% in terms of weight. Here Krypton arc lamp is used as pump source which is kept in parallel position to Nd:YAG rod. Both the lasing source and pump source are kept inside an elliptical gold plated cavity. The whole Nd:YAG rod exhibit desirable optical, mechanical and thermal properties. Which makes it widely used lasing media for high power lasing operation. Use of Brewster's angle surface either in one or both end helps to eliminate the requirement for anti reflection coating as well as enhance the surface reflection. In general size of Nd:YAG rod is within quarter inch to half inch in diameter and five to six inch long. Photographic view of laser generation unit is given in fig. 4.2.

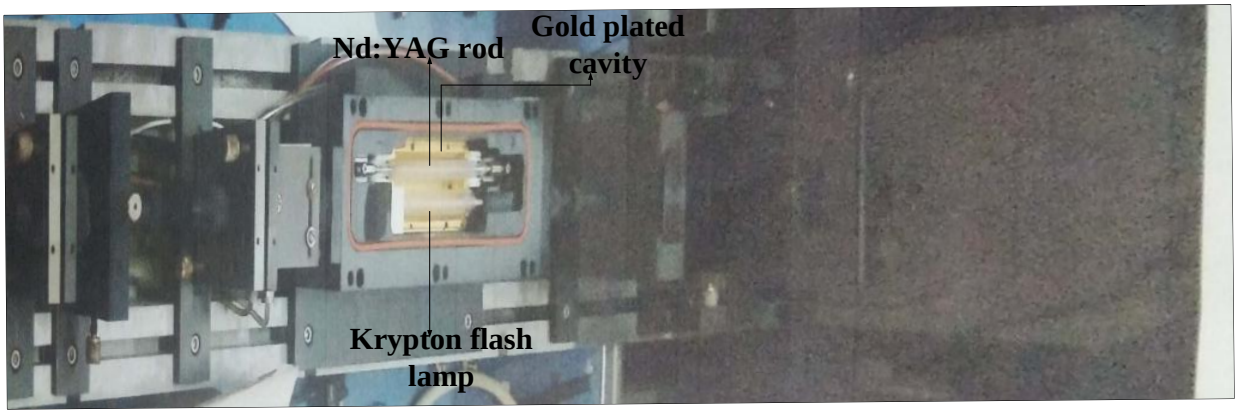

Fig. 4.2 Image of laser head

4.1.2 Resonators

Internal mirrors, also known as "resonator" or "cavity" mirrors, are used to generate, maintain and amplify the laser beam by forming a reflective "resonator" around the Nd:YAG crystal. The simplest optical resonator, the Fabry-Perot resonator, consists of one plane and other hemispherical mirrors located opposite to one another. The schematic view of resonator is given in fig.4.3. They are centered to a common optical axis and are aligned perpendicular to this axis. Back internal mirror, is designed to reflect (100%) the beam back into the laser resonator for continuous amplification whereas front internal mirror has reflectivity of 80%. The outside surface of the front mirror usually has an anti-reflective coating for improved transmission efficiency. The inside surface has a partially reflective coating to reflect a specified percentage of the beam back into the resonator.

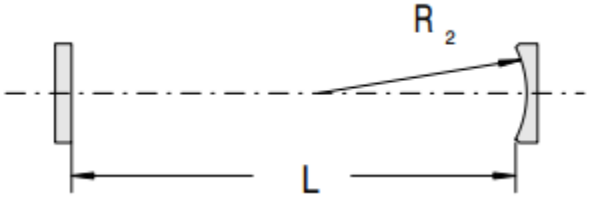

Fig 4.3 Hemispherical resonator

4.1.3 Intra cavity aperture

Aperture restricts the amplification to occur along the off axis of the resonator. This aperture is nothing but two pin holes on the optical axis of resonator and is in working condition when the laser is to be operated in Fundamental mode, i.e., a perfect circular spot of interaction on the work substrate, examined under a transmission electron microscope (TEM_{00}). As this aperture is used inside the cavity, it is known as intra cavity aperture.

4.1.4 Intra cavity safety shutter

An electrically controlled safety shutter is important part in the laser cavity. It is a mechanical device which helps out to terminate lasing operation without turning off the main power switch as per requirement. Photographic view of intra cavity shutter is given in fig 4.4. This beam attenuator is located inside the cavity and actuated by toggle switch. Blocking of lasing operation is performed by blocking the path of laser beam and preventing the emission of laser radiation out of head assembly enclosure. This shutter can be controlled either by auto mode or by manual mode.

Fig 4.4 Image of intra cavity safety shutter.

4.1.5 Lamp current controller Unit

This unit ignites and controls the intensity pumping device (krypton arc lamp) which governs the laser output. High voltage pulse is used to trigger with high impedance krypton arc lamp. Lamp current controller unit not only provide a system to regulate the current flowing through the lamp after discharge is developed in the lamp but also favour a special feature of standby mode to prevail the discharge in the lamp. Operational life of flash lamp is enhanced by aforesaid special feature. Power supply unit is also equipped with interlocking system which only steer the ignition of the lamp, if the cooling arrangement is in working state. Image of power supply unit is given fig 4.5.

Fig 4.5 Image of lamp current controller unit

4.2 Beam delivery unit

It consists of beam expander, bending mirror, focusing lens and protective lens. Beam expander helps to travel a certain distance with same intensity. After which the beam falls on the beam bender which kept at 45 degree. Beam bender, bend the beam at 90 degree to send this beam to workpiece via focusing lens. Power density and depth of focus of the laser beam on the spot of irradiation is mainly depends on focal length of the focusing lens. The type (Gaussian or other) and mode (TEM_{00} or other) of the beam also depends on the focusing lens. To get the proper machining efficiency, co-inside of beam center with the lens center is must necessary thing, as this thing is governed by the alignment of focusing lens. Length of focus is chosen as per machining requirement, as a lower focal length provides small depth of focus with high power density and vice versa. Protective lens is a specially coated glass lens which protects helps to avoid any damage of focusing lens from vapor plume or moisture during laser machining process. Pictorial view of beam delivery system is given in fig.4.6.

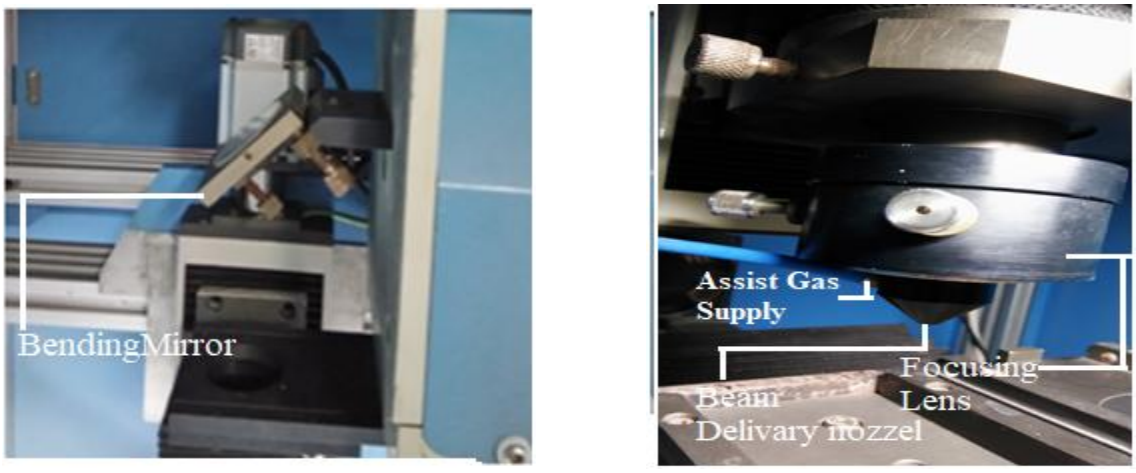

(i) (ii)

Fig.4.6. Image of beam delivery unit.

4.2.1 Sub system of beam delivery unit

A high definition CCD camera and a monitor are the parts of this subsystem. Proper focusing is necessary to achieve efficient processing as laser beam machining is a thermo-optical process. Image of job surface is displayed on the monitor which is captured by CCD camera and helps to kept the job sample at the proper focal length of the beam with the aid of CNC controlled XYZ work station. CCD camera is connected with the monitor by a BNC cable. Image of CCD camera is given in fig.4.7.

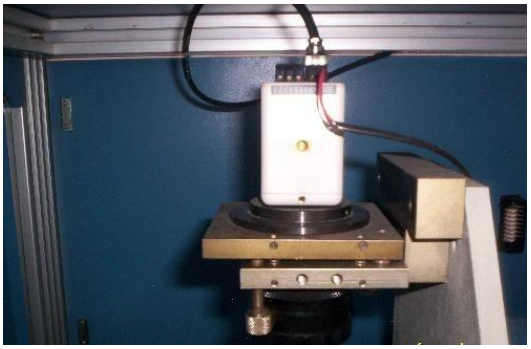

Fig 4.7. Image of CCD camera

4.2.2 Q-Switch and R.F. Driver unit

Q-switch is one of the most important components of beam delivery system which transforms the continuous wave beam into pulsed beam with very high peak power. 27.2 MHz radio frequency (RF source) helps for resonators modulation on the pulse repetition frequency (ranging from 0.1 kHz to 19.9 kHz) during acousto-optic Q-switch operated Nd:YAG laser operation. RF driver is used to generate the radio frequency. A temperature interlock system is incorporated in the driver unit for avoid any electronic malfunction. In-situ cooling system also attached with it to cool the driver properly for repetitive operations. Piezo-electric acoustic transducer bounded transparent material generally quartz is the main component of the acousto-optic Q-switch. Change or modulation of the reflective index of the quartz has been periodically governed by the crystal and velocity of acoustic wave of crystal which generate during application of RF signal to transducer. Stimulated emission is not in operational condition when the RF signal to Q-switch is on and populates with the number of atoms in excited state. Restoration of optical feedback by removal of RF signal initiate immediate decay of excited atoms to normal state which generates an avalanche of photons and that's come out as high peak power laser beam. Cooling system is incorporated in the Q-switch unit to avoid any thermal damage during operate at high frequency. Pictorial view of RF-Q-Switch driver unit is given in fig4.8.

Fig 4.8. Image of RF-Q Switch driver unit

4.3 Cooling unit

Integration of cooling system in laser generation unit is one of the most necessary thing to avoid any damage to the generation system as well as proper functioning, i.e., any damage to Nd:YAG rod, krypton lamp, Gold plated cavity and Q-switch. This unit consists of two substances such as 3-phase chiller system and Heat exchanger and pump systems. Schematic diagram of cooling unit has given in figure 4.9. 3-phase chiller system is used for providing the chilled water to the heat exchanger. Heat exchanger and pump systems, which are mainly used for circulating the de-ionized water through resin filter via water to water heat exchanger to the laser head & Q-switch. The specification details of chiller units are shown in table 4.2. The de-ionized water with high optical transparency and low electrical conductivity is used in this cooling system to avoid ant chemical reaction in the subsystems of laser generation unit as well as for proper functioning. The heat from de-ionized water subsequently removed by water-to water heat exchanger connected to an outside water source. A solenoid controls the outside flow condition (on/off) to regulate the de-ionized water temperature as per requirement.

Table 4.2 Specification of the Chiller Unit.

Properties	**Description**
Electrical requirement	415V AC supply
De-ionized water tank capacity	5 Litre
De-ionized water resistance	≥200 KΩ/cm
De-ionized water flow rate	20 litre/min
De-ionized water operating temperature	24^0C ±1^0C

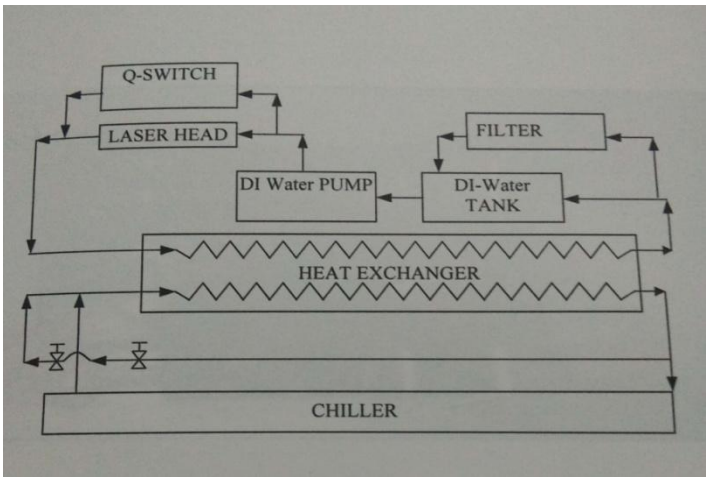

Fig 4.9. Schematic illustration of cooling unit

4.4 CNC controlled Workstation

As the laser beam machining system is working on the opto-thermal properties of material, proper focusing of the work substrate is necessary to get desired machining characteristics. To get the above mentioned condition a precise work station is needed. In this system a CNC controlled X-Y-Z axes based workstation is included. Steeper motors are attached to each axes based on lead screw for precise movement and connected to a CNC controller unit which controls the movement by the mean of different softwares for various laser operations. In this system Z axis is attached to the focus lens of the laser system which helps to perform the machining at variable focus distance. Specification of CNC controlled work station is given in table 4.3 whereas pictorial image is given in 4.10.

Table 4.3 Specification of CNC table unit

Properties	**Description**
Axis of travel (X-Y axis)	150mm x 150mm
Focusing vertical travel	50mm
Position accuracy	00.02 mm over travel 250mm
Repeatability	0.01 mm over travel of 250mm
Resolution	1 μm
Table working area	150mm x 150mm
Clamping	Using newly developed fixture
Feed rate (X, Y, & Z axis)	25 mm/sec
Control system	CNC open loop system

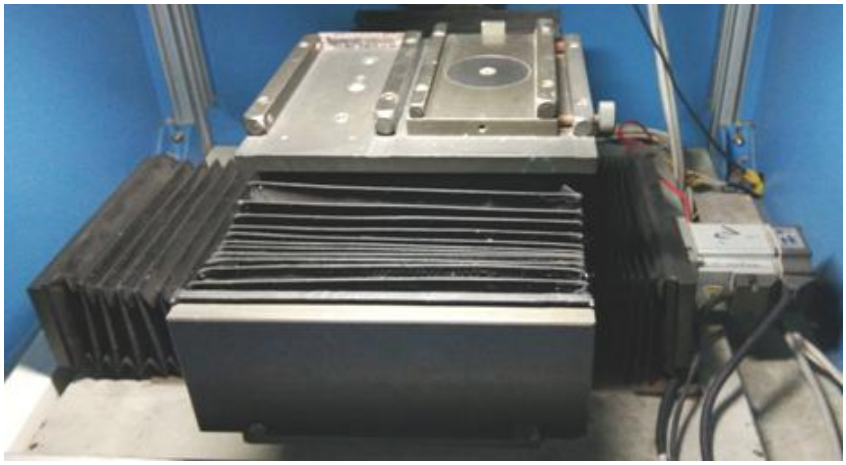

Fig 4.10. CNC controlled work station.

4.5 Fixtures for Laser micromachining

4.5.1 Need for fixtures

Any kind of subtractive machining always require proper fixture to hold the work substrate of various shape any size. In laser based micromachining operations, i.e, drilling, cutting, marking, milling, surface modification, proper alignment of work substrate with uniform holding pressure leads to minimize of heat affected zone variance and leads to get desired machining output with dimensional accuracy.

4.5.2 Workpiece holding device

A duralumin made light weight job holding device is used to hold and clamp the work substrate during machining. Part list of the various component of the tool holding device is given in table 4.3. A photographic image of job holding device is given in fig 4.11. whole job holding device is chemically black coated to avoid reflection of light.

Table 4.4: List of components of job holding device

Component name	Number of component	Manufacturing material
Base plate with T slot	1	Duralumin
Mounting Bar	2	Duralumin
Elliptical slotted clamps	4	Spring steel
Spring dwell pins (M4×8)	4	Spring steel
Washer (M6×1.5)	4	Mild steel
Hexagonal nut (M6)	4	Mild steel
Stud (M6)	4	Mild steel
Counter sink head screw with hexagonal socket (M4×25)	6	Mild steel
T-Bolt (M8×35)	2	Mild steel
T-Nut	4	Mild steel

Fig 4.11. Job holding device

4.6 Assist Gas supply Unit

An assist gas supply unit has attached with LBM system which is mainly used to remove the machined particle from the machining zone as well as for cooling of machining zone. Assist gas supply unit consists of compressor or specific gas container, oil moisture separator, pressure valve. The assist gas supply line passes through the oil & moisture separator and Pressure regulator before reached the nozzle of beam delivery system, from where it comes out of the nozzle co-axially with the laser beam and impinged on the irradiate spot. Oil & moisture separator is used for purification of compressed air or gas. Pressure regulator is used to supply compressed air or gas at various pressures as per requirement to the machining zone. An inlet of assist gas is presented in between the protective lens and outlet of the specially designed conical nozzle of the beam delivery system which photographically represented in fig.4.6.(ii). In this set up assist gas comes out from the same delivery nozzle of laser beam. A schematic illustration of assist gas supply unit is given below in fig 4.12 and another schematic diagram of beam and assist gas supply nozzle is illustrated in figure 4.13.

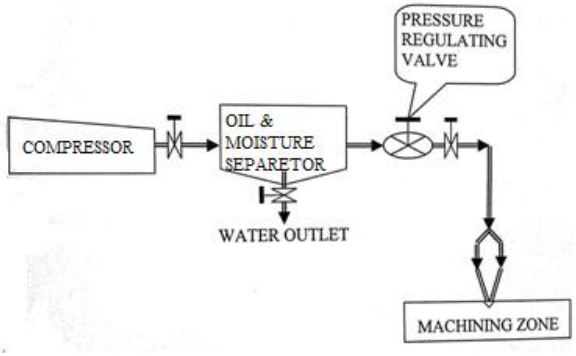

Fig.4.12 Schematic diagram of assist gas supply unit.

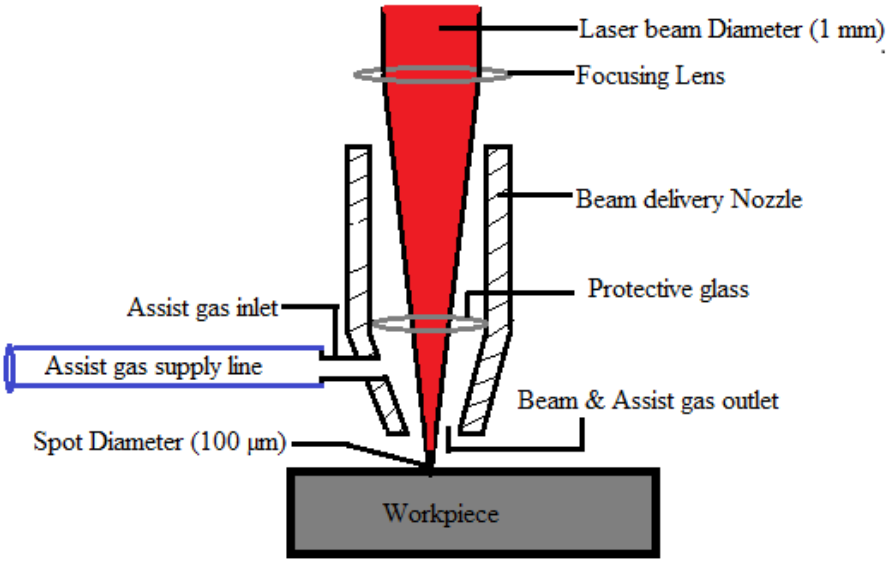

Fig. 4.13 Schematic diagram of beam delivery nozzle

4.7 Development of Underwater Workpiece holding unit

Workpiece holding unit for underwater laser beam operation has been designed and fabricated at workshop. Transparent PMMA sheets with different thickness are used for fabrication of workpiece holding device. First, all PMMA plates with different thickness are cut in proper size according to the design by power Shaw. Then these sheets are attached to each other with the aid of chloroform. During this said process, chloroform is injected in between two plates and uniform pressure is applied on these plates with the help of two table vice placed parallel two each other at a specified distance. The alignment of each sheet is measured preciously with sprit level (accuracy level 0.001mm). This specially designed underwater workpiece holding unit is placed over the CNC controlled workstation. An opaque piece of PMMA is used to make a T bolt (M2.5×5) which is used as jammer to hold the job sample in a specific place in specially designed underwater workpiece holding unit. Schematic view of developed workpiece holding unit is given in fig 4.14.

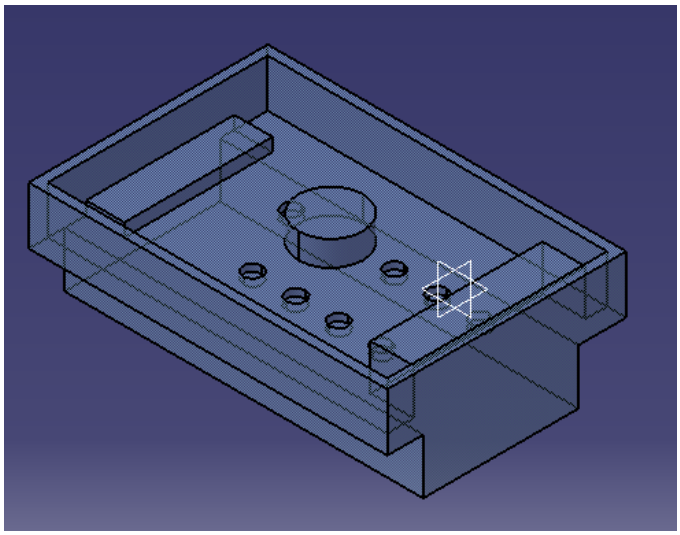

Fig 4.14. Schematic view of underwater workpiece holding unit

The pulsed Nd:YAG laser system is calibrated before performing the experiments. The sub-systems specially the tool holding devices or the work-table are calibrated through the spirit level with accuracy range of 1 micron. The beam delivery system and the laser power on the spot of irradiation is checked with the IR plate and laser power meter manufactured by Ophir. To avoid any vibration of the CNC- based work platform monthly maintenance of the lead screw is performed which enhance the repeatability of the process during each experiment. Though the average laser power of the machine is described as 75 watts but during experiments it is observed that the highest achievable average laser power is 45watts when the lamp current is at it's highest value of 30 amp. In this research work lamp current is considered as an input process variable inspite of laser power, as it is a function of lamp current and generally maintains a linear relationship.

4.7 Methodology used for Experimental planning and analysis

4.7.1 Taguchi Methodology

Taguchi's approach provides the designer with a systematic and efficient approach for conducting experimentation to determine near optimum settings of design parameters for performance and cost. The method emphasizes passing quality back to the design stage, seeking to design a product/process, which is insensitive to quality problems. The Taguchi method utilizes orthogonal arrays to study a large number of variables with a small number of experiments. Using orthogonal arrays significantly reduces the number of experimental configuration to be studied. The conclusion drawn from small-scale experiments are valid over

the entire experimental resign spanned by the control factors and their settings. This method can reduce research and developmental cost by simultaneously studying a large number of parameters. In order to analyze the results, the Taguchi method uses a statistical measure of performance called signal-to-noise (S/N) ratio. The S/N ratio takes both the mean and the variability into account. The S/N equation depends on the criterion for the quality characteristics to be optimized. After performing the statistical analysis of S/N ratio, an analysis of variance (ANOVA) needs to be employed for estimating error variance and for determining the relative importance of various factors. Using the Taguchi method for parameter design, the predicted optimum setting need not corresponds to one of the rows of the matrix experiments. Therefore, an experimental confirmation is run using the predicted optimum levels for the control parameters being studied. The purpose is to verify that the optimum conditions suggested by matrix structured experiments do indeed lead to the projected improvement. If observed and projected improvements match, the suggested optimum conditions will be adopted. The corrective actions include finding better quality characteristics, or S/N ratios, or different control factors and levels, or studying a few specific interactions among the control factors may be adopted. An efficient way to study the effect of several control factors simultaneously is to plan matrix experiments using orthogonal arrays. Orthogonal arrays offer many benefits. First, the conclusion arrive from such experiments are valid over the entire experimental region by the control factor and their settings. Second, there is a large saving in the experimental effort. Third, the data analysis is very easy. Finally, it can detect noises from the additive model. An orthogonal array for a particular robust design project can be constructed from the knowledge of the number of control factors, their levels, and the desire to study the specific interactions [77]. The key features of this approach are as follows:

(a) Orthogonal Array :

In array rows are represent the number of experiments to be conducted.

Determination of S/N Ratio Curve:

S/N ratio is a mathematically transformed form for quality/performance characteristics, the maximization of which minimizes quality loss and also improves (Statistically) the additivity of control factor effect. From the each experimental result S/N value can be calculated as

$$\eta = -10\log\left[\frac{1}{n}\sum_{i=1}^{n} y_i^2\right] \tag{4.1}$$

For the smaller is better type problem and

$$\eta = -10\log\left[\frac{1}{n}\sum_{i=1}^{n} \frac{1}{y_i^2}\right] \tag{4.2}$$

For larger is better type problem.

Where η denotes the S/N ratio calculated from the observed or experimental value y_i represents the experimental observed value of the i^{th} experiment, and n is the number of times each experiment is repeated. The over mean value of η can be calculated as:

$$m = \frac{1}{n}\sum_{i=1}^{n} \eta_i \tag{4.3}$$

The effect of the factor level is defined as the division it causes from the overall mean. The average S/N ratio at any level suppose A_3 for experiments 7,8 and 9 which is denoted by m_{A3} is given by

$$m_{A3} = \frac{1}{3}[\eta_7 + \eta_8 + \eta_9] \tag{4.4}$$

Thus, the effect of that parameter at level A3 is given by (m_{A3}-m).

By taking the numerical values of η, the average numerical value m_{Aj} for each level of the factors can be obtained. These averages are obtained graphically which is known as S/N ratio curve.

4.7.2 Taguchi based Grey Relation analysis

Optimization of multiple quality characteristics is much more complicated than that of a single quality characteristic [77]. Improving one particular quality characteristic would possibly lead to serious degradation of the other critical quality characteristics. To solve this problem, the grey relational analysis first established by Dr. Deng in 1982, can provide a solution to a system in which the model is uncertain or the information is incomplete. In grey relational method, experimental information is classified as white, black, or grey. Representing white as full of

information and black as lack of information, the grey represents the primitive data with poor, incomplete and uncertain information, and the incomplete relationship of the information among these data is called the grey relation. Grey relation analysis is used to measure an approximate correlation between sequences [78]. In grey relational analysis, the dimensions of factors considered are usually different, and their magnitude difference is large. Therefore, the original data is normalized to make the magnitude of the original data in the range of zero and one. Next, a grey relational coefficient is calculated to express the relationship between the ideal and actual normalized experimental results. Then, the grey relational grade is computed by averaging the grey relational coefficient corresponding to each quality characteristic. The level with the highest grey relational grade is considered as optimum process parameter level [79]. The steps of the grey relational analysis are given in below,

Step 1: Grey relational generating

Step 2: Calculating the grey relational coefficient

Step 3: Calculating the grey relational grade

Grey relational generating

In Grey Relation analysis, the orders of magnitude of the factors are different. Because of this the input data must be pre processed to transform the original sequence to a comparable sequence. For this purpose, the experimental results are normalized in the range of zero and one, the process is called grey relational generating. The normalized results, x_{ij}, for lower-the-better and higher-the-better quality characteristic can be expressed [80] as

$$x_{ij} = \frac{\max_j y_{ij} - y_{ij}}{\max_j y_{ij} - \min_j y_{ij}} \tag{4.5}$$

$$x_{ij} = \frac{y_{ij} - \min_j y_{ij}}{\max_j y_{ij} - \min_j y_{ij}} \tag{4.6}$$

Where, y_{ij} is the i^{th} quality characteristic in the j^{th} experiment. Larger normalized results correspond to the better quality and the best-normalized result should be equal to 1.

Determination of Grey relational coefficients

A grey relational coefficient is calculated to display the relationship between the optimal and actual normalized experimental results. The grey relational coefficient can be expressed [80] as

$$\xi_{ij} = \frac{\min_i \min_j \left| x_i^{\,0} - x_{ij} \right| + \zeta \max_i \max_j \left| x_i^{\,0} - x_{ij} \right|}{\left| x_i^{\,0} - x_{ij} \right| + \zeta \max_i \max_j \left| x_i^{\,0} - x_{ij} \right|} \tag{4.7}$$

Where, $x_i^{\,0}$ is the ideal normalized result (i.e. best normalized result=1) for the i^{th} quality characteristics and ζ is a distinguishing coefficient, which is defined in the range of $0 \leq \zeta \leq 1$. In this study, the value of ζ is taken as 0.5 (which is generally adopted in most previous studies) for calculating the grey relational coefficients.

Grey relational Grades determination

The grey relation grade can be calculated from equation no. 4.7 [80] by taking the average of the grey relational coefficients and applies the same or different weightage on various quality characteristics under investigation.

$$\gamma_j = \frac{1}{m} \sum_{i-1}^{m} w_i \xi_{ij} \tag{4.8}$$

Where, γ_j is the grey relational grade for the j^{th} experiment, w_i is the weighting factor for the i^{th} quality characteristic and m is the number of quality characteristics.

Optimal grey relation grade determination

After getting the optimal parameter settings for desired microhole characteristics, the next step is to verify the feasibility of the proposed Taguchi based grey method. The optimum grey relational grade, γ_{opt}, is calculated as:

$$\gamma_{opt} = \gamma_m + \sum_{i-1}^{q} \left(\bar{\gamma}_i - \gamma_m \right) \tag{4.9}$$

where, γ_m is the total mean of the grey relational grade, γ_i, is the mean of the grey relational grade of i^{th} parameter at the optimal level, and q is the number most influencing of microhole drilling parameters

4.7.3 Response surface methodology (RSM)

Response surface methodology (RSM) is a sequential procedure to build empirical model with combination of mathematical and statistical techniques. RSM has been developed by Box and Draper (1987) to model experimental responses which later used for into the modeling of numerical experiments. Design of experiments to find relationship between process variables with machining responses is the main aspect of RSM. An adequate functional relationship between a response of interest, y, and a number of associated control (or input) variables denoted by x1, x2, ... , xk is generated by response surface modeling. Generally two models, i.e. first degree model and second degree model is used in response surface methodology. Models are given below,

First degree model,

$$y = \beta_0 + \sum_{i=1}^{k} \beta_i x_i + \in \tag{4.10}$$

Second degree model,

$$y_u = \beta_0 + \sum_{j=1}^{k} \beta_j x_j + \sum_{j=1}^{k} \beta_{jj} x_j^2 + \sum_{i<j} \sum_{j=2}^{k} \beta_{ij} x_i x_j \tag{4.11}$$

Where, y_u= Corresponding response,

X_{iu}= coded value of the i^{th} process parameters for the u^{th} experiment,

K = Number of process parameters.

$\beta_0, \beta_i, \beta_j$ = Second order regression co-efficient.

Establishment of relationship between machining response with controllable process variables, determination of significance of controllable factors and determination of optimum parametric settings within the predefined design space are the purpose of considering of aforesaid model.

Second degree model is mostly used method of RSM. Central composite, Box- Behnken and 3^k factorial designs are the frequently used second degree design techniques.

4.7.3.1 Central Composite Design (CCD)

Central composite design (CCD) helps to construct second degree model efficiently [81]. It consists of factorial points, central points, and axial points. Additional axial and center points are

added in the first degree model to develop second order model. Characterization of the response surface has been determined by analysis of variance for fitting the data to the second-order.

4.7.3.2 Analysis of Variance (ANOVA)

A better feel for the relative effect of the different factors can be obtained by the decomposition of the variance, which is commonly known as analysis of variance (ANOVA). The purpose in conducting ANOVA is to determine the relative magnitude of the of each factor on the objective function η and to estimate the error variance. In Robust Design, ANOVA also used to choose from among many alternatives the most appropriate quality characteristics and S/N ratio for a specific problem. ANOVA used to investigate which machining parameters affected the observed values significantly. In the present investigation, ANOVA and the F-test applied to analyze the experimental data. The related meaning and equations are as follows:

$$S_m = \frac{(\sum \eta_i)^2}{q}, \qquad S_r = \sum \eta_1^2 - S_m \tag{4.12}$$

$$S_A = \frac{\sum \eta_{Ai}^2}{N} - S_m, \qquad S_E = S_T - \sum S_a \tag{4.13}$$

$$V_A = \frac{S_A}{f_A}, \qquad F_{AB} = \frac{V_A}{V_E} \tag{4.14}$$

Where,

S_m is the sum of square, based on the mean,

S_T is the sum of square, based on total variation,

S_A is the sum of square, based on parameter A,

S_E is the sum of square, based on error

q is no of experiment

η_i is the mean value of each experiment (i=1,….,q)

η_{Ai} is the sum of i^{th} level of parameter A (i=1,2 or i=1,2,3),

N is the repeating number of each parameter A level,

f_A is the freedom degree of parameter A

V_A is the variation of parameter A,

F_{AB} is the F-test value of parameter A,

$F_{0.05}$, n_1, n_2 is as quoted from the "Table for Statisticians". The contribution of the input parameter is defined as significant if the calculated values exceed F0.05, n1, n2.

4.7.4 Sensitivity Analysis

Sensitivity analysis is the investigation about the dominance of uncertainty or imprecision of input values of a model in a decision making process. The main aim of sensitivity analysis is to describe about the influence of any small change of input variables of a model on output. Assessment of model precision for system performance and information regarding relative significance of errors in various parameters can be provided by sensitivity analysis. Sensitivity analysis is very much meaningful for developers as well as user of a model due to addressing about significance and interactions among individual parameters [82].

The experiment based scientific investigation of nanosecond pulsed Nd:YAG laser for drilling and cutting purpose on various advanced engineering materials has been demonstrated in the next two chapters. In view of limited resources, mainly geometrical aspects of machining characteristics are considered during the scientific investigation.

Chapter 5

5. Experimental studies on laser beam microdrilling

From the beginning of civilization, the materials have been processed into useful components or tools, by modifying their physical properties like size, shape and texture. This has been done through different processes, namely cutting, welding, bending, machining, punching, marking, cladding, alloying etc. The advancement of technology during the last few decades causes to the development of many hard-to-machine materials, such as titanium, stainless steel, high-strength temperature- resistant alloys, ceramics, refractories, fiber reinforced composites, superalloys, nanomaterials etc. These materials are not suitable to be machined by the conventional machining processes because of their high hardness, strength, brittleness, toughness and low machinability properties. Sometimes, the machined components require high surface finish and dimensional accuracy which is very difficult to achieve by the conventional machining processes. Moreover, the rise in temperature and the residual stress generated in & around the machining zone by those machining processes are not at all desirable or acceptable. In these circumstances pulsed Nd:YAG laser beam may be used as a powerful tool for micromachining of those materials because the laser beam can be focused to micron-sized spot diameter with varying thermal load which can be controlled by changing the pulse length.

From the manufacturing point of view, the geometrical as well as metallurgical features of the laser drilled section are very important. Formations of taper, heat-affected zone (HAZ), recast layer are most undesired machining responses during laser microdrilling. Pulsed Nd:YAG laser beam microdrilling on aluminum 5052 alloy and silicon carbide 30% boron nitride (SiC30BN) have been conducted to study the effect of different controllable process variables on microdrilling characteristics and try to achieve optimum microdrilling condition for desired microdrilling condition with the aid of different optimization technique. In depth study on effect of environment like different assist gas has been also investigate here.

5.1 Parametric study on laser beam microdrilling of Aluminum 5052 alloy with compressed air as an assist medium

In aluminum alloys, aluminum (Al) is the predominant metal. The typical alloying elements are copper, magnesium, manganese, silicon and zinc. Aluminum alloys are widely used in engineering structures and components where light weight or corrosion resistance is required. Aluminum 5052 is known for exceptional performance in extreme environments. It is highly resistant to corrosion attack in seawater, industrial chemical environments or in any hostile environment. It also retains exceptional strength after welding. It also has very good cold formability. It has medium to high tensile strength and fatigue strength alloy. 5052 alloys are commonly used in aircraft, other aerospace structures, amphibious vehicles like boat building and shipbuilding, and other marine and salt-water sensitive shore applications. Aluminum is increasingly used in micro systems technology such as electrodes in biotechnology applications also [83].

5.1.1 Material Specification

Aluminum 5052 sheets of thickness 0.78 mm are used as the workpiece material. Chemical composition and the physical and mechanical properties of the Aluminum 5052 are given in Table 1 and Table 2, respectively.

Table 5.1 Chemical composition of Aluminum alloy 5052 [84]

Element	**Precentage**
Manganese(Mn)	0.0-0.10
Iron(Fe)	0.0-0.40
Copper(Cu)	0.0-0.10
Magnesium(Mg)	2.2-2.8
Silicon(Si)	0.0-0.25
Zinc(Zn)	0.0-0.10
Chromium(Cr)	0.15-0.25
Others(Total)	0.0-0.15
Aluminum(Al)	Balance

Table 5.2 Physical & mechanical Properties of Aluminum alloy 5052 [84]

Property	**Value**
Density	2.68 kg/m^3
Tensile strength	210 MPa
Elongation	14 %
Modulus of elasticity	70 GPa
Melting point	605 ^{0}C

5.1.2 Design of experiments

Through-holes have been drilled in all experiments, and each experiment was repeated three times. Lamp current, pulse frequency, pulse width and assist gas pressure have been chosen as independently controllable process variables. Hole taper and hole circularity are considered as process responses. Compressed air has been chosen as assist gas for this experiment. A total of 32 sets of experiments have been carried out according to the central composite rotatable second-order design based on response surface methodology (RSM). The levels of selected parameters are shown in Table 5.3.

Table 5.3 Level of the process parameters

Parameters	**Symbol**	**Levels**				
		-2	-1	0	1	2
Lamp current (Amp)	x_1	21	22	23	24	25
Pulse frequency (kHz)	x_2	0.2	0.6	1.0	1.2	1.8
Pulse width (%)	x_3	1	2	3	4	5
Air pressure (kg/cm^2)	x_4	0.5	1.0	1.5	2.0	2.5

Average values of these repeated experiments (3 times) are taken for further analysis. A general second-order polynomial response surface model has been developed to establish the mathematical relationship between the machining responses, and process parameters.

5.1.2.1 Measurement of job sample and machining responses

The thickness of the job sample is measured at different sections by a digital micrometer having a least count of 0.001 mm. After completion of the experiments, microscopic views of the microdrilled holes for both top and bottom surfaces has taken at 10X magnification with the help of an optical measuring microscope (Olympus STM6). Hole taper is measured for each experimental result by analyzing the microscopic view of perimeters of drilled holes at entry and exit using an image analysis software.

$$\text{Taper(rad)} = \frac{\text{Hole\_dia}_{\text{Top}} - \text{Hole\_dia}_{\text{Bot}}}{2 \times \text{Thickness}} \tag{5.1}$$

The hole circularity at top and bottom surface has been measured by using the ratio of minimum to maximum Feret's diameters of the drilled hole. All the machining responses are measured three times each for all the experimental runs and average of this is accounted for further analysis. Experimental observations are listed in table 5.4

5.1.3 Results and discussion

Table 5.4 Experimental results

Experiment No.	Lamp Current (Amp)	Pulse frequency (kHz)	Pulse Width (%)	Assist air Pressure (kg/cm^2)	Hole Taper (rad)	Hole circularity
1	22	0.6	2	1.0	0.03699	0.89700
2	24	0.6	2	1.0	0.02614	0.89270
3	22	1.4	2	1.0	0.03868	0.86400
4	24	1.4	2	1.0	0.02724	0.82673
5	22	0.6	4	1.0	0.03452	0.87500
6	24	0.6	4	1.0	0.01922	0.91400
7	22	1.4	4	1.0	0.03430	0.85450
8	24	1.4	4	1.0	0.01934	0.87250
9	22	0.6	2	2.0	0.02680	0.87550
10	24	0.6	2	2.0	0.01842	0.86750
11	22	1.4	2	2.0	0.02699	0.87700
12	24	1.4	2	2.0	0.01820	0.85090
13	22	0.6	4	2.0	0.03418	0.82789
14	24	0.6	4	2.0	0.01897	0.87600
15	22	1.4	4	2.0	0.03374	0.86291
16	24	1.4	4	2.0	0.01787	0.87520
17	21	1.0	3	1.5	0.03324	0.89300
18	25	1.0	3	1.5	0.01084	0.90850
19	23	0.2	3	1.5	0.02682	0.85600
20	23	1.8	3	1.5	0.02905	0.82150
21	23	1.0	1	1.5	0.02937	0.86950
22	23	1.0	5	1.5	0.02529	0.87240
23	23	1.0	3	0.5	0.03398	0.88000
24	23	1.0	3	2.5	0.02596	0.86150
25	23	1.0	3	1.5	0.03004	0.86500
26	23	1.0	3	1.5	0.03072	0.86200
27	23	1.0	3	1.5	0.03007	0.86770
28	23	1.0	3	1.5	0.03147	0.87050
29	23	1.0	3	1.5	0.03059	0.86100
30	23	1.0	3	1.5	0.02929	0.86350
31	23	1.0	3	1.5	0.03034	0.86200

Statistical software MINITAB 17 is used here to establish second order polynomial models which are further used for sensitivity analysis.

5.1.3.1 Second order polynomial modelling of responses

The effect of the process parameters on the responses have been correlated by using RSM-based empirical model, established as follows.

$$Y_{Circularity} = 6.034 - 0.4241\ X_1 + 0.4533\ X_2 - 0.2898\ X_3 - 0.1014\ X_4 + 0.008894\ X_1X_1 - 0.07340\ X_2X_2 + 0.001444\ X_3X_3 + 0.00558\ X_4X_4 - 0.02248\ X_1X_2 + 0.012067\ X_1X_3 + 0.00136\ X_1X_4 + 0.01798\ X_2X_3 + 0.07504\ X_2X_4 - 0.00806\ X_3X_4. \quad (5.2)$$

$$Y_{Taper} = -0.9841 + 0.09198\ X_1 + 0.0167\ X_2 + 0.02913\ X_3 - 0.0284\ X_4 - 0.002055\ X_1*X_1 - 0.00362\ X_2*X_2 - 0.000730\ X_3*X_3 - 0.000290\ X_4*X_4 - 0.000207\ X_1*X_2 - 0.001368\ X_1*X_3 + 0.000537\ X_1*X_4 - 0.000689\ X_2*X_3 - 0.00133\ X_2*X_4 + 0.004500\ X_3*X_4 \quad (5.3)$$

Where X_1, X_2 , X_3 and X_4 indicate coded values of the process parameters, e.g., lamp current, pulse frequency, pulse width and assist air pressure, respectively.

5.1.3.2 ANOVA analysis

The ANOVA analysis result of the quadratic model for hole taper is given in table 5.5. Adequacy of the model is measured by the values of R^2, adjusted R^2 and predicted R^2 which are in the reasonable agreement and close to 1. P-value for the model as well as for all the process parameters in single term is less than 0.05 indicates that the model along with the all the process parameters are statistically significant at 95% confidence level The lack-of-fit value of 0.178 implies that it is not significant which is desired.

Table 5.5 ANOVA analysis of Hole taper

Source	**DF**	**Adj SS**	**Adj MS**	**F-Value**	**P-Value**
Model	14	0.001279	0.000091	115.4	0.000
Linear	4	0.001031	0.000258	326.20	0.000
X_1	1	0.000883	0.000883	1117.39	0.000
X_2	1	0.000001	0.000001	1.64	0.041
X_3	1	0.000010	0.000010	12.64	0.003
X_4	1	0.000137	0.000137	173.12	0.000
Square	4	0.000133	0.000033	41.96	0.000
2-Way Interaction	6	0.000115	0.000019	24.15	0.000
Error	16	0.000013	0.000001		
Lack-of-Fit	10	0.000010	0.000001	2.17	0.178

Source	DF	Adj SS	Adj MS	F-Value	P-Value
Pure Error	6	0.000003	0.000000		
Total	30	0.001291			
S	R-sq	R-sq (adj)		R-sq (pred)	
0.0008891	99.02%	98.16%		95.29%	

The ANOVA analysis results of the quadratic model for hole circularity is given in table 5.6. Adequacy of the model is measured by the values of R^2, adjusted R^2 and predicted R^2 which are in the reasonable agreement and close to 1. P-value for the model as well as for all the process parameters in single term is less than 0.05 indicates that the model along with the all the process parameters are statistically significant at 95% confidence level The lack-of-fit value of 0.707 implies that it is not significant which is desired.

Table 5.6 ANOVA analysis of Hole circularity

Source	DF	Adj SS	Adj MS	F-Value	P-Value
Model	14	0.012490	0.000892	91.38	0.000
Linear	4	0.002685	0.000671	68.74	0.000
X_1	1	0.000220	0.000220	22.57	0.000
X_2	1	0.001852	0.0001852	189.73	0.000
X_3	1	0.000006	0.000006	0.66	0.047
X_4	1	0.000605	0.000605	62.00	0.000
Square	4	0.003989	0.000997	102.14	0.000
2-Way Interaction	6	0.005817	0.000969	99.30	0.000
Error	16	0.000156	0.000010		
Lack-of-Fit	10	0.000084	0.000008	0.70	0.707
Pure Error	6	0.000072	0.000012		
Total	30	0.012647			
S	R-sq	R-sq (adj)		R-sq (pred)	
0.0031247	98.76%	97.68%		95.40%	

5.1.3.3 Parametric analysis

Figure 5.1 represents the effect of lamp current and pulse frequency on hole taper when the other process variables are kept constant at their respective mid values. Here hole taper shows a linear relationship with both the process variables and decreases with increase in lamp current and slightly increases with increases in pulse frequency. From the surface plot it is observed that lowest hole taper can be achieved at highest value of lamp current with lowest value of pulse frequency. At that specific parameter settings laser power density at the irradiate spot is highest

which helps to removal the material uniformly throughout the drilled hole to make the hole less tapered.

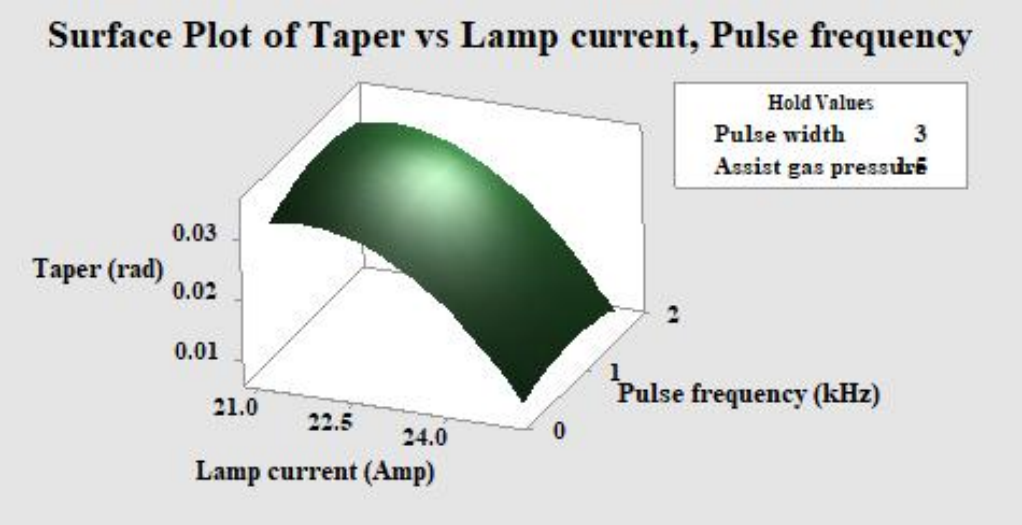

Fig. 5.1 Surface plot of hole taper vs lamp current vs pulse frequency

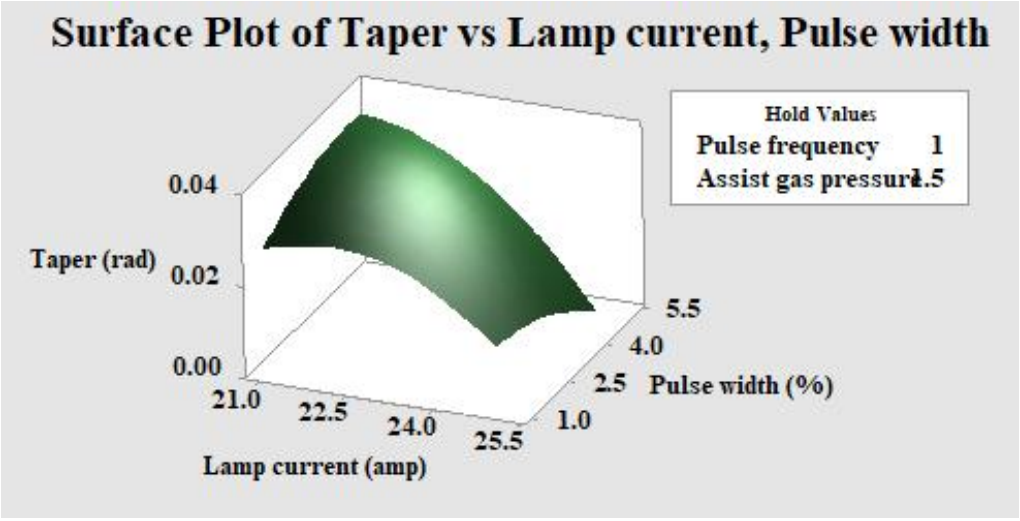

Fig. 5.2 surface plot of hole taper vs lamp current vs pulse width

From the surface plot given in fig. 5.2 it is observed that taper shows a decreasing tendency with increase in lamp current and pulse width. Increase in lamp current and pulse width means increase in thermal energy of the laser beam and peak power which helps to remove the material uniformly throughout the drilled hole to decrease the hole taper. Moderate or comparatively high value of pulse width helps to penetrate a more, due to higher peak power along with more thermal energy at higher lamp current. Thus this kind of plot emerges.

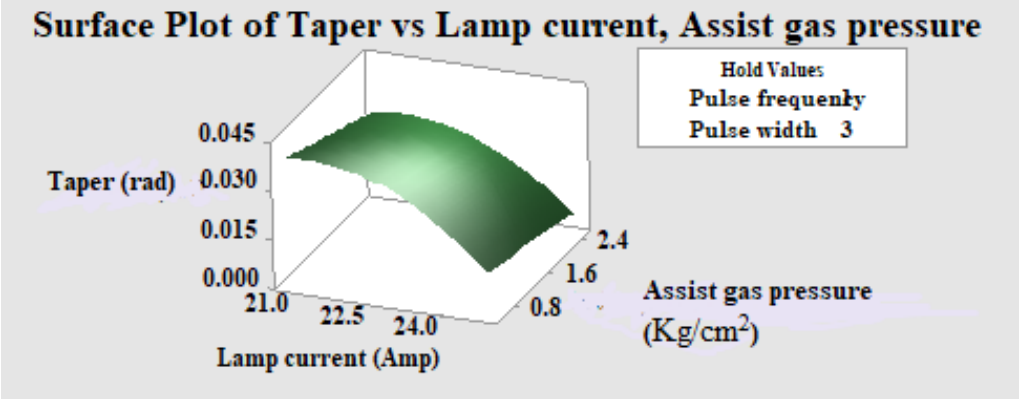

Fig. 5.3 surface plot of hole taper vs lamp current vs assist gas pressure

From fig. 5.3 it is found that hole taper decreases with increase in lamp current and assist gas pressure also. Increase in assist gas pressure helps to remove the molten debris and debris in vapour form, from the machining zone properly leads to decrease in hole taper by avoiding resolidification on the hole wall. Increase in thermal energy due to increase in lamp current, assist in uniform material removal throughout the machined hole leads to decrease in hole taper. Increased lamp current helps to pump more thermal energy into the system which leads to decrease in hole taper by reducing the discrimination of material removal from the top of the machining zone and drilled hole vertically.

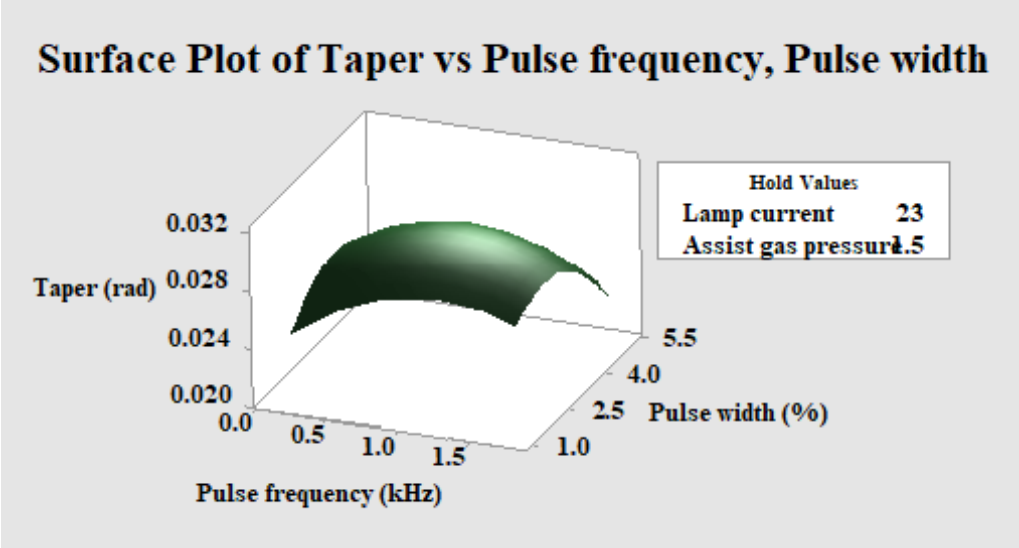

Fig. 5.4 surface plot of hole taper vs pulse frequency vs pulse width

It has been viewed from surface plot given in fig 5.4 that hole taper marginally increase upto certain value of pulse frequency and pulse width after which, it decreases when the other two process variable, i.e., lamp current and assist gas pressure kept constant at 23 amp & 1.5 kg/cm^2

respectively. From the plot it has been observed that lowest hole taper may be achieved at lowest value of pulse frequency in addition of lowest value of pulse width. Decrease in peak power with increase in pulse width leads to lesser penetration of laser beam at the time of interaction with workpiece may be the reason behind increase in hole taper. But further increase in pulse width, generates more energy per pulse which in combination with certain value of pulse frequency may helps to remove the material evenly throughout the machining zone vertically. Thus hole taper decreases.

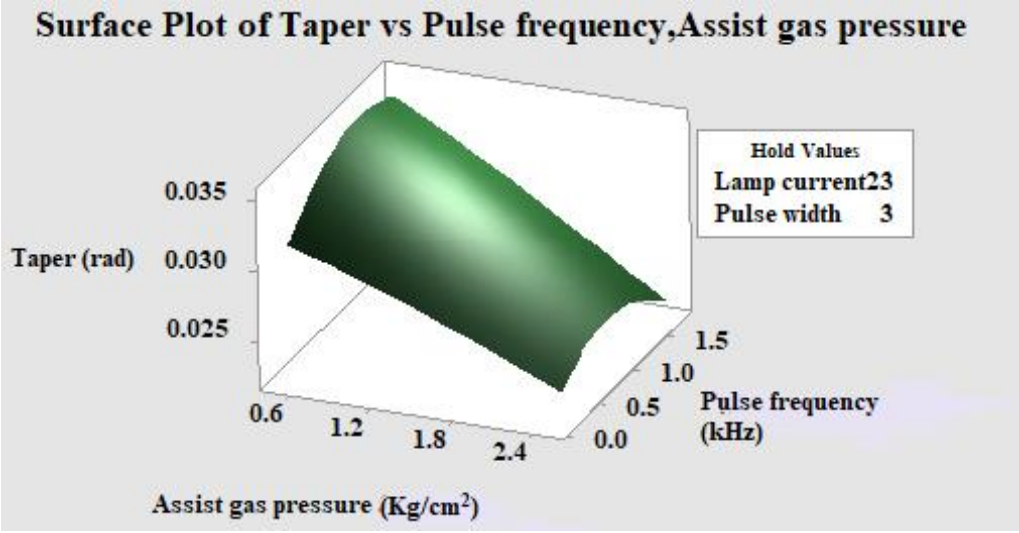

Fig. 5.5 surface plot of hole taper vs pulse frequency vs assist gas pressure

It is observed from fig. 5.5 that hole taper increases with increase in pulse frequency upto certain value but decreases with further increase in pulse frequency whereas hole taper decreases with increase in assist gas pressure linearly. Energy per pulse decreases with increase in pulse frequency may not insert adequate amount of thermal energy which leads to comparatively lesser amount of melt pool and debris at the zone of irradiation. That may not be removed properly with aid of respective assist air pressure and pressure created by plasma plume, results in resolidification around the wall of drilled hole. These may be the reasons behind observed phenomenon for hole taper. But further increase in pulse frequency may increase the cumulative pulse energy which helps to remove material throughout the drilled hole properly by respective assist gas pressure thus and taper decreases.

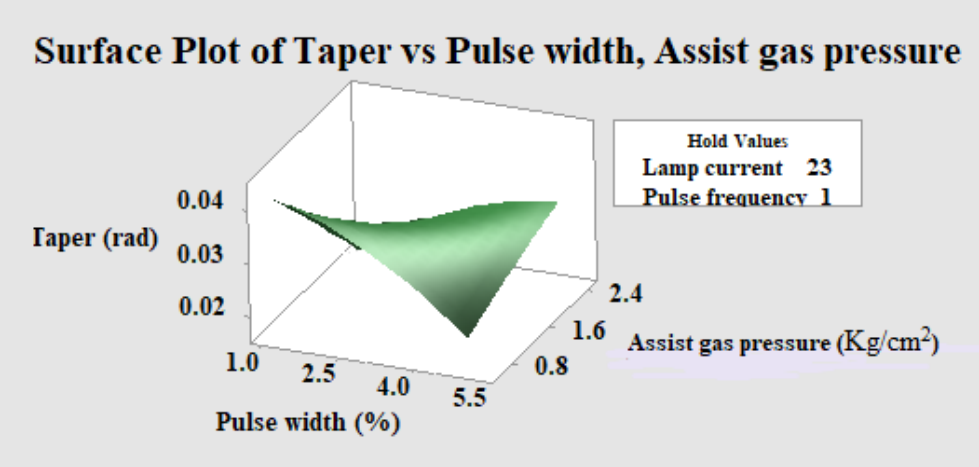

Fig. 5.6 surface plot of hole taper vs pulse width vs assist gas pressure

From the surface plot fig 5.6, it is viewed that hole taper is decreased with increase in assist air pressure but decreases with increase in pulse width when lamp current kept constant at 23 amp and pulse frequency at 1 kHz. Decrease in peak power with increase in pulse width, results in lesser depth of penetration when laser beam interact with workpiece. That may lead to non uniform material removal from drilled hole. Thus hole taper increases. Increase in assist gas pressure not only helps to remove debris from machining zone but also added some extra energy into the process by endothermic reaction on the melt pool which may leads to remove more material from the hole, results in decrease in hole taper.

Figure 5.7 represents the effect of lamp current and pulse frequency on machining response, i.e. circularity of the drilled hole at top surface when the other process variables are kept constant at their respective mid value.

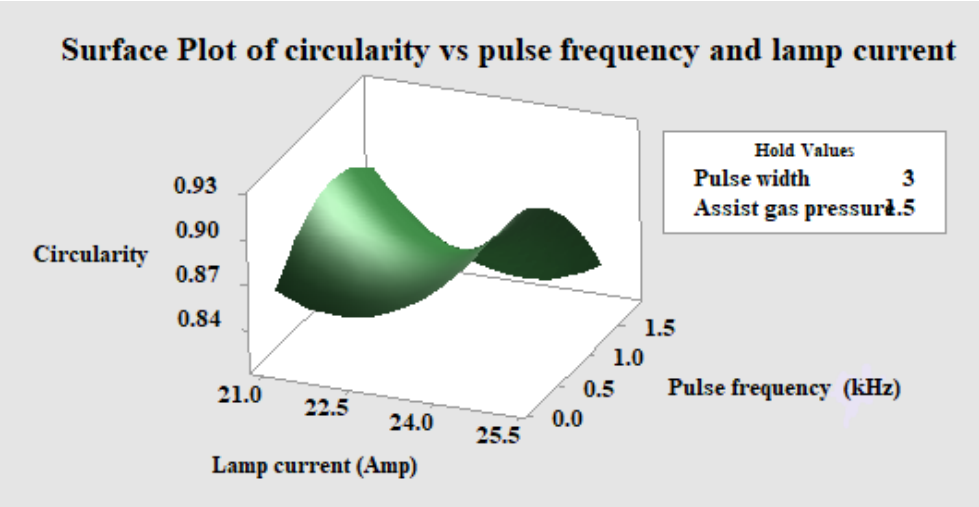

Fig. 5.7 Surface plot of hole circularity vs lamp current vs pulse frequency

Figure 5.7 represents the effect of lamp current and pulse frequency on machining response, i.e. circularity of the drilled hole at top surface when the other process variables are kept constant at their respective mid value. Hole circularity initially decreases with increase in pulse frequency but decrease after a certain value of pulse frequency whereas circularity decreases upto 22.5 amp lamp current then circularity increases with increase in lamp current. From the figure it is also observed that highest value of hole circularity may be achieved at highest value of lamp current with moderate value of pulse frequency which may helps to remove material uniformly from the top surface of the workpiece to get desired geometrical shape.

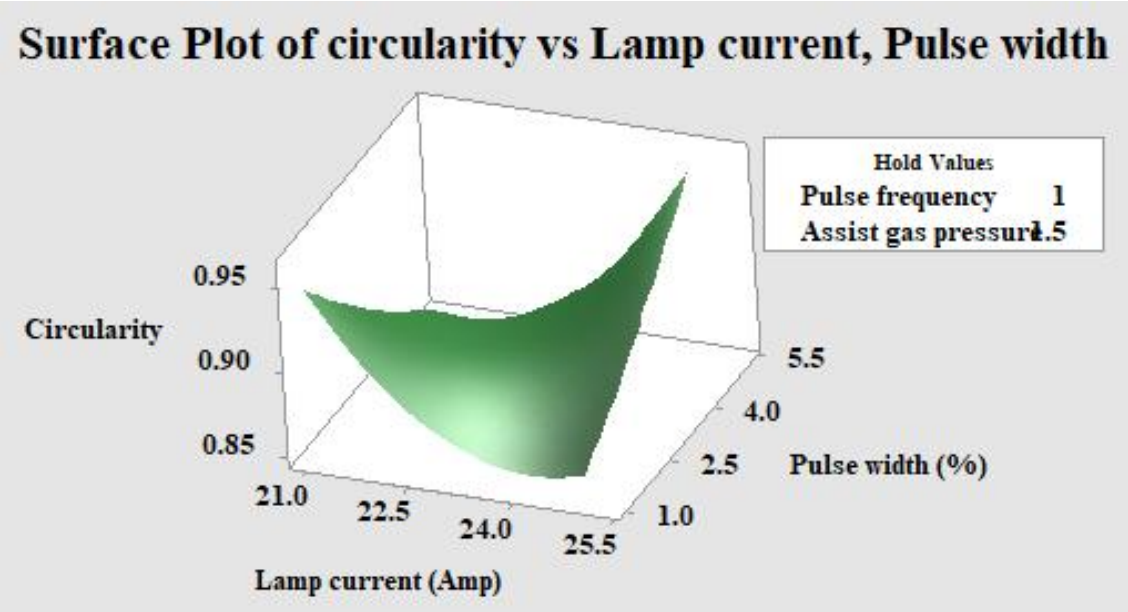

Fig. 5.8 Surface plot of hole circularity vs lamp current vs pulse width

From the surface plot given in fig. 5.8 it is observed that hole circularity decreases with increase in lamp current upto certain value then increases, but linearly increases with pulse width. As the average power increases with increase in pulse duration, hole geometry in entry side may be enhanced by standardized material removal, thus hole circularity increased. Increase in lamp current helps to induct more thermal energy into the system which may generate comparatively more amount of melt pool. That melt pool may effects the entry hole geometry, if not properly move away from spot of irradiation. By this phenomenon hole circularity may be decreased. Further increase in lamp current may helps to instant vaporization form the top surface leads to get desired geometrical shape of drilled hole on the top surface of the workpiece.

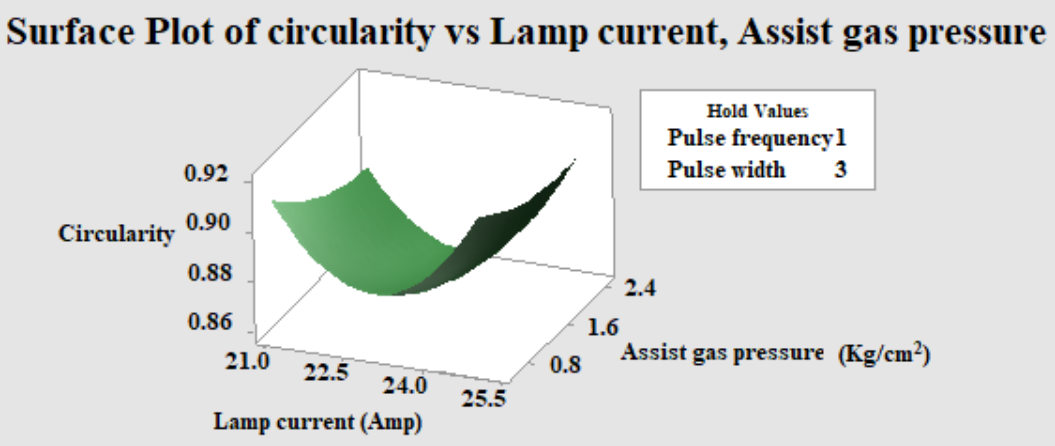

Fig. 5.9 Surface plot of hole circularity vs lamp current vs assist gas pressure

From fig. 5.9 it is found that hole circularity initially decreases upto certain value of lamp current (23 amp) then increases with increase in value of lamp current but decreases a little bit with increase in assist gas pressure when other two variable kept constant at 1 kHz of pulse frequency and 3% of pulse width. The turbulence, created by assist gas at higher value of assist gas pressure at the machining zone, may be the reason behind marginal fall in the value of circularity. Thermal efficiency may not be adequate upto the aforesaid value of lamp current due to influence of assist air pressure, may be the reason behind observed phenomenon. But further increase in lamp current may helps to induct adequate amount of thermal energy to get proper geometrical shape at the hole entry, leads to increase in hole circularity.

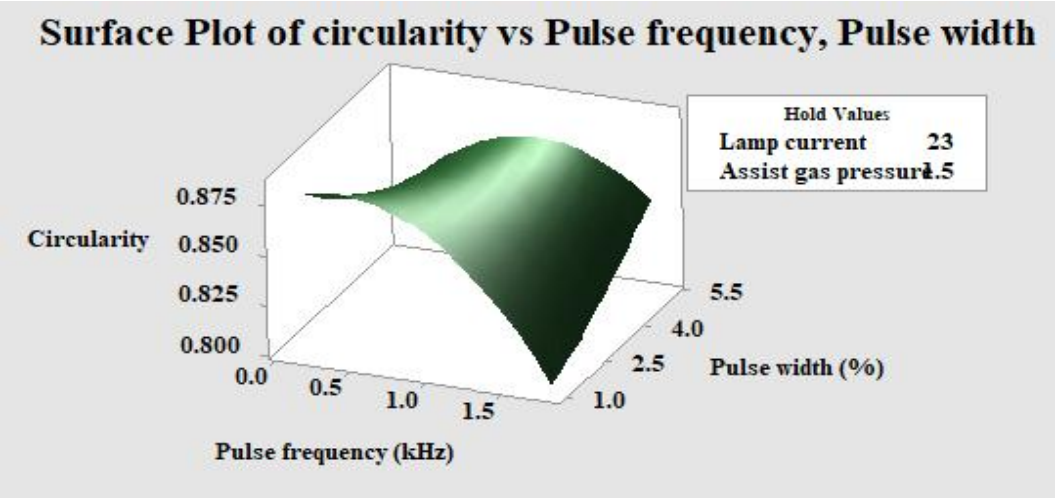

Fig. 5.10 Surface plot of hole circularity vs pulse frequency vs pulse width

It has been viewed from surface plot given in fig 5.10 that hole circularity decreases with increase in pulse frequency but increases with increase in pulse width when the other two

process variable, i.e., lamp current and assist gas pressure kept constant at 23 amp & 1.5 kg/cm^2 respectively. From the plot it is evident that lowest value of pulse frequency with highest value of pulse width helps to get desired value of hole circularity. As the energy per pulse are decreases with increase in pulse frequency, circularity decreases due to non uniformity in material removal from the top surface of the machining zone. On the other hand average power of the focused laser beam increases with increase in pulse width may enhance the chance of uniform material removal from the top surface of the machining spot which leads to create an uniform edge at the top surface of drilled hole. Thus circularity of hole increases.

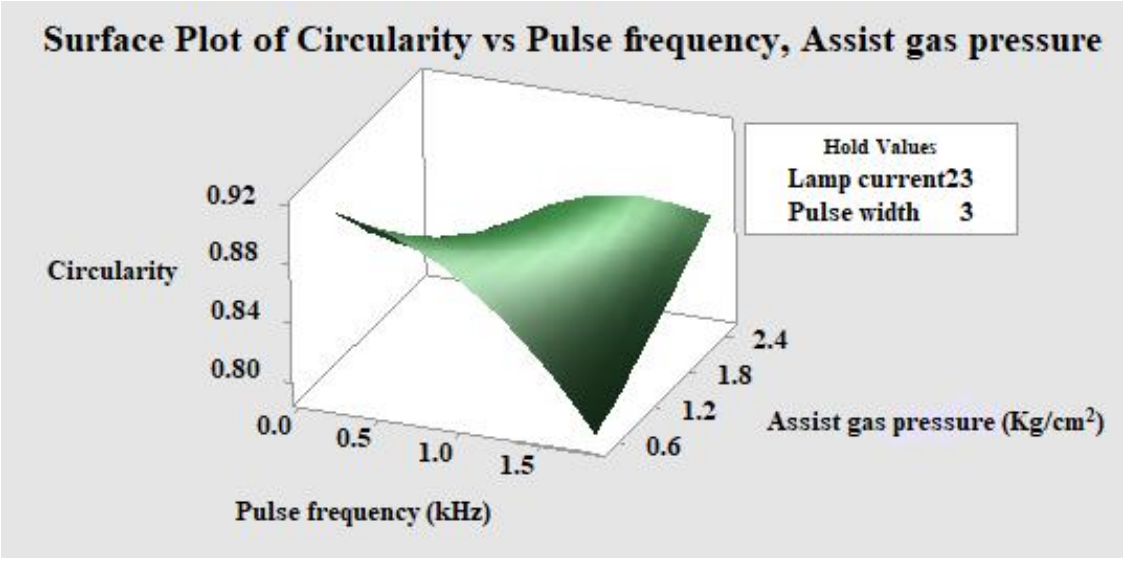

Fig. 5.11 Surface plot of hole circularity vs pulse frequency vs assist gas pressure

It is observed from fig. 5.11 that hole circularity decreases with increase in pulse frequency but increases with increase in assist gas pressure. Higher value of assist gas pressure helps to proper removal of gaseous or molten debris from the machining zone which avoids any resolidification on the edge of hole or adjacent area of the drilled hole, results in increase in circularity. Decrease in energy per pulse with increase in pulse frequency may not insert adequate amount of thermal energy on the machining spot which may leads to uneven heating at top surface of workpiece. Thus circularity decreases.

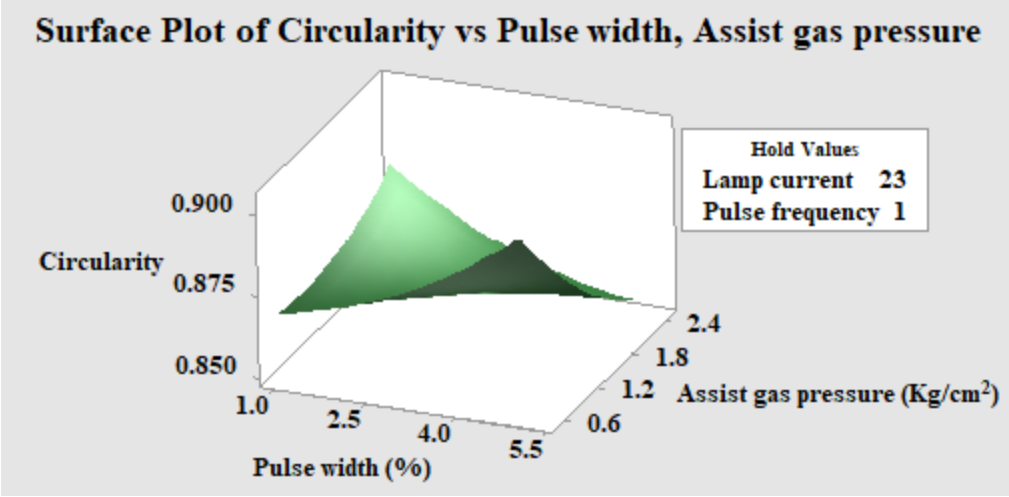

Fig. 5.12 Surface plot of hole circularity vs pulse width vs assist gas pressure

From the surface plot fig 5.12 it is viewed that circularity increases with increase in pulse width but decreases with increase in assist gas pressure. Decrease in peak power with increase in pulse width, results in increase in average laser power which enhance the uniformity of material removal from the top surface of the irradiate zone, may leads to increase in hole circularity. But the uneven heating value on the top surface due to the higher value of assist gas pressure may be the reason behind decrease in circularity. Microscopic view of laser drilled hole is given in fig.5.13.

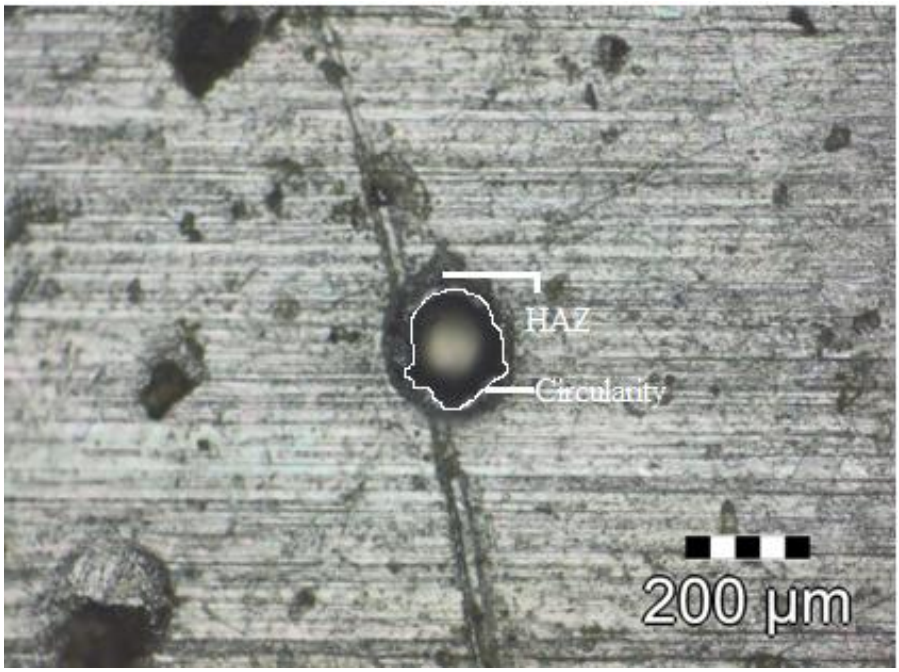

Fig. 5.13 Microscopic view of laser drilled hole at top surface

5.1.4 Sensitivity analysis of machining responses

To obtain the sensitivity equation of circularity (C) with respect to process variables, the equation (5.2) is partially differentiated with respect to process variables. Thus equations (5.4),(5.5),(5.6) and (5.7) are the sensitivity equations of circularity with respect to lamp current, pulse frequency, pulse width and assist air pressure respectively.

$$\delta C/\delta X_1 = -0.4241+0.017788X_1-0.02248X_2+0.012067X_3+0.00136X_4 \quad (5.4)$$

$$\delta C/\delta X_2 = 0.4533-0.1468X_2-0.02248X_1+0.01798X_3+0.07504X_4 \quad (5.5)$$

$$\delta C/\delta X_3 = -0.2898+0.002888X_3+0.012067X_1+0.01798X_2-0.00806X_4 \quad (5.6)$$

$$\delta C/\delta X_4 = -0.1014+0.01116X_4+0.00136X_1+0.07504X_2-0.00806X_3 \quad (5.7)$$

Equations (5.8), (5.9),(5.10)and (5.11) are represent the sensitivity equation of hole taper(T) with respect to lamp current, pulse frequency, pulse width, and assist air pressure respectively which is get by partially differentiated eq. no (5.3).

$$\delta T/\delta X_1 = 0.09198-0.00411X_1-0.000207X_2-0.001368X_3+0.000537X_4 \quad (5.8)$$

$$\delta T/\delta X_2 = 0.0167-0.00724X_2-0.000207X_1-0.000689X_3-0.00133X_4 \quad (5.9)$$

$$\delta T/\delta X_3 = 0.02913-0.00146X_3-0.001368X_1-0.000689X_2+0.004500X_4 \quad (5.10)$$

$$\delta T/\delta X_4 = -0.0284-0.00058X_4+0.000537X_1-0.00133X_2+0.004500X_3 \quad (5.11)$$

Sensitivity analysis is carried out to examine the influence of an input variable to the outputs within the design space considered in this research work. Positive values of sensitivities means that the output variable increases as the input variable increases and a negative value means that the output variable increases as the input variable decreases [82].

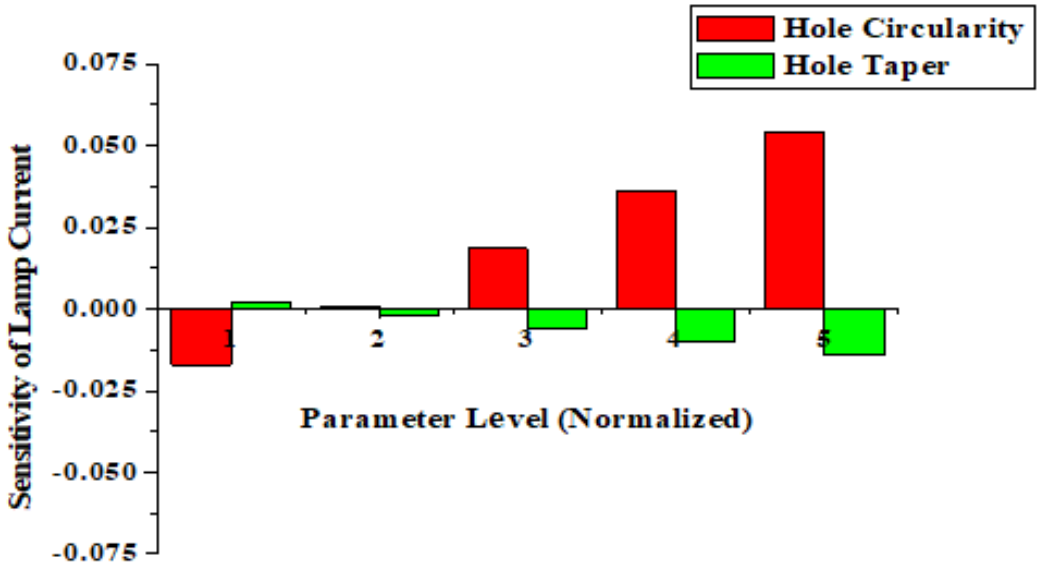

Fig.5.14 Sensitivity of lamp current in respect of machining responses

It is evident from figure 5.14 that, the sensitivity of lamp current on hole taper is negative. It indicates that with the increase in lamp current, hole taper decreases. Higher lamp current generates high thermal energy, which produces large taper. The low energy of laser beam generates small taper. High-energy laser beam at higher lamp current with a small incident time, may removes more material from the top surface almost instantly, rather than throughout the depth which increases the tapering effect. Also from the figure we infer that sensitivity of hole circularity gradually changes from negative to positive. This implies that the circularity increases with lamp current. This is due to the reason that when lamp current increases, the energy of laser beam also increases which in turn increases the material removal from the top surface of the work piece, due to which circularity improves.

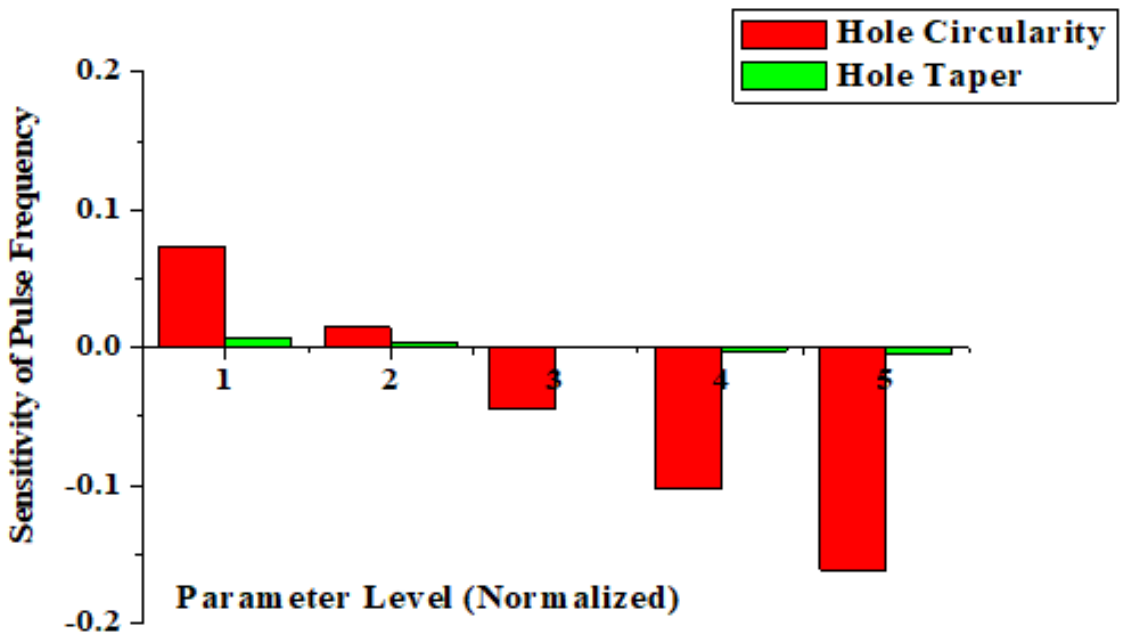

Fig.5.15 Sensitivity of pulse frequency in respect of machining responses

From figure 5.15 it is evident that sensitivity of pulse frequency on hole taper is positive for lower values of pulse frequency and negative for higher value of pulse frequency. The negative value of pulse frequency sensitivity of hole taper indicates a decrease in the value of hole taper with increase of pulse frequency. At high pulse frequencies, small taper is observed but at low pulse frequencies, large taper is generated. At a low pulse frequency, comparatively high beam energy is generated, which remove more material from top surface results in the high tapered hole. Again at lower pulse frequency, less energy beam generates small taper of micro-hole. From figure 5 we can see that sensitivity of pulse frequency on hole circularity gradually changes from positive to negative. This because, initially when pulse frequency increases, the pulse-off time becomes shorter and the beam energy generated becomes lower, as a result the material which melts and solidifies with less disorder and produces higher circularity. After a certain limit when pulse frequency again increases, the pulse-off time becomes very short, and the material does not get time to be solidified, due to which agitation and disorder takes place in molten material during material removal process, and it results in a lower circularity.

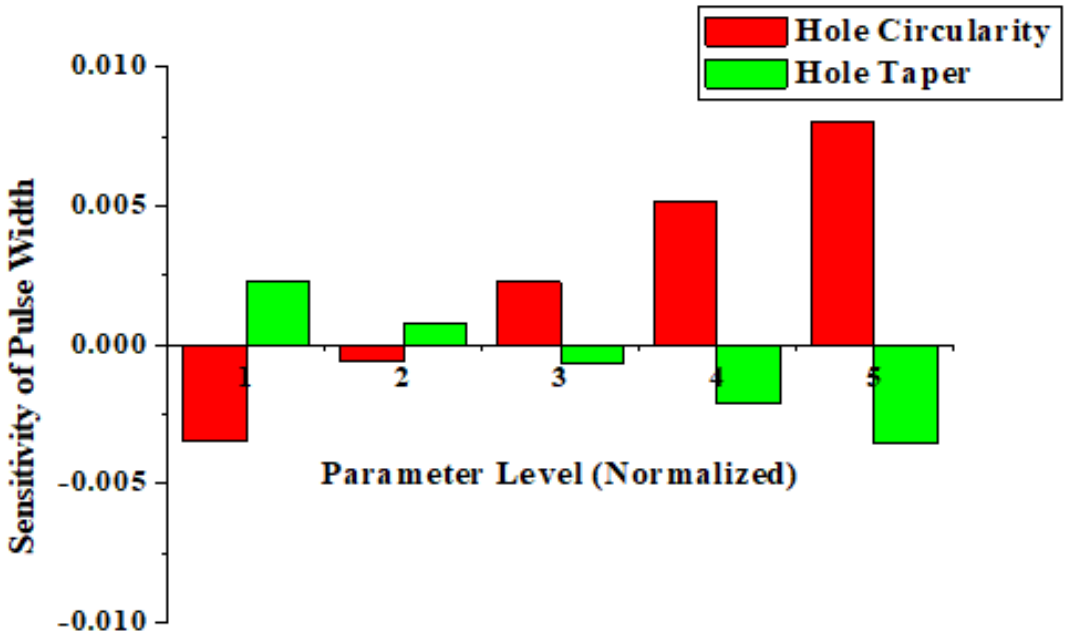

Fig 5.16 Sensitivity of pulse width in respect of machining responses

From figure 5.16 it is evident that the hole taper is positive with lower pulse width values and negative with higher pulse width values. The pulse width has positive effect on taper, and as pulse width increases, taper increases. At lower pulse widths, high concentrated beam energy causes quick penetration in the work piece thus, material removal throughout the depth is almost equal, results in less taper is formed at lower pulse width. Sensitivity of pulse width on hole circularity shows a different trend unlike hole taper. At higher pulse width due more interaction time of laser beam with workpiece, remove more material hence circularity is increased and vice versa.

The sensitivity of air pressure on hole taper and circularity is shown in figure 5.17. The hole taper has negative air pressure sensitivities. Lower assisted air pressure is unable to compensate the excess heat generated and the top hole diameter increases. Increase in assist air pressure helps remove extra heat due to which material gets solidified at the entrance of the hole, which causes less material removal from the top surface and the hole taper decreases with increase in air pressure. However, at higher level of assist air pressure molten material is ejected from the top surface rapidly, thus a larger hole taper is generated. The sensitivity of air pressure on circularity changes gradually from negative to positive. Circularity increases with increase in air pressure. Low assist air pressure removes less amount of heat from the drilling zone. However, at higher

level of assist air pressure, the amount of excess heat is removed rapidly. The higher air pressure also assist to eject molten material from the drilling zone. As a result, circularity increases with increase in air pressure at high lamp current.

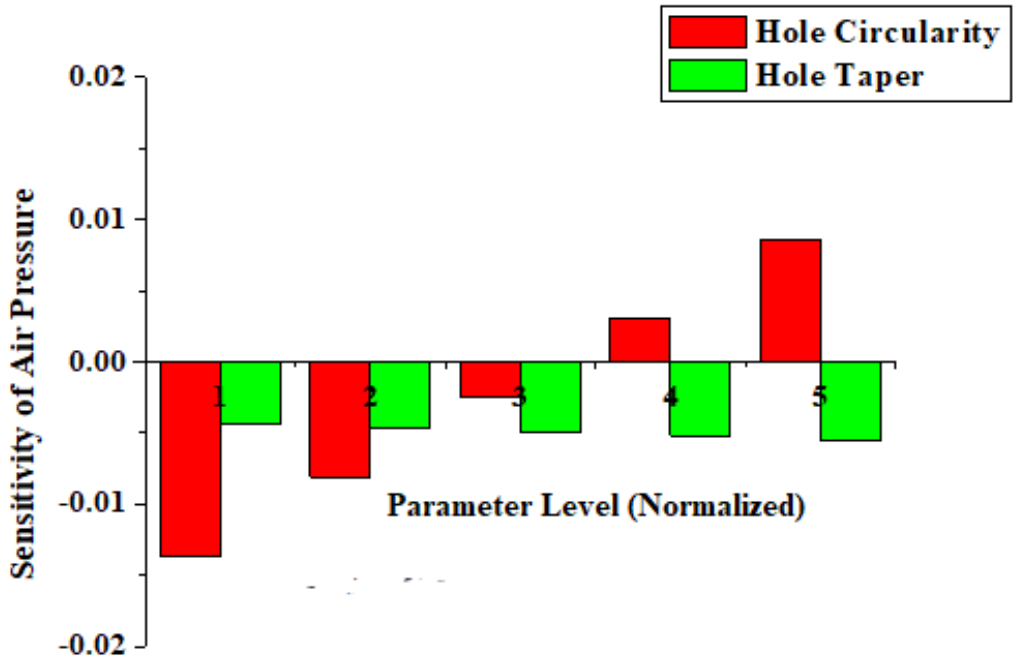

Fig.5.17 Sensitivity of assist gas pressure in respect of machining responses

Figure 5.18-5.21 represents the 3D contour plot for all the dominant interactions of process variables for hole taper. It is observed from the plots that hole taper from 0.005 rad to 0.02 rad is the mostly feasible region can be achieved under present set of parametric combinations. Higher value of lamp current with high assist air pressure, comparative higher value of pulse width are the parametric condition to achieve the feasible result of hole taper. It is also observed from the plot 5.18 that effect of pulse frequency is very less for hole taper which also justify the results of ANOVA analysis for hole taper.

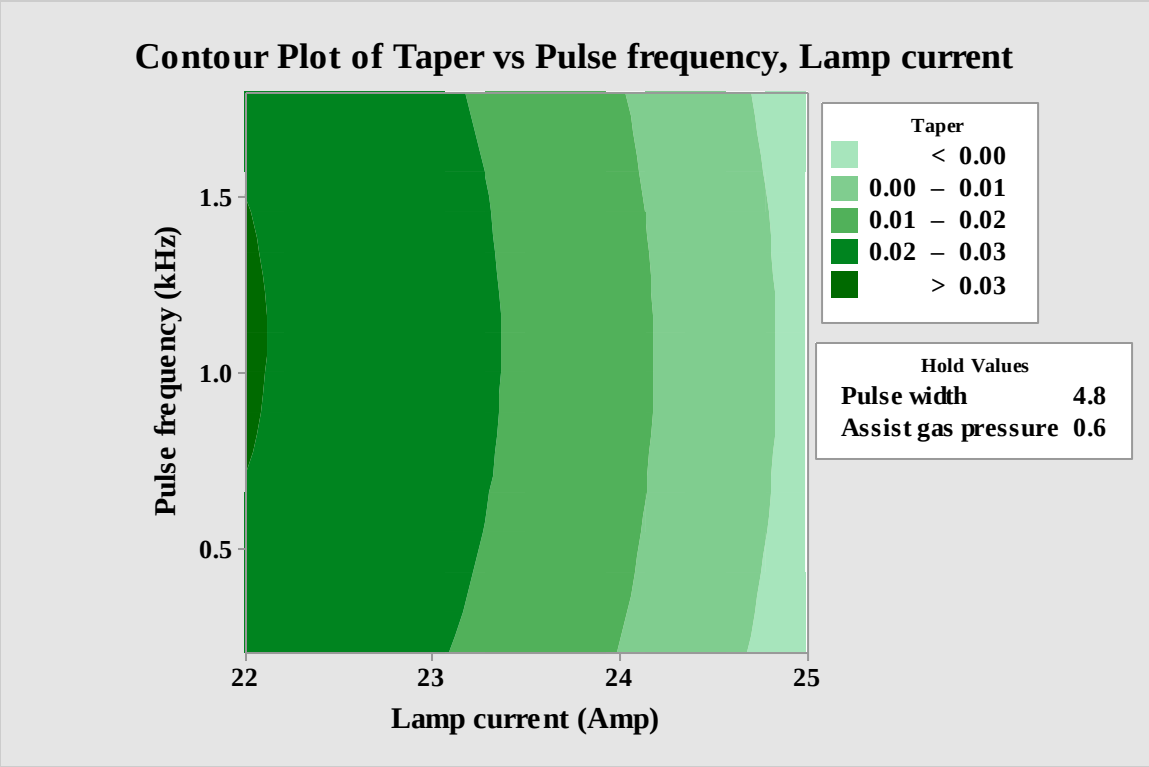

Fig. 5.18 Contour plot of hole taper vs pulse frequency vs lamp current

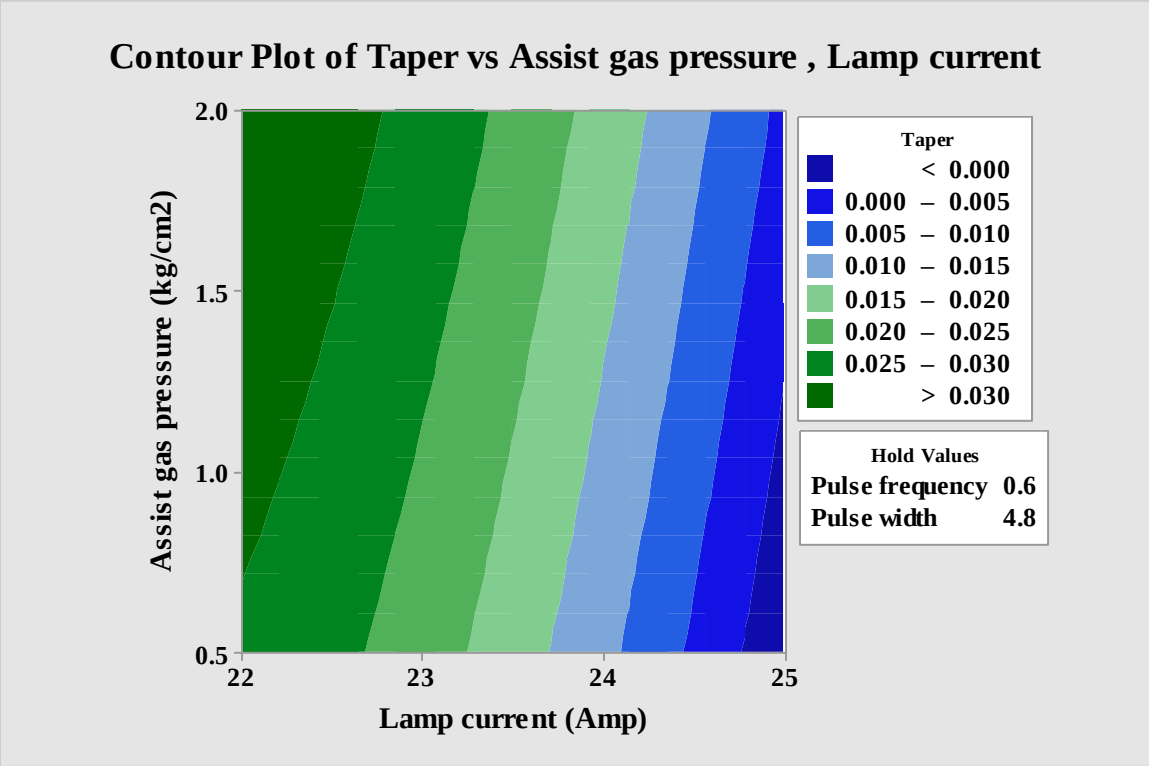

Fig. 5.19 Contour plot of hole taper vs assist gas pressure vs lamp current

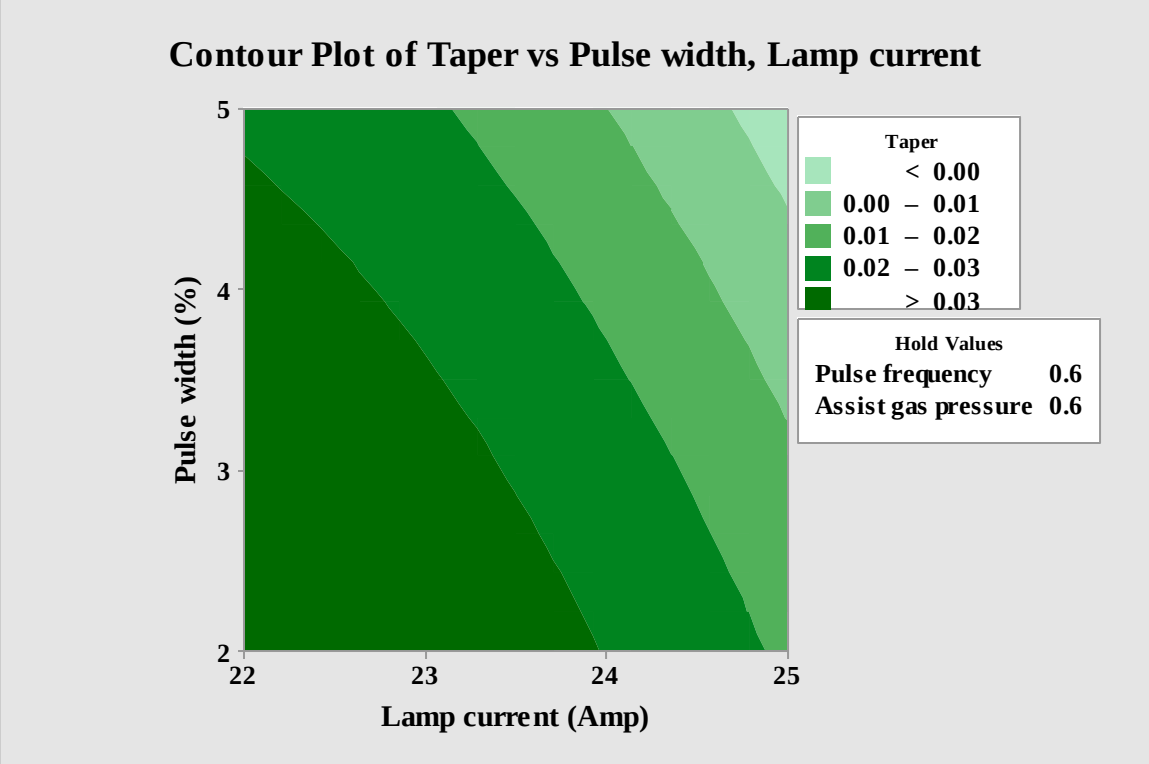

Fig. 5.20 Contour plot of hole taper vs pulse width vs lamp current

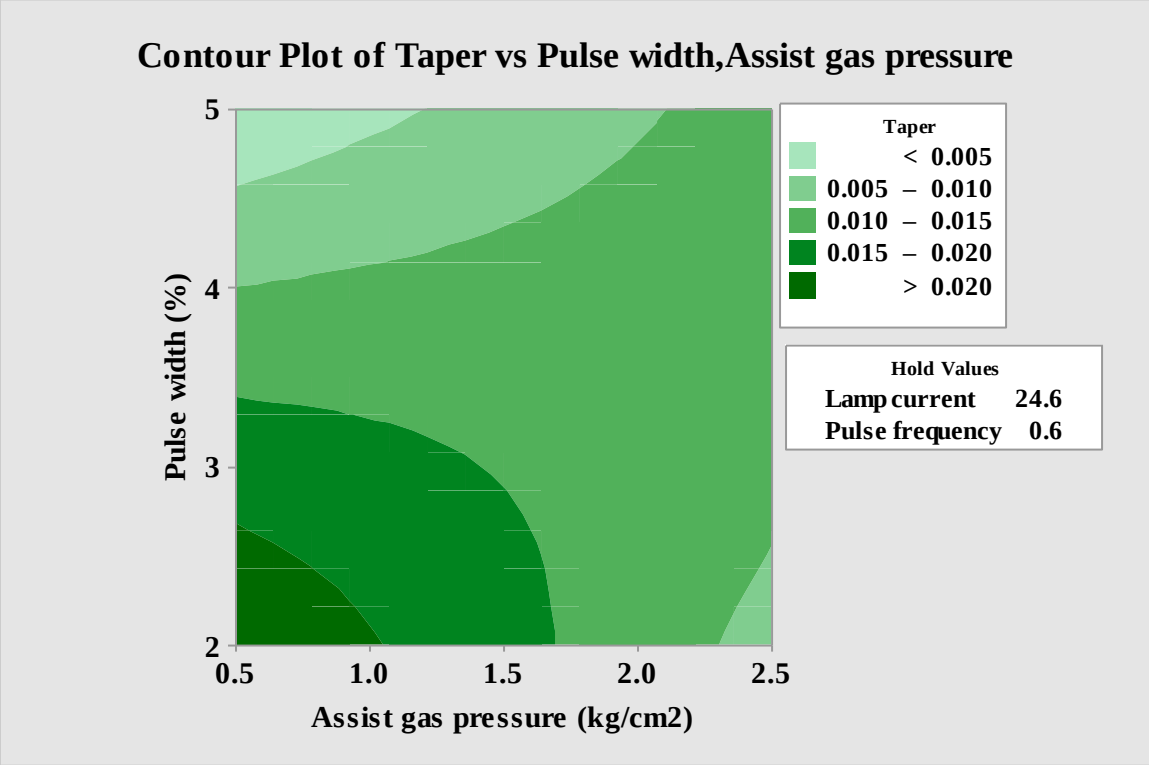

Fig. 5.21 Contour plot of hole taper vs pulse width vs Assist gas pressure

Figure 5.22- 5.25 represents the 3D contour plot for all the dominant interactions of process variables for hole circularity. It is evident from plots that hole circularity in between 0.85 to 0.92 is most feasible range to be achieved by any combination of process variables. Lower value of pulse frequency with lower value of assist gas pressure, higher value of lamp current and higher value of pulse width helps to get feasible region of hole circularity.

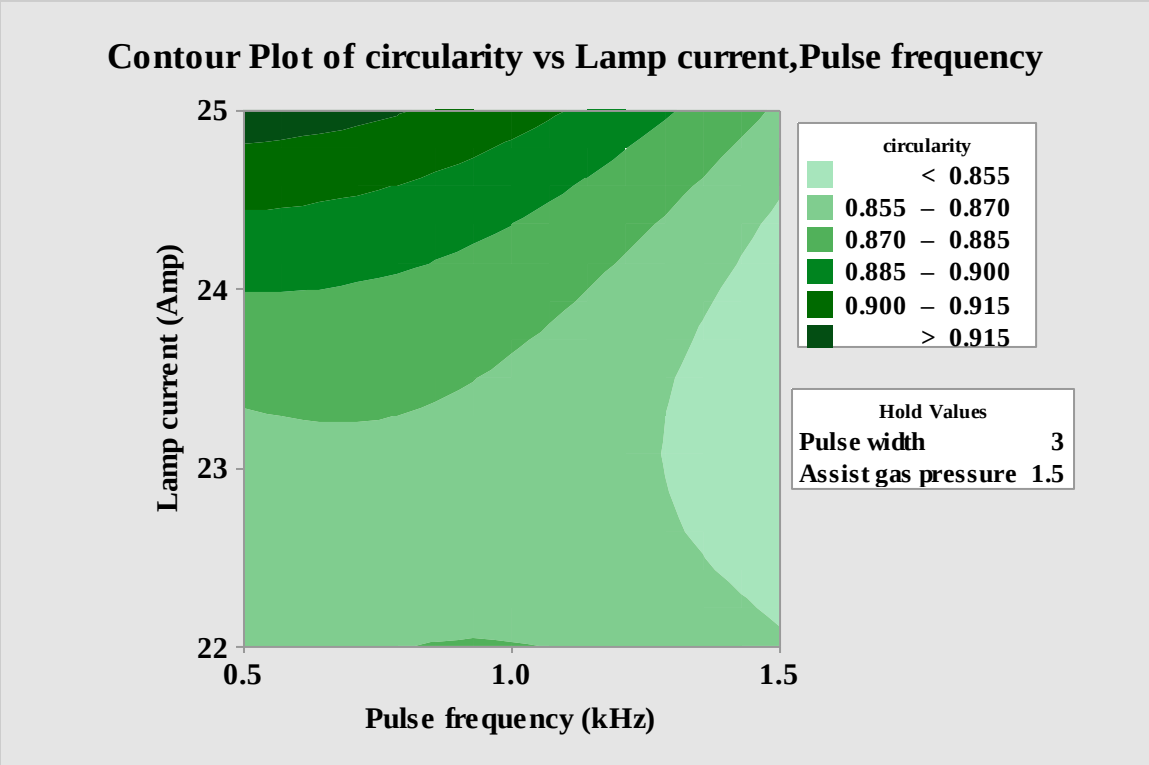

Fig. 5.22 Contour plot of hole circularity vs pulse frequency vs lamp current

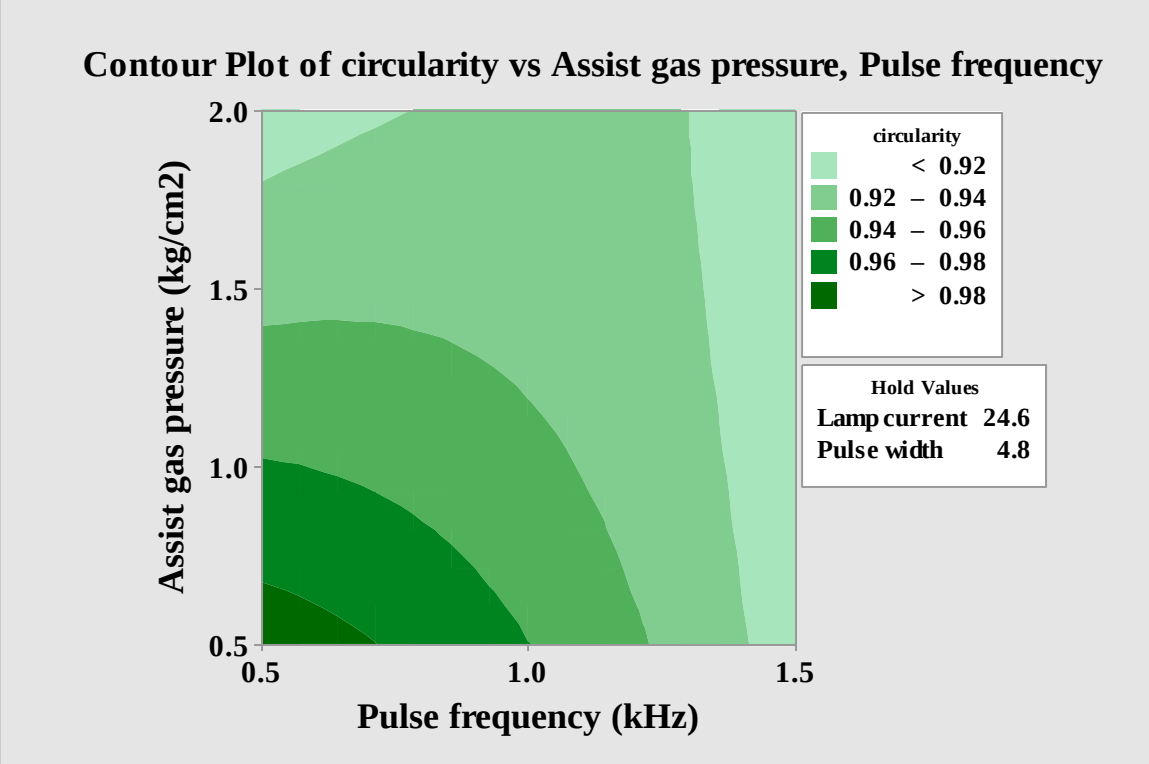

Fig. 5.23 Contour plot of hole circularity vs pulse frequency vs assist gas pressure

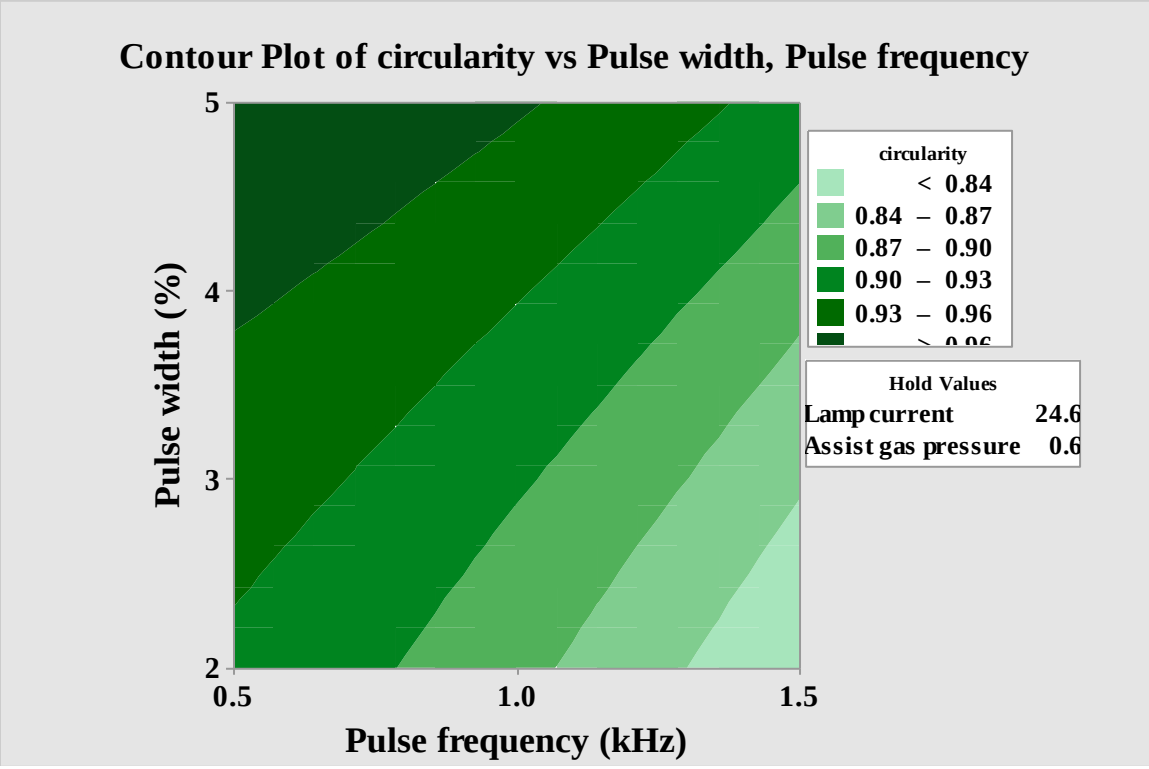

Fig. 5.24 Contour plot of hole circularity vs pulse frequency vs pulse width

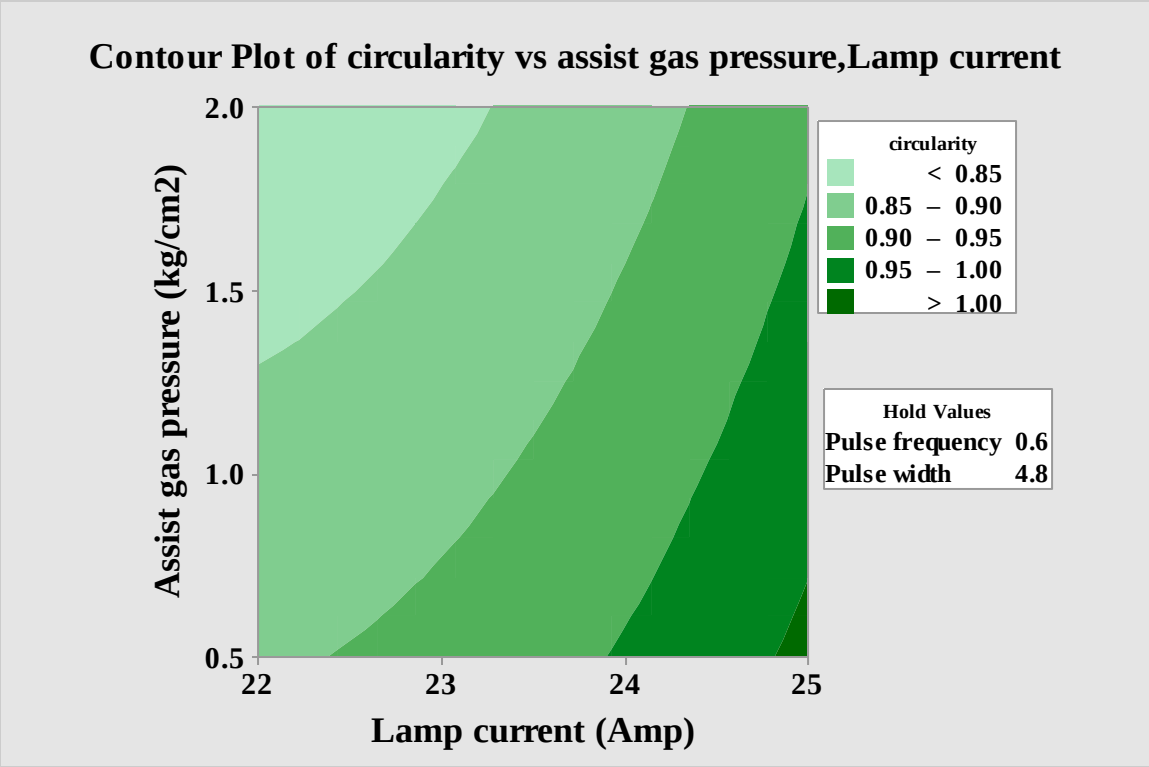

Fig. 5.25 Contour plot of hole circularity vs lamp current vs assist gas pressure

5.1.5 Determination of optimal process parameter settings

Fig.5.26 and fig 5.27 shows the optimization results for the maximum hole circularity and minimum hole taper based on the mathematical model developed by using Eq. (5.7) and Eq. (5.8) . To get ideal machining response, the value of the weight for linear desirability function (d) is considered as 1.

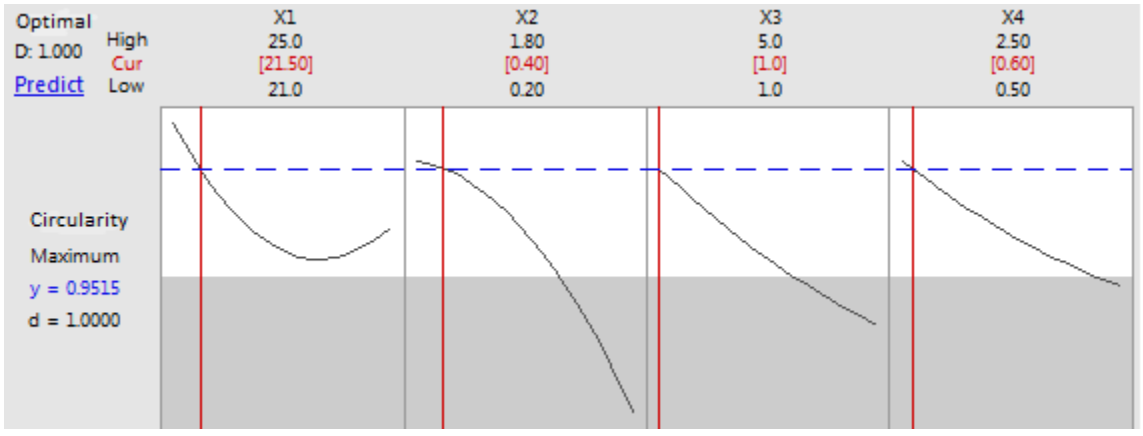

Fig 5.26 Single objective optimization in respect of hole circularity

It is found from the figure that maximum hole circularity of 0.09515 dimension can be achieved at process parameter settings of 21.50 A lamp current, 0.4 kHz pulse frequency, 1% pulse width, and 0.6 kg/cm^2 of assist gas pressure.

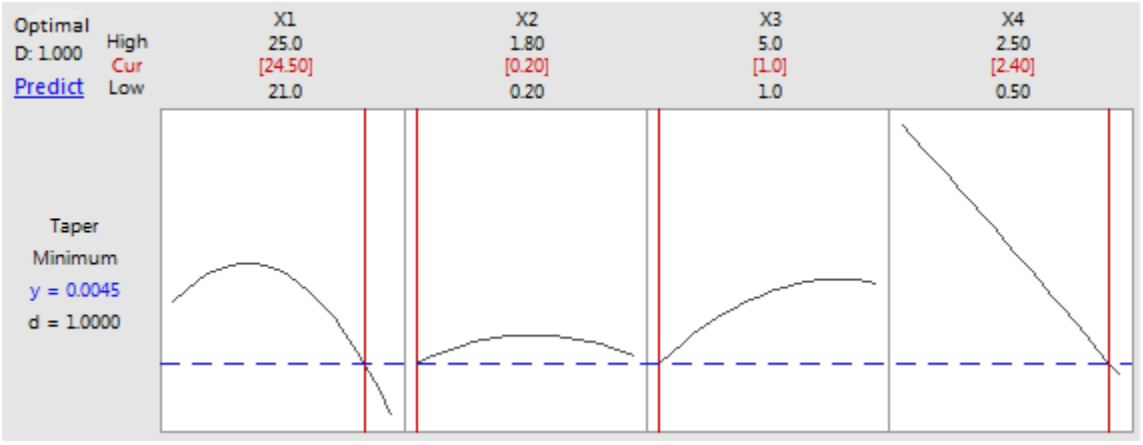

Fig 5.27 Single objective optimization in respect of hole taper

It is found from the figure that minimum hole taper of 0.0045 dimension can be achieved at process parameter settings of 24.50 A lamp current, 0.2 kHz pulse frequency, 1% pulse width, and 2.40 kg/cm^2 of assist gas pressure.

Multi-response optimization of maximum hole circularity with minimum hole taper are shown in fig 5.28. Here two responses have been optimized simultaneously. The label above composite desirability refers to the current process parameters setting and changes for moving the factor settings interactively. The label is optimal when the optimization plot is created. It is found from the figure 5.28 that maximum hole circularity 0.9807 along with minimum hole taper of 0.0033 dimension can be achieved at process parameter settings of 24.60 A lamp current, 0.6 kHz pulse frequency, 4.8% pulse width, and 0.6 kg/cm^2 of assist gas pressure. The value of composite desirability factor (D) is 1 which is desired. Microscopic view of drilled hole at optimal parameter settings are given in 5.29.

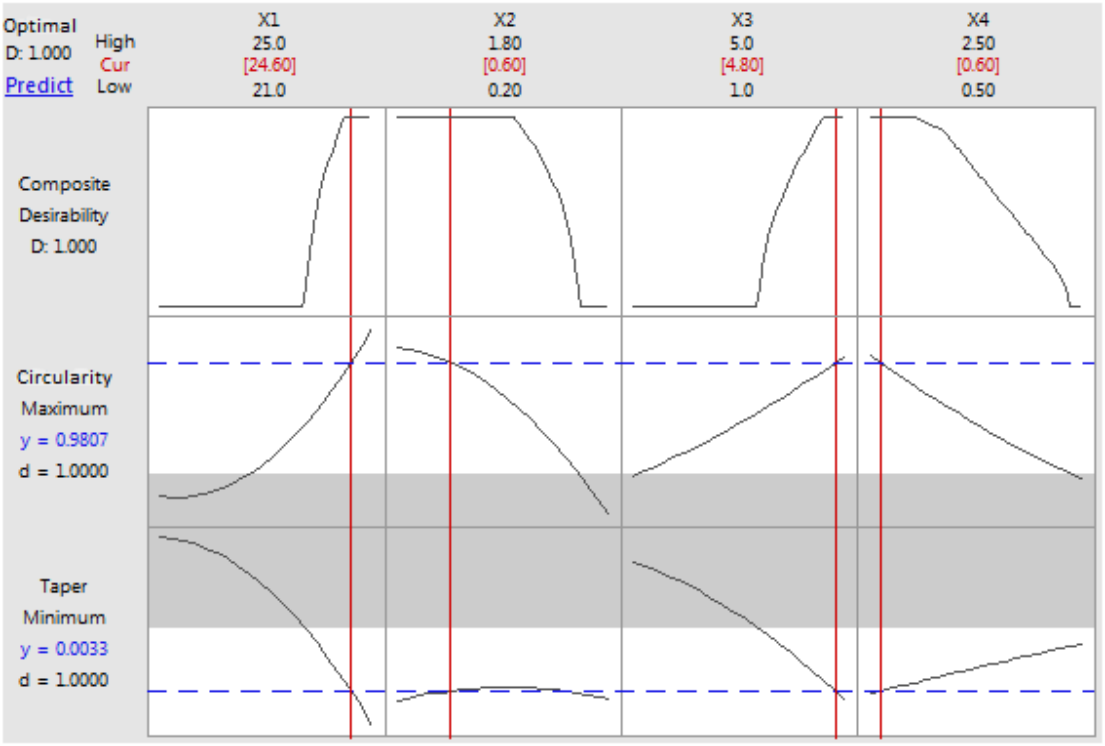

Fig 5.28 Multi-objective optimization in respect of machining characteristics

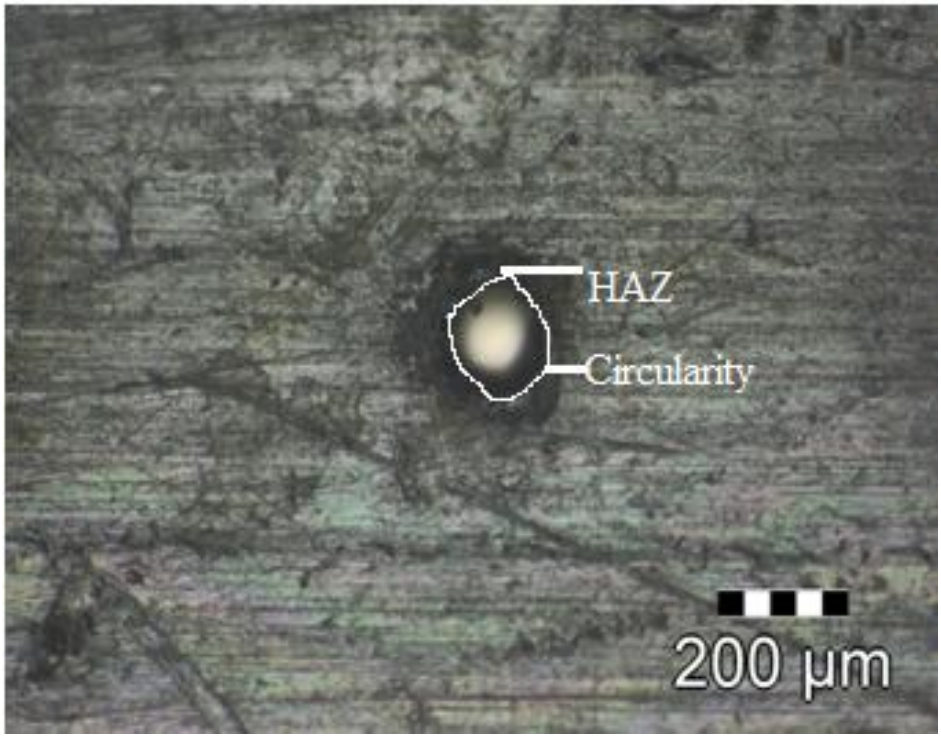

5.29 Microscopic view of drilled hole at Optimal parametric condition

5.1.5.1 Validation of the developed model

Five confirmation experiments are conducted with optimal process parameter settings. The actual results are calculated as the average of three measured results for each response. Result of validation experiments and predicted values and calculated percentage error of confirmation experiments which indicate that the developed models can yield nearly accurate results. Results of validation experiments are given in table 5.7.

TABLE 5.7 Validation test

Lamp current (amp)	Pulse frequency (kHz)	Pulse width (%)	Assist air pressure (kg/cm^2)		Hole circularity	Hole taper (rad)
24.6	0.6	4.8	0.6	Predicted	0.9807	0.0033
				Actual	0.9359	0.0079
				% of error	4.57	1.39

5.1.6 Outcome of the study

In this experimental study microdrilling operation is successfully carried out on aluminum alloy with high reflectivity. Parametric analysis has been conducted to understand the effect of process variables on machining characteristics. RSM based CCD technique is used here to design various combination of process variables, i.e, lamp current, pulse frequency, pulse width and assist pressure to perform microdrilling. ANOVA analysis helps to check the adequacy of the developed mathematical model. It is found from the ANOVA analysis that all the process variables are statistically significant to hole taper and hole circularity. It is also observed that laser power in terms of lamp current is the most significant process variable for hole taper and pulse frequency is the least significant whereas pulse frequency is the most significant process variable for hole circularity and pulse width is the least significant. Single and multi objective optimization has also been carried out to get optimal parameter settings for lower hole taper with higher hole circularity.

5.2. Laser beam microdrilling of SiC30BN nanocomposite material

A nanocomposite is a multiphase solid material where one of the phases has one, two or three dimensions of less than 100 nanometers (nm), or structures having nano-scale repeat distances between the different phases that make up the material. The mechanical, electrical, thermal, optical, electrochemical, catalytic properties of the nanocomposite differ vastly from that of the parent materials. Nanocomposite materials, mechanical properties are different from conventional composite material due to its very high aspect ratio [85]. Pulsed Nd: YAG laser has great ability for micro-machining because of higher laser beam intensity at low mean power, good focusing characteristics due to small pulse duration in nano to femtosecond scale. Due to formation of a thermal gradient at that laser beam and work piece interface, the bond strength of nanocomposite material is reduced to a great extent which helps for easy material removal. That makes application of laser beam machining more advantageous for micromachining of nanocomposite over other conventional and non conventional manufacturing technique [86]. However, no such comprehensive research work or any technology guidance is available for Nd:YAG laser beam microdrilling of Silicon Carbide 30% Boron Nitride (SiC-30 BN) nanomaterials. Nanosecond Pulsed Nd: YAG laser percussion microdrilling of Silicon Carbide 30% Boron Nitride (SiC-30BN) nanocomposite material has been performed for determination of optimum laser machining Process parameters to get desired machining responses. To study the effect of different environment, two types of assist gas is used during the experimental study. All the experiments are carried out as per Taguchi methodology though Taguchi method uses a special design of orthogonal arrays to study the entire process parameter space with a small number of experiments only.

5.2.1 Parametric study on laser beam microdrilling of SiC-30BN nanocomposite material with compressed air as an assist medium.

Experiments are performed on Silicon Carbide 30% Boron Nitride (SiC-30BN) nanocomposite with aide of dry compressed air as an assist gas to study the effects of different controllable process variables on machining responses. During this study compressed air gas is also selected as an process parameter and try to find out whether this parameter have any significance on the quality characteristics of drilled microhole.

5.2.1.1 Experimental Planning

1.57 mm thick Silicon Carbide 30% Boron Nitride (SiC-30BN) nanocomposite has been considered as workpiece material for experimental study. Properties of SiC-30BN nanocomposite is listed in Table 5.8 [87]. Q-switched pulsed (120 ns) Nd:YAG laser with 1064 nm wavelength is used in this study to create array of micro holes via laser micro drilling technique. The distance (centre to centre) between two micro holes kept constant at 2 mm.

Table 5.8 Properties of SiC-30BN Nanocomposite [87]

Property	Unit	Values
Yield Stress	MPa	263.2 ± 6
Young's Modulus	GPa	230±5
Fracture Strength	MPa	380±10
Density	gm/cc	2.906

Lamp current, pulse frequency and pulse width are considered as the controllable process parameters to carry out the experiment. Assist gas pressure and focal distance are also chosen as controllable process variable for this experimental study. Emphasis has given on in depth study of assist medium along with change in focal distance and schematic illustration of focal distance change is given in fig. no.5.24.

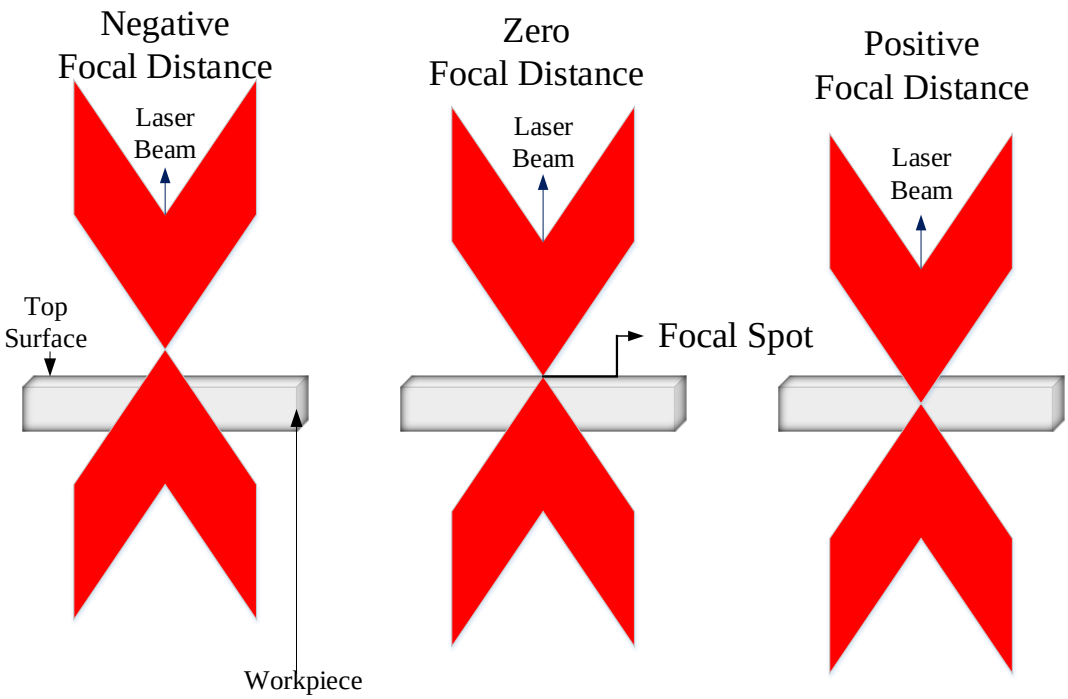

Fig.5.30 Schematic diagram illustrating different focal distance

From figure 5.30 it has been observed that with change in focal distance laser beam either interacts with top surface of the workpiece or its fall just beneath the top surface or just above the top surface of workpiece. That's lead to change on energy density on the point of interaction which may vary the machining responses. The experiments are carried out according to the arrangement of the L_{27} orthogonal array system based on Taguchi methodology. The ranges of these parameters are selected on the basis of trial experiments conducted by using one factor at a time approach. Ranges of the parameters are listed in table no, 5.9.

Table 5.9 Machining Parameters and Their Levels

Process Parameters	Level		
	1	2	3
Lamp current (L)(amp)	23.5	24.5	25.5
Pulse frequency (γ)(kHz)	1	2	3
Pulse width (w) (%)	2	4	6
Assist gas pressure (compressed Air) (p) (kg/cm^2)	0.4	0.7	1.0
Focal distance (F) (µm)	-200	0	200

In this process compressed air is axially flow on the spot of irradiation. Pressure gauge which is attached with the gas delivery system (details has been given in previous chapter) helps to maintain the desired assist gas (compressed air) pressure to get desired machining characteristics. The geometrical aspects i.e. hole Taper, hole circularity and Heat affected zone (HAZ) width are considered as process responses.

5.2.1.1.1 Measurements of machining outcome

STM 6 Olympus measuring microscope At 10 X magnification is used to capture the images of diameter of the micro hole. A Mitutoyo manufactured digital micrometer with 1 µm resolution is used to measure the thickness of the workpiece material. Images of microhole are captured by the microscope from where the hole diameter are measured by image analysis software (Feret's diameter measurement technique). This measurement replicate 3 times for each hole and average is taken for further analysis. The machining responses are calculated by the equations given below and the values are taken for further analysis.

$$HAZwidth(mm) = \frac{HAZdia_{Top} - Holedia_{Top}}{2} \qquad (5.12)$$

$$Taper(rad) = \frac{Hole\_Dia_{Top} - Hole\_Dia_{Bot}}{2 \times Thickness} \qquad (5.13)$$

5.2.1.2 Results and discussion

All the results for air as an assist gas are documented in table 5.10.

Table 5.10 Experimental results

EXP. No.	Lamp current (Amp)	Pulse frequency (kHz)	Pulse width (%)	Assist gas pressure (compressed air) (kg/cm^2)	Focal distance (mm)	Taper (rad)	HAZ width (mm)	Circularity
1	1	1	1	1	1	0.0821	0.2038	0.939
2	1	1	1	1	2	0.0605	0.2179	0.928
3	1	1	1	1	3	0.0435	0.2084	0.932
4	1	2	2	2	1	0.1005	0.1966	0.945
5	1	2	2	2	2	0.0835	0.1943	0.921
6	1	2	2	2	3	0.0793	0.1784	0.927
7	1	3	3	3	1	0.0901	0.1825	0.880
8	1	3	3	3	2	0.0865	0.1798	0.875
9	1	3	3	3	3	0.0649	0.1854	0.863

EXP. No.	Lamp current (Amp)	Pulse frequency (kHz)	Pulse width (%)	Assist gas pressure (compressed air) (kg/cm^2)	Focal distance (mm)	Taper (rad)	HAZ width (mm)	Circularity
10	2	1	2	3	1	0.0482	0.2504	0.937
11	2	1	2	3	2	0.0350	0.2465	0.932
12	2	1	2	3	3	0.0274	0.2436	0.909
13	2	2	3	1	1	0.0989	0.2037	0.912
14	2	2	3	1	2	0.0903	0.2074	0.904
15	2	2	3	1	3	0.0582	0.2123	0.894
16	2	3	1	2	1	0.1121	0.1976	0.869
17	2	3	1	2	2	0.0995	0.2020	0.845
18	2	3	1	2	3	0.0649	0.1916	0.858
19	3	1	3	2	1	0.1250	0.2350	0.923
20	3	1	3	2	2	0.1200	0.2263	0.908
21	3	1	3	2	3	0.0787	0.2259	0.905
22	3	2	1	3	1	0.1203	0.2503	0.929
23	3	2	1	3	2	0.0905	0.2501	0.898
24	3	2	1	3	3	0.0834	0.2371	0.906
25	3	3	2	1	1	0.1470	0.2376	0.900
26	3	3	2	1	2	0.1117	0.2409	0.892
27	3	3	2	1	3	0.0870	0.2203	0.878

Statistical software MINITAB 17 is used here to analyze the experimental observations.

5.2.1.2.1 Parametric analysis

Effect of Controllable process on machining responses are elaborately discussed in this section, Mean ratio plot of HAZ width is graphically represent here in fig. 5.31. From the fig. 5.31 it is found that HAZ width gradually decreases with increase in lamp current and focal distance upto mid level of input parameter but increases with further increase in input parameters value. Whereas HAZ width sharply decrease with increase in assist compressed air flow upto mid level then increases. HAZ width increase upto mid level with increase in pulse frequency and pulse width and then decreases. Increase in lamp current results in more excitement of photons via more pumping which produce more amount of laser, thus laser energy on the irradiate spot may be increase which supply more thermal energy on and around the irradiate spot. For aforesaid condition thermal energy cannot distributed properly throughout the machining surface as well as beneath it, results in more HAZ width after mid level.

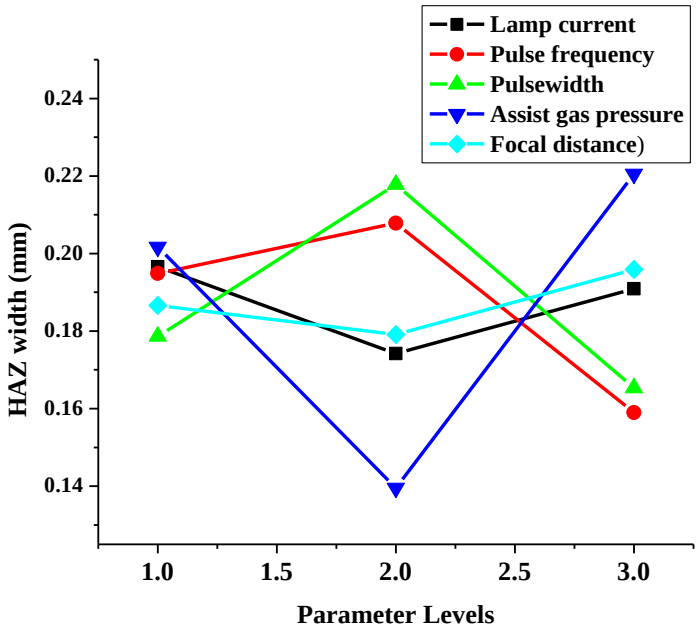

Fig.5.31 Effects of Nd:YAG laser microdrilling process parameters on HAZ width.

With negative and positive focal distance the area of interaction is more than focal distance at zero, i.e., just on the top surface of workpiece, results lower HAZ width than other two position. Energy per pulse is decreased with increase in pulse width for which HAZ width is reduced after a certain value of pulse width. With increase in pulse frequency energy density on the machining zone is reduced results in decrease in HAZ width. Axially flowed compressed air constantly deviate the laser beam to focused on the predefined spot in the nano scale along with proper cooling results in decrease in HAZ width but further increase in air pressure along with influence of other process variables results in uneven heating on the machining zone to produce more HAZ width.

From the graphical representation given in fig. 5.32, it has been found that taper decreases with increase in lamp current and focal distance whereas marginally increase with pulse frequency, pulse width and assist gas pressure upto mid level than decreases marginally. Laser power increases with increase in lamp current which may helps to remove material uniformly from top surface of the machining zone and from the drilled hole thereafter, results in decrease in hole taper. Change in focal distance from -200 µm to +200 µm in respect of top surface of the workpiece along with Gaussian beam profile of laser may produce uniform dimensional hole.

The amount of laser energy incorporated into the machining area is changed reciprocally with change in pulse frequency that may be the reason behind the observed phenomenon.

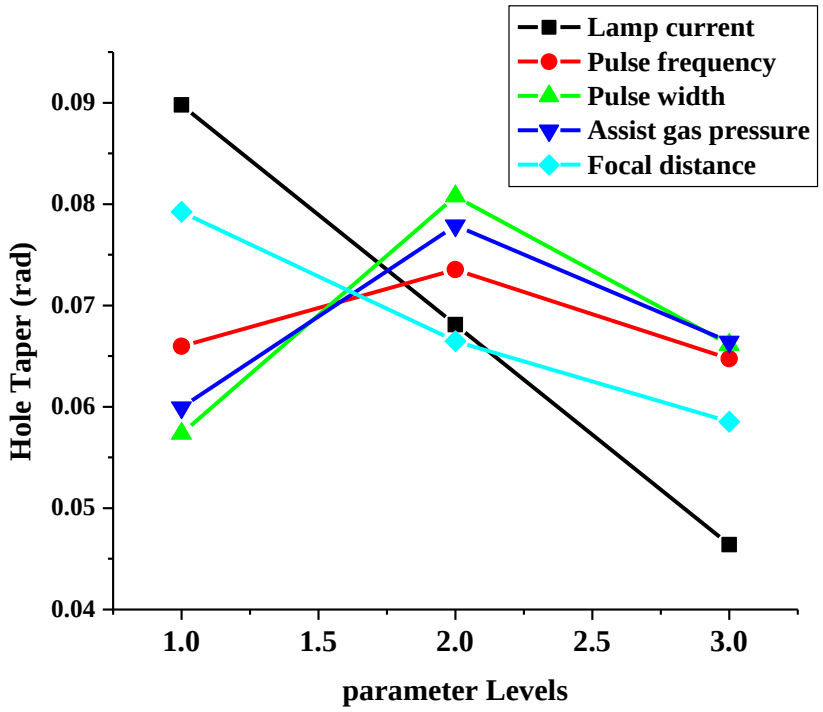

Fig.5.32 Effects of Nd:YAG laser microdrilling process parameters on hole taper.

Increase in peak power with decrease in pulse width helps to more penetration during laser drilling, results in increase in hole taper upto mid level of pulse width. Further increase in pulse width may decrease in peak power but comparatively increase in average power and interaction time may results in decrease in hole taper. Cooling effect of assist compressed air creates uneven heating in & around the machining zone results in non uniform material removal from the irradiate spot. But further increase in air pressure helps to remove material from the irradiate zone, specially from micro drilled hole to make the hole dimension uniform. Thus the taper is reduced.

From the graphical illustration of relation between process variables and machining response given in fig. 5.33, it has been found that hole circularity decreases with increase in pulse frequency and focal distance whereas decreases upto mid level with increase in lamp current and assist air pressure thereafter increases with further increase in value of afore said controllable variables. Laser beam with lesser energy is impinged on the workpiece at higher pulse frequency

and vice versa. That phenomenon may leads to uneven material removal from top surface which may hamper the dimensional accuracy of hole entry, results in decrease in hole circularity. Increase in lamp current produce more thermal energy into the machining process which may leads to non uniform material removal from the machining zone, results in decrease in geometrical dimension of hole entry but further increase in lamp current tends to removal of material by vaporisation which helps to maintain the shape of hole entrance uniform to produce hole with increased circularity.

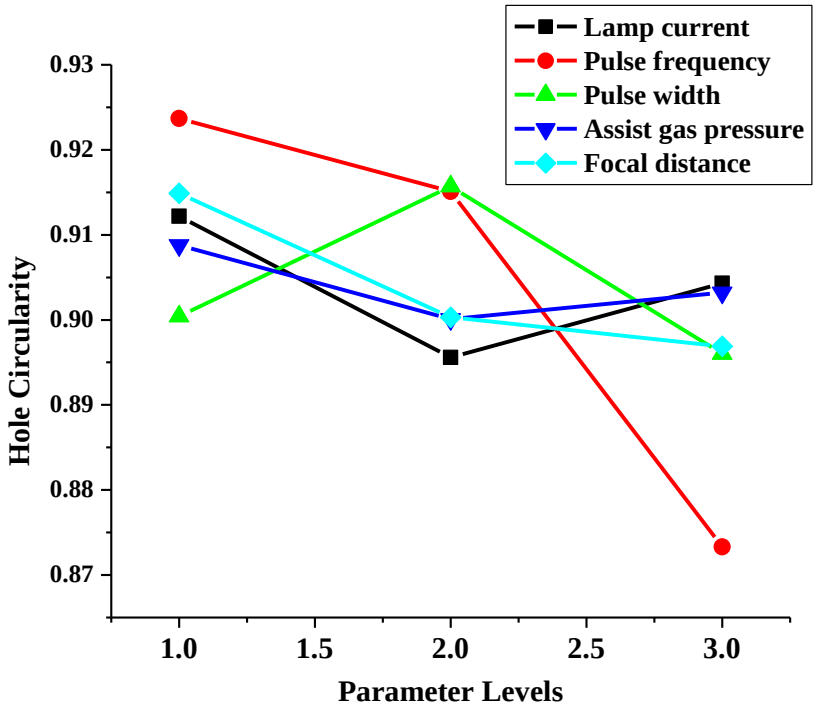

Fig.5.33 Effects of Nd:YAG laser microdrilling process parameters on hole circularity**.**

Assist air pressure helps to removal of molten debris from machining zone as well as cool the machining zone which may helps to generate uniform hole circularity that may be the reason behind observed nature of graph. Increased peak power at lower values of pulse width leads to more penetration which helps to generate a uniform hole entry but increase in pulse width leads to decrease in peak power that's result in uneven heating on the machining zone and produce non uniform hole entry. Change in focal distance to positive direction indicates at increase in area of interaction which may leads to uneven heating on the top surface of irradiation, results in decrease in hole circularity.

5.2.1.2.2 ANOVA of machining responses

Table 5.11 Results of ANOVA for hole taper (Air)

Source	DF	Adj SS	Adj MS	F	P	% of contribution
Lamp current	2	0.008469	0.004235	105.90	0.000	57.04
Pulse frequency	2	0.000407	0.000204	5.09	0.019	2.74
Pulse width	2	0.002517	0.001258	31.47	0.000	16.95
Assist Air pressure	2	0.001489	0.000745	18.62	0.000	10.03
Focal distance	2	0.001966	0.000983	24.58	0.000	13.24
Error	16	0.000640	0.000040			
Total	26	0.015488				
S		R-sq		R-sq(adj)		R-sq(pred)
0.0063235		95.8%		93.29%		88.24%

From the ANOVA analysis at 95% confidence level it is observed that all the process variables are statistically significant. The values of regression analysis, i.e., R-sq (95.8%), R-sq (adj) (93.29%) & R-sq (pred) (88.24%) indicates at the acceptability of the outcome within the pre-defined design space. All the controllable process variables have an great impact on machining responses. From the calculation of contribution percentage it is found that lamp current is the mostly influenced followed by pulse width, focal distance, assist air pressure and pulse frequency.

Table 5.12 Results of ANOVA for HAZ width (Air)

Source	Degrees of Freedom	Sum of Square	Mean of Square	F	P	% Contribution
Lamp Current	2	0.007900	0.003950	107.63	0.000	56.62
Pulse Frequency	2	0.002714	0.001357	36.98	0.000	19.46
Pulse Width	2	0.001303	0.000651	17.75	0.000	9.34
Assist Air Pressure	2	0.001778	0.000889	24.23	0.000	12.75
Focal Distance	2	0.000255	0.000128	3.48	0.036	1.83

Source	Degrees of Freedom	Sum of Square	Mean of Square	F	P	% Contribution
Error	16	0.000587	0.000037			
Total	26	0.014538				
S	R-sq		R-sq(adj)		R-sq(pred)	
0.0088199	94.13%		90.46%		83.28%	

If the value of P is less than 0.05, the process parameter is considered significant. From the table it is found that all the process parameters other than Focal Distance are statistically significant for HAZ Width. Percentage contribution column in ANOVA result table indicates at the degree of influence of all the process parameters on the microhole characteristics. According to the table it is found that Lamp Current (56.62%) has the most dominant factor followed by Pulse Frequency (19.46%), Assist gas pressure (12.75%), Pulse width (9.34%) and Focal Distance (1.83%). From the table it has been observed that S-values of the responses are smaller and R-Sq, R-Sq (adj) and R-Sq (pred) values of responses are moderately high, from which it can be concluded that the data for each response are well fitted in the developed models.

Table 5.13 Results of ANOVA for hole circularity (Air)

Source	DF	Adj SS	Adj MS	F	P	% of contribution
Lamp current	2	0.001251	0.000626	13.66	0.000	6.87
Pulse frequency	2	0.013056	0.006528	142.53	0.000	71.69
Pulse width	2	0.001915	0.000957	20.90	0.000	10.51
Assist air pressure	2	0.000347	0.000173	3.79	0.000	1.91
Focal distance	2	0.001643	0.000822	17.94	0.038	9.02
Error	16	0.000733	0.000042			
Total	26	0.063510				
S		R-sq		R-sq(adj)		R-sq(pred)
0.0067676		96.13%		93.71%		88.98%

From the ANOVA analysis at 95% confidence level it is observed that all the process variables are statistically significant. The values of regression analysis, i.e., R-sq (96.13%), R-sq (adj) (93.71%) & R-sq (pred) (88.98%) indicates at the acceptability of the outcome within the pre-defined design space. All the controllable process variables have an great impact on machining responses. From the calculation of contribution percentage it is found that pulse frequency is the mostly influenced followed by pulse width, focal distance, lamp current and assist air pressure.

5.2.1.3 Determination of optimal parameter settings

5.2.1.3.1 Single objective optimization based on Taguchi methodology

Experimental observations are further used to determine the optimal parameter settings. Firstly the experimental results are used to carry out single objective optimization by Taguchi based optimization technique. The results of single optimization for each machining responses are listed in table no. 5.14

Table 5.14 Single objective optimization of responses

Machining responses	Optimal parameter settings	Optimal Value
Hole taper (rad)	L2 γ1 w2 p3 F3	0.0173
HAZ width (mm)	L1 γ3 w3 p2 F3	0.1585
Circularity	L3 γ3 w1 p1 F3	0.959

5.2.1.3.1.1 Confirmation test based on single objective optimization results

Five experiments with optimal parameter settings for each machining responses has been carried out. The average of experimental results is taken for confirmation test. Table 5.15 furnished the result of confirmation test.

Table5.15 confirmation test of single objective optimization technique

Machining responses	Optimal parameter settings	Optimal Value	Experimental value (average)	% of error
Hole taper (rad)	L2 γ1 w2 p3 F3	0.0173	0.018	4.04
HAZ width (mm)	L1 γ3 w3 p2 F3	0.1585	0.17	7.25
Circularity	L3 γ3 w1 p1 F3	0.959	0.924	3.64

5.2.1.3.2 Taguchi based Grey relation analysis for multi objective optimization

Also multiple objective optimization is performed here by Grey based Taguchi optimization technique. As per previously said in last chapter, all the normalized grey value and grey relation coefficient values are documented in table no.5.16. During the calculation of the grey relation grade 40% weightage is given on hole taper and HAZ width whereas 20% weightage is given on hole circularity.

Table 5.16 Grey Relation analysis results

EXP. No.	GRG Taper	GRG HAZ width	GRG Circularity	GRC Taper	GRC HAZ width	GRC Circularity	GRG	grade
1	0.5411	0.2829	0.9400	0.5215	0.4108	0.8929	0.1811	16
2	0.7159	0.2047	0.8300	0.6377	0.3860	0.7463	0.1810	15
3	0.7341	0.2573	0.8700	0.6529	0.4023	0.7937	0.1880	10
4	0.0000	0.2946	1.0000	0.3333	0.4148	1.0000	0.1664	19
5	0.1353	0.3610	0.7600	0.3664	0.4390	0.6757	0.1521	26
6	0.3501	0.2545	0.8200	0.4348	0.4014	0.7353	0.1593	24
7	0.4735	0.4004	0.3500	0.4871	0.4547	0.4348	0.1525	25
8	0.5370	0.5200	0.3000	0.5192	0.5102	0.4167	0.1624	23
9	0.5495	0.3285	0.1800	0.5260	0.4268	0.3788	0.1495	27
10	0.4239	0.0249	0.9200	0.4646	0.3390	0.8621	0.1629	22
11	0.5906	0.1280	0.8700	0.5498	0.3644	0.7937	0.1715	18
12	0.7248	0.0000	0.6400	0.6450	0.3333	0.5814	0.1638	21
13	0.5457	0.3534	0.6700	0.5239	0.4361	0.6024	0.1654	20
14	0.8113	0.3894	0.5900	0.7260	0.4502	0.5495	0.1859	11
15	0.7996	0.3783	0.4900	0.7139	0.4458	0.4950	0.1804	14
16	0.5953	0.8831	0.2400	0.5527	0.8105	0.3968	0.2049	6
17	0.6673	1.0000	0.0000	0.6005	1.0000	0.3333	0.2312	1
18	0.8813	0.8610	0.1300	0.8082	0.7825	0.3650	0.2264	3
19	0.7938	0.7877	0.7800	0.7080	0.7019	0.6944	0.2272	2
20	0.8735	0.7102	0.6300	0.7981	0.6331	0.5747	0.2194	4
21	0.8366	0.5920	0.6000	0.7537	0.5507	0.5556	0.2026	8

EXP. No.	GRG Taper	GRG HAZ width	GRG Circularity	GRC Taper	GRC HAZ width	GRC Circularity	GRG	grade
22	0.8171	0.0021	0.8400	0.7322	0.3338	0.7576	0.1849	12
23	1.0000	0.2386	0.5300	1.0000	0.3964	0.5155	0.2037	7
24	1.0778	0.0706	0.6100	1.1843	0.3498	0.5618	0.2174	5
25	0.8191	0.3700	0.5500	0.7343	0.4425	0.5263	0.1842	13
26	0.8560	0.2192	0.4700	0.7764	0.3904	0.4854	0.1789	17
27	0.9689	0.1930	0.3300	0.9414	0.3825	0.4274	0.1904	9

The optimal parameter setting determined by using Grey based Taguchi method is *L*3*γ*1*w*3*p*2*f*1. The grey relational grade of each factor level is calculated as the average for the same level in each column. Microscopic view of drilled micro hole is given below in fig. 5.34.

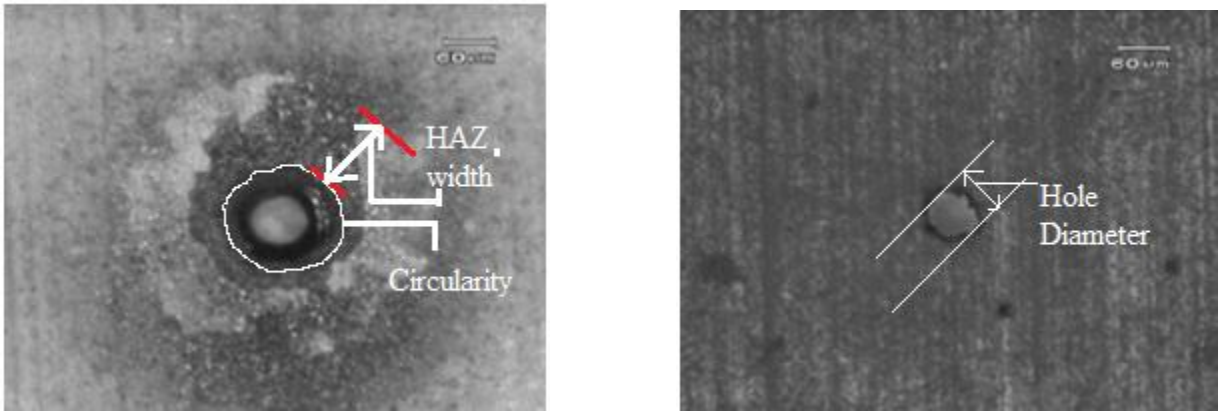

Fig.5.34 (a,b) Microscopic view of the microhole (a) Hole at top, (b)Hole at bottom

5.2.1.3.2.1 Confirmation test for multi objective optimization

Three additional experiments are performed with optimal parameter settings of multi objective optimization and average of those three results is taken for confirmation test. Table 5.17 furnishes the predicted value of grey relation grade and result of confirmation test.

Table 5.17 Results of confirmation test

	Initial Parameter setting	**Optimal parameters**	
		Prediction	**Experiment**
Level	*L3γ1w3p2f1*	*L2γ3w1p2f2*	*L2γ3w1p2f2*
Taper (rad)	0.0561	-	0.0484
HAZ width (mm)	0.2084	-	0.2005
Circularity	0.923		0.928
Grey Relation Grade	0.2272	0.2312	0.2381

.

From the table it is found that hole quality characteristics viz. Hole taper is improved from 0.0561 rad to 0.0484 rad (13.72%), HAZ width is improved from 0.2084 to 0.2005 (3.79%) and circularity improved marginally from 0.923 to 0.928 (0.54%). Lamp current at 24.5 amp, pulse frequency at 3 kHz, pulse width at 1%, assist air pressure at 0.7 kg/cm^2 and focal distance at zero position (focal point on the top surface) are the optimal parameter settings to get desired machining response.

5.2.2 Parametric study on laser beam microdrilling of SiC30BN nanocomposite material with argon gas as an assist medium.

Some previous research work indicates that environment in & around the thermal machining zone have a great impact on quality of responses. For laser machining operation especially for laser percussion microdrilling process, use of different kind of reactive or inert gas have some affect on the machining responses. From previous literature review it is found that reactive gases like oxygen, nitrogen may have some adverse affect during the machining for which inert gases like helium, or argon is the most preferable one to use as an assist gas. Property like complete inertness at very high temperature makes inert gases a suitable alternative to get desired homogeneity in & around the drilled microhole by laser beam. In this experimental investigation industrial argon gas with 99% purity has been used to study the effect on machining characteristics. Cooling efficiency of argon gas is much more than any other inert gas and low cost than other industrial inert gas makes it's a suitable alternative of compressed air as an assist gas for laser micromachining process. Properties of argon gas is listed below in table 5.18,

Table 5.18 Properties of argon gas [88]

Properties	**Unit**	**Values**
Phase at STP		Gas
Boiling Point	°C	-185.848
Density at STP	kg/m^3	1.784
Heat of vaporization	kJ/kg	162.3
Thermal conductivity	$W/(m^2 \times K)$	17.72×10^{-3}
Specific gravity		1.39
Specific heat (Cp)	kJ/kg×°C	0.523

5.2.2.1 Experimental Planning

Table 5.19 Machining Parameters and Their Levels

Process Parameters	**Level**		
	1	2	3
Lamp current (*L*)(amp)	23.5	24.5	25.5
Pulse frequency (*γ*)(kHz)	1	2	3
Pulse width (*w*) (%)	2	4	6
Assist gas pressure (Argon) (*p*) (kg/cm^2)	0.4	0.7	1.0
Focal distance (*F*) (μm)	-200	0	200

In this study also, the range of selected parameters are kept constant as previous study though the assist gas is changed to argon. Taguchi methodology for five factors at three levels is used for the implementation of the plan of orthogonal array experiments. A L27 orthogonal array with five columns and 27 rows is employed in this work

STM 6 Olympus measuring microscope At 10 X magnification is used to capture the images of diameter of the micro hole. A Mitutoyo manufactured digital micrometer with 1 μm resolution is used to measure the thickness of the workpiece material. Images of microholes are captured by the Olympus manufactured optical microscope (STM 6), from where the hole diameter are measured by image analysis software through Feret's diameter measurement technique. This measurement procedure is replicated 3 times for every hole and the average is taken for further analysis. Then HAZ width and hole taper is measured by equ no. 5.12& 5.13 respectively whereas hole circularity is measured by image j software.

5.2.2.2 Results and Discussion

Machining responses, i.e., hole taper, HAZ width and circularity are calculated as per previously give formulae. Experimental results are documented in the table 5.20 given below,

Table 5.20 Experimental lay out and Results

EXP. No.	Lamp Current	Pulse Frequency	Pulse Width	Assist Gas Pressure	Focal Distance	Taper	HAZ width	Circularity
1	1	1	1	1	1	0.080750	0.20350	0.9240
2	1	1	1	1	2	0.063720	0.2170	0.9190
3	1	1	1	1	3	0.061940	0.20380	0.9140
4	1	2	2	2	1	0.133490	0.201630	0.9280
5	1	2	2	2	2	0.120300	0.189630	0.9250
6	1	2	2	2	3	0.099370	0.208880	0.9150
7	1	3	3	3	1	0.087340	0.182500	0.9010
8	1	3	3	3	2	0.081150	0.160880	0.8950
9	1	3	3	3	3	0.079940	0.195500	0.8850
10	2	1	2	3	1	0.092180	0.250380	0.9290
11	2	1	2	3	2	0.075930	0.231750	0.9040
12	2	1	2	3	3	0.062850	0.254880	0.8940
13	2	2	3	1	1	0.080310	0.191000	0.9220
14	2	2	3	1	2	0.054422	0.184500	0.9060
15	2	2	3	1	3	0.055560	0.186500	0.9020
16	2	3	1	2	1	0.075471	0.095250	0.8900
17	2	3	1	2	2	0.068455	0.074125	0.8840
18	2	3	1	2	3	0.047596	0.099250	0.8860
19	3	1	3	2	1	0.056129	0.112500	0.9340
20	3	1	3	2	2	0.048354	0.126500	0.9370
21	3	1	3	2	3	0.051957	0.147875	0.9260
22	3	2	1	3	1	0.053854	0.254500	0.9280
23	3	2	1	3	2	0.036029	0.211750	0.9120
24	3	2	1	3	3	0.028444	0.242125	0.9070
25	3	3	2	1	1	0.053664	0.188000	0.9100
26	3	3	2	1	2	0.050061	0.215250	0.8960
27	3	3	2	1	3	0.039063	0.220000	0.9030

The observed data from the set of experiments have been used as inputs to MINITAB software for parametric optimization i.e for achieving minimum taper and HAZ width with maximum circularity condition.

5.2.2.2.1 Parametric Analysis

Statistical software MINITAB is used here to get response table of means of machining responses. The effects of the process parameters such as the lamp current, pulse frequency, pulse width, assist gas pressure and focal length on the hole taper, HAZ width and hole circularity, during laser microdrilling are graphically represented (Origin 6.1 software) by plots 5.35-5.37 given below,

From the figure 5.35 it is observed that hole taper slightly decreases with increase in lamp current upto mid level (24.5 amp) after that sharply increases with increase in lamp current. Generally higher thermal energy is add into the process by increase the lamp current which leads to decrease in taper by uniform material removal throughout the drilled hole. But further increase in lamp current results in generation of comparatively more melt pool which may removed properly from machining zone thus increase in hole taper.

Comparatively low energy beam interacts with workpiece at higher pulse frequency results in non uniform melt pool generation on the machining zone may results in increase in hole taper. Increase in Pulse width results in uniform material removal from machining zone due to high peak power. For which taper shows a decreasing tendency upto mid level of pulse width but further increase in Pulse width causes higher heating value in top surface than bottom surface results in increase in taper. It is found that, Taper increases with gas pressure upto 2^{nd} level and thereafter starts decreasing. At initial stage, lower value of assist gas pressure is not capable to removal of molten debris from the machining zone results in increase in hole taper but further increase in assist gas pressure results in uniform removal of debris in & around the drilled micro hole, leads to decrease in taper. It has been shown from the figure that hole taper decreases with increase in Focal Distance. Equality in material removal from machining zone due to travel of the focal point towards the top surface of workpiece and 200 μm under the top surface, generates low hole taper.

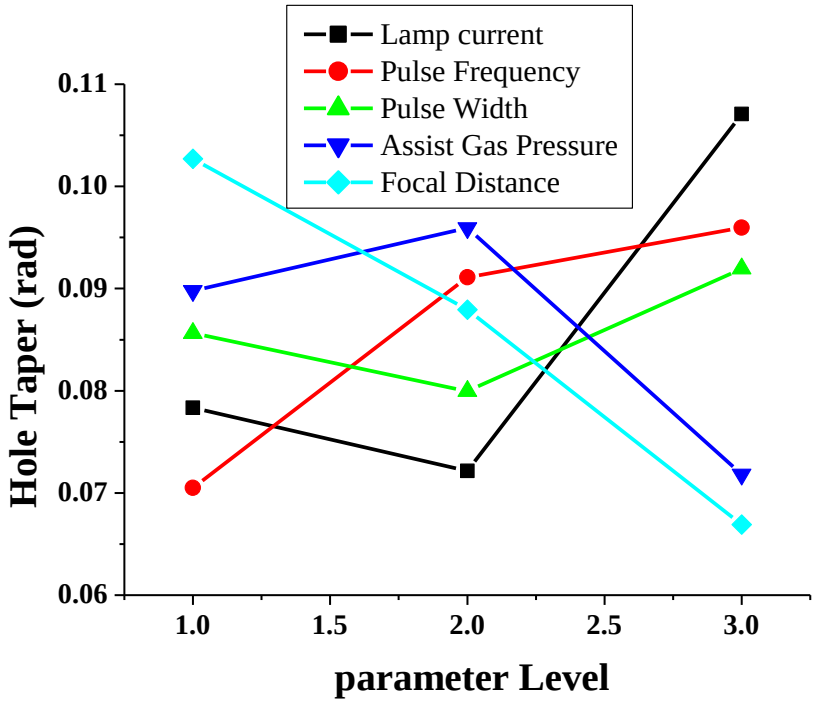

Fig.5.35 Effects of Nd:YAG laser microdrilling process parameters on hole taper.

From the figure it is observed that HAZ width increases monotonically over the entire range lamp current. As per know lamp current excites the pumping action to produce more laser, results in integration of more thermal energy into the process leads to increase in HAZ width. HAZ width decreases with increase in pulse frequency throughout the range due to generation of comparatively low energy beam at higher value of pulse frequency. HAZ width shows a marginal increasing tendency upto mid level of pulse width after which decreases gradually. At lower pulse widths less HAZ is generated, than that of higher pulse widths due to less interaction time and heat diffusion between laser beam and workpiece material and vice versa. HAZ width is found to be decreases upto mid level thereafter increase with increase in assist gas pressure. Cooling effect of assist gas, helps to reduce HAZ width upto mid level but further increase in assist gas pressure generates turbulence on the machining zone, results in uneven heating on the spot of irradiation which may leads to increase in HAZ width. It has been observed that HAZ width fractionally increases upto mid level of focal distance then decreases with further increase in focal distance.

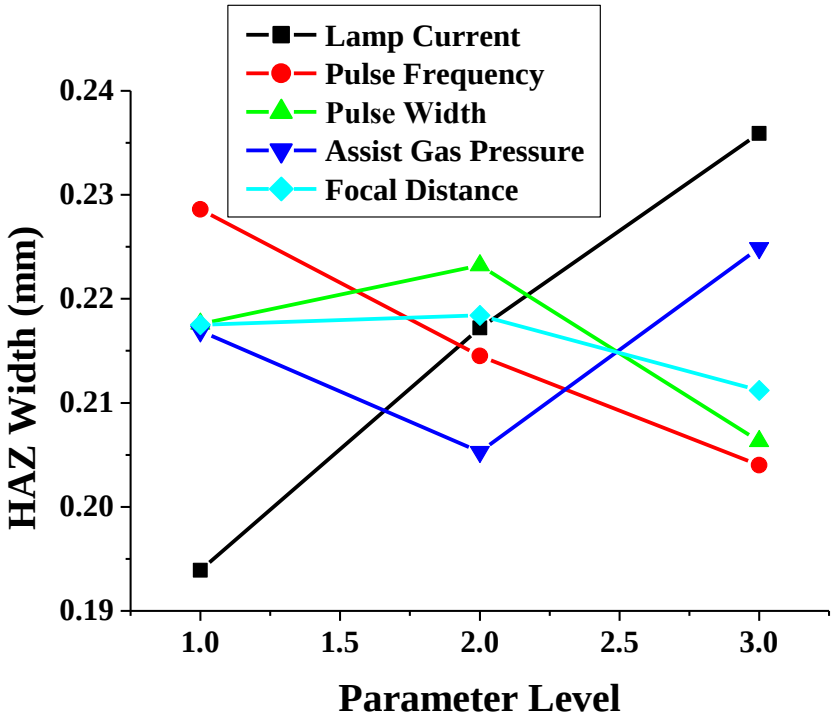

Fig.5.36 Effects of Nd:YAG laser microdrilling process parameters on HAZ width.

Initially when focal distance changed from -200 µm above the top surface to the top surface of the workpiece, the energy density on the irradiation spot is increased thus HAZ width marginally increased. After that, spot of irradiation moves under the top surface which may decrease the energy density on the top surface. Thus HAZ width decreases.

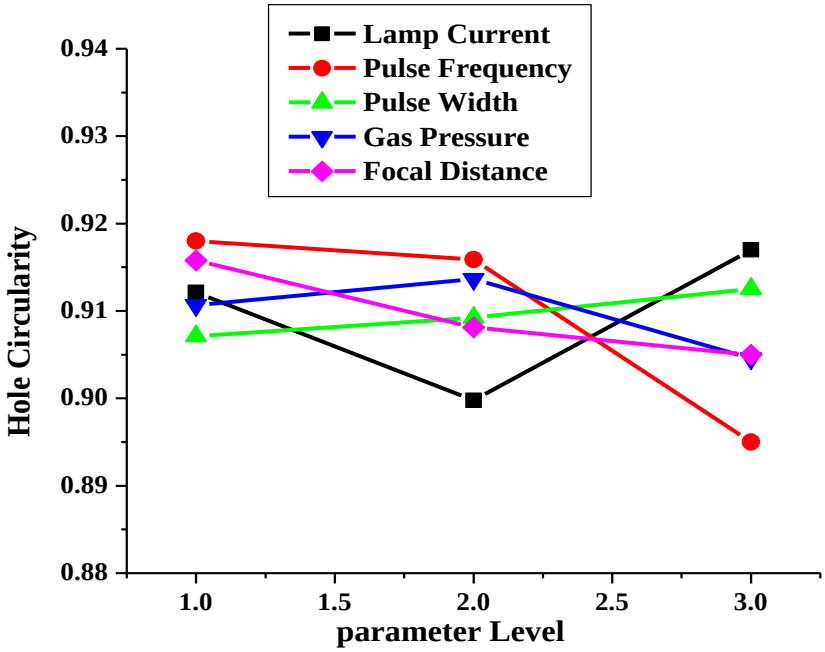

Fig.5.37 Effects of Nd:YAG laser microdrilling process parameters on hole circularity.

It has been seen from the graph plot that with increase in lamp current, Circularity decreases up to mid level (24.5 amp), and then it increases. Generally, higher laser beam power generates higher thermal energy which produces better circularity by uniform material removal from machining zone, leads to create circular hole entry. Increase in pulse frequency means lesser time between two consecutive pulses which results instant melting as well as vaporization from the top surface of the workpiece. For aforesaid condition, unevenness may create in & around the machining zone on top surface, thus circularity decreases. Hole circularity shows a linear relationship with pulse width. Increase in average power along with more interaction time may generate uniform material removal from top surface which affects the geometrical aspects and circularity increases. It is observed from the plot that hole circularity marginally increases with gas pressure upto mid level (0.7 kg/cm^2) and thereafter starts decreasing. Increased assist gas pressure helps to remove molten as well as gaseous debris from machining zone and helps to create proper geometrical shaped drilled hole, results in increase in circularity. Uneven heating produced by turbulence due to higher value of assist gas pressure may generate non uniform material removal from top surface of the workpiece. This is may be reason behind observed quality characteristics. When the focal distance changes, the area of interaction between laser

beam and workpiece material on the top surface along with power density changes, that's may lead to decrease in hole circularity.

5.2.2.2.2 ANOVA of machining responses

Table 5.21 Results of ANOVA for hole taper (Argon)

Source	Degrees of Freedom	Sum of Square	Mean of Square	F	P	% Contribution
Lamp current	2	0.006883	0.003442	44.24	0.000	34.49
Pulse frequency	2	0.003581	0.001791	23.02	0.000	17.95
Pulse width	2	0.000487	0.000243	3.13	0.071	2.44
Assist gas pressure	2	0.002665	0.001332	17.13	0.000	13.35
Focal distance	2	0.006341	0.003170	40.75	0.00	31.77
Error	16	0.001245	0.000078			
Total	26	0.021202				
S	R-sq		R-sq(adj)		R-sq(pred)	
0.0060581	95.96%		93.44%		88.50%	

Whereas from the table 5.21 it is found that all the process parameters other than pulse width are statistically significant for hole taper. Percentage contribution column in ANOVA result table indicates at the degree of influence of all the process parameters on the hole taper. According to the table it is found that Lamp Current (34.49%) has the most dominant factor followed by Focal Distance (31.77%), Pulse Frequency(17.95%) , Assist gas pressure (13.35%) and Pulse width (2.44%). It can be concluded that the data for each response are well fitted in the developed models and the results of regression analysis is also desirable for hole taper given in table no. 5.21.

Table 5.22 Results of ANOVA for HAZ width (Argon)

Source	Degrees of Freedom	Adj SS	Adj MS	F	P	% of contribution
Lamp current	2	0.002440	0.001220	7.75	0.004	3.99
Pulse frequency	2	0.011534	0.005767	36.66	0.000	18.91
Pulse width	2	0.013426	0.006713	42.67	0.000	22.01
Assist gas pressure	2	0.032320	0.016160	102.73	0.000	52.99
Focal distance	2	0.001274	0.000637	4.05	0.038	2.1
Error	16	0.002517	0.000157			
Total	26	0.063510				
S		R-sq		R-sq(adj)		R-sq(pred)
0.0125422		96.04%		93.56%		88.71%

From the ANOVA analysis at 95% confidence level it is observed that all the process variables are statistically significant. The values of regression analysis, i.e., R-sq (96.04%), R-sq (adj) (93.56%) & R-sq (pred) (88.71%) indicates at the acceptability of the outcome within the pre-defined design space. All the controllable process variables have a great impact on machining responses. From the calculation of contribution percentage it is found that assist air pressure is the mostly influenced followed by pulse width, pulse frequency and lamp current. Focal distance is the least contributed process variable.

Table 5.23 Results of ANOVA for hole circularity (Argon)

Source	Degrees of Freedom	Sum of Square	Mean of Square	F	P	% of Contribution
Lamp current	2	0.001251	0.000626	13.66	0.000	6.87
Pulse frequency	2	0.013056	0.006528	142.53	0.000	71.71
Pulse Width	2	0.001915	0.000957	20.90	0.000	10.52
Assist gas pressure	2	0.000347	0.000173	3.73	0.045	1.88
Focal distance	2	0.001643	0.000822	17.94	0.000	9.02
Error	16	0.000733	0.000046			
Total	26	0.018945				
S	R-sq		R-sq(adj)		R-sq(pred)	
0.0067676	96.13%		93.71%		88.98%	

If the value of P is less than 0.05, the process parameter is considered significant. From the table 5.23 it is found that all the process parameters are statistically significant for circularity. Percentage contribution column in ANOVA result table indicates at the degree of influence of all the process parameters on the microhole characteristics. According to the table it is found that Pulse Frequency (71.71%) has the most dominant factor followed by Pulse width (10.52%), Focal Distance (9.02%), Lamp Current (6.87%) and Assist gas pressure (1.88%). From the table it has been observed that S-values of the responses are smaller and R-Sq, R-Sq (adj) and R-Sq (pred) values of responses are moderately high, from which it can be concluded that the data for each response are well fitted in the developed models.

5.2.2.3 Determination of optimal parameter settings

5.2.2.3.1 Single objective optimization based on Taguchi methodology

Experimental observations are further used to determine the optimal parameter settings. Firstly the experimental results are used to carry out single objective optimization by Taguchi based optimization technique. The results of single optimization for each machining responses are listed in table no. 5.24.

Table5.24 Single objective optimization of responses

Machining responses	**Optimal parameter settings**	**Optimal Value**
Hole taper (rad)	L3 γ3 w1 p1 F3	0.0146
HAZ width (mm)	L2 γ3 w3 p2 F2	0.0682
Circularity	L3 γ1 w3 p2 F1	0.940

5.2.2.3.1.1 Confirmation test for Taguchi based single objective optimization

Additional five experiments have been carried out as per optimal parametric conditions for each of the machining responses. Average is taken and listed in the table of confirmation test given below.

Table 5.25 Confirmation test of single optimization technique

Machining responses	**Optimal parameter settings**	**Optimal Value**	**Experimental value (average)**	**% of error**
Hole taper (rad)	L3 γ3 w1 p1 F3	0.0146	0.0155	6.16
HAZ width (mm)	L2 γ3 w3 p2 F2	0.0682	0.0701	2.79
Circularity	L3 γ1 w3 p2 F1	0.940	0.929	1.17

5.2.2.3.2 Taguchi based Grey relation analysis for multi objective optimization

Also multiple objective optimization is performed here by Grey based Taguchi optimization technique. As per previously said, all the normalized grey value and grey relation coefficient values are documented in table no. During the calculation of the grey relation grade 40% weightage is given on hole taper and HAZ width whereas 20% weightage is given on hole circularity.

Table 5.26 Grey Relation analysis results

EXP. No.	GRG Taper	GRG HAZ width	GRG Circularity	GRC Taper	GRC HAZ width	GRC Circularity	GRG	grade
1	0.5426	0.6472	0.7547	0.5223	0.5863	0.6709	0.1925	12
2	0.7232	0.4514	0.6604	0.6437	0.4768	0.5955	0.1891	13
3	0.8654	0.5833	0.5660	0.7879	0.5455	0.5354	0.2135	4
4	0.3888	0.7472	0.8302	0.4500	0.6642	0.7465	0.1983	9
5	0.5309	0.7792	0.7736	0.5160	0.6936	0.6883	0.2072	6
6	0.5661	1.0000	0.7358	0.5354	1.0000	0.6543	0.2483	1
7	0.4758	0.9431	0.3208	0.4882	0.8978	0.4240	0.2131	5
8	0.5059	0.9806	0.2075	0.5029	0.9626	0.3869	0.2212	2
9	0.6865	0.9028	0.0189	0.6146	0.8372	0.3376	0.2161	3
10	0.8261	0.0000	0.8491	0.7419	0.3333	0.7681	0.1946	10
11	0.9365	0.0542	0.3774	0.8872	0.3458	0.4454	0.1941	11
12	1.0000	0.0944	0.1887	1.0000	0.3557	0.3813	0.2062	7
13	0.4022	0.6486	0.7170	0.4554	0.5873	0.6386	0.1816	15
14	0.4741	0.5972	0.4151	0.4874	0.5538	0.4609	0.1696	18
15	0.7425	0.5292	0.3396	0.6600	0.5150	0.4309	0.1854	14
16	0.2918	0.7333	0.1132	0.4138	0.6522	0.3605	0.1662	19
17	0.3972	0.6722	0.0000	0.4534	0.6040	0.3333	0.1632	20
18	0.6865	0.8167	0.0377	0.6146	0.7317	0.3419	0.2023	8
19	0.1839	0.2139	0.9434	0.3799	0.3888	0.8983	0.1624	21
20	0.2258	0.3347	1.0000	0.3924	0.4291	1.0000	0.1762	17
21	0.5711	0.3403	0.7925	0.5383	0.4311	0.7067	0.1764	16
22	0.2232	0.0014	0.8302	0.3916	0.3336	0.7465	0.1465	24
23	0.4724	0.0042	0.5283	0.4866	0.3343	0.5146	0.1437	25
24	0.5318	0.1847	0.4340	0.5164	0.3801	0.4690	0.1508	23
25	0.0000	0.1778	0.4906	0.3333	0.3782	0.4953	0.1279	27
26	0.2952	0.1319	0.2264	0.4150	0.3655	0.3926	0.1302	26
27	0.5017	0.4181	0.3585	0.5008	0.4621	0.4380	0.1576	22

The optimal parameter setting determined by using Grey based Taguchi method is *L1γ2w2p2f3*. The grey relational grade of each factor level is calculated as the average for the same level in each column.

5.2.2.3.2.1 Confirmation Test on results of multi objective optimization

To verify the feasibility of the proposed Taguchi based grey method, confirmation test is carried out. The results of confirmation test is given below in table no.5.27

Table 5.27 Results of confirmation test

	Initial Parameter setting	**Optimal parameters**	
		Prediction	**Experiment**
Level	*L1γ1w1p1f3*	*L1γ2w2p2f3*	*L1γ2w2p2f3*
Taper (rad)	0.0483	-	0.0403
HAZ width (mm)	0.1125	-	0.0728
Circularity	0.914		0.918
Grey Relation Grade	0.2312	0.2411	0.2414

Three additional experiments are performed with levels at optimal parameter settings and average of those three results is taken for confirmation test. Table furnishes the predicted value of grey relation grade and result of confirmation test. From the table it is found that hole quality characteristics viz. taper is improved from 0.0483 to 0.03403 (16.56%), HAZ width is improved from 0.1125 mm to 0.0728 mm (35.28 %) and circularity is improved from 0.914 to 0.918 (0.44%). Optical image of drilled microhole on the top surface of workpiece at different assist medium (compressed air and argon gas) with corresponding optimum parameter settings are given in fig. 5.38 and 5.39.

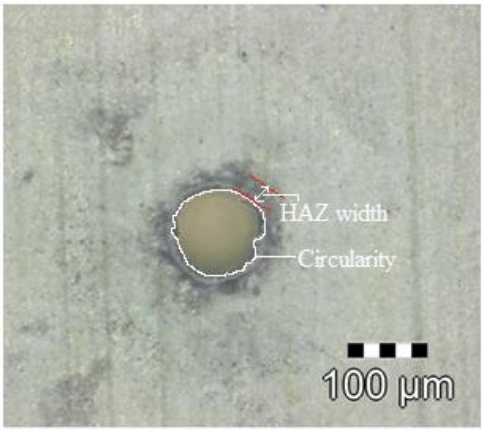

5.38 Microscopic view of microhole at top surface with optimum parameter settings (*L2γ3w1p2f2*) with compressed air

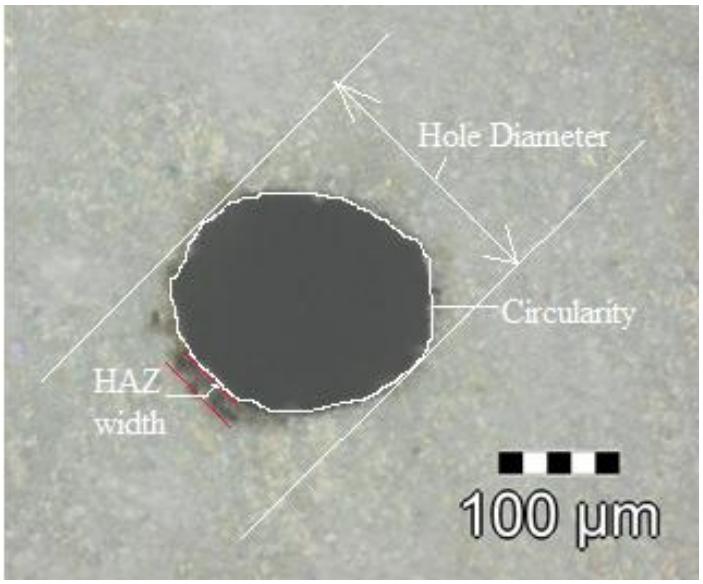

5.39 Microscopic view of microhole at top surface with optimum parameter settings (*L1γ2w2p2f3*) with Argon gas

5.2.2.4 Outcome of the study

Solid state flash pumped Nd:YAG laser with 1064 nm wavelength is applied in the experimental study to make through microhole via laser percussion drilling technique. Silicon carbide 30% boron nitride nanocomposite material is chosen as workpiece material. Taguchi based L_{27} orthogonal array technique is used here to design and carry out the experiments. Different kind of assist gas, i.e. compressed air and argon is applied here to carry out the laser microdrilling operation on ceramic nanocomposite material. Same design space is applied during application of different assist gas. Parametric study and their corresponding phenomenon are discussed elaborately. From the ANOVA analysis it is concluded that all the process parameters are statistically significant for the three machining responses. Taguchi based Grey relation analysis has been carried out for multiobjective optimization. Confirmation test after multiobjective optimization indicates at the enhancement of all the process criteria at predicted process parameter settings simultaneously which justify the application of the technique for multiobjective optimization for laser microdrilling of SiC-30BN nanocomposite material.

5.2.3 Comparative study of the effect of different assist medium on laser micro-drilling of SiC30BN

During laser microdrilling of SiC-30BN nanocomposite by pulsed Nd:YAG laser at 1064 nm wavelength two different environment, i.e., compressed air and argon gas is used at same parametric condition when other all the controllable process variable are kept as same parametric settings on same workpiece. A comparative study is conducted here to study the effect of different assist gas/ environment on preselected machining response. From figure 5.38 & 5.39 it is observed that the top microhole diameter for argon gas is more than the top hole diameter get during application of compressed air. The shear stress applied by argon gas on the melt pool gives more momentum than the force applied by compressed air leads to quick removal/displacement of the molten debris from the spot of irradiation. Thus that kind of micro hole is formed with varied diameter along with different assist gas [89].

From figure 5.40 (a-e) it is observed that the effect of environment is very much visible on hole taper with each process parameters at three different levels. Deviation in hole taper is much more during application of argon gas whereas deviation is comparatively less during application of compressed air. It is also viewed that minimum value of hole taper is less when argon gas is applied and average value of hole taper is much more when compressed air is used as assist gas. From the ANOVA results it is evident that lamp current in respect of average working power, is the most significant process parameter for both environment. The percentage contribution of lamp current is 57.04% and 34.49% for compressed air and argon gas as assist medium respectively.

Form figure 5.41 (a-e) Within the same design space, it is observed that the impact of argon gas on HAZ width is much more than compressed air as assist gas. Minimum value of HAZ width can be obtained when argon gas is used as assist gas. It also observed the average value of HAZ width is comparatively much less during application of argon as assist gas than compressed air as assist gas. The cooling efficiency of argon gas helps to cool down the machining zone more quickly than compressed air as well as oxygen present in compressed air helps to introduce more energy to the system by exothermic reaction, results in increase in HAZ width.

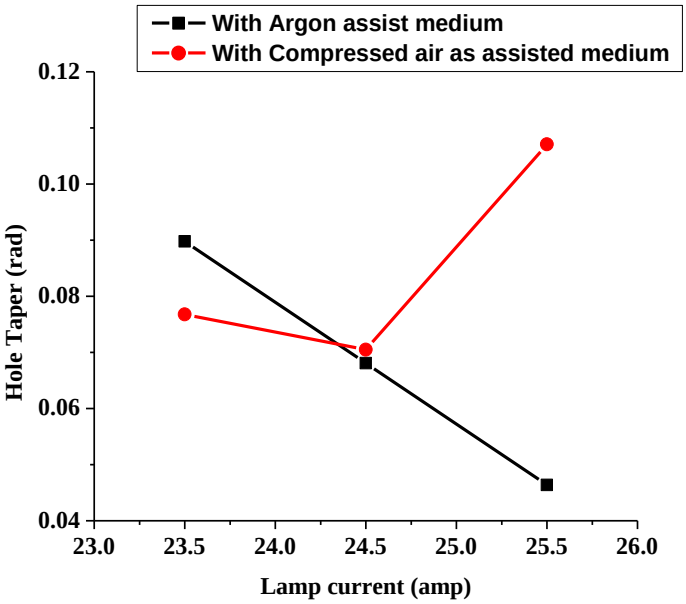
With Argon assist medium
With Compressed air as assisted medium
Hole Taper (rad)
0.12
0.10
0.08
0.06
0.04
23.0
23.5
24.0
24.5
25.0
25.5
26.0
Lamp current (amp)

(a)

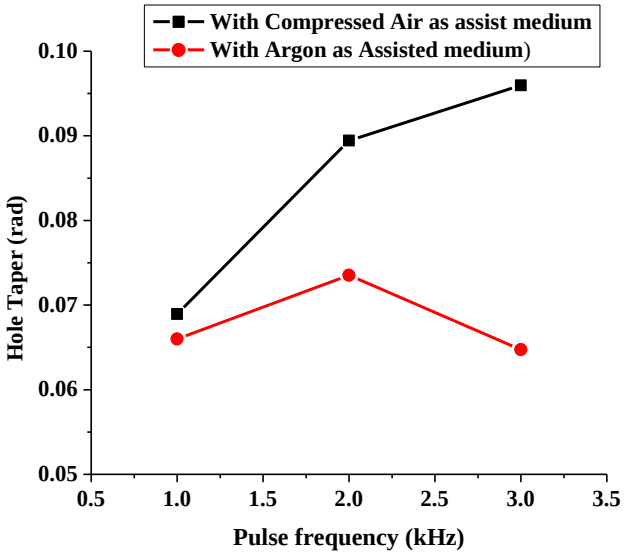
With Compressed Air as assist medium
With Argon as Assisted medium)
Hole Taper (rad)
0.10
0.09
0.08
0.07
0.06
0.05
0.5
1.0
1.5
2.0
2.5
3.0
3.5
Pulse frequency (kHz)

(b)

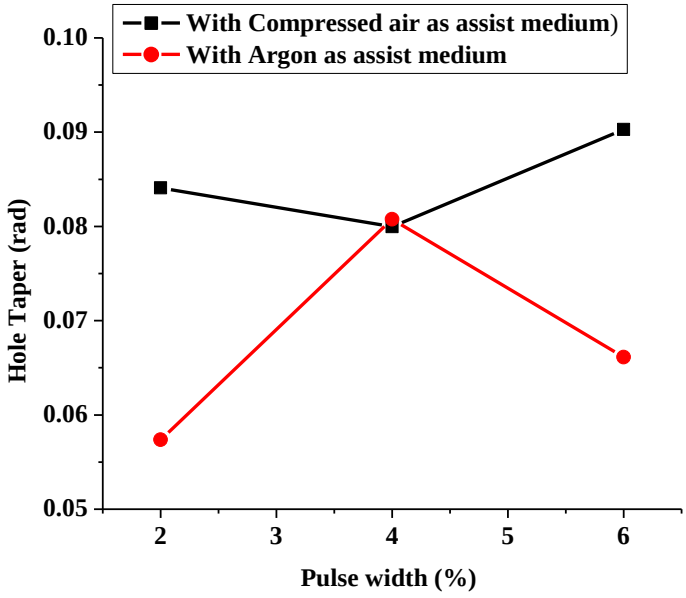
With Compressed air as assist medium)
With Argon as assist medium
Hole Taper (rad)
0.10
0.09
0.08
0.07
0.06
0.05
2
3
4
5
6
Pulse width (%)

(c)

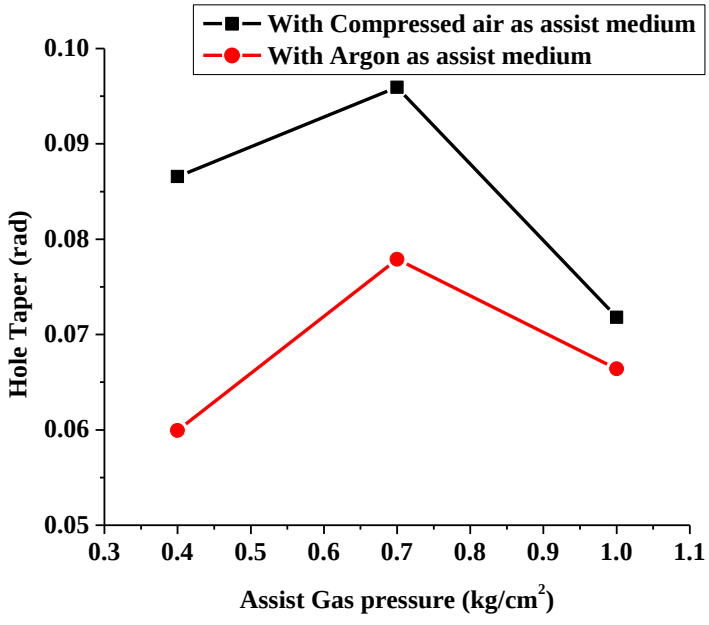
With Compressed air as assist medium
With Argon as assist medium
Hole Taper (rad)
0.10
0.09
0.08
0.07
0.06
0.05
0.3
0.4
0.5
0.6
0.7
0.8
0.9
1.0
1.1
Assist Gas pressure (kg/cm2)

(d)

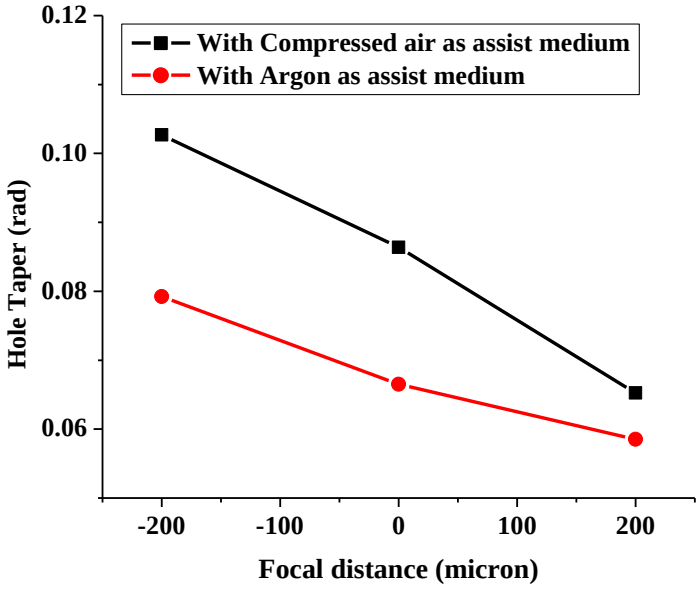

(e)

Fig.5.40 (a-e) Comparative plot of hole taper with different assist medium for controllable process variables.

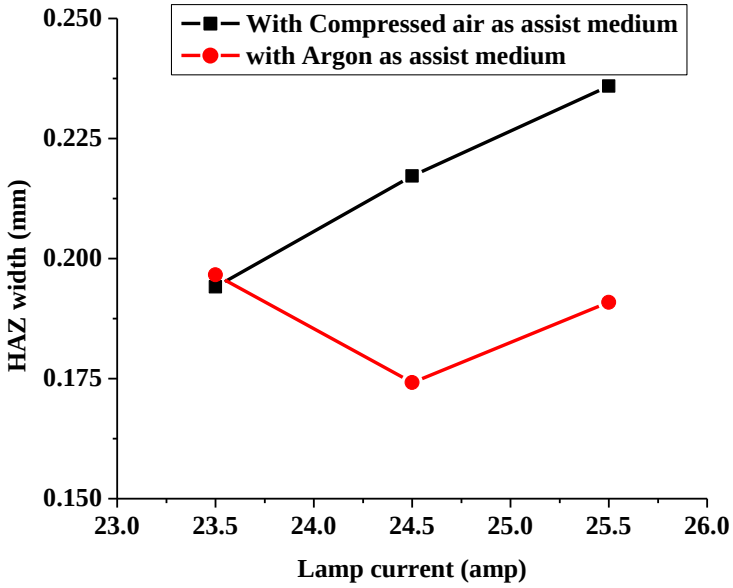

(a)

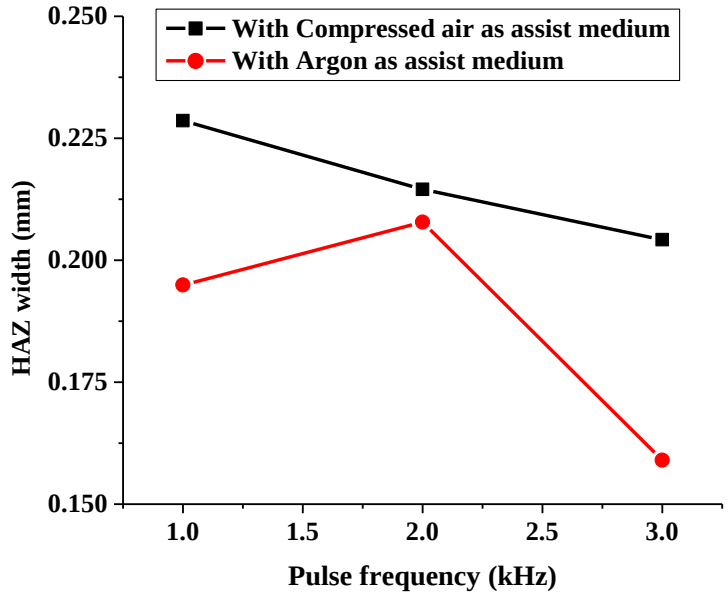
With Compressed air as assist medium
With Argon as assist medium
HAZ width (mm)
0.250
0.225
0.200
0.175
0.150
1.0
1.5
2.0
2.5
3.0
Pulse frequency (kHz)

(b)

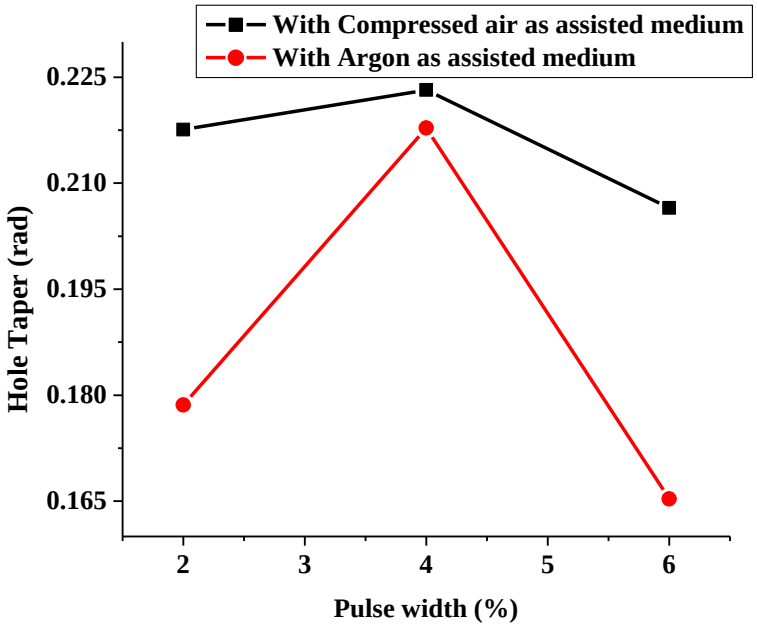
With Compressed air as assisted medium
With Argon as assisted medium
Hole Taper (rad)
0.225
0.210
0.195
0.180
0.165
2
3
4
5
6
Pulse width (%)

(c)

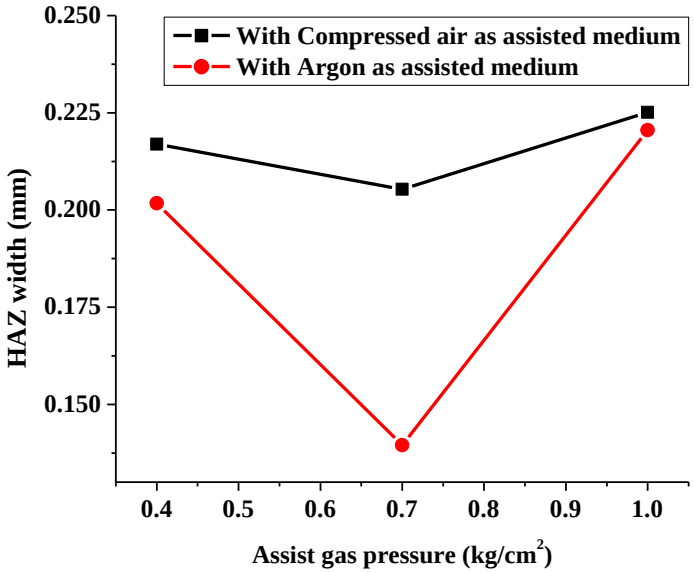

(d)

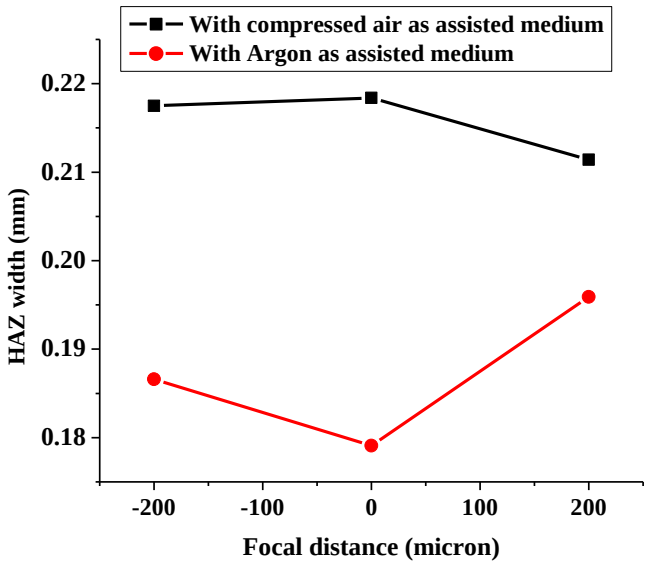

(e)

Fig.5.41 (a-e) Comparative plot of HAZ width with different assist medium for controllable process variables

Similarly, like hole taper, deviation for HAZ width is less when compressed air is used as assist gas. From the result of ANOVA it is evident that argon as the assist gas is most significant process variable (52.99%) whereas the compressed air is the third valuable contributor (12.75%) to heat affected zone width when used separately as assist gas during laser microdrilling of ceramic nanocomposite. Within the same design space, it is observed that the impact of argon gas on HAZ width is much more than compressed air as assist gas. Minimum value of HAZ width can be obtained when argon gas is used as assist gas. It also observed the average value of HAZ width is comparatively much less during application of argon as assist gas than compressed air as assist gas. The cooling efficiency of argon gas helps to cool down the machining zone more quickly than compressed air as well as oxygen present in compressed air helps to introduce more energy to the system by exothermic reaction, results in increase in HAZ width. On the other hand, higher surface tension on the machining zone along with increased viscosity of melt pool during application of compressed air results in more HAZ width than HAZ width obtain during application of argon gas [90]. Similarly, like hole taper, deviation for HAZ width is less when compressed air is used as assist gas. From the result of ANOVA it is evident that argon as the assist gas is most significant process variable (52.99%) whereas the compressed air is the third valuable contributor (12.75%) to heat affected zone width when used separately as assist gas during laser microdrilling of ceramic nanocomposite.

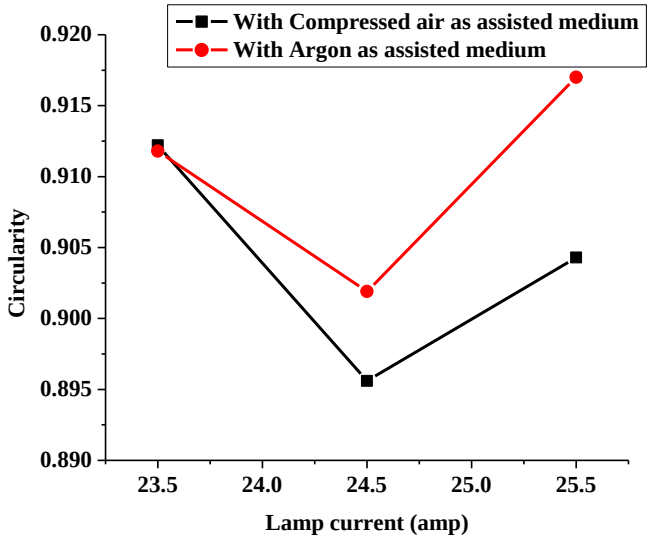

(a)

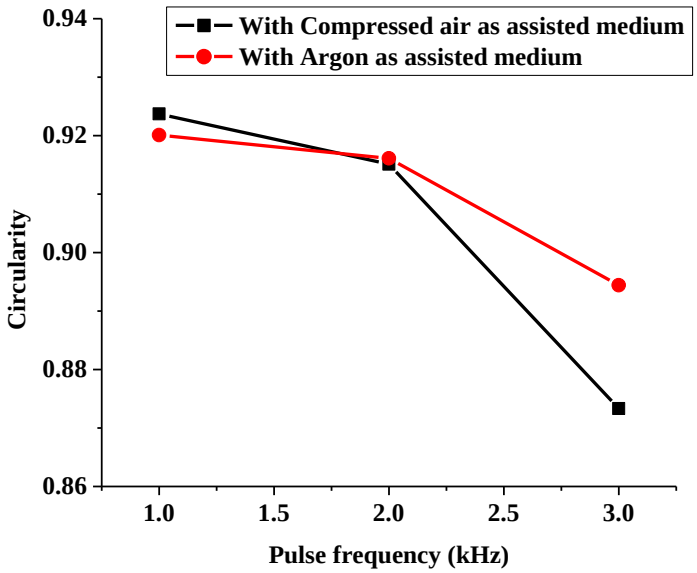
With Compressed air as assisted medium
With Argon as assisted medium
Circularity
0.94
0.92
0.90
0.88
0.86
1.0
1.5
2.0
2.5
3.0
Pulse frequency (kHz)

(b)

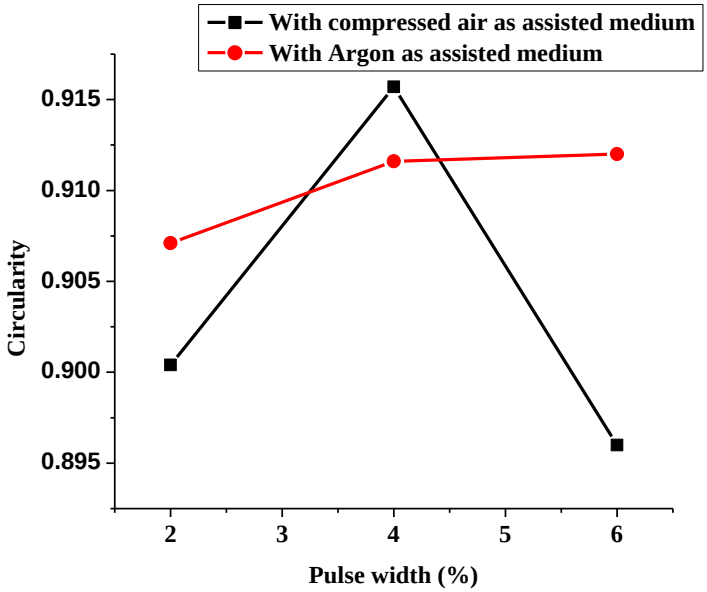
With compressed air as assisted medium
With Argon as assisted medium
Circularity
0.915
0.910
0.905
0.900
0.895
2
3
4
5
6
Pulse width (%)

(c)

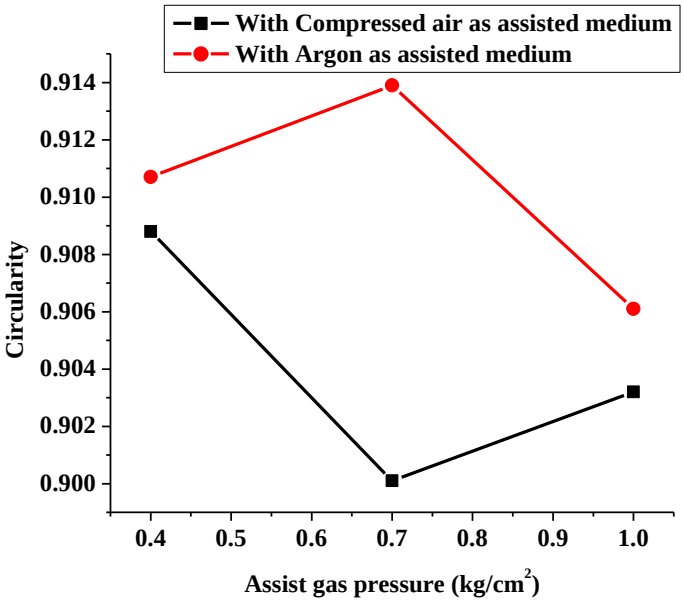

(d)

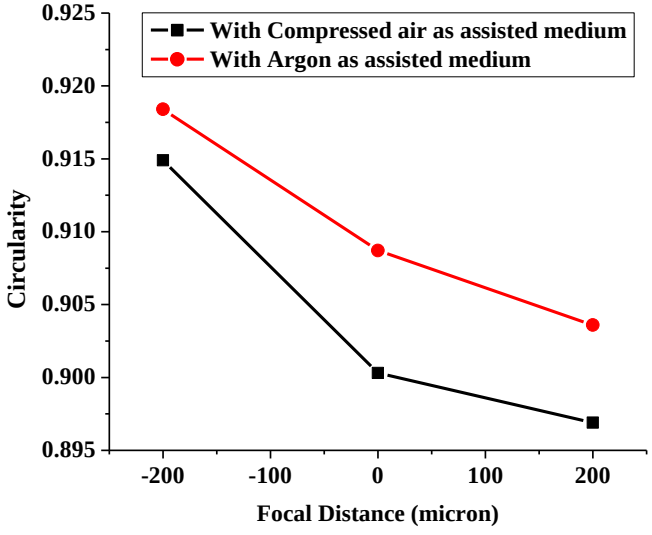

(e)

Fig.5.42 (a-e) Comparative plot of hole Circularity with different assist medium for controllable process variables

It is observed from the comparative plot 5.42 (a-e) that effect of environment in terms of different assist gas have little bit less effect on circularity of the hole other than focal distance and assist gas pressure. As the circularity of hole depends on the pressure of assist gas instead of the nature of it and same design space is used for both the assist gas, that kind of comparative plot is observed.

Chapter 6

6. Experimental studies on laser beam microcutting

In different types of laser based manufacturing techniques, laser cutting is characterized by high speed, reliable and full/semi automated 2-Dimentional material processing method to produce a high aspect ratio and clean cut width. During laser cutting process, a high intensity laser beam is focused on the target region of the workpiece which subsequently heats up the surface of the irradiate zone by absorbing the thermal energy of the laser beam. Cutting front is generally produced by expulsion of melt pool and vapour of the material from the machining zone by the assistance of pressurized gas flow coaxially/axially. From the quality and quantitative point of view assist the gas flow has a great impact on the laser cutting process. It helps to get cleaner cut width along with less heat affected zone (HAZ) in terms of quality aspect. Chemical reactions like oxidization at elevated temperature at the machining zone may enhance the material removal which indicates at the quantitative aspect. Now-a day, laser cutting process is applied in the industries to process a wide range of materials such as wood, ferrous and non ferrous metals, polymers, ceramics, composite materials, superalloys to nanocomposite materials also. In modern technologies, miniaturization is an important trend to fabricate microparts for biotechnological, microelectronics, telecommunication, MEMS, and medical applications. Laser beam micromachining is utilized for the generation of microproducts with better flexibility in the dimensional design. Photo-thermal or photochemical ablation is the mechanism behind the material removal in micron or in sub-micron range during laser beam micromachining operation. Laser beam with wavelength in the range in near infrared (1.06μm) to deep Ultraviolet (150nm) is commonly used in micromachining operation. Photon energy increases with shorter wavelength enhance the material removal, results in less thermal damages like melting, charring of adjacent unirradiate material. Pulsed Nd:YAG laser with shorter wavelength has great ability for micromachining because of higher laser beam intensity at low mean power, good focusing characteristics with small spot diameter.

6.1 Parametric study of laser microcutting on Hydroxyapatite (HAp) bioceramic with compressed air as an assist medium

Compared to metals, ceramics have many advantages such as high-temperature strength, high hardness, chemical resistance, low density, superior wear resistance combined with a low coefficient of friction and lower thermal and electrical conductivity. Ceramic materials can keep these properties at elevated temperature also [91]. Ceramics that are considered for bio-applications are commonly termed as bio-ceramics. These are usually polycrystalline inorganic silicates, oxides, and carbides. They are refractory in nature and possess high compressive strength. Bio-ceramics can be sub-classified as bioinert, bioactive, and biodegradable materials. During recent decades, both an ageing population and a democratization of high-risk sports have led to a surge of bone-related diseases and bone fractures, which must be treated. There are many instances where repair or replacement of a considerable part of lost bone tissue is necessary. Substituting lost bone tissue with artificial material have some advantages as well as drawbacks like immune reaction and subsequent rejection of the implant also. Therefore, the artificial bone replacement material must have some similarities in structure and composition to human bone [92]. One of the most widely used materials in this field is hydroxyapatite (HAp), $Ca_5(PO_4)_3(OH)$. Hydroxyapatite composites have been successfully used for the repair, reconstruction, and replacement of diseased or damaged parts of the body, especially bone due to its excellent biocompatibility, osteo-conductivity, non-Inflammatory, non-Immunogenic and low chemical reactivity. HAp is known to be bioactive and biocompatible due to its chemical similarity with bone minerals. Apart from chemical composition and mechanical properties of this artificial material, a suitable modification of the surface topography can increase the bioactivity and may achieve a stronger bone-implant fixation [93]. Apart from that, coating of hydroxyapatite is often applied on metallic implants (most commonly titanium/titanium alloys and stainless steels) to alter the surface properties [94]. Hydroxyapatite has also employed in forms such as powders, porous blocks or beads to fill bone defects or voids. These may arise when large sections of bone have had to be removed (e.g. bone cancers) or when bone augmentations are required (e.g maxillofacial reconstructions or dental applications) [95]. The brittle nature of HAp with low fracture toughness, make this material hard to machine with any contact type conventional or non conventional machining process [93]. The effect of process parameter on machining response during Direct laser interference patterning (DLIP) method to

produce periodic patterns on hydroxyapatite by A Nd:YAG laser operating at 266 and 355nm wavelengths and a pulse duration of 10 ns has also studied [96]. Some researchers also try to find out the effect of pulsed Nd:YAG laser treatment for plasma-sprayed hydroxyapatite coatings to get wide range of microstructures [97]. An extensive research work is much needed to generate technology guidance for direct laser processing in terms of microgrooving of such a useful bio-material for modern medical apparatus industries.

Experimental investigation has been carried out here to check the feasibility of laser grooving of Hydroxyapetite in its pure form by nano-second pulsed Nd:YAG laser with wavelength in near infrared region. Lamp current, pulse frequency, assist air pressure, and cutting speed are chosen as independent controllable process parameters whereas pulse width kept fixed during the experiment. Overcut and Groove Depth are chosen as machining response. Taguchi method coupled with grey relational analysis is, therefore, used as statistical design of experiment tools for simultaneous optimization of both the quality characteristics. With the frame of this experimental study, the effects of process parameters on groove qualities are also discussed. The effectiveness of the proposed optimization process is demonstrated and validated by experimental results.

6.1.1 Experimental details:

Hydroxyapatite (HAp), $Ca_5(PO_4)_3(OH)$ bioceramic material have been used for experimental study. Properties of hydroxyapatite (HAp) bioceramic material are listed in Table 6.1.

Table 6.1 Properties of hydroxyapatite (HAp), $Ca_5(PO_4)_3(OH)$ bioceramic [88]

Property	**Value**
Density	2.4625 g/cm^3
Bending Strength	38 MPa
Modulus of Elasticity	76 GPa
Toughness	1.31 MPa m $^{1/2}$
Hardness	3 GPa
Co efficient of Heat expansion	11.6×10^{-6} K^{-1}
Co efficient of Lattice thermal expansion	9.9×10^{-6} / ˚C

The ranges of aforesaid process parameters are selected on the basis of trial experiments which are conducted by using one factor at a time approach. During the trial experiments it is observed

that the effect of pulse width on machining responses is very less, relatively with other process parameter for which it is kept constant during the experimental runs. In the experiment single pass grooving operation has been carried out. Taguchi methodology for four factors at three levels is used here for the implementation of orthogonal array design. The experiments are carried out according to the arrangement of the orthogonal array L_9 orthogonal array with four columns and 9 rows. Laser beam machining parameters and corresponding levels are listed at table no. 6.2.

Table 6.2 Machining Parameters and respective levels

Process Parameter	**Level**		
	1	**2**	**3**
Lamp current (L)(amp)	22	23	24
Pulse frequency (γ)(kHz)	4	5	6
Assist Air Pr. (p) (kg/cm^2)	0.6	0.8	1.0
Cutting speed (v) (mm/sec)	4	8	12

Overcut and depth of groove during this single pass blind cut/grooving operation are selected as the machining responses under observation. Target width of the cut during experiments are set to be 1 mm. Optical measuring microscope (Olympus STM6) at 10x magnification is used to capture the image of microgroove, after which the upper kerf width and groove depth of the workpiece material is determined by image analysis software from where overcut is measured. The observed data from the set of experiments have been used as input data to MINITAB software for parametric optimization i.e. for achieving desired machining condition.

Overcut = Upper kerf width – (Target width + Spot diameter) (6.1)

Here target width is kept fixed at 1mm and spot diameter of laser beam is 0.1 mm (by default) for Gaussian beam system with TEM_{00} mode.

6.1.2 Experimental observations and discussion

All the experimental value is documented in table 6.3.

Table 6.3 Experimental results

Exp no.	Lamp current (Amp)	Pulse frequency (kHz)	Assist gas pressure (kg/cm^2)	Cutting Speed (mm/sec)	Upper kerf width (mm)	Overcut (mm)	Groove depth (mm)
1	1	1	1	1	1.13644	0.03644	0.34222
2	1	2	2	2	1.1968	0.09680	0.21452
3	1	3	3	3	1.1725	0.07250	0.19916
4	2	1	2	3	1.1281	0.02810	0.22905
5	2	2	3	1	1.16407	0.06407	0.19952
6	2	3	1	2	1.1483	0.04830	0.25607
7	3	1	3	2	1.1506	0.05060	0.35416
8	3	2	1	3	1.20118	0.10118	0.32272
9	3	3	2	1	1.17212	0.07212	0.32622

6.1.2.1 Parametric analysis

The effects of the process parameters such as the lamp current, pulse frequency, assist air pressure and cutting speed on the overcut and groove depth are discussed here in details.

From figure 6.1, overcut has been found to be a decreasing tendency upto 23 amp lamp current then it increases with further increase in lamp current upto 24 amp. Generally higher thermal energy generates with increase in lamp current which may produces uniform material removal from top surface results in decrease in overcut. But with further increase in lamp current generates more thermal energy which removes more material from top surface than later which results in increase in overcut. It is observed from fig.6.1 that overcut, first increases with increase in pulse frequency upto 5 kHz then decreases. At low pulse frequency high laser intensity generates and vice versa. At low pulse frequency, instant melting and vaporization from the top surface due to high laser power and then decreases with increases in pulse frequency. Increase in assist gas pressure causes rapid removal of melt pool and debris from machining zone may produces more material removal, results in little increase in overcut. But further increase in assist gas pressure causes results in uneven heating value on the machining zone, decrease in melt layer

surface temperature for which less amount of material is removed. As a result low overcut is observed. It is shown from the fig. 6.1 that overcut increases with increase in cutting speed. Though interaction time as a function of cutting speed is decreased with increase in cutting speed, the propagation of fractured dominated material removal takes place abruptly from the travel path of laser beam with aid of assist gas pressure, results in increase in overcut.

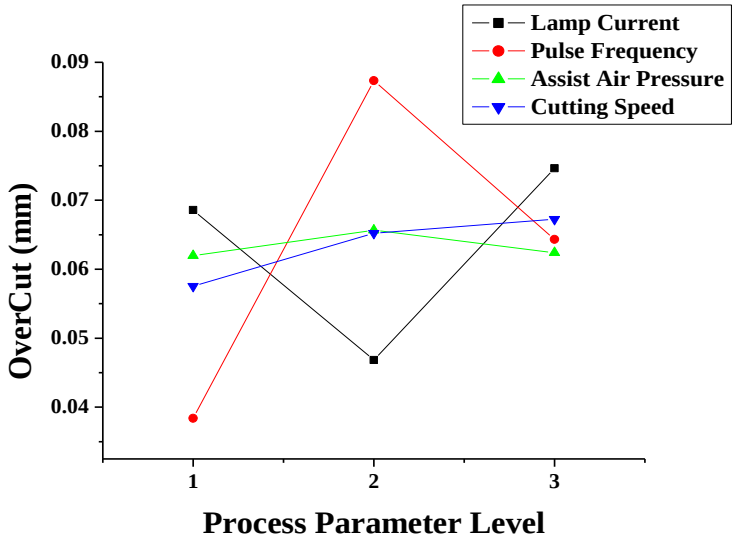

Fig. 6.1. Effect of process parameters on Overcut

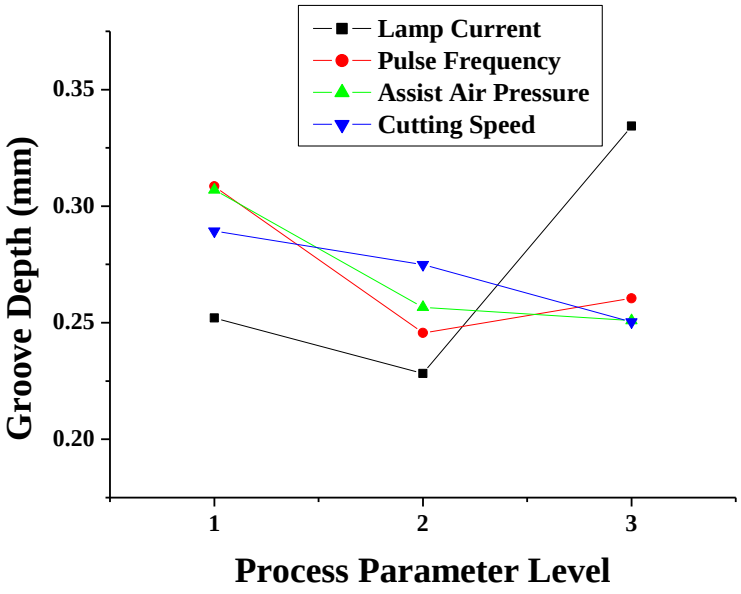

Fig. 6.2 Effect of process parameters on groove depth

From figure 6.2, Groove depth has been found to be a decreasing tendency upto 23 amp lamp current then it increases with further increase in lamp current upto 24 amp. Generally, higher laser beam power generates higher thermal energy which produces better material removal results in increase in groove depth at top surface. Groove depth also shows a decreasing tendency upto 5 kHz pulse frequency but with further increase in pulse frequency results in increased groove depth. At lower value of pulse frequencies, it gives low spot over lapping, alongwith discontinuous power density which results low groove depth and vice versa. It has been observed from fig. 6.2 that groove depth decreases with increase in assist air pressure. Increase in assist gas pressure cause uneven heating value with non uniform wall shear stress in the machining zone of the work piece for which less amount of material is removed. As a result low groove depth is observed. Increase in cutting speed reduces the interaction time between workpiece and laser beam results in low material removal rate. For which groove depth has been showing a decreasing tendency with increase in cutting speed.

6.1.2.2 ANOVA of machining responses

The analysis of variance (ANOVA) is the most widely used method of statistical analysis of quantitative data. To determine the relative significances of the machining process parameters considered during experimentation, the analysis of variance (ANOVA) test has been performed for both the responses and the results are documented in table no 6.4 & 6.5. Percentage contribution column in ANOVA result table indicates at the degree of influence of all the process parameters on the machining characteristics. In this ANOVA analysis The F ratio value is calculated by using the pooled error mean square [73] due to degrees of freedom for error value is equal to zero.

Table 6.4 Results of the ANOVA for Overcut

Source	**Degrees of Freedom**	**Sum of Square**	**Mean of Square**	**F**	**% Contribution**
Lamp Current	2	0.001283	0.000642	53.5	25.33
Pulse Frequency	2	0.003601	0.001801	150.0833	71.07
Assist Air Pressure	2	0.000025	0.000012	1	0.47
Cutting Speed	2	0.000158	0.000079	6.5833	3.12
Error	0				
Total	8	0.005067			

ANOVA analysis for overcut is listed in Table no.6.4. From the table it is found that all the process parameters have some effect on overcut. According to the table it is found that pulse frequency (71.07%) is the most dominant factor followed by lamp current (25.34%) cutting speed (3.12%), and assist air pressure (0.47%).

Table 6.5 Results of ANOVA for Groove depth

Source	**Degrees of Freedom**	**Sum of Square**	**Mean of Square**	**F**	**% Contribution**
Lamp Current	2	0.01862	0.00931	7.9786	56.17
Pulse Frequency	2	0.00648	0.00324	2.7763	19.54
Assist Air Pressure	2	0.00572	0.00286	2.4490	17.24
Cutting Speed	2	0.00234	0.00117	1	7.04
Error	0				
Total	8	0.033153			

ANOVA analysis for Groove depth is listed in Table no.6.5. From the table it is found that all the process parameters have some effect on Groove depth. According to the table it is found that lamp current (56.17%) is the most dominant factor followed by Pulse frequency (19.55%), assist air pressure (17.24%) and cutting speed (7.04%).

6.1.3 Determination of optimal parameter settings

6.1.3.1 Single objective optimization based on Taguchi methodology

Experimental observations are further used to determine the optimal parameter settings. Firstly single objective optimization by Taguchi based optimization technique has been carried out. The results of single optimization for each machining responses are listed in table 6.6.

Table 6.6 Single objective optimization of responses

Machining responses	**Optimal parametric settings**	**Optimal value**
Overcut	$L2\gamma 1p1v1$	0.0146
Groove Depth	$L3\gamma 1p1v1$	0.4244

6.1.3.1.1 Confirmation test for Taguchi based single objective optimization

Five additional experiments are carried out for confirmation test separately for both the machining responses and the average of experimental results are taken for confirmation test and given in table no. 6.7.

Table 6.7 confirmation test of single objective optimization technique

Machining responses	**Optimal parametric settings**	**Optimal value**	**Experimental value (average)**	**% of error**
Overcut	$L2\gamma1p1v1$	0.0186	0.0192	3.23
Groove Depth	$L3\gamma1p1v1$	0.4244	0.4087	3.7

6.1.3.2 Taguchi based Grey relation analysis for multi objective optimization

Multiple objective optimization is performed here by Grey based Taguchi optimization technique. As per previously said in chapter 4, all the normalized grey value and grey relation coefficient values are documented in table no.6.8. During the calculation of the grey relation grade same weightage (50%) is given on overcut and groove depth.

Table 6.8 Results of Grey relation analysis

Exp. no.	**Overcut (mm)**	**Groove Depth (mm)**	**Grey relation generating**		**Grey relation coefficient**		**Grey relation grade**	**Order**
			Overcut	**Groove Depth**	**Overcut**	**Groove Depth**		
1	0.03644	0.34222	0.8437	0.9230	0.7619	0.8665	0.840337	1
2	0.09680	0.21452	0.8823	0.0991	0.8095	0.3569	0.352059	9
3	0.07250	0.19916	0.9360	0.0000	0.8865	0.3333	0.392389	8
4	0.02810	0.22905	1.0000	0.1928	1.0000	0.3825	0.691254	3
5	0.06407	0.19952	0.8039	0.0023	0.7182	0.3339	0.418890	7
6	0.04830	0.25607	0.8893	0.3672	0.8188	0.4414	0.542680	5
7	0.05060	0.35416	0.8233	1.0000	0.7389	1.0000	0.809451	2
8	0.10118	0.32272	0.7503	0.7972	0.6670	0.7114	0.522367	6
9	0.07212	0.32622	0.0000	0.8197	0.3333	0.7350	0.594295	4

The optimal parameter setting determined by using Grey based Taguchi method is $L1\gamma 1p1v1$. The grey relational grade of each factor level is calculated as the average for the same level in each column.

6.1.3.2.1 Confirmation test

Three additional experiments are performed at optimal parameter settings and average of those three experimental results is taken for confirmation test. Table 6.9 furnishes the predicted value of grey relation grade and result of confirmation test.

Table 6.9 Results of confirmation test.

	Initial parameter setting	**Optimal parameters**	
		Prediction	**Experiment**
Level	$L1\ \gamma\ 1\ p1v1$	$L3\gamma 1\ p1v1$	$L3\gamma 1\ p1v1$
Overcut (mm)	0.03644	-	0.03044
Groove Depth (mm)	0.34222	-	0.35162
Grey Relation Grade	0.840337	0.954113	0.95404

From the table it is found that machined grove quality characteristics i.e. overcut is improved from 0.03644 mm to 0.03044 mm whereas groove depth is improved from 0.34222 mm to 0.35162 mm. This result shows that the use of Taguchi based grey relation analysis is effective for improvement of groove quality characteristics during laser grooving of hydroxyapatite (HAp). The overall characteristics are improved from 0.840337 to 0.954113. The results of confirmation test justify the application of the proposed method and leads to continuous improvement of groove geometry in laser grooving of hydroxyapatite (HAp). Photographic View of the micro groove on hydroxyapatite (HAp) is given in figure 6.3.

Scanning Electron Microscopic image of experiment no.4 has shown in Fig 6.4 gives the clear image of groove portion, and from the figure it is also depicted that the machined material in it's pure form is very porous and non homogeneous in nature.

Fig.6.3 Photographic view of the microgroove on HAp

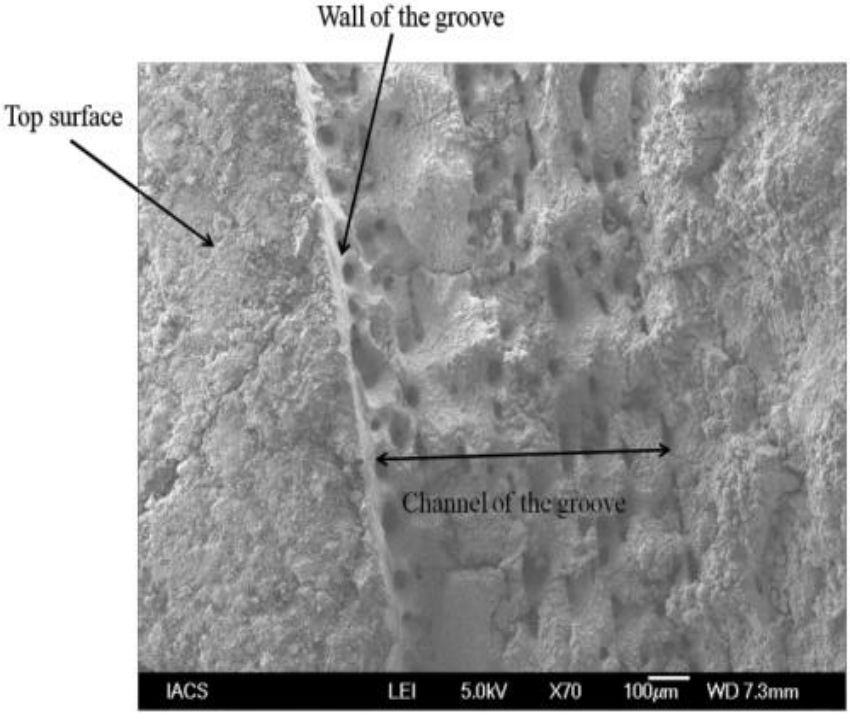

Fig 6.4 Scanning Electron Microscope image of the microgroove

For which during machining the material removal mechanism is mainly governed by crack propagation method rather than melting and vaporization. Multiple microcrack are seen on the bed of machined surface. As the material removal is dominated by crack formation followed by propagation of those cracks, the surface profile of the machined zone is very much rough. It is also observed that edge of the kerf is clearly visible in one side whereas other side isn't properly formed as the material may be comes out as a chuck.

6.1.4 Outcome of the study

Laser grooving process is used here successfully, for grooving operation on Hydroxyapatite in its pure form. From the optical and SEM images it is clearly observed that it is very difficult to do any machining on the surface of hydroxyapatite (HAp) in it's pure form. Material removal mechanism during formation of groove is mainly governed by crack formation rather than ablation. Taguchi based grey relational analysis is used here to optimize the laser grooving process with the multiple performance characteristics on hydroxyapatite (HAp). From the ANOVA analysis it has been found that statistically all the process parameters have influence on both the machining responses. Lamp current is the most dominating process parameter for both overcut and groove depth. The outcome of the study demonstrates the feasibility of the proposed multiobjective optimization technique for laser grooving of hydroxyapatite (HAp) and helps to obtain optimum parameter settings for overall improvement (13.53%) of machined groove characteristics when both the response are consider simultaneously.

6.2 Laser beam microcutting of Inconel 625 superalloy

In recent times demands for high performances nickel based superalloys are increased vary rapidly in aerospace and power generation industries [98]. Nickel based superalloys have high tensile, creep and rupture strength at elevated temperatures with excellent ductility and toughness at low temperature; make them attractive toward various application in manufacturing industries. In which Inconel 625 superalloy also have superior resistance to a wide range of corrosive environments as well as to high-temperature effects such as oxidation and carburization. These properties of Inconel 625 make it an excellent choice for sea water application, aerospace field, nuclear and chemical processing field. The solid solution strengthening effects of the refractory metals, niobium and molybdenum, in a nickel–chromium matrix are the reason for mechanical properties viz. very high toughness and strength of Inconel 625 superalloy in the temperature range from cryogenic to ultra hot environment. Properties like high hardness, low thermal conductivity and high work hardening rates make it difficult to machine material with excessive tool wear and poor surface finish [99]. Comparatively high absorptive short wavelength pulsed Nd: YAG laser may be enables to cut this kind of hard to machine material. Selections of cutting parameters along with assist medium are the most dominating factors to get desired cut profile during pulsed laser beam cutting process. Extensive research work is required to make technological guidelines of laser material processing of Inconel 625 in absences/ very few of previous documentation. On the basis of above mentioned circumstances, in depth study of pulsed laser machining of Inconel 625 superalloy is carried out in different assisted medium.

6.2.1 Parametric study on laser beam microcutting of Inconel 625 superalloy with compressed air as an assist medium

6.2.1.1 Experimental details

A pulsed Nd:YAG laser-based CNC machining system, manufactured by M/s Sahajanand Laser Technology, India, is used for the experimental study. A specially designed workpiece holding unit is placed over the CNC controlled work table. Inconel 625 superalloy with 8mm×8mm×0.9mm dimension has been considered as workpiece material for experimental study. Properties of Inconel 625 are listed in table 6.10 [100].

Table.6.10 Properties of Inconel 625

Property	**Unit**	**Value**
Yield Strength	MPa	414-645
Ultimate Tensile Strength	MPa	827-1034
Modulus of Elasticity	GPa	207.5
Poission's Ratio	-	0.278
Elongation	%	60-30
Density	Gram/cc	8.44
Hardness	Brinell	145-220

Lamp current, pulse frequency, pulse width, cutting speed and assist gas pressure are considered as the controllable process parameters to carry out the experiment. Kerf width, depth of cut and heat affected zone (HAZ) width are considered as process responses. Here compressed air is selected as an assist gas. Compressed air is co-axially flow with laser beam and impinged on the irradiate spot. Compressed air is passed through the air & oil separator which helps to remove impurities from compressed air and this dry compressed air struck the workpiece as per required pressure by the help of pressure regulator which is also attached to compressed air delivery system like oil & moisture separator. The ranges of these process parameters are selected on the basis of trial experiments conducted by using one factor at a time approach. Experiments have been carried out according to the central composite rotatable second-order design based on response surface methodology. Range of all controllable input process variables are listed in Table 6.11. A CNC programme is written to make the blind linear cut with 5 mm length on the job sample. The CNC programme is inserted into the interfacing software provided with the Nd:YAG system to perform the cutting process.

Table.6.11 Process parameters levels

Process Parameter	Unit	Symbol	Levels				
			-2	-1	0	1	2
Lamp current	Amp	x_1	20	22	24	26	28
Pulse frequency	kHz	x_2	2	4	6	8	10
Pulse width	%	x_3	2	4	6	8	10
Cutting speed	mm/sec	x_4	1.0	1.5	2.0	2.5	3.0
Assist gas pressure	kg/cm^2	x_5	0.5	1	1.5	2	2.5

Response surface modeling was used to establish the mathematical relationship between the response, y_u and the various machining parameters, with the eventual objective of determining the optimum operating conditions for the system.

Olympus optical measuring microscope has been used to capture the image of cut region at 20x magnification from where kerf width (KW), depth of cut and HAZ width are calculated by image analysis software.

$$HAZwidth(mm) = \frac{HAZ_{Top} - Kerfwidth_{Top}}{2} \tag{6.2}$$

Responses are measured at three different places for each cut. Average measured values of responses are listed in table no.6.12. Image of the blind cut is given in figure no. 6.5. Minitab 17 Software is used for analysis of the measured responses and determining the mathematical models with best fits.

6.2.1.2 Results and discussion

Table. 6.12 Experimental results

Exp. No.	Lamp current (Amp)	Pulse frequency (kHz)	Pulse width (%)	Cutting speed (mm/sec)	Assist air pressure (kg/cm^2)	Kerf width (KW) (mm)	Depth of cut (mm)	Heat affected zone width (mm)
1	22	4	4	1.5	1	0.0645	0.0128	0.09005
2	26	4	4	1.5	1	0.0830	0.0142	0.14615
3	22	8	4	1.5	1	0.0677	0.0126	0.09020
4	26	8	4	1.5	1	0.0788	0.0154	0.16725
5	22	4	8	1.5	1	0.0654	0.0132	0.09770
6	26	4	8	1.5	1	0.0837	0.0135	0.12950
7	22	8	8	1.5	1	0.0684	0.0107	0.09325
8	26	8	8	1.5	1	0.0769	0.0128	0.14525

Exp. No.	Lamp current (Amp)	Pulse frequency (kHz)	Pulse width (%)	Cutting speed (mm/sec)	Assist air pressure (kg/cm^2)	Kerf width (KW) (mm)	Depth of cut (mm)	Heat affected zone width (mm)
9	22	4	4	2.5	1	0.0695	0.0098	0.10660
10	26	4	4	2.5	1	0.0835	0.0108	0.13480
11	22	8	4	2.5	1	0.0636	0.0119	0.09795
12	26	8	4	2.5	1	0.0692	0.0139	0.14505
13	22	4	8	2.5	1	0.0684	0.0086	0.10980
14	26	4	8	2.5	1	0.0833	0.0090	0.11965
15	22	8	8	2.5	1	0.0691	0.0102	0.09370
16	26	8	8	2.5	1	0.0692	0.0115	0.11225
17	22	4	4	1.5	2	0.0667	0.0119	0.08094
18	26	4	4	1.5	2	0.0855	0.0122	0.15535
19	22	8	4	1.5	2	0.0621	0.0131	0.08995
20	26	8	4	1.5	2	0.0701	0.0141	0.17810
21	22	4	8	1.5	2	0.0707	0.0143	0.09945
22	26	4	8	1.5	2	0.0823	0.0138	0.14545
23	22	8	8	1.5	2	0.0660	0.0143	0.10835
24	26	8	8	1.5	2	0.0680	0.0145	0.16740
25	22	4	4	2.5	2	0.0675	0.0105	0.09335
26	26	4	4	2.5	2	0.0854	0.0099	0.13070
27	22	8	4	2.5	2	0.0638	0.0142	0.09175
28	26	8	4	2.5	2	0.0660	0.0152	0.13645
29	22	4	8	2.5	2	0.0673	0.0119	0.12205
30	26	4	8	2.5	2	0.0826	0.0113	0.13145
31	22	8	8	2.5	2	0.0670	0.0146	0.09979
32	26	8	8	2.5	2	0.0739	0.0141	0.12360
33	20	6	6	2	1.5	0.0590	0.0136	0.08800
34	28	6	6	2	1.5	0.0875	0.0141	0.16990
35	24	2	6	2	1.5	0.0791	0.0101	0.13925
36	24	10	6	2	1.5	0.0712	0.0125	0.13959
37	24	6	2	2	1.5	0.0784	0.0130	0.11075
38	24	6	10	2	1.5	0.0780	0.0124	0.10400
39	24	6	6	1	1.5	0.0758	0.0125	0.10574
40	24	6	6	3	1.5	0.0801	0.0098	0.09650
41	24	6	6	2	0.5	0.0828	0.0119	0.14455
42	24	6	6	2	2.5	0.0793	0.0132	0.15455

Exp. No.	Lamp current (Amp)	Pulse frequency (kHz)	Pulse width (%)	Cutting speed (mm/sec)	Assist air pressure (kg/cm^2)	Kerf width (KW) (mm)	Depth of cut (mm)	Heat affected zone width (mm)
43	24	6	6	2	1.5	0.0850	0.0109	0.14340
44	24	6	6	2	1.5	0.0859	0.0109	0.15050
45	24	6	6	2	1.5	0.0862	0.0120	0.14885
46	24	6	6	2	1.5	0.0878	0.0118	0.14820
47	24	6	6	2	1.5	0.0851	0.0116	0.14840
48	24	6	6	2	1.5	0.0906	0.0116	0.14025
49	24	6	6	2	1.5	0.0929	0.0116	0.14715
50	24	6	6	2	1.5	0.0950	0.0115	0.14125
51	24	6	6	2	1.5	0.0955	0.0118	0.14319
52	24	6	6	2	1.5	0.0941	0.0119	0.14605

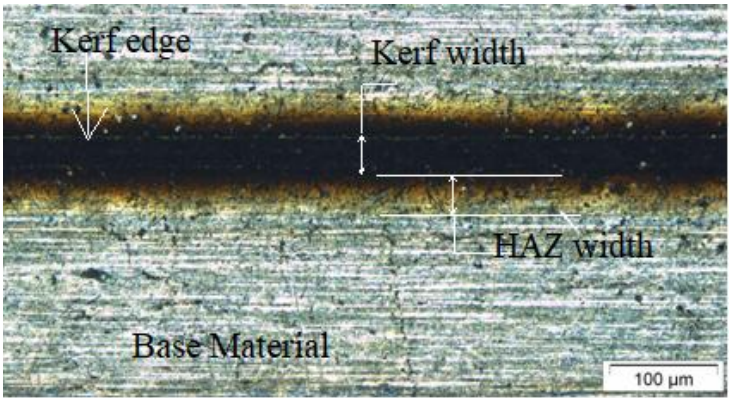

Fig 6.5 Image of blind cut with compressed air

6.2.1.2.1 Development of Second order polynomial model

$$Y_{KW} = 0.089295 + 0.005661X_1 - 0.003313X_2 + 0.000415X_3 - 0.000466X_4 + 0.000900X_5 - 0.004633X_1^2 - 0.004151X_2^2 - 0.002873X_3^2 - 0.003539X_4^2 - 0.002160X_5^2 - 0.002863X_1X_2 - 0.000424X_1X_3 - 0.000500X_1X_4 - 0.000078X_1X_5 + 0.000818X_2X_3 - 0.001048X_2X_4 - 0.001179X_2X_5 + 0.000047X_3X_4 - 0.000322X_3X_5 + 0.000089X_4X_5 \quad (6.3)$$

$$Y_{Depth} = 0.0945 - 0.006129X_1 - 0.002368X_2 + 0.000193X_3 - 0.00283X_4 - 0.00273X_5 + 0.000144X_1^2 - 0.000015X_2^2 + 0.000073X_3^2 - 0.000389X_4^2 + 0.001011X_5^2 + 0.000064 X_1X_2 - 0.000048 X_1X_3 - 0.000113X_1X_4 - 0.000344X_1X_5 - 0.000088X_2X_3 + 0.000694X_2X_4 + 0.000350X_2X_5 - 0.000181X_3X_4 + 0.000613X_3X_5 + 0.001625X_4X_5 \quad (6.4)$$

$Y_{HAZ\ width} = -1.477+0.07973X_1-0.00543X_2+0.06491X_3+0.4109X_4-0.0654X_5-0.001067X_1^2-0.000413X_2^2-0.002415X_3^2-0.04490X_4^2+0.00353X_5^2+0.000916X_1X_2-0.001583X_1X_3-0.008300X_1X_4 + 0.001944X_1X_5-0.000549X_2X_3-0.004469X_2X_4 +0.000812X_2X_5 -0.000398X_3X_4+0.003684X_3X_5-0.00704X_4X_5$ (6.5)

6.2.1.2.2 ANOVA of machining responses

ANOVA analysis of the quadratic models with other adequacy measures R2, adjusted R2 and predicted R2 are documented in Table 6.13, 6.14 and 6.15.

Table. 6.13 ANOVA result of Kerf width

Source	**DF**	**Adj SS**	**Adj MS**	**F value**	**P value**
Model	20	0.004573	0.000229	159.63	0.000
Linear	5	0.001769	0.000354	246.99	0.000
Lamp current	1	0.001282	0.001282	894.91	0.000
Pulse frequency	1	0.000439	0.000439	306.50	0.000
Pulse width	1	0.000007	0.000007	4.82	0.036
Cutting speed	1	0.000009	0.000009	6.07	0.019
Assist gas pressure	1	0.000032	0.000032	22.63	0.000
Square	5	0.002423	0.000485	338.33	0.000
2 way Interaction	10	0.000381	0.000038	26.60	0.000
Error	31	0.000044	0.000001		
Lack of Fit	22	0.000027	0.000001	0.63	0.822
Pure Error	9	0.000018	0.000002		
Total	51	0.004617			
Value of S 0.0011968		R sq 99.04 %	R sq (adj) 98.42 %	R sq (pred) 97.39 %	

From the table 6.13 it is observed that the associated p-value of less than 0.05 indicates that the model term can be considered as statistically significant at 95% confidence level. Value of lack of fit of the model is more than 0.05 which indicates at non significant as desired. From the table it is found that lamp current (72.47%) is the most dominating factor followed by pulse frequency (24.82%), assist gas pressure (1.83%) whereas cutting speed and pulse width have very negligible contribution. From the regression analysis result in terms of value of S, R-sq, R-sq(adj) and R-sq(pred), it may be concluded that the data for each response are well fitted in the developed model.

Table.6.12 ANOVA result of depth of cut

Source	**DF**	**Adj SS**	**Adj MS**	**F value**	**P value**
Model	20	0.000130	0.000006	52.92	0.000
Linear	5	0.000064	0.000013	104.02	0.000
Lamp current	1	0.000004	0.000004	32.35	0.000
Pulse frequency	1	0.000023	0.000023	185.84	0.000
Pulse width	1	0.000001	0.000001	5.94	0.021
Cutting speed	1	0.000025	0.000025	200.90	0.000
Assist gas pressure	1	0.000012	0.000012	95.07	0.000
Square	5	0.000017	0.000003	27.69	0.000
2 way Interaction	10	0.000049	0.000005	39.99	0.000
Error	31	0.000004	0.000001		
Lack of Fit	22	0.000002	0.000001	0.78	0.696
Pure Error	9	0.000001	0.000001		
Total	51	0.000134			
Value of S 0.0003503		R sq 97.15 %	R sq (adj) 95.32 %	R sq (pred) 91.70 %	

From table 6.14 it is observed that the associated p-value of less than 0.05 for the model (i.e. , α = 0.05, or 95% confidence level) indicates that the model terms are statistically significant. The lack-of-fit value of the model indicates non-significance, as this is desirable. ANOVA results show that all the input process parameters are significant. Values of other adequacy measures R-sq, adjusted R-sq and predicted R-sq are in reasonable agreement and are close to100%, which indicate adequacy of the model. F-value (0.9) and P-value (0.696) of the Lack-of-Fit implies that it is not significant relative to the pure error, as this is desired. From the table it is observed that statistically, cutting speed (38.65%) is the most dominating factor followed by pulse frequency (35.75%), assist gas pressure (18.29%), lamp current (6.22 %) and pulse width (1.14%).

Table.6.15 ANOVA result of HAZ width

Source	**DF**	**Adj SS**	**Adj MS**	**F value**	**P value**
Model	20	0.033674	0.001684	126.74	0.000
Linear	5	0.019742	0.003948	297.23	0.000
Lamp current	1	0.018806	0.018806	1415.65	0.000
Pulse frequency	1	0.000058	0.000058	4.33	0.046
Pulse width	1	0.000061	0.000061	4.61	0.040
Cutting speed	1	0.000592	0.000592	44.56	0.000
Assist gas pressure	1	0.000226	0.000226	16.98	0.000
Square	5	0.008541	0.001708	128.58	0.000
2 way Interaction	10	0.005391	0.000539	40.58	0.000
Error	31	0.000412	0.000013		
Lack of Fit	22	0.000302	0.000014	1.13	0.450
Pure Error	9	0.000110	0.000012		
Total	51	0.034086			
Value of S 0.0036448		R sq 98.79 %	R sq (adj) 98.01%	R sq (pred) 96.42 %	

From table 6.15 it is observed that the associated p-value of less than 0.05 for the model (i.e. , α = 0.05, or 95% confidence level) indicates that the model terms are statistically significant. The lack-of-fit value of the model indicates non-significance, as this is desirable. ANOVA results show that all the input process parameters are significant contribution of Pulse width and pulse frequency is very less. Values of other adequacy measures R-sq, adjusted R-sq and predicted R-sq are in reasonable agreement and are close to100%, which indicate adequacy of the model. F-value (0.9) and P-value (0.450) of the Lack-of-Fit implies that it is not significant relative to the pure error, as this is desired. From the table it is observed that statistically, lamp current (95.26 %) is the most dominating factor followed by cutting speed (3.00%) and assist gas pressure (1.14%).

6.2.1.2.3 Parametric analysis

The effects of the process parameters such as the lamp current, pulse frequency assist air pressure and cutting speed on kerf width, depth of cut and HAZ width are discussed here in details.

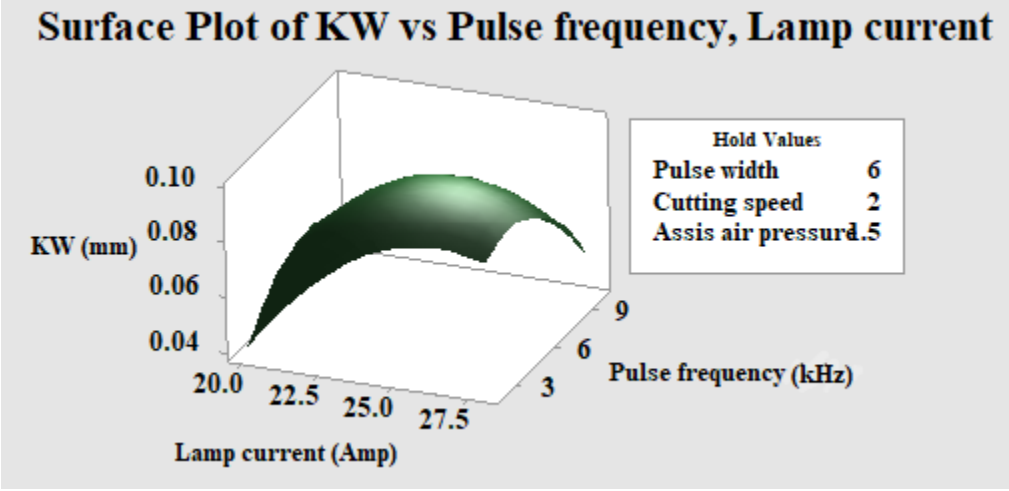

Figure 6.6. Surface plot of Kerf width with lamp current and pulse frequency

From fig.6.6 it is observed that kerf width first increase with increase in lamp current but it marginally decreases with lamp current after 26 A. Firstly increase in lamp current generates more laser power for which amount molten material increases, results in increase in kerf width. But when lamp current exceeds 26 A value, excess amount of molten material is formed in machining zone which cannot properly removed by assist gas from the machining zone and results in decrease in kerf width. Kerf width marginally increases with increases in pulse frequency upto 4 kHz then gradually decreases. At low pulse frequency comparatively high

energy beam is generated which removes more material from the top surface of the workpiece and vice versa. From the fig. it can be concluded that low kerf width can be achieved at lowest lamp current with highest value of pulse frequency.

From fig. 6.7 it is observed that kerf width first increases with increase in lamp current but it marginally decreases with increase in lamp current after 26 A whereas incase of cutting speed kerf width gradually increases upto mid value of cutting speed then decreases . In beginning due to increase in lamp current along with low cutting speed at that point of time, more laser power is transferred to machining zone results in increase in kerf width but further increase in cutting speed results in decrease in interaction time between laser beam and workpiece results in decrease in kerf width inspite of higher laser power at higher lamp current.

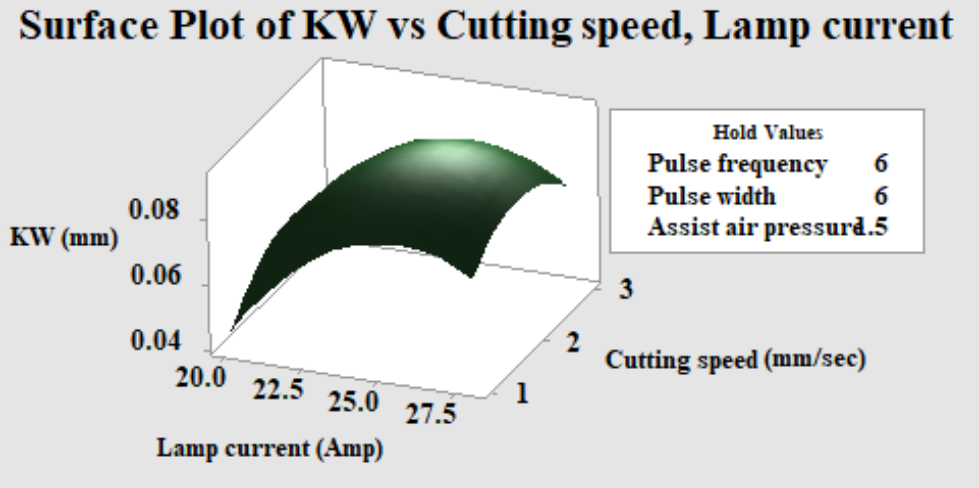

Fig. 6.7 Surface plot of Kerf width with lamp current and cutting speed

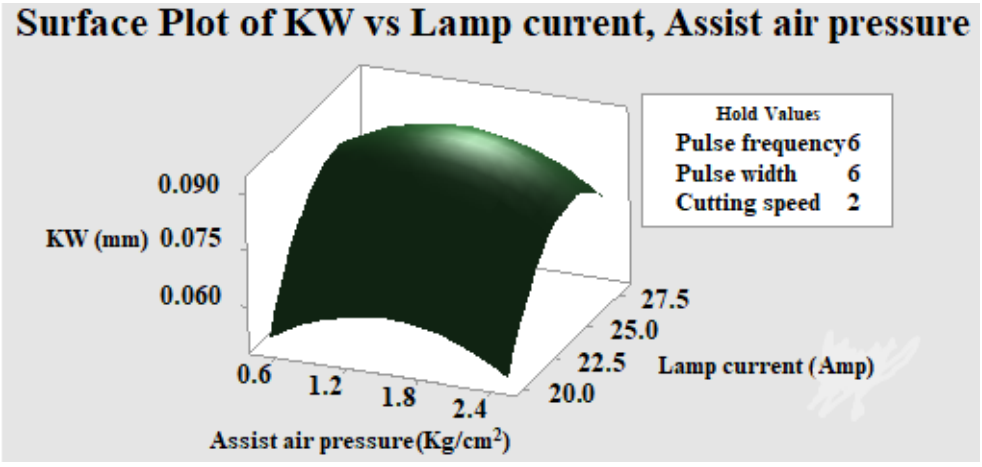

Fig. 6.8 Surface plot of Kerf width with lamp current and assist air pressure

From the surface plot it has been evident that kerf width increases with increase in both the lamp current and assist gas pressure upto a certain value than decreases marginally in case of lamp current and markedly with assist gas pressure when others process parameters are kept constant at pre-selected mid value. Laser power density at irradiate zone increases with increase in lamp current which helps to melt more material, that removes from the machining zone with the aid of co-axially flown assist gas. But after a certain value of lamp current melt pool generation is increased whereas increased air pressure helps to resolidify the molten debris around the side wall of the cut due to the cooling effect of compressed air. For the above said reasons, this kind of phenomenon can be observed.

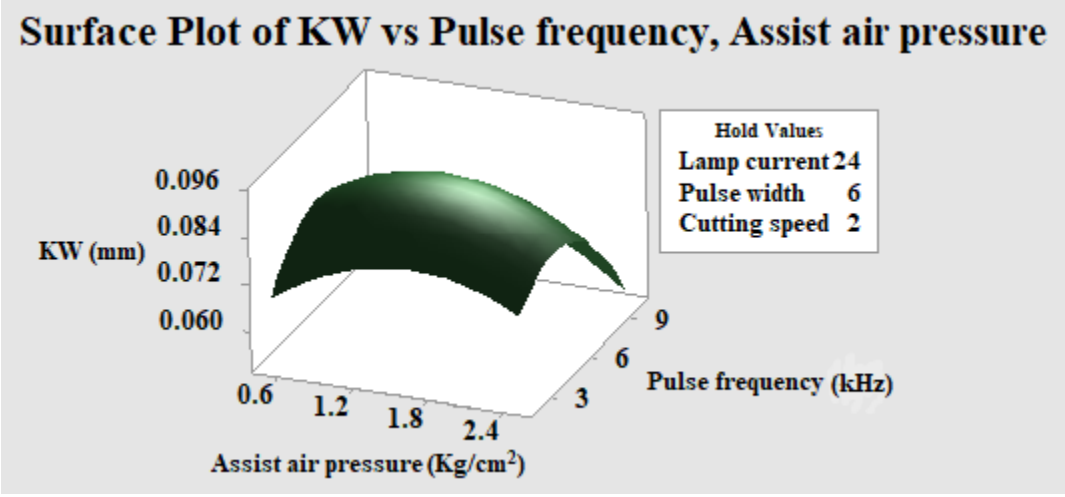

Fig. 6.9 Surface plot of Kerf width with pulse frequency and assist air pressure

From the plot it has been observed that kerf width is increasing with increase in the value of assist air pressure and pulse frequency upto a certain value of chosen design space but further increase on the value of controllable variable results in decrease in kerf width. From the plot it also find that desired lowest value of kerf can be achieved at the combination of highest value of pulse frequency with highest value of assist air pressure. At the aforesaid parameter settings debris in molten or vapour form, generate at the machining zone may be properly removed from machining zone to produce clean and narrow kerf which is desirable.

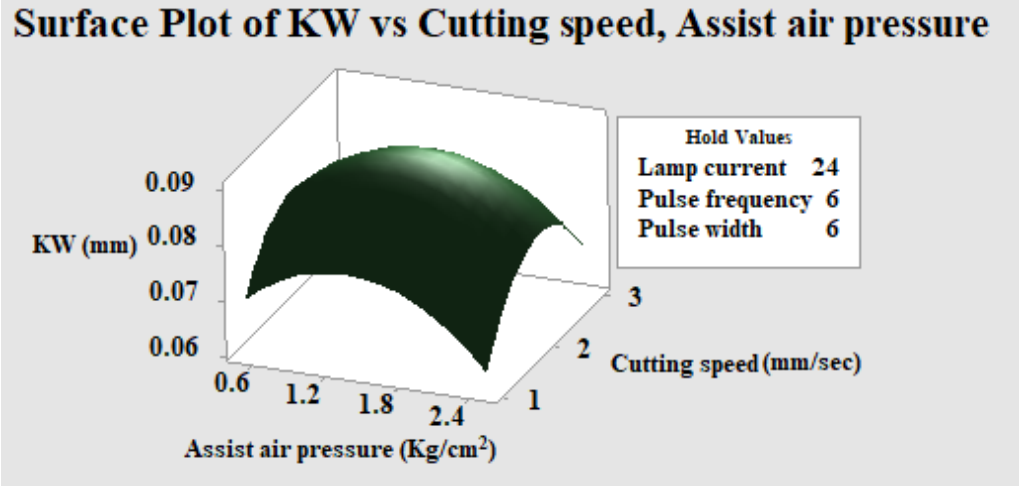

Fig. 6.10 Surface plot of Kerf width with assist air pressure and cutting speed

From fig.6.10 it is observed that lowest kerf width achieved at highest value of cutting speed and lowest value of assist air pressure. During aforesaid parametric condition interaction time between laser beam and work piece is very small but due to moderate value (hold value) of lamp current some adequate amount of melt pool may be formed which may not be properly removed by assist gas at that lowest value. That result in resolidification of the molten material along kerf edges and inner wall of the cut profile, make the kerf width narrow.

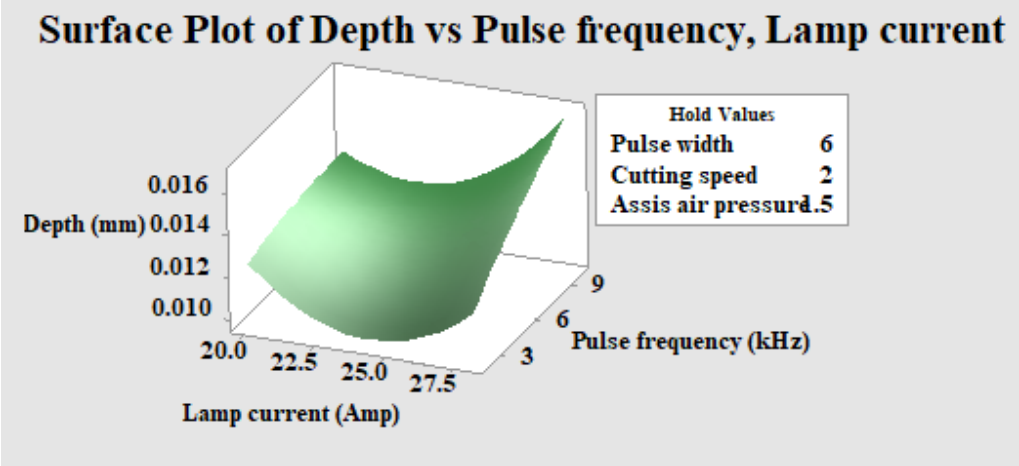

Fig. 6.11 Surface plot of depth of cut with lamp current and pulse frequency

Depth of cut shows a linear relationship with pulse frequency and gradually increases with increase in pulse frequency. Depth of cut shows parabolic nature of surface plot to lamp current which means initially decreasing tendency with increase in lamp of current but increases with further increase in lamp current. Highest value of depth of cut may be achieved at highest value

of pulse frequency with highest value of lamp current. At this parameter settings laser energy density on the irradiate spot is moderate amount of debris is produced in the machining zone which may be removed properly by the assist gas to create desired value of depth of cut.

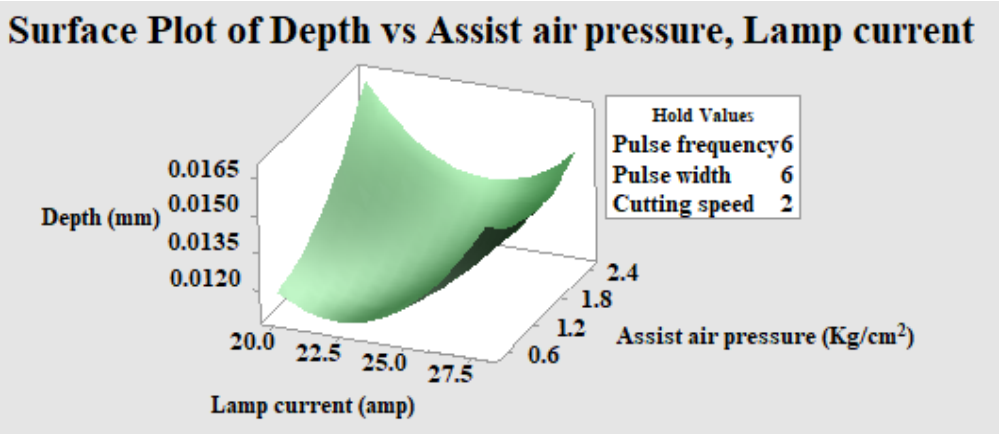

Fig. 6.12 Surface plot of depth of cut with Assist air pressure and lamp current

It is observed from the plot 6.12 that higher value of depth of cut can be achieved at lower value of lamp current with higher value assist air pressure. With this parameter settings debris may be properly remove from the machining zone along with that compressed air which flown co-axially with laser beam to impinged on the machining zone may incorporate some extra thermal energy into the machining zone due to exothermic reaction happened on melt pool. These may be reasons behind observed phenomenon.

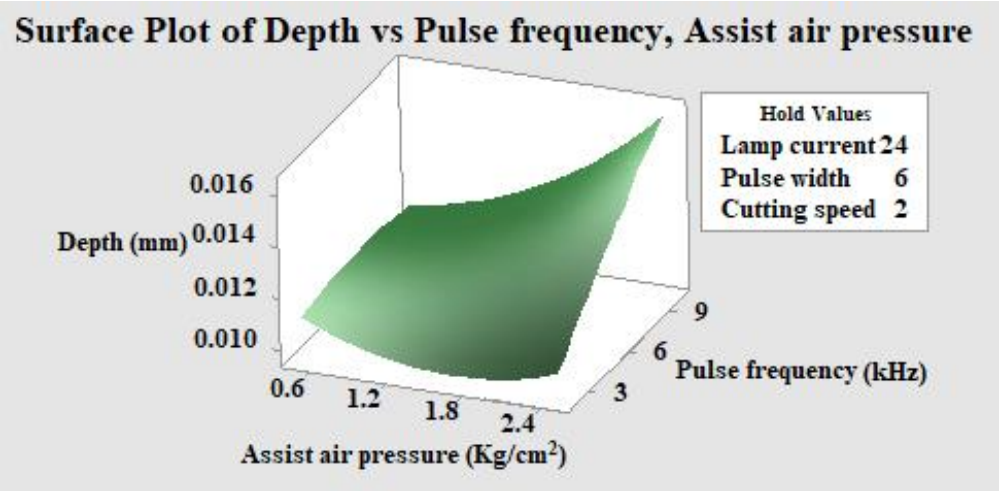

Fig. 6.13 Surface plot of depth of cut with Assist air pressure and pulse frequency

Form the surface plot 6.13 it is evident that highest value of depth of cut can be achieved at combination of highest value of pulse frequency and assist air pressure when the other process variable kept constant at their respective mid value. Energy per pulse is reduced with increase in pulse frequency which incorporate moderate thermal energy to the system to produce debris which removed from the machining zone properly by higher value of assist air pressure instantly along with this the assist pressure at higher value may enhance recoil pressure on the melt pool which helps the better depth of cut.

From the surface plot 6.14 it is observed that highest depth of cut can be achieved at combination of highest value of pulse width and assist air pressure. At higher value of pulse width pulse on time is more which with moderate value of cutting speed (2mm/sec) input sufficient thermal energy in to the system for material removal. Assist air pressure in its higher value helps to remove those molten debris from the machining zone properly. The cooling effect of compressed air may enhance surface tension on the melt pool which may helps the melt pool to move in longitudinal direction to get more depth.

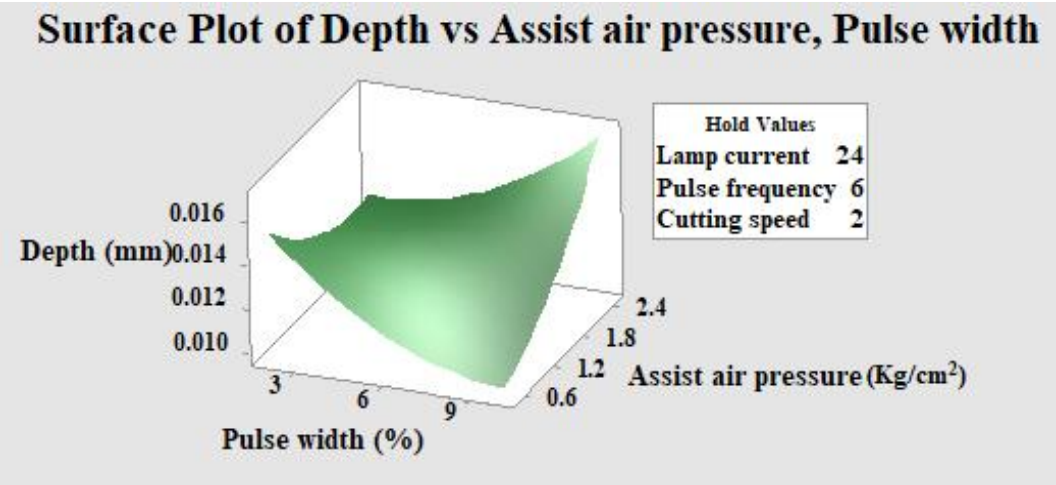

Fig. 6.14 Surface plot of depth of cut with Assist air pressure and pulse width

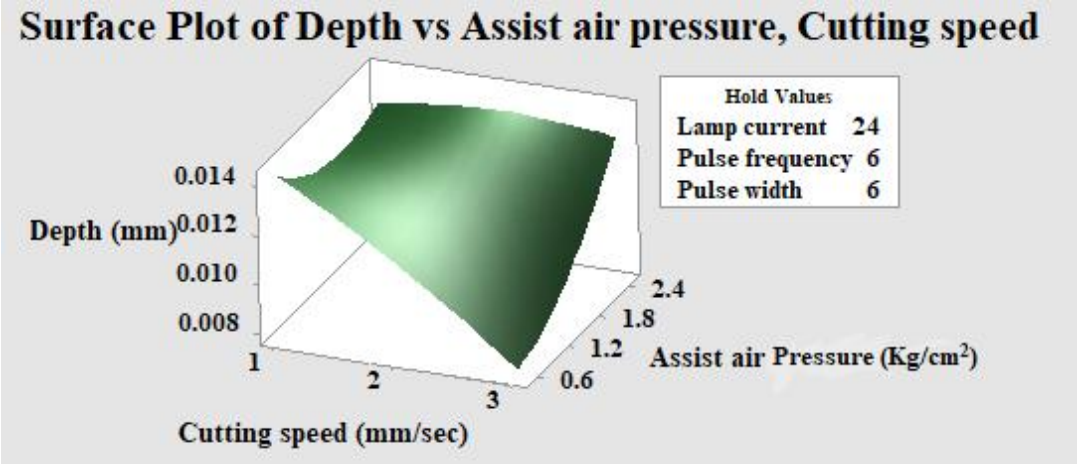

Fig. 6.15 Surface plot of depth of cut with assist air pressure and cutting speed

Depth of cut increases with increases with increase in assist air pressure whereas decreases with increase in cutting speed when other process variables kept constant at their respective pre selected mid value. Increased in cutting value indicates at decrease in contact time of laser beam with workpiece at a certain point. That means the irradiate points may not get sufficient energy to melt or vaporize, results in decrease in depth. Whereas higher assist pressure helps to proper removal of debris from machining zone along with incorporate some extra energy via exothermic reaction on machining zone.

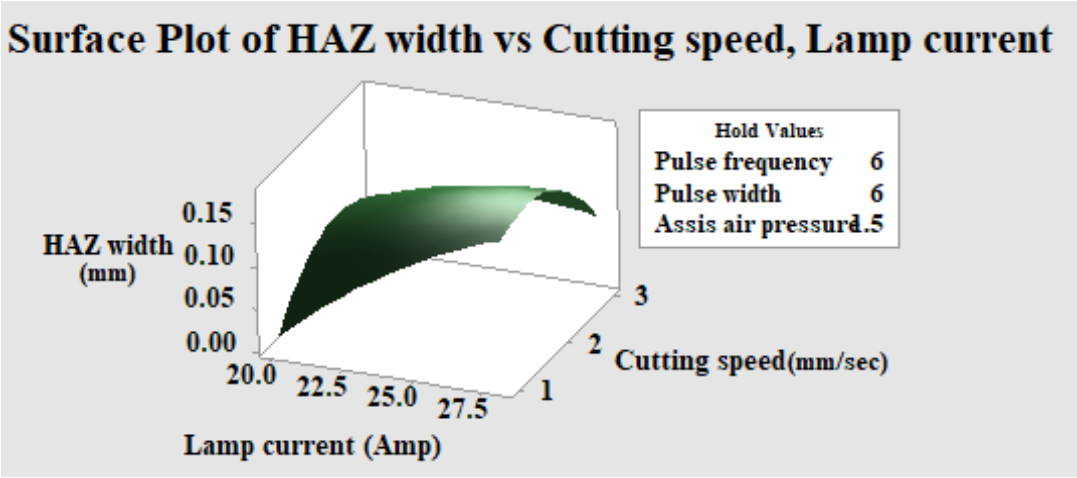

Fig. 6.16 Surface plot of HAZ width with lamp current and cutting speed

It has been observed from the plot 6.16 that HAZ width is increased with increase in lamp current, as it incorporate more thermal energy into the system. In case of cutting speed, HAZ

width initially increases with increase in cutting speed after which it decreases with further increase in cutting speed.

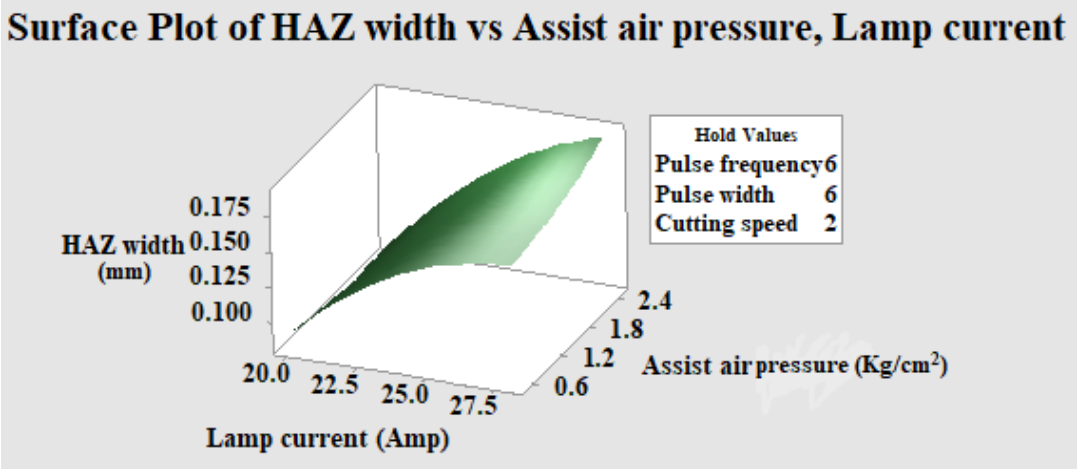

Fig. 6.17 Surface plot of HAZ width with lamp current and assist air pressure

As a combined effect with lamp current irradiate zone gets enough thermal energy upto certain value of cutting speed, results in increase in HAZ width. Later, irradiate points may not get sufficient thermal energy due comparatively lesser interaction time, which decrease heat affected region with further increase in cutting speed,

From the pot 6.17 it is evident that lowest HAZ width may be achieved at a combination of lowest value of lamp current and lowest value of assist air pressure. At this parametric setting lowest energy density along with the cooling effect of assist compressed air flow plays a vital role on smaller HAZ formation around the machining zone.

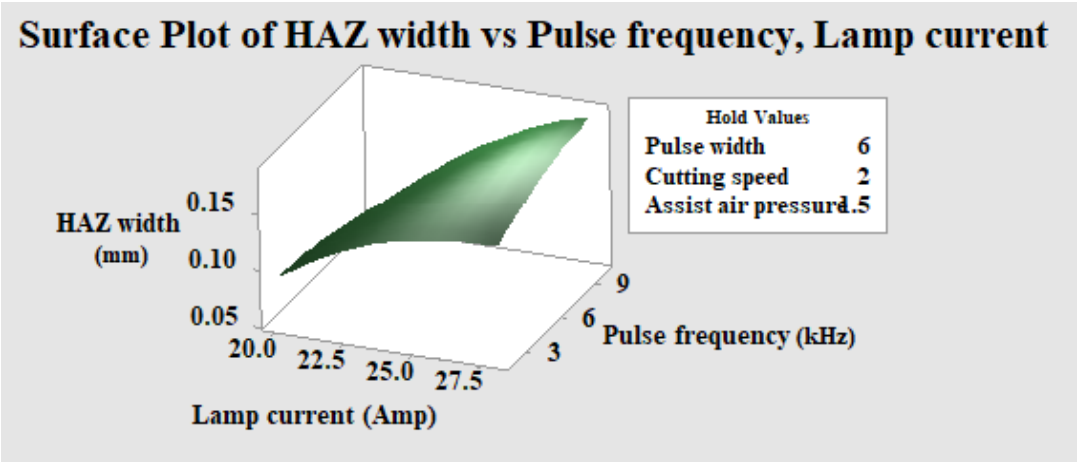

Fig. 6.18 Surface plot of HAZ width with lamp current and pulse frequency

Surface plot 6.18 of HAZ width with lamp current and pulse frequency demonstrates that HAZ width increases with increase in lamp current and pulse frequency when other process variables are kept constant at their corresponding mid values. Lowest energy density at the spot irradiation is achieved at lowest value of lamp current and highest value of pulse frequency which helps to lesser thermal diffusion around the machining zone, results in lower value of HAZ width.

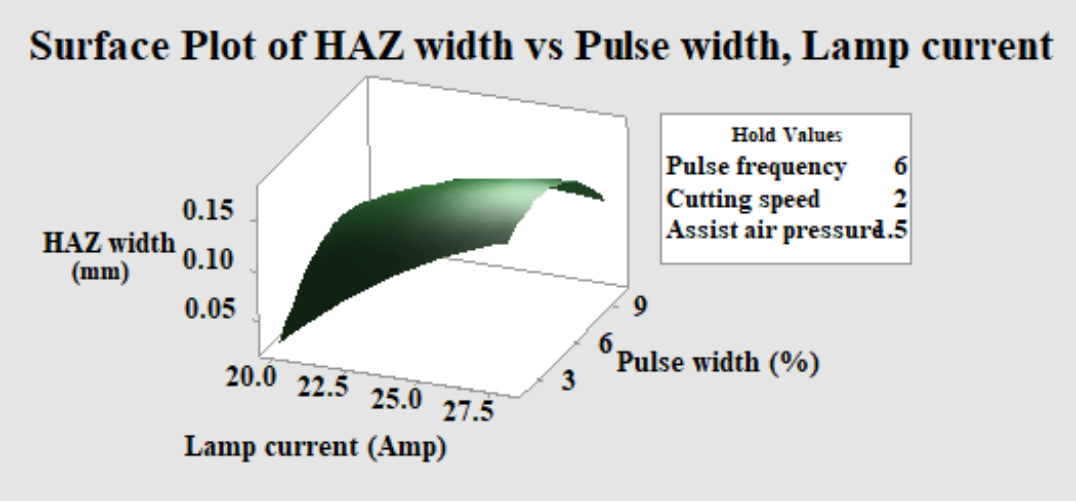

Fig. 6.19 Surface plot of HAZ width with lamp current and pulse width

From the plot 6.19 it is observed that HAz width is increases with increase in lamp current due to increase of thermal energy by the more intensified laser beam interaction with workpiece. Whereas HAZ width marginally increases then decreases with further increase in pulse width. Initially peak power plays a vital role for transformation of phase, solid to liquid which leads to produce cut by removal of that debris from machining zone, results in increase in melt pool formation which try to solidify during longer laser off time by conduction of heat to the adjacent zone. That leads to increase in HAZ width. But further increase in pulse width means decrease in pulse off time which may along with moderate cutting speed helps to restrict the thermal diffusion into a comparatively narrower zone, results in decrease in HAZ width.

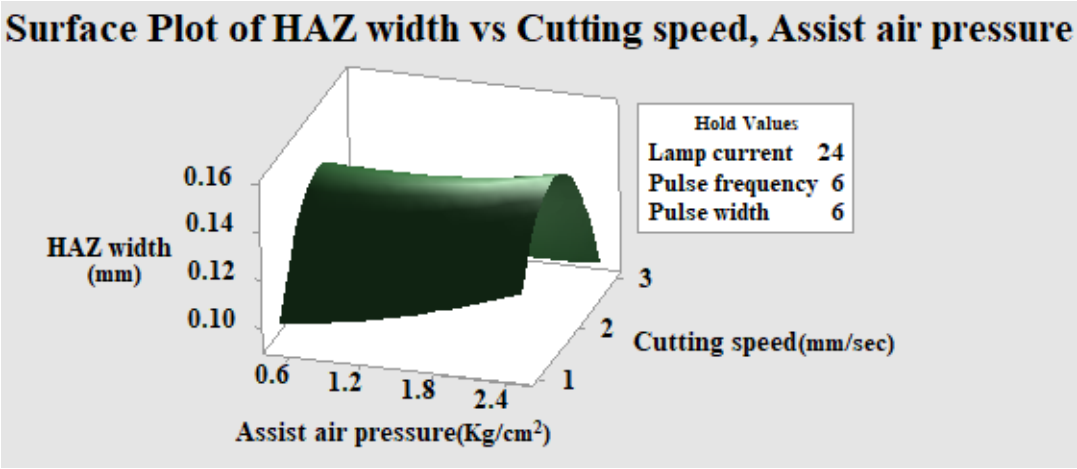

Fig. 6.20 Surface plot of HAZ width with cutting speed and assist air pressure

From the plot 6.20 it is observed that lowest HAZ width can be achieved at combination of lowest assist pressure with highest cutting speed. At this particular parameter setting comparatively lesser interaction time with lower value of assist air pressure helps to proper cooling of machining zone, leads to restriction of heat affected zone. For aforesaid reasons lowest HAZ width may be achieved.

6.2.1.3 Sensitivity analysis

Sensitivity analysis shows if the objective function will increase or decrease with the change in the process parameters and hence considered as the first and most important step in optimization problems. Thus sensitivity analysis determines which process parameter can be modified for getting improved result. Mathematically sensitivity of design objective function is obtained through partial derivative of the function with respect of the variables [79].

To obtained the sensitivity equation for machining responses, i.e. kerf width, depth of cut and HAZ width with respect to controllable variables, respective second order polynomial equations 6.3,6.4 & 6.5 are partially differentiated with respect to corresponding process parameters.

Partially derived equation for kerf width (KW)

$\delta KW/\delta X_1 = 0.005661 - 009266X_1 - 0.002863X_2 - 0.000424X_3 - 0.000500X_4 - 0.000078X_5$ (6.6)

$\delta KW/\delta X_2 = -0.003313 - 0.008302\ X_2 - 0.002863X_1 + 0.000818X_3 - 0.001048X_4 - 0.001179X_5$ (6.7)

$\delta W/\delta X_3 = 0.000415 - 0.005746X_3 - 0.000424X_1 + 0.000818X_2 + 0.000047X_4 - 0.000322X_5$ (6.8)

$\delta KW/\delta X_4 = -0.000466 - 007186X_4 - 0.000500X_1 - 0.001048X_2 + 0.000047X_3 + 0.000089X_5$ (6.9)

$\delta KW/\delta X_5 = 0.000900 - 0.00432X_5 - 0.000078X_1 - 0.001179X_2 - 0.000322X_3 + 0.000089X_4$ (6.10)

Partially derived equation for depth of cut (D)

$\delta D/\delta X_1 = 0.006129+0.000288X_1+0.000064X_2-0.000048X_3-0.000113X_4-0.000344X_5$ (6.11)

$\delta D/\delta X_2 = -0.002368-0.00003X_2+0.000064X_1-0.000088X_3+0.000694X_4+0.000350X_5$ (6.12)

$\delta D/\delta X_3 = 0.000193+0.000146X_3-0.000048X_1-0.000088X_2-0.000181X_4+0.000613X_5$ (6.13)

$\delta D/\delta X_4 = -0.00283-0.000778X_4-0.000113X_1+0.0000694X_2-0.000181X_3+0.001625X_5$ (6.14)

$\delta D/\delta X_5 = -0.00273+0.002022X_5-0.000344X_1+0.000350X_2+0.000613X_3+0.001625X_4$ (6.15)

Partially derived equation for HAZ width (HW)

$\delta HW/\delta X_1 = 0.07973-0.002134X_1+0.000916X_2-0.001583X_3-0.008300X_4+0.001944X_5$ (6.16)

$\delta HW/\delta X_2 = -0.00534-0.000826X_2+0.000916X_1-0.000549X_3-0.004469X_4+0.000812X_5$ (6.17)

$\delta HW/\delta X_3 = 0.06491-0.00483X_3-0.001583X_1-0.000549X_2-0.000398X_4+0.003684X_5$ (6.18)

$\delta HW/\delta X_4 = 0.4109-0.08818X_4-0.008300X_1-0.004469X_2-0.000398X_3-0.00704X_5$ (6.19)

$\delta HW/\delta X_5 = -0.0654+0.00706X_5+0.001944X_1+0.000812X_2+0.003684X_3-0.00704X_4$ (6.20)

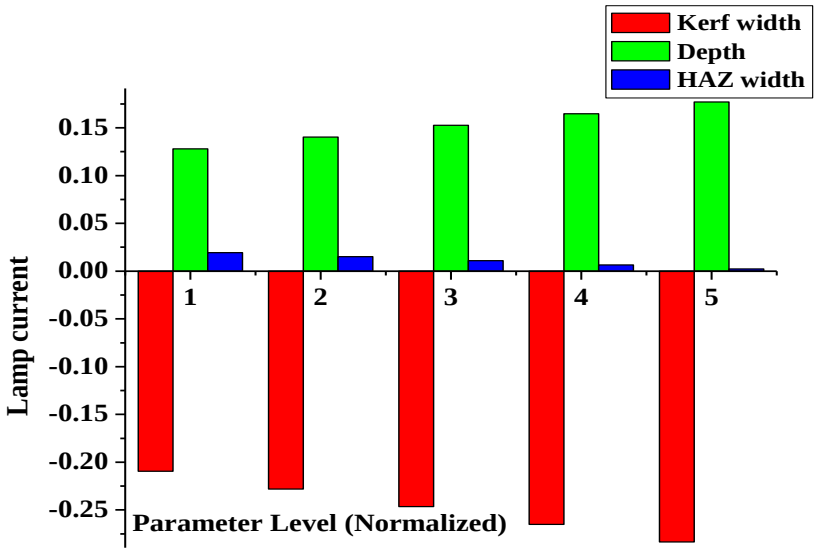

Fig.6.21: Sensitivity of lamp current on machining responses

From the plot 6.21 it is evident that, depth and HAZ width have a positive value of sensitivity whereas kerf width has negative sensitivity. It indicates that if the value of lamp current changes is positive direction, depth and HAZ width increases but kerf width decreases. It also finds from the plot that machining responses are more sensitive to lamp current at lower values than upper.

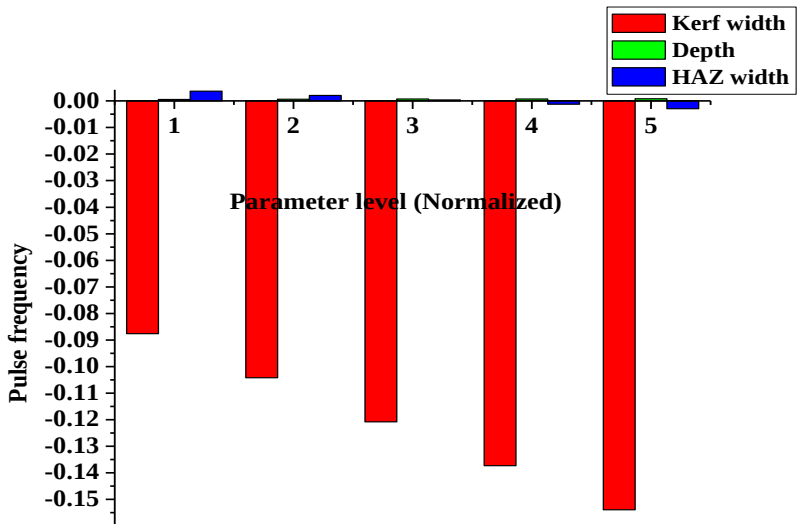

Fig6.22: Sensitivity of pulse frequency on machining responses

It is observed from the plot 6.22 that pulse frequency shows a negative sensitivity with kerf width and marginally sensitive in positive value to depth of cut whereas HAZ width has a merely positive sensitivity initially but later shows a little negative sensitivity. Aforesaid plots demonstrate that pulse frequency more sensitive to kerf width than other two responses when all the other parameters kept constant at their corresponding mid value. It is also found that initially high energy per pulse with comparatively more time between two pulses (more cooling off time) leads to generate residual stress at the solid liquid boundary of the machining zone. But cooling off time is less during higher value of pulse frequency leads to comparatively lower HAZ width. For aforesaid reasons that kind of sensitivity plot may be seen. Lower pulse frequency comparatively generates higher value of pulse energy at the spot of irradiation which helps to form more melt pool. This excess amount of molten debris may not properly removed from the zone of machining by moderate air pressure leads to non uniform kerf width along the travel path of laser. As well as the pulse energy generates at higher value of pulse frequency may not adequate to form a kerf at the machining zone. For the above said reason that kind of sensitivity plot may arise.

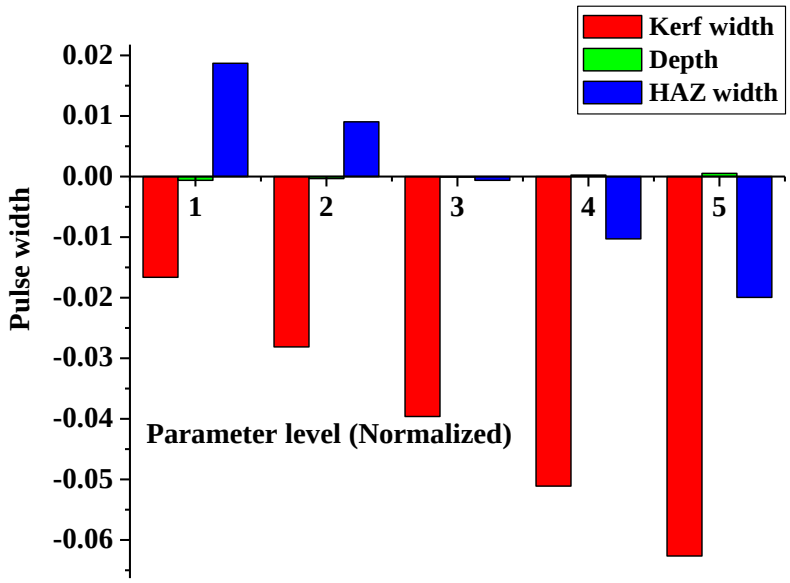

Fig6.23: Sensitivity of pulse width on machining responses

It has been observed from the plot that depth has a negative sensitivity with pulse width but shows a positive sensitivity at later stage within the chosen design space. Lower value of pulse width means higher value of peak power which helps to more penetration during interaction with workpiece. That means increase in pulse width leads to decrease in depth. Kerf width shows a negative sensitivity with pulse width and HAZ width shows initially positive sensitivity upto certain level then negative sensitivity. high concentrated beam energy is generate at low pulse width than higher pulse width for which a little change in pulse width in the lower region may vary the kerf width more than at higher pulse width.

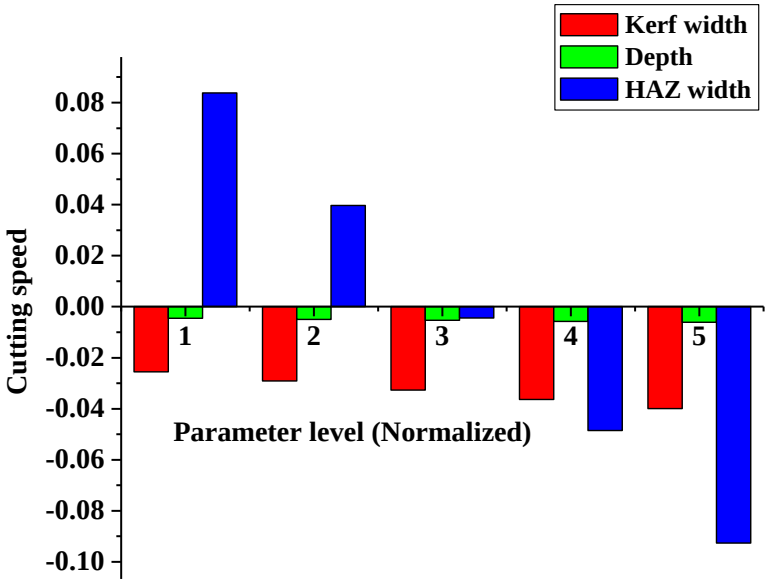

Fig 6.24: Sensitivity of cutting speed on machining responses

It is evident from the plot that kerf width and depth is negatively sensitive to cutting speed whereas HAZ width is positively sensitive at lower value of cutting speed and negatively sensitive after a certain value of cutting speed. The plot indicates that HAZ width is more sensitive than other two machining responses. Kerf width and HAZ width is more sensitive to cutting speed at their respective lower values than upper levels. Sensitivity varies with interaction time which is gradually decreases with increasing cutting speed.

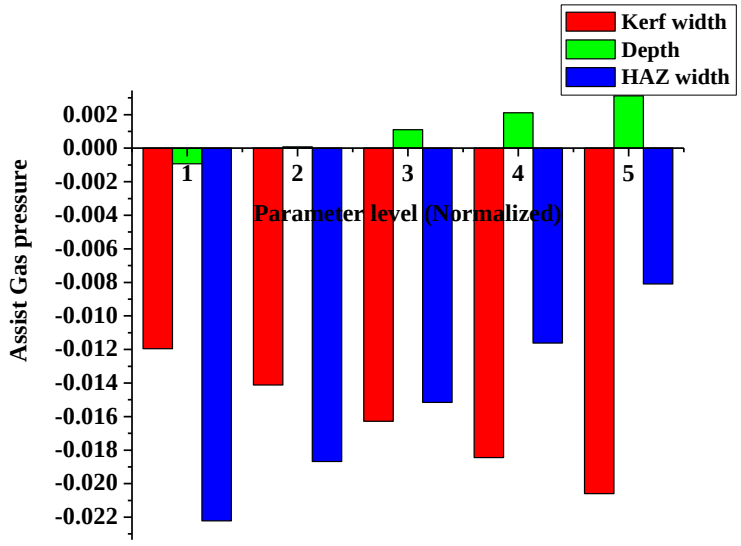

Fig 6.25: Sensitivity of assist gas pressure on machining responses

It is observed from the plot that kerf width and HAZ width are negatively sensitive to assist gas pressure whereas depth is negatively sensitive with lower value of assist gas pressure and positive sensitive with higher value of assist gas pressure. It is also found that kerf width is more sensitive at lower value of assist gas pressure whereas depth and HAZ width is more sensitive at higher value of assist gas pressure when the other process variables kept constant at pre selected mid range. Debris in vapour /molten form is generated during laser beam workpiece interaction are removed from machining zone properly by the lower value of assist gas pressure flow co-axially. But higher value of assist air pressure added some extra energy to the process which may leads to increase in heat affected zone. For the aforesaid reasons that kind of sensitivity plot may be observed.

Fig. 6.26 exhibits the contour plot for investigating the influences of different combinations for dominant process variables on kerf width. A large number of combinations are represented by each contour curve. Good interaction between the process variables and response is indicated by elliptical shape whereas circular shape indicates no interaction between the variables. From the plot it is observed that significant interaction between the variables are mainly happened for pulse frequency with lamp current and lamp current with assist gas pressure. Contour plot of depth of cut and HAZ width are given in fig. 6.27 and 6.28 respectively. From the fig.6.27 it is observed that most significant interaction between dominant process variables are pulse width with lamp current and assist air pressure with lamp current. For HAZ width it is observed that HAZ width with upper value of 0.15 mm and lower value of 0.12 mm is most feasible region to get during experiments when all the variables are kept constant in their respective mid value.

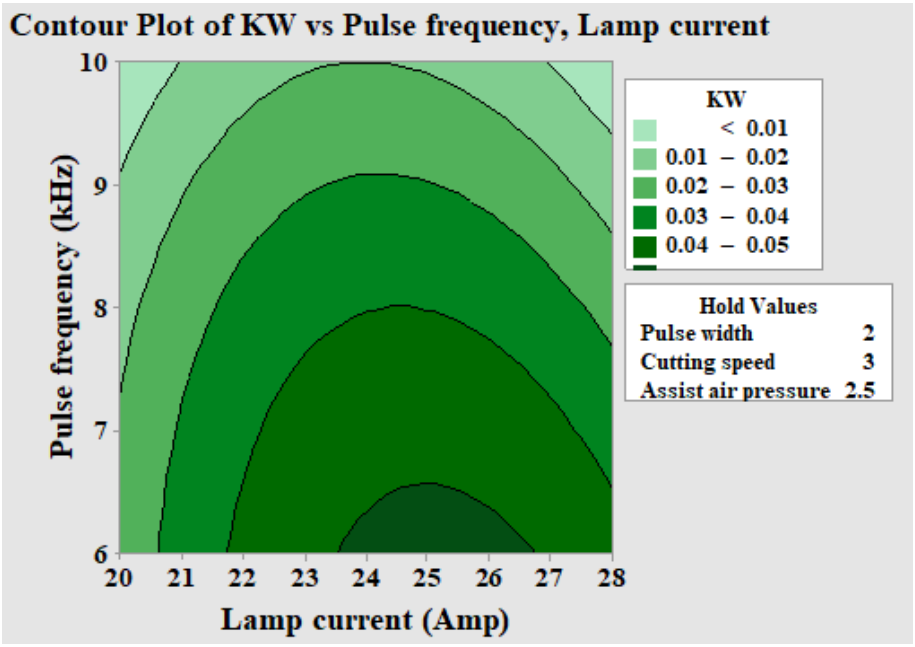
Contour Plot of KW vs Pulse frequency, Lamp current
Pulse frequency (kHz)
10
9
8
7
6
20 21 22 23 24 25 26 27 28
Lamp current (Amp)
KW
< 0.01
0.01 – 0.02
0.02 – 0.03
0.03 – 0.04
0.04 – 0.05
Hold Values
Pulse width 2
Cutting speed 3
Assist air pressure 2.5

(a)

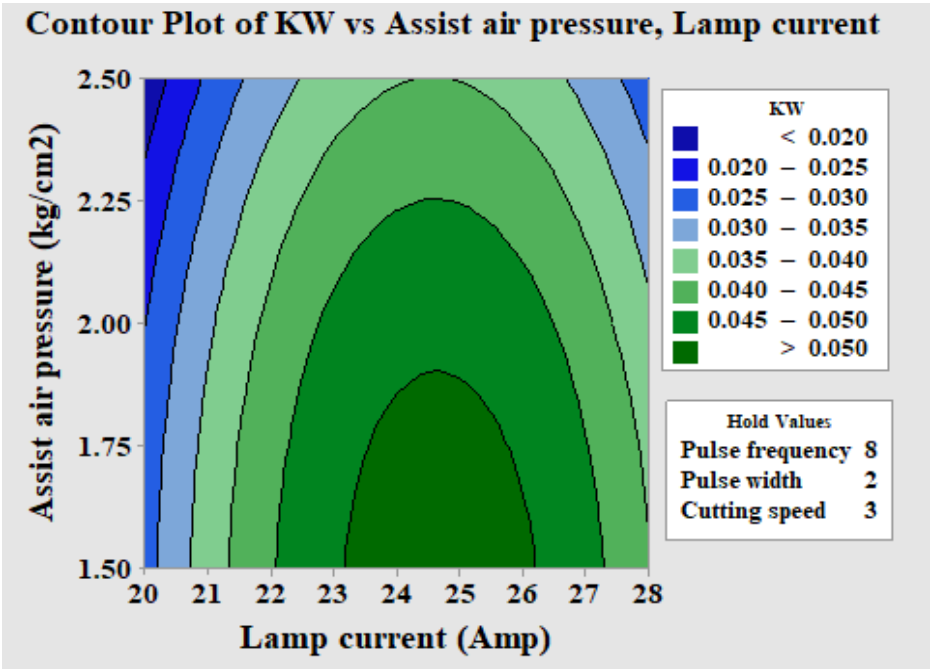
Contour Plot of KW vs Assist air pressure, Lamp current
Assist air pressure (kg/cm2)
2.50
2.25
2.00
1.75
1.50
20 21 22 23 24 25 26 27 28
Lamp current (Amp)
KW
< 0.020
0.020 – 0.025
0.025 – 0.030
0.030 – 0.035
0.035 – 0.040
0.040 – 0.045
0.045 – 0.050
> 0.050
Hold Values
Pulse frequency 8
Pulse width 2
Cutting speed 3

(b)

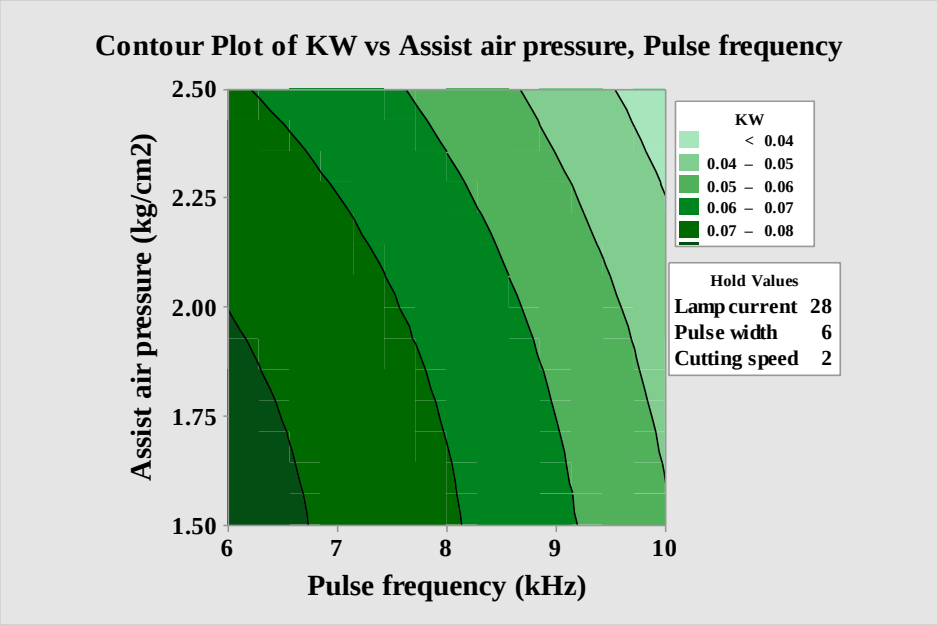

(c)

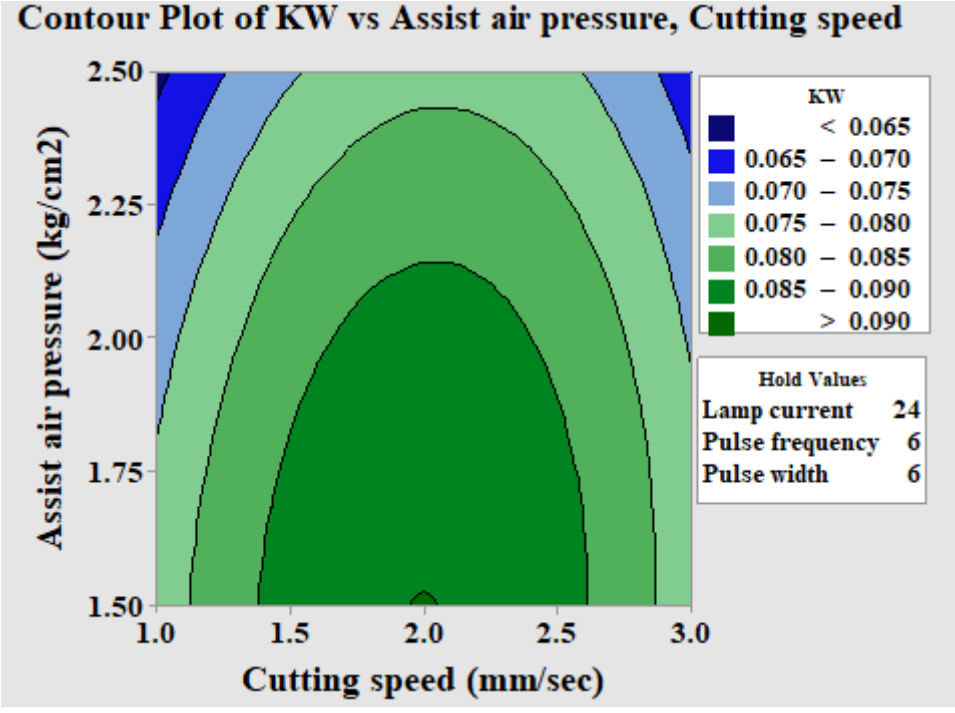

(d)

Fig. 6.26 (a,b,c,d) contour plots of kerf width with all process variables.

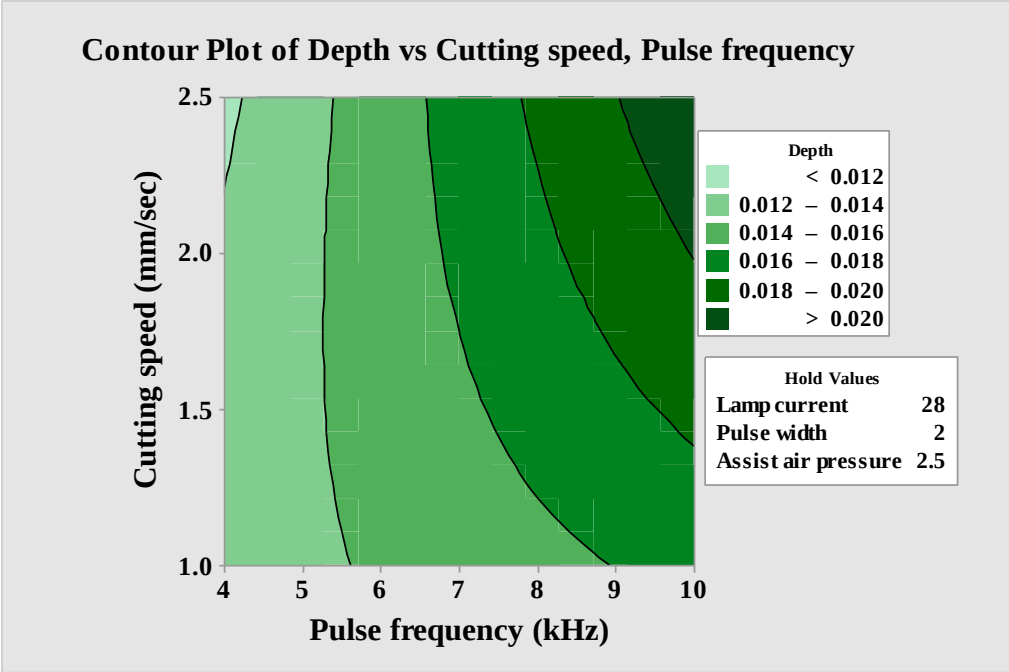
Contour Plot of Depth vs Cutting speed, Pulse frequency
Cutting speed (mm/sec)
2.5
2.0
1.5
1.0
4
5
6
7
8
9
10
Pulse frequency (kHz)
Depth
< 0.012
0.012 – 0.014
0.014 – 0.016
0.016 – 0.018
0.018 – 0.020
> 0.020
Hold Values
Lamp current 28
Pulse width 2
Assist air pressure 2.5

(a)

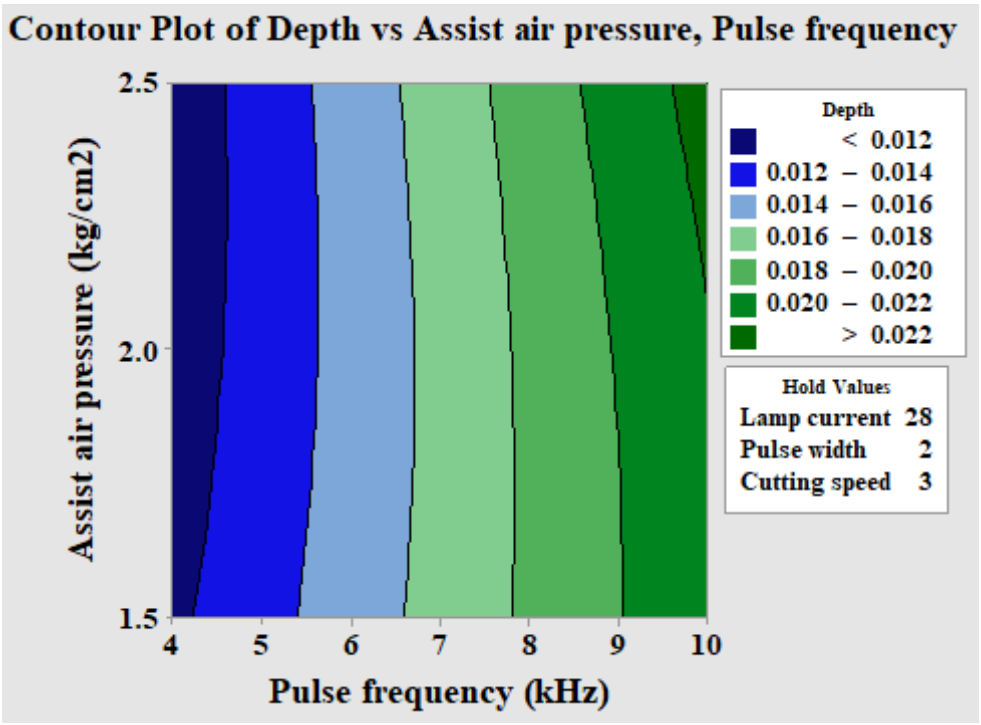
Contour Plot of Depth vs Assist air pressure, Pulse frequency
Assist air pressure (kg/cm2)
2.5
2.0
1.5
4
5
6
7
8
9
10
Pulse frequency (kHz)
Depth
< 0.012
0.012 – 0.014
0.014 – 0.016
0.016 – 0.018
0.018 – 0.020
0.020 – 0.022
> 0.022
Hold Values
Lamp current 28
Pulse width 2
Cutting speed 3

(b)

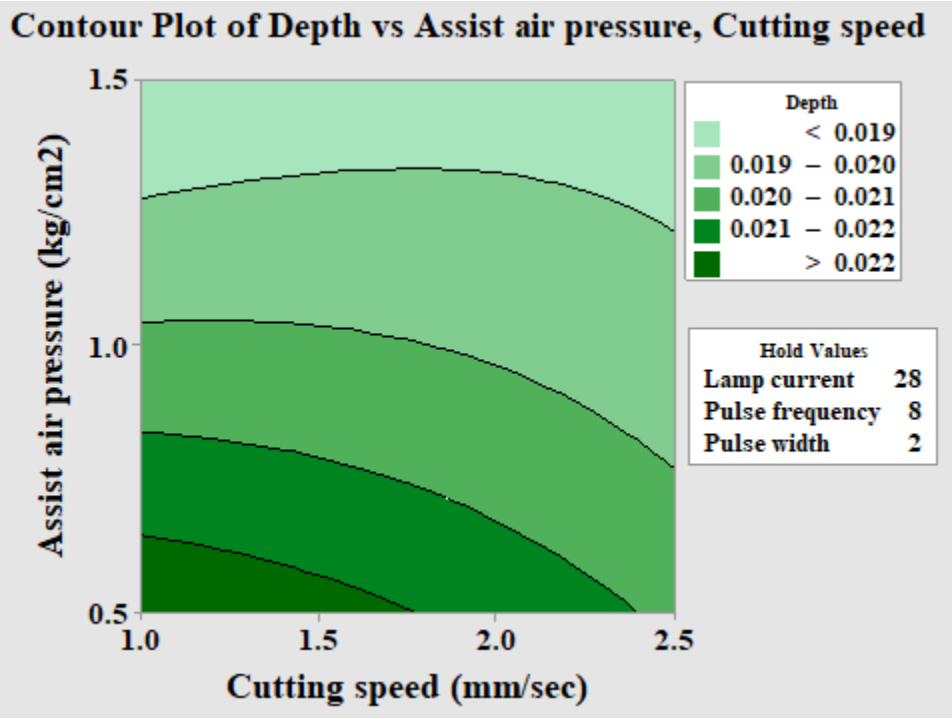

(c)

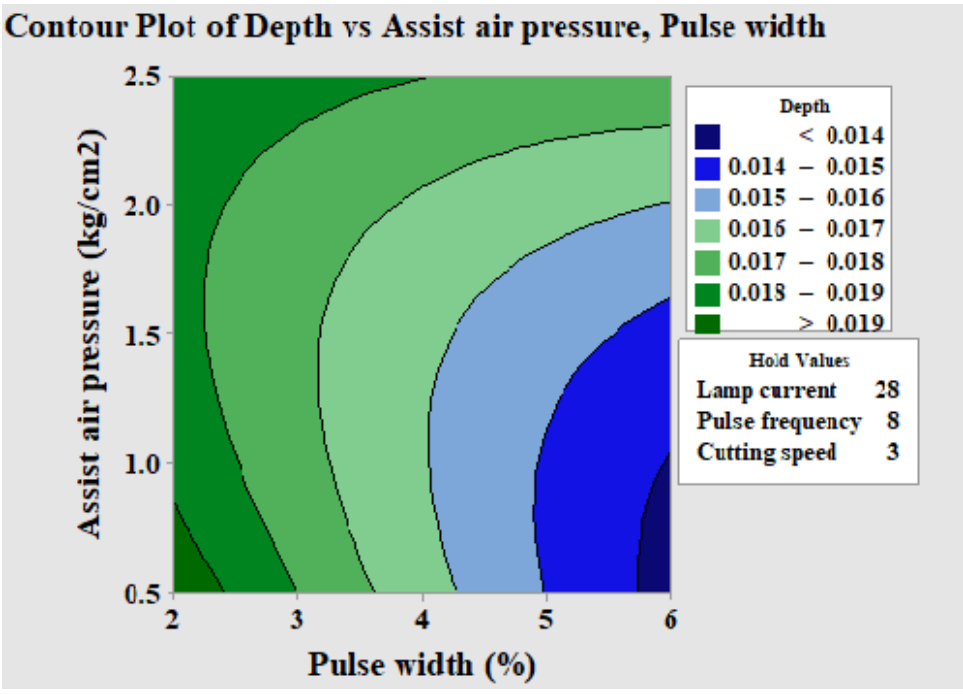

(d)

Fig. 6.27 (a,b,c,d) Contour plots of depth of cut with dominant process variables.

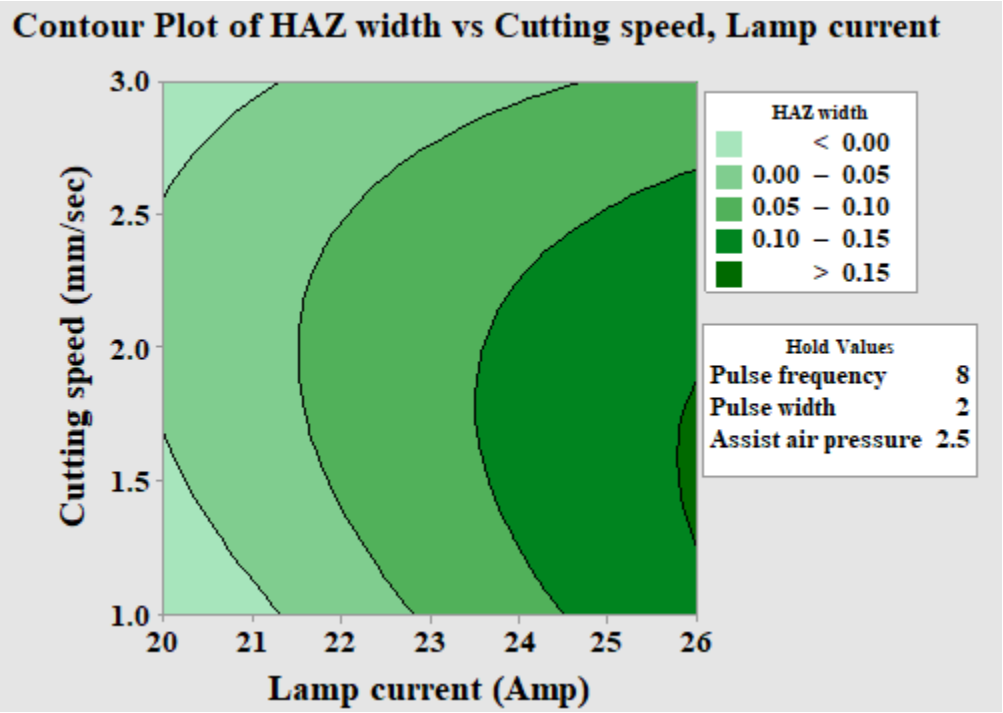
Contour Plot of HAZ width vs Cutting speed, Lamp current
Cutting speed (mm/sec)
3.0
2.5
2.0
1.5
1.0
20
21
22
23
24
25
26
Lamp current (Amp)
HAZ width
< 0.00
0.00 – 0.05
0.05 – 0.10
0.10 – 0.15
> 0.15
Hold Values
Pulse frequency 8
Pulse width 2
Assist air pressure 2.5

(a)

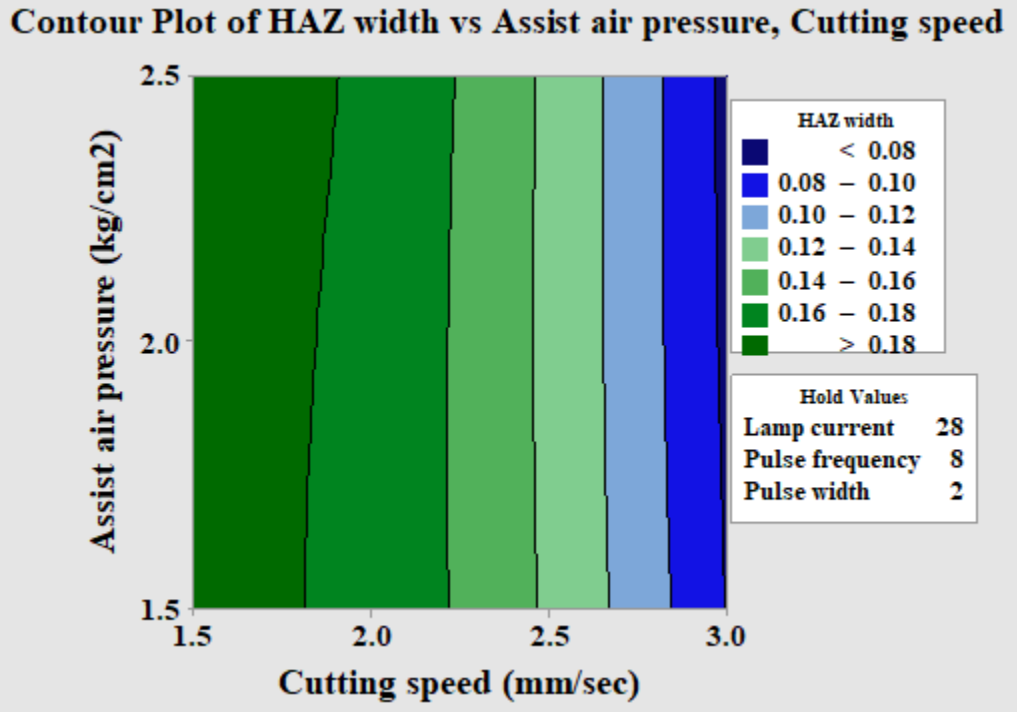
Contour Plot of HAZ width vs Assist air pressure, Cutting speed
Assist air pressure (kg/cm2)
2.5
2.0
1.5
1.5
2.0
2.5
3.0
Cutting speed (mm/sec)
HAZ width
< 0.08
0.08 – 0.10
0.10 – 0.12
0.12 – 0.14
0.14 – 0.16
0.16 – 0.18
> 0.18
Hold Values
Lamp current 28
Pulse frequency 8
Pulse width 2

(b)

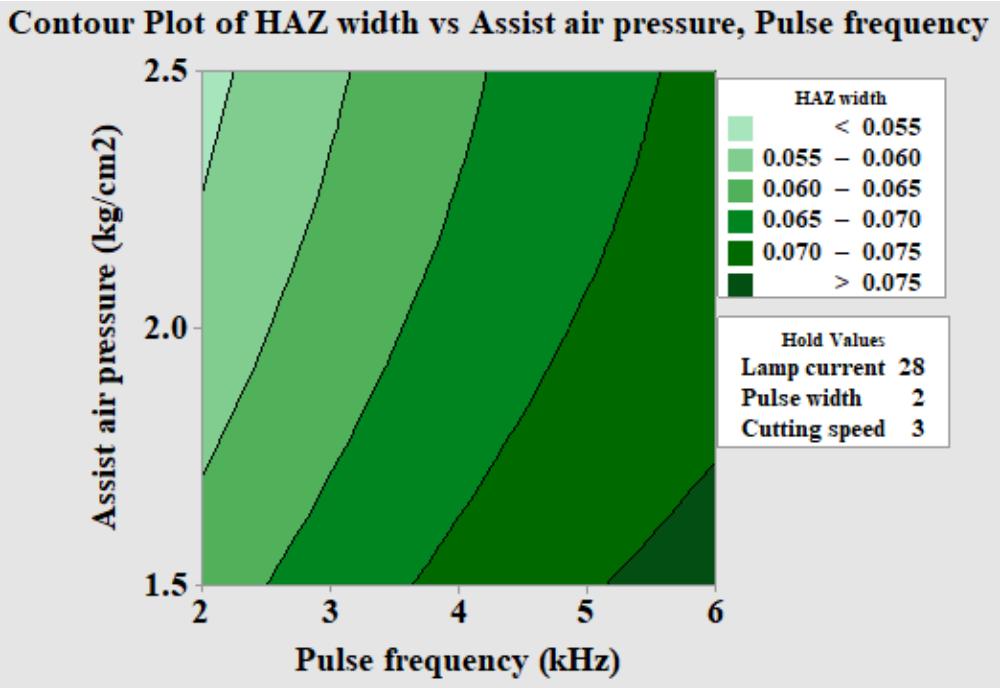

(c)

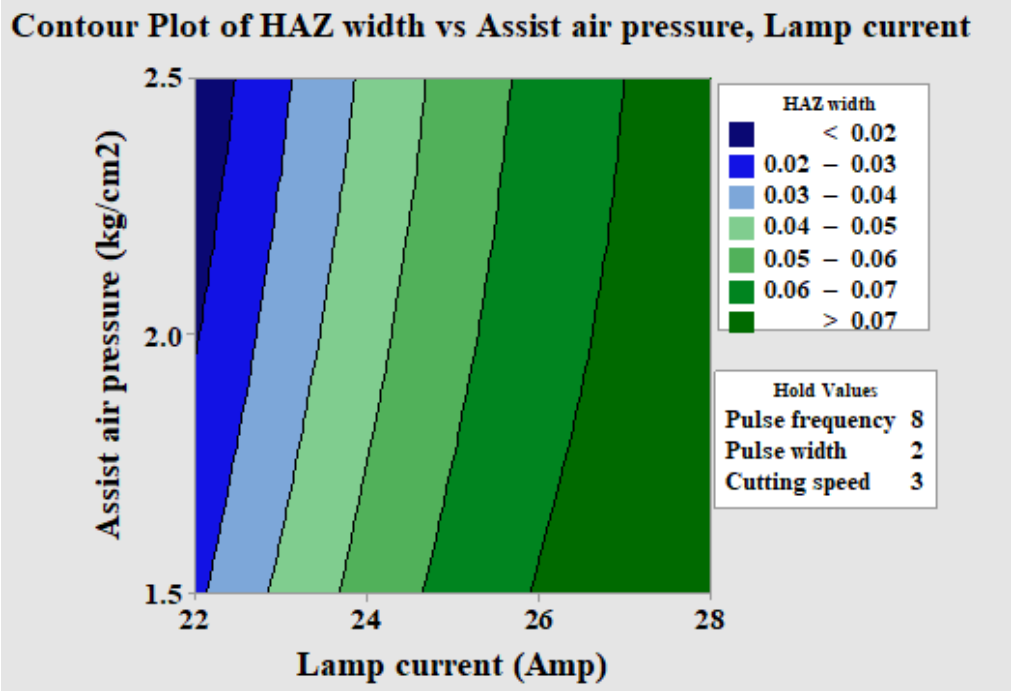

(d)

Fig. 6.28 (a,b,c,d) Contour plots of depth of cut with dominant process variables.

6.2.1.4 Determination of optimal process parameter settings

Fig.6.29, 6.30 and fig 6.31 shows the single objective optimization results for the minimum kerf width, minimum HAZ width and maximum depth of cut based on the polynomial model developed by using Eq. 6.3,6.4 and 6.5.To get ideal machining response, the value of the weight for linear desirability function (d) is considered as 1.

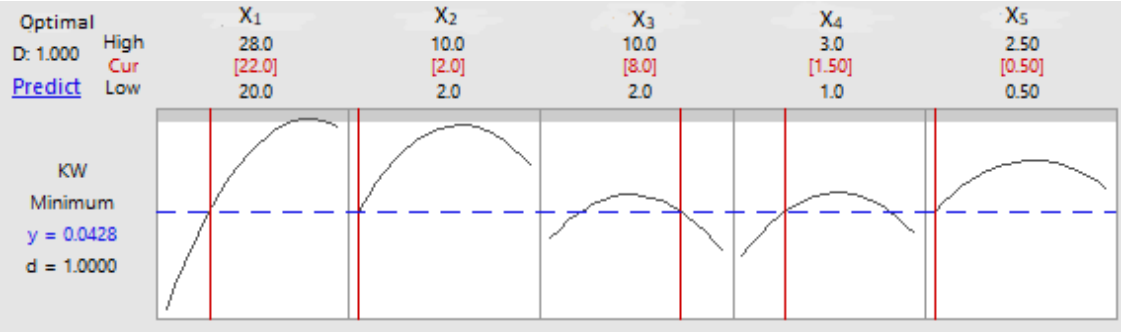

Fig 6.29 Single objective optimization in respect of kerf width

It is found from the figure that minimum kerf width of 0.0428 mm can be achieved at process parameter settings of 22 Amp lamp current (X_1), 2.0 kHz pulse frequency (X_2), 8% pulse width (X_3), 1.50 mm / sec of cutting speed (X_4) and 0.5kg/cm^2 of assist gas pressure (X_5).

It is found from the figure that maximum depth of cut 0.0216 mm can be achieved at process parameter settings of 28 Amp lamp current (X_1), 10.0 kHz pulse frequency (X_2), 4% pulse width (X_3), 3 mm / sec of cutting speed (X_4) and 2.5kg/cm^2 of assist gas pressure (X_5).

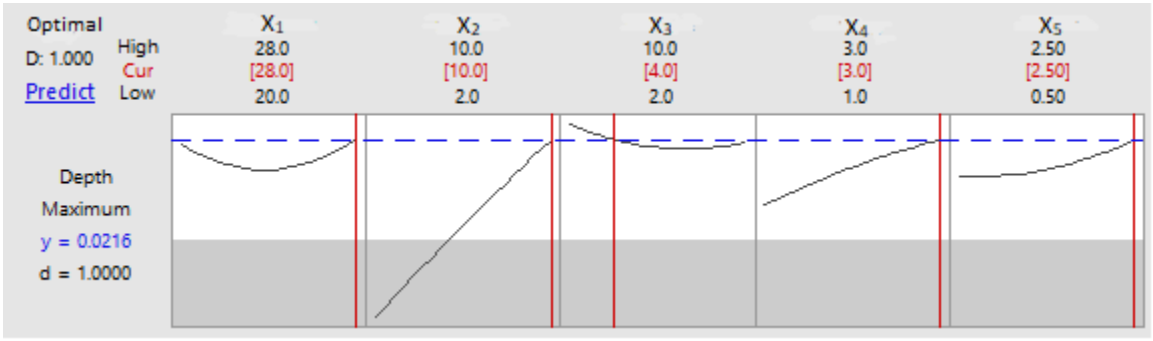

Fig 6.30 Single objective optimization in respect of depth of cut

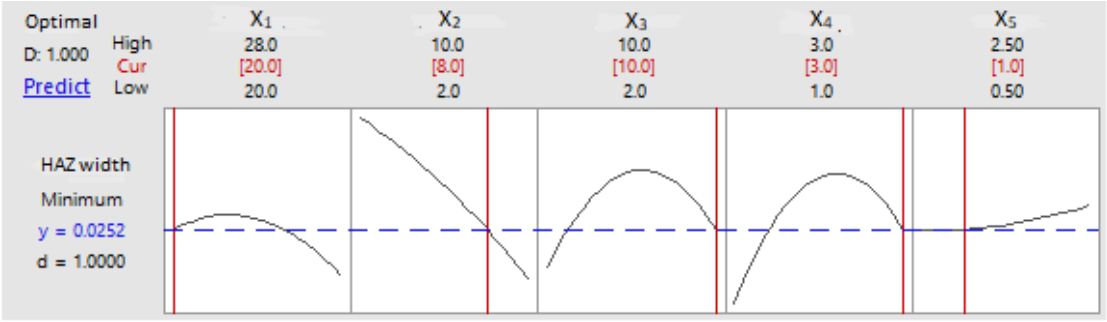

Fig 6.31 Single objective optimization in respect of HAZ width

It is found from the figure that minimum HAZ width of 0.0252 mm can be achieved at process parameter settings of 20 Amp lamp current (X_1), 8.0 kHz pulse frequency (X_2), 10% pulse width (X_3), 3 mm / sec of cutting speed (X_4) and 1.0 kg/cm^2 of assist gas pressure (X_5).

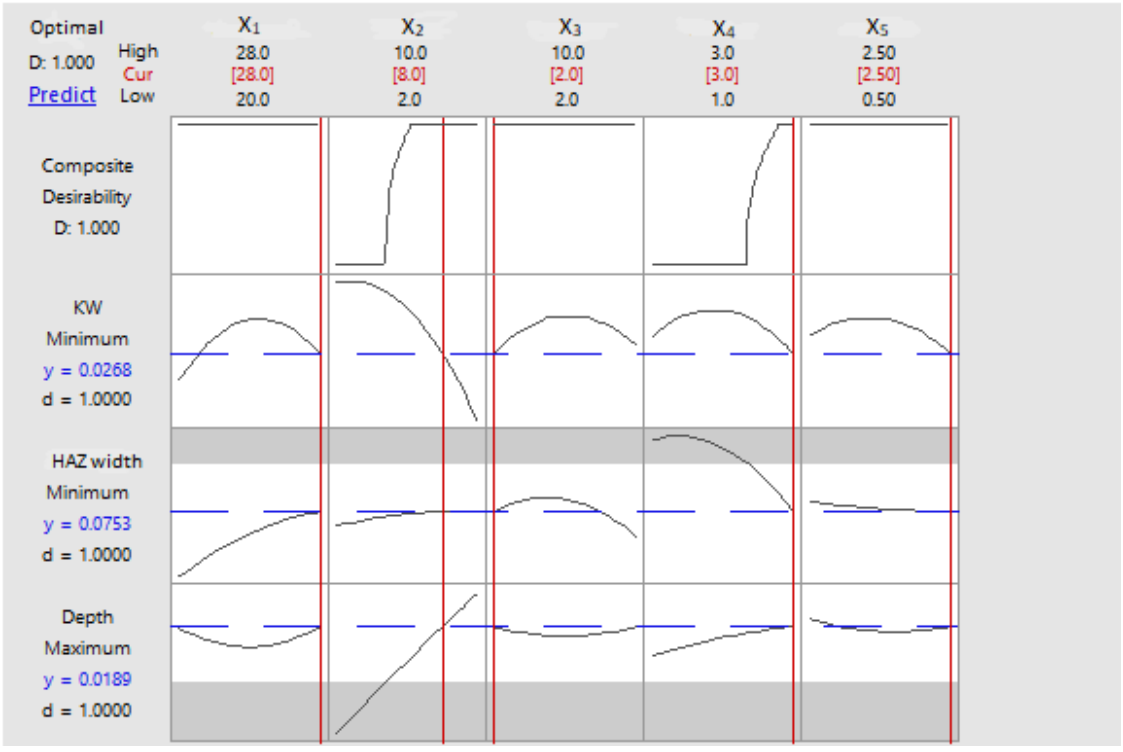

Fig 6.32 Multi-objective optimization in respect of machining responses

From figure 6.32 it is observed that kerf width of 0.0268 mm, HAZ width of 0.0753 mm and depth of 0.0189 mm can be achieved with optimum parameter settings of 28 amp of lamp current (X_1), 8 kHz pulse frequency (X_2), 2% of pulse width (X_3) , 3mm/sec cutting speed (X_4) and 2.50 kg/cm^2 assist air pressure (X_5).

6.2.1.4.1 Confirmation test

Five additional experiments are carried as per optimal settings based on multiobjective optimization performed. Average of experimental results are taken into account for confirmation test and given below in table 6.16

Table 6.16 Confirmation test of laser microcutting with aide of assist gas pressure

Machining responses	Predicted value at Optimal parametric settings	Experimental value at Optimal parametric settings	% of error
Kerf width (mm)	0.0268	0.0281	4.85
Depth of cut (mm)	0.0189	0.0184	2.65
HAZ width (mm)	0.0753	0.0789	4.78

6.2.2 Parametric study on laser beam microcutting of Inconel 625 superalloy at submerged condition in water

Undesired quality aspects, i.e. kerf taper, dross formation, heat affected zone, recast layer, burr formation, difficulties in debris removal and desired surface morphology during laser cutting sometimes remove or partially corrected by irradiate the workpiece material at submerged condition.

Advantages of laser beam cutting at submerge condition [31]

1) Narrow heat affected zone is generated due to low thermal load on workpiece.
2) Strong hydrodynamic force generates by bubble dynamics, carry away the debris from machining zone.
3) Shorter wavelength of irradiate laser beam at liquid helps to increase the absorptivity of workpiece at submerged condition.
4) Risk of atmosphere contamination is reduced at submerged condition.

Sometimes water solution of salts or bases or acids are used during submerged laser beam machining to improve the etch rate and finish quality. To improve the wetting quality of water film on workpiece surface organic additive are added.

6.2.2.1 Experimental set up

In this study same laser system with same beam characteristics is used to carry out the experiments. Only submerged condition is added in place of assist gas at required pressure to perform the experiments as per five factor five level design of central composite design based response surface methodology. The schematic diagram of the underwater pulsed Nd:YAG laser based CNC machining system is shown in fig.6.33.

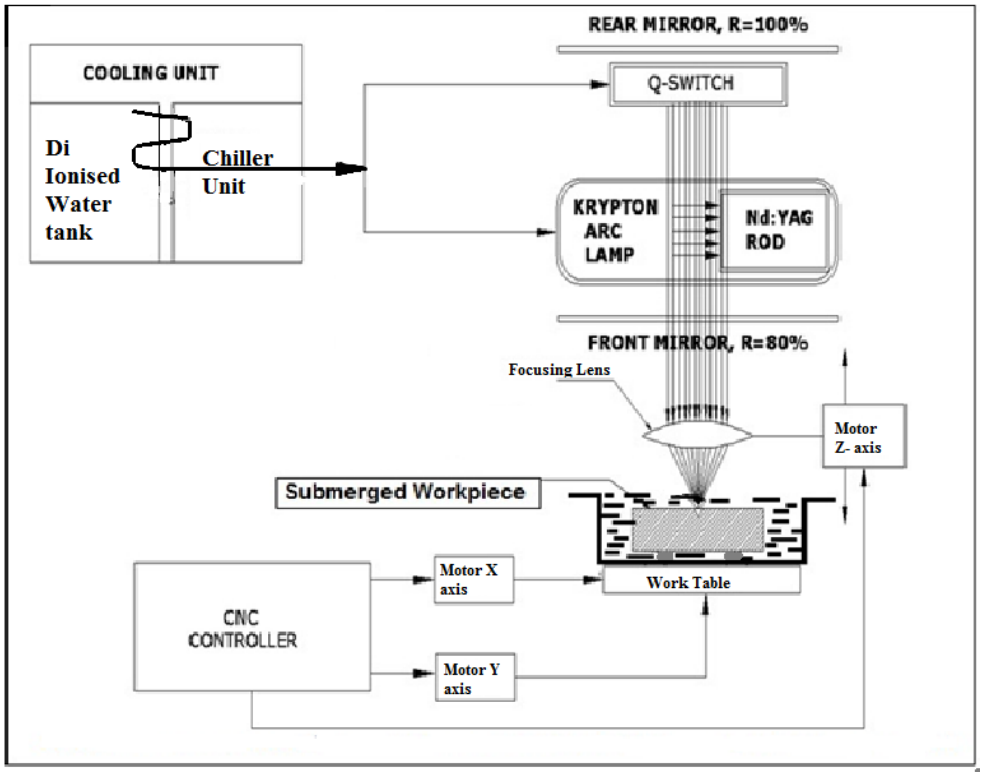

Fig. 6.33. Schematic diagram of Pulsed Nd:YAG laser beam machining set up at submerged condition [31].

In this experimental procedure a water film from one to five mm is used to carry out the experiments. For that laser beam comes from outside and first interact with water film then travel a distance trough the water to incident on workpiece substrate. Workpiece is hold here in submerged condition by pouring water externally. Height of water column over the workpiece is maintained preciously by placing the slip gauge over the workpiece material. From the dimension of slip gauge the height of water column over the surface of workpiece material is controlled as requirement. A steady state of water column is maintained during the experiment. De-ionized water at room temperature (20-22 °C) has been used as submerged medium because of its non-reactive nature to work-piece material even at elevated temperatures and easy availability. The bubbles accumulated near the fusion region are removed from the machining zone by a thin stick after each experimental run and wait for few minutes for stabilization of stagnant water. Jammer is used for tightly fixed the workpiece in a position.

Range of all controllable input process variables for underwater laser machining i.e. lamp current, pulse frequency, pulse width, cutting speed and height of water level as selected are listed in Table 6.17.

TABLE 6.17 Process parameters levels

Process Parameter& Symbol	Unit	Value of α	Levels	
			Lowest (-2)	Highest (+2)
Lamp Current (x_1)	Amp	2.00	20	28
Pulse Frequency (x_2)	kHz		2	10
Pulse Width (x_3)	%		2	10
Cutting Speed (x_4)	mm/sec		1	3
Height of Water Level (x_5)	mm		1	5

Image of machining responses, are captured by Olympus (STM 6) optical microscope at 20x magnification and measured by image analysis software provide with it which is listed in table no. 6.18. Image of blind cut at submerged condition is given in figure no. Each response has been measured at three different locations across the cut to reduce the measurement error and their statistical average has been taken for further analysis.

6.2.2.2 Experimental results and discussion

Table 6.18 Experimental results

Exp. No.	Lamp current (Amp)	Pulse frequency (kHz)	Pulse width (%)	Cutting speed (mm/sec)	Height of water level (mm)	Kerf width (mm)	Depth of cut (mm)	Heat affected zone width (mm)
1	22	4	4	1.5	2	0.1346	0.0271	0.06582
2	26	4	4	1.5	2	0.1836	0.0243	0.07205
3	22	8	4	1.5	2	0.0933	0.0274	0.05652
4	26	8	4	1.5	2	0.1039	0.0230	0.07403
5	22	4	8	1.5	2	0.1141	0.0272	0.06717
6	26	4	8	1.5	2	0.1886	0.0275	0.07583
7	22	8	8	1.5	2	0.0860	0.0274	0.06133
8	26	8	8	1.5	2	0.0963	0.0257	0.07983
9	22	4	4	2.5	2	0.1193	0.0315	0.06440
10	26	4	4	2.5	2	0.1571	0.0255	0.07280
11	22	8	4	2.5	2	0.0912	0.0232	0.04652
12	26	8	4	2.5	2	0.0910	0.0189	0.06787
13	22	4	8	2.5	2	0.1052	0.0274	0.06833
14	26	4	8	2.5	2	0.1640	0.0280	0.07682

Exp. No.	Lamp current (Amp)	Pulse frequency (kHz)	Pulse width (%)	Cutting speed (mm/sec)	Height of water level (mm)	Kerf width (mm)	Depth of cut (mm)	Heat affected zone width (mm)
15	22	8	8	2.5	2	0.0843	0.0198	0.05060
16	26	8	8	2.5	2	0.0854	0.0216	0.07402
17	22	4	4	1.5	4	0.1355	0.0220	0.05582
18	26	4	4	1.5	4	0.2294	0.0204	0.06347
19	22	8	4	1.5	4	0.0941	0.0233	0.05132
20	26	8	4	1.5	4	0.1156	0.0225	0.07473
21	22	4	8	1.5	4	0.1477	0.0243	0.05177
22	26	4	8	1.5	4	0.1997	0.0241	0.06120
23	22	8	8	1.5	4	0.0866	0.0229	0.05150
24	26	8	8	1.5	4	0.0949	0.0248	0.07607
25	22	4	4	2.5	4	0.1301	0.0265	0.05097
26	26	4	4	2.5	4	0.2176	0.0231	0.06157
27	22	8	4	2.5	4	0.0919	0.0187	0.03750
28	26	8	4	2.5	4	0.0942	0.0188	0.06297
29	22	4	8	2.5	4	0.1270	0.0257	0.04867
30	26	4	8	2.5	4	0.2043	0.0268	0.06110
31	22	8	8	2.5	4	0.0756	0.0161	0.04193
32	26	8	8	2.5	4	0.0824	0.0213	0.06718
33	20	6	6	2	3	0.0945	0.0225	0.04162
34	28	6	6	2	3	0.1526	0.0222	0.07380
35	24	2	6	2	3	0.1837	0.0307	0.06198
36	24	10	6	2	3	0.0707	0.0231	0.05858
37	24	6	2	2	3	0.1255	0.0189	0.06557
38	24	6	10	2	3	0.1291	0.0196	0.06850
39	24	6	6	1	3	0.1358	0.0299	0.06588
40	24	6	6	3	3	0.1378	0.0255	0.05267
41	24	6	6	2	1	0.1188	0.0309	0.07733
42	24	6	6	2	5	0.1400	0.0254	0.05488
43	24	6	6	2	3	0.1428	0.0286	0.06233
44	24	6	6	2	3	0.1349	0.0287	0.06232
45	24	6	6	2	3	0.1311	0.0289	0.06472
46	24	6	6	2	3	0.1359	0.0278	0.06167
47	24	6	6	2	3	0.1289	0.0301	0.06405
48	24	6	6	2	3	0.1371	0.0270	0.06360
49	24	6	6	2	3	0.1238	0.0301	0.06412
50	24	6	6	2	3	0.1277	0.0279	0.06410
51	24	6	6	2	3	0.1264	0.0291	0.06292
52	24	6	6	2	3	0.1328	0.0281	0.06130

6.2.2.2.1 Development of Second order polynomial model

Response surface modeling (central composite design) is used to establish the mathematical relationship between the response and variable process parameters. The second order polynomial equations are given below

$$Y_{KW} = -0.925 + 0.0605 X_1 + 0.0862 X_2 + 0.0082 X_3 + 0.0031 X_4 - 0.0052 X_5 - 0.000645 X_1X_1 - 0.000417 X_2X_2 - 0.000413 X_3X_3 + 0.00291 X_4X_4 - 0.00112 X_5X_5 - 0.003672 X_1X_2 - 0.000105 X_1X_3 - 0.00152 X_1X_4 + 0.001680 X_1X_5 - 0.000213 X_2X_3 + 0.00106 X_2X_4 - 0.003453 X_2X_5 + 0.00037 X_3X_4 - 0.000627 X_3X_5 + 0.00141 X_4X_5 \quad (6.21)$$

$$Y_{Depth} = -0.1572 + 0.01547 X_1 + 0.00207 X_2 + 0.00202 X_3 + 0.01059 X_4 - 0.00984 X_5 - 0.000391 X_1X_1 - 0.000107 X_2X_2 - 0.000585 X_3X_3 - 0.000897 X_4X_4 - 0.000114 X_5X_5 + 0.000076 X_1X_2 + 0.000251 X_1X_3 + 0.000138 X_1X_4 + 0.000293 X_1X_5 - 0.000054 X_2X_3 - 0.001755 X_2X_4 + 0.000109 X_2X_5 - 0.000417 X_3X_4 + 0.000109 X_3X_5 + 0 .000404 X_4X_5 \quad (6.22)$$

$$Y_{HAZ\ width} = 0.63058 + 0.007893X_1 - 0.001267X_2 + 0.001022X_3 - 0.002791X_4 - 0.005027X_5 - 0.001270X_1^2 - 0.000626X_2^2 + 0.001061X_3^2 - 0.000879X_4^2 + 0.000830X_5^2 + 0.003362X_1X_2 + 0.000316X_1X_3 + 0.000607X_1X_4 + 0.000820X_1X_5 + 0.000844X_2X_3 - 0.002134X_2X_4 + 0.001911X_2X_5 + 0.000410X_3X_4 - 0.01027X_3X_5 - 0.000711X_4X_5 \quad (6.23)$$

6.2.2.2.2 ANOVA of machining responses

To test the adequacy of the developed mathematical models for Kerf width, depth of cut and HAZ width, Analysis of variance (ANOVA) and subsequently F- and p-value tests have been carried out. ANOVA analysis of the quadratic model with other adequacy measures R^2, adjusted R^2 and predicted R^2 are given in Table 6.18, table 6.19 & Table 6.20.

TABLE 6.18. ANOVA result of kerf width at submerged condition

Source	DF	Adj SS	Adj MS	F-Value	P-Value
Model	20	0.068474	0.003424	45.47	0.00
Linear	5	0.058979	0.011796	156.67	0.00
Lamp current	1	0.012522	0.012522	166.32	0.00
Pulse frequency	1	0.043371	0.043371	576.06	0.00
Pulse width	1	0.000444	0.000444	5.89	0.021
Cutting speed	1	0.000805	0.000805	10.69	0.003

Source	DF	Adj SS	Adj MS	F-Value	P-Value
Height of water column	1	0.001837	0.001837	24.40	0.00
Square Term	5	0.000495	0.000099	1.32	0.283
2-way Interaction	10	0.009	0.0009	11.95	0.00
Error	31	0.002334	0.000075		
Lack-of-Fit	22	0.002041	0.000093	2.85	0.093
Pure Error	9	0.000293	0.000033		
Total	51	0.070808			
S	R-sq		R-sq(adj)	R-sq(pred)	
0.0086769	96.70%		94.58%	88.71%	

From table 6.18 it is observed that the associated p-value is less than 0.05 (i.e. , $\alpha = 0.05$, or 95% confidence level) of the model, indicates that the model terms are statistically significant. The lack-of-fit value of the model indicates non-significance, as this is desirable. All the input process parameters along with the 2 way interaction term are significant and have some effect on machining responses. From the table it is observed that statistically pulse frequency (73.54%) is the most dominating factor for kerf width followed by lamp current (21.23%), height of water (3.12%), cutting speed (1.36%) and pulse width (0.75%). Values of other adequacy measures R-sq, adjusted R-sq and predicted R-sq are in reasonable agreement and are close to100%, which indicate adequacy of the model.

TABLE 6.19. ANOVA result of depth of cut at submerged condition

Source	DF	Adj SS	Adj MS	F-Value	P-Value
Model	20	0.000681	0.000034	37.49	0.00
Linear	5	0.000237	0.000047	52.05	0.00
Lamp current	1	0.000005	0.000005	5.98	0.20
Pulse frequency	1	0.000127	0.000127	139.23	0.00
Pulse width	1	0.000006	0.000006	6.91	0.013
Cutting speed	1	0.000022	0.000022	24.47	0.00
Height of water column	1	0.000076	0.000076	83.65	0.00
Square Term	5	0.000288	0.000058	63.39	0.00
2-way Interaction	10	0.000157	0.000016	17.25	0.00
Error	31	0.000028	0.000001		
Lack-of-Fit	22	0.000019	0.000001	0.90	0.603
Pure Error	9	0.000009	0.000001		
Total	51	0.000710			
S	R-sq		R-sq(adj)	R-sq(pred)	
0.0009534	96.03%		93.47%	88.72%	

From table 6.19 it is observed that the associated p-value of less than 0.05 for the model (i.e. , α = 0.05, or 95% confidence level) indicates that the model terms are statistically significant. The lack-of-fit value of the model indicates non-significance, as this is desirable. ANOVA results show that all the input process parameters are significant. Values of other adequacy measures R-sq, adjusted R-sq and predicted R-sq are in reasonable agreement and are close to100%, which indicate adequacy of the model. F-value (0.9) and P-value (0.603) of the Lack-of-Fit implies that it is not significant relative to the pure error, as this is desired. From the table it is observed that statistically, pulse frequency (53.50 %) is the most dominating factor followed by height of water level (32.14%), cutting speed (9.40%), pulse width (2.66%) and lamp current (2.29 %).

TABLE 6.20. ANOVA result of HAZ width at submerged condition

Source	DF	Adj SS	Adj MS	F-Value	P-Value
Model	20	0.004807	0.000240	196.8	0.00
Linear	5	0.003921	0.000784	641.99	0.00
Lamp current	1	0.002492	0.002492	2040.49	0.00
Pulse frequency	1	0.000064	0.000064	52.53	0.00
Pulse width	1	0.000042	0.000042	34.19	0.00
Cutting speed	1	0.000312	0.000312	255.17	0.00
Height of water column	1	0.001011	0.001011	827.58	0.00
Square Term	5	0.000148	0.000030	24.22	0.00
2-way Interaction	10	0.000739	0.000074	60.49	0.00
Error	31	0.000038	0.000001		
Lack-of-Fit	22	0.000026	0.000001	0.85	0.645
Pure Error	9	0.000012	0.000001		
Total	51	0.004845			

S	R-sq	R-sq(adj)	R-sq(pred)
0.0011052	99.22%	98.71%	97.72%

ANOVA analysis of the second order polynomial model with other adequacy measures R-sq, adjusted R-sq and predicted R-sq are listed in Table 6.18 The associated p-value of less than 0.05 for the model (i.e., α = 0.05, or 95% confidence level) indicates that the model terms are statistically significant. It is found from ANOVA analysis that all the input process parameters are statistically significant. Lamp current is the most dominant (63.56%) process variable on machining response, followed by height of water column (25.78%), cutting speed (7.95%), pulse frequency (1.64%) and pulse width (1.07%). Values of other adequacy measures R-sq, adjusted

R-sq and predicted R-sq are in moderate range and are close to100%, which reflects adequacy of the model.

6.2.2.2.3 Parametric Study

From the fig 6.34 it is observed that kerf width marginally increases with increase in height of water level then decreases with further increase in height of water level. With increase increase in water column bubbles formation and their collapsing is move away from fusion zone results in increase in material removal. But further increase in water column results in increase of travel distance for laser beam to interact with work substrate. For that absorption of laser energy by water increased, results in decrease in material removal. With increase in lamp current more laser power generates which travels through the thin water column to interact with workpiece, For which may be more material in removed from fusion zone due to hydrodynamic mechanism.

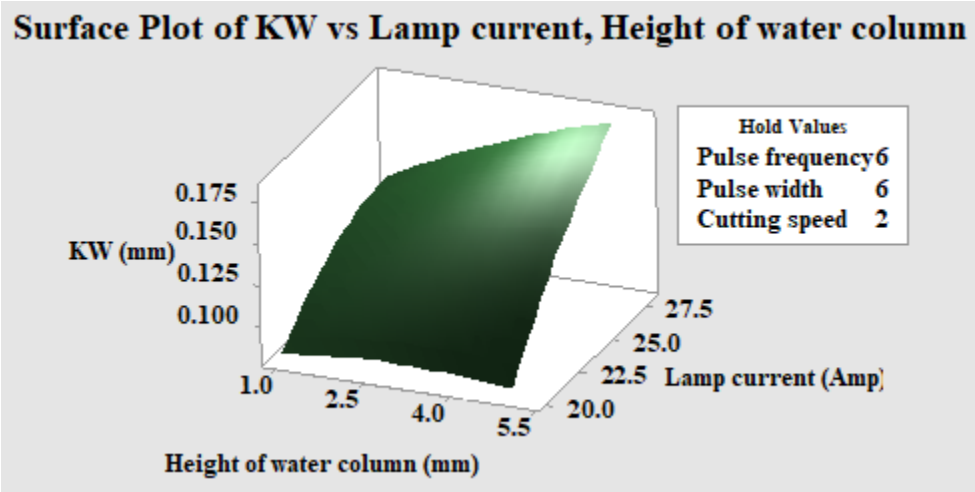

Fig.6.34 Surface plot of kerf width vs height of water column vs lamp current

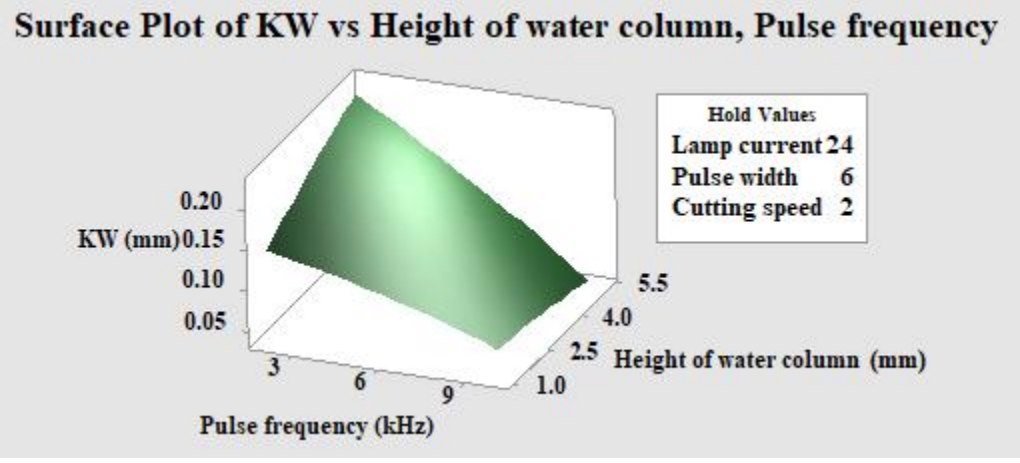

Fig. 6.35 Surface plot of kerf width vs pulse frequency vs height of water column

From the fig 6.35 it is observed that kerf width decreases with increase in pulse frequency whereas increases with increase in height of water. At low pulse frequency comparatively high energy beam is generated which removes more material from the top surface of the workpiece. With the aid of the hydrodynamic effects, water may carry away the molten debris from the machining zone results in increase in kerf width with increase in height of water column at low pulse frequency. But at higher pulse frequency, kerf width decrease with increase in height of water. Such behaviors could be attributable to the following reasons. Lower beam energy generates at higher pulse frequency and vice versa. For which amount of energy loss of laser beam at high pulse frequency and high height of water column is more, results in less amount of material removal. For that desired low kerf width can be achieved at high pulse frequency and high height of water column.

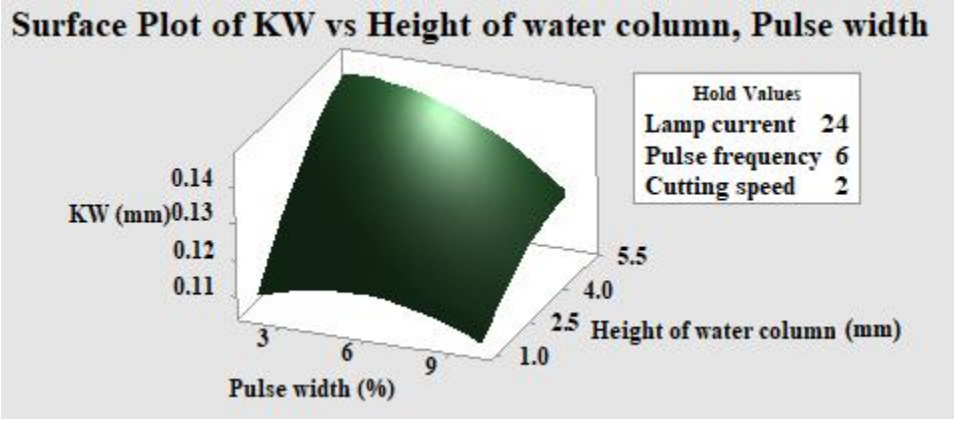

Fig. 6.36 Surface plot of kerf width vs pulse width vs height of water column

From the plot, it has been observed that with increase in pulse width kerf width (KW) slightly increases but decreases with further increase. In case of relationship with height of water column kerf width shows a linear relationship and increases with increase in height of water column when other process variables are kept constant at moderate value. As peak power decreases with increase in pulse width, the energy per pulse irradiate on the targeted spot on the work surface may not be sufficient to make adequate amount of melt pool at submerged condition which is removed later from the spot. That may be reason behind observed phenomenon. In integration with aforesaid phenomenon, the hydrodynamic effect due to increase in water layer/column helps to remove the debris in particle and in molten form from the machine zone properly, results in increase in kerf width. Thus minimum kerf width can be achieved at higher value of pulse width with lower value of height of water column.

Kerf width shows a decreasing tendency with increase in cutting speed but increases with increase in height of water column in fig. 6.37. Due to less interaction time with increase in pulse width results in less amount of heat energy per unit area of irradiation. Therefore less amount of material is removed from the top surface. With increase in height of water column turbulence zone in water may be move a little from laser–workpiece material interaction zone and molten material may be removed by the hydrodynamic effect of water column results in increase in kerf width.

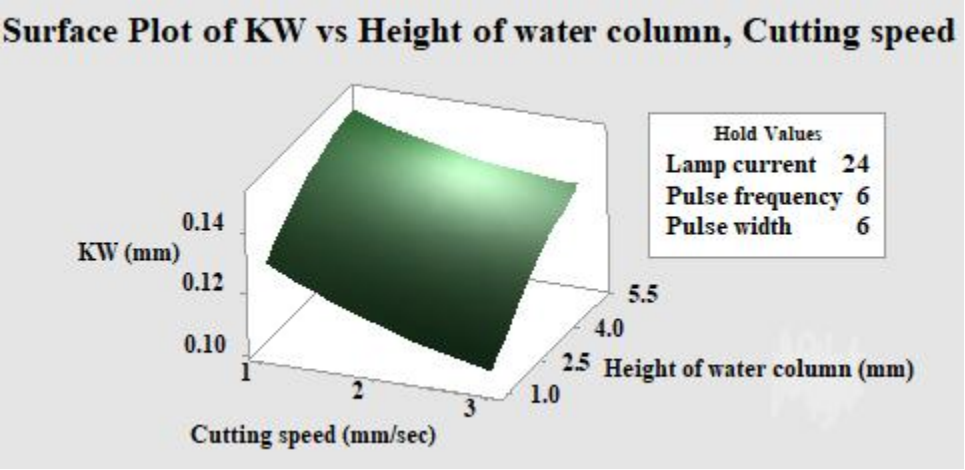

Fig. 6.37 Surface plot of kerf width vs cutting speed vs height of water column

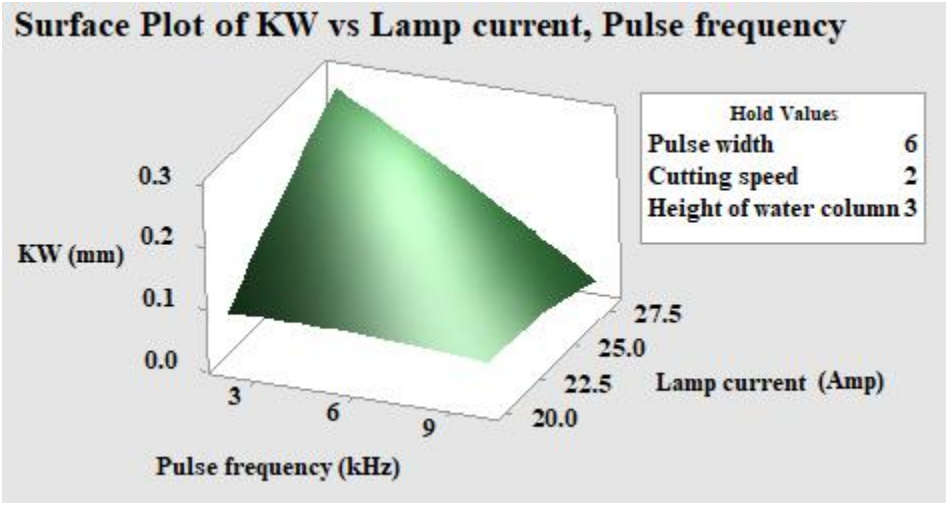

Fig. 6.38 Surface plot of kerf width vs pulse frequency vs lamp current

From the fig. 6.38 it is observed that kerf width increases with increase in lamp current whereas decreases with increases in pulse frequency. Lower kerf width is generated at high frequency with low lamp current. At low lamp current with high pulse frequency less energy beam is generated which may not give sufficient heat input to the machining zone due to loss of energy

during passing through the water column for excess amount of material removal results in low kerf width.

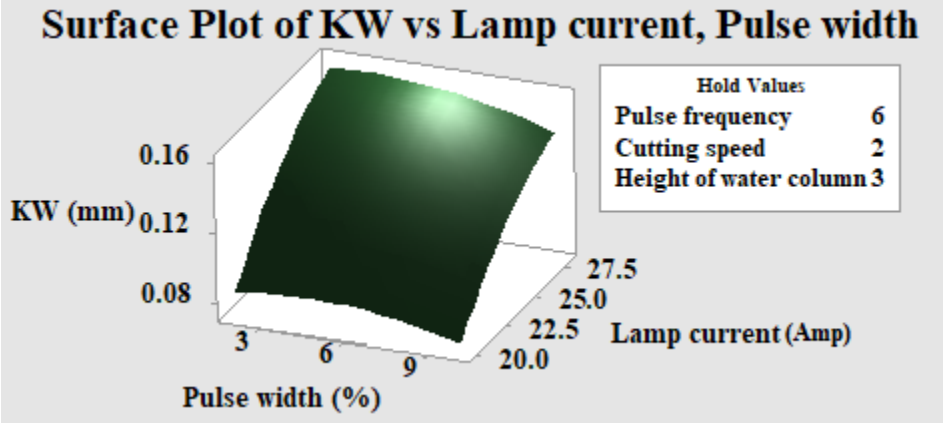

Fig. 6.39 Surface plot of kerf width vs lamp current vs pulse width

From the figure 6.39 it is observed that lamp current have more effect on kerf width than pulse width. Where kerf width increases with increase in lamp current upto certain limit then showing a tendency to decrease, kerf width marginally decreases with increase in pulse width. As the lamp current increases the photon energy and corresponding beam energy also increases. Increase in pulse width means increase of percentage of pulse on time results in more interaction time. But during laser beam machining at submerged condition, higher energy photons along with higher pulse width cause more amount of plasma generation which prevents the laser beam to interact with machining zone with moderate energy. That's the reason of showing decreasing tendency of kerf width at highest value of lamp current and pulse width.

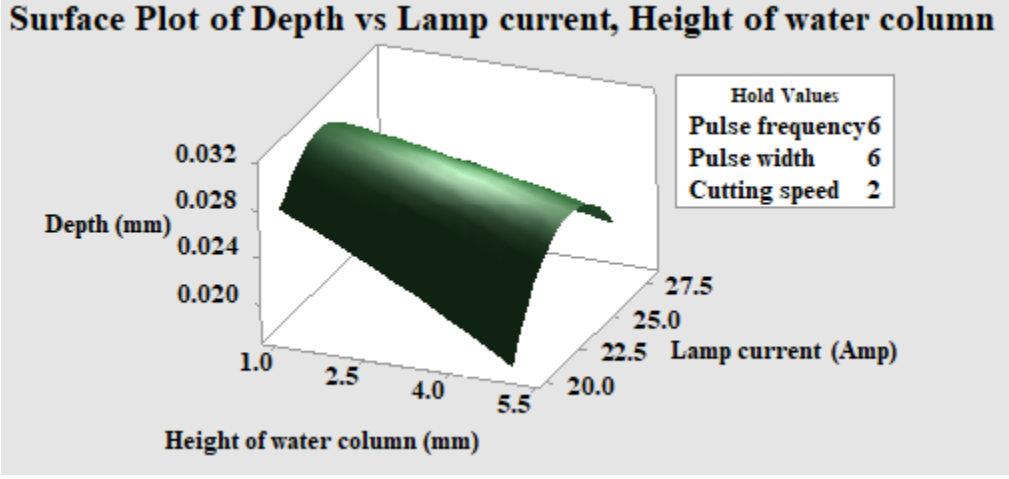

Fig. 6.40 Surface plot of depth of cut vs lamp current vs height of water column

Depth of cut increases upto certain value and then decreases with further increase of lamp current whereas decreases with increase in height of water in figure 6.40. But at highest level of lamp current depth of cut shows a different tendency to increase with increase in height of water column. The reason behind the variation of depth of cut may be at highest level of lamp current amount of laser power generates is more and reached beyond threshold which can penetrates through the plasma vapour layer produced during increase in lamp current, results in increase in increase in depth of cut.

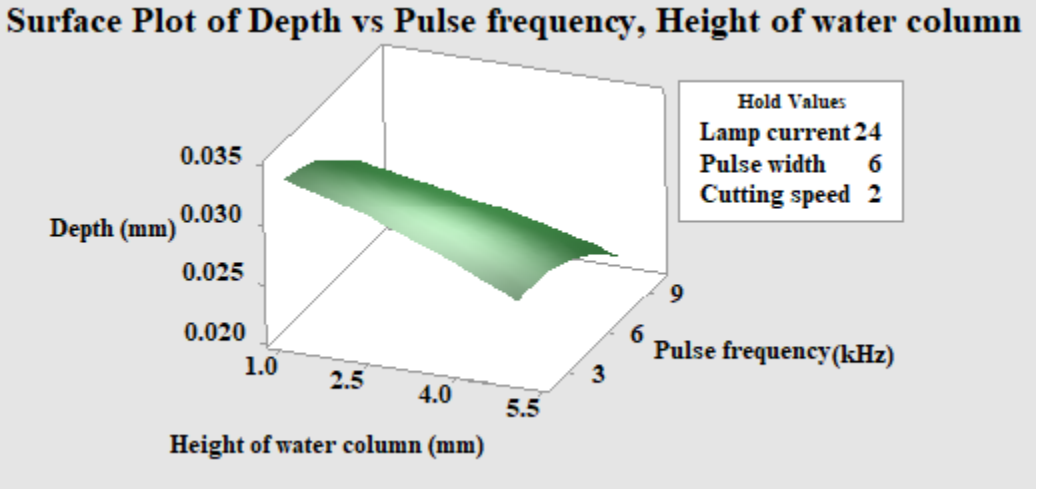

Fig. 6.41 surface plot of depth of cut vs pulse frequency vs height of water column

Depth of cut shows a decreasing tendency with increase in the value of both process parameter, i.e. pulse frequency and height of water column in figure 6.41. With increase in height of water due to refraction effect laser spot diameter decreased which results in increased shear force along the work surface and decreased penetration force along the formation of water wave during laser beam machining at submerged condition. With increase in pulse frequency comparatively less energy beam is generated which cannot interact with workpiece material at moderate energy due to loss of energy during passing through excess height of water column on account of the Beer–Lambert's law above the workpiece surface. For that laser beam cannot yield the ablation threshold limit at the bottom of cut region results less material removal from the machining zone generates low depth of cut and vice versa.

It has been observed from the plot that a curved surface is generate with respect to pulse width which means depth of cut sharply increases with increase in pulse width upto certain value of pulse width within the specified range after which it decreases with further increase in pulse

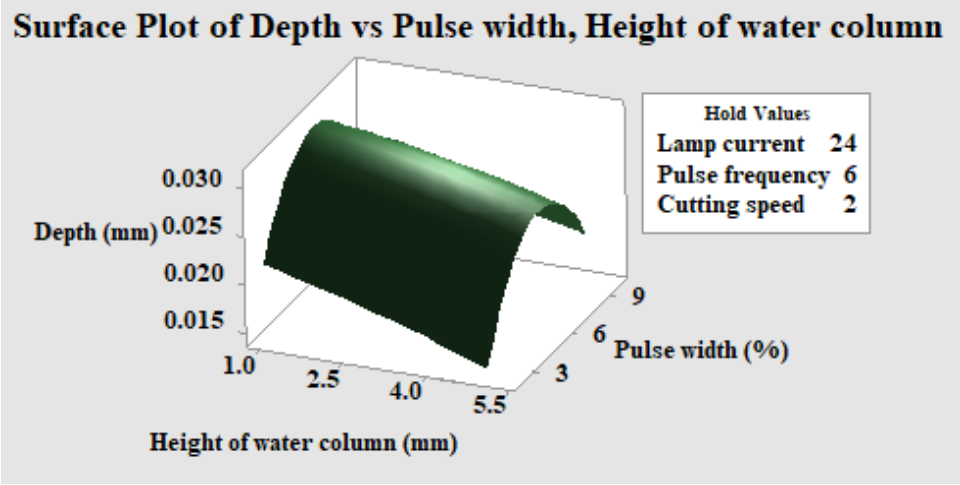

Fig. 6.42 surface plot of depth of cut vs pulse width vs height of water column

width. Increase in height of water column results in decrease in depth of cut. From the plot it has been found that highest value of depth of cut can be achieved at the lowest value of height of water column with moderate value (around 6%) of pulse width. More thermal energy is required to perform the cutting operation at submerged condition with increase in water column height due to loss of thermal energy. For which depth of cut is reduced with increase in height of water column. As pulse width increases, dominance of average power over peak power is started to perform the process. In addition interaction time per pulse with work sample also increases. Combination of these two factor helps to create moderate energy at the spot of irradiation in submerged condition to melt and remove the material subsequently. The pressure of water column as well as the cooling affect may enhance the chance of resolidification of the molten debris/melt pool at the solid liquid interface of the machining zone, results in decrease in depth of cut.

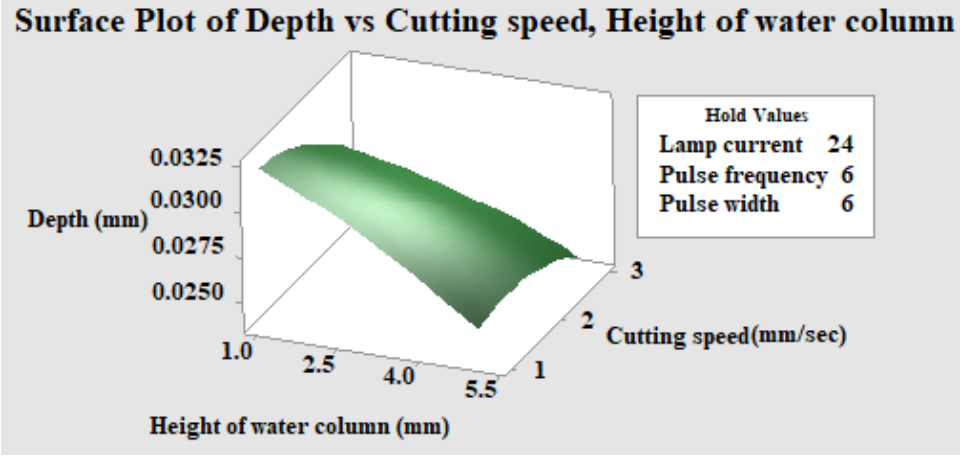

Fig. 6.43 surface plot of depth of cut vs cutting speed vs height of water column

Depth of cut is decreases with increase in height of water column and cutting speed. Surface plot demonstrate that highest value of depth of cut may be achieved at the lowest value of height of water column with lowest value of cutting speed. At the said parametric settings the energy density on the spot at submerged condition is highest, as the thermal energy loss of laser beam due to absorption by water column is lowest along with highest value of interaction time of laser beam with work substrate due to lowest cutting speed. These may be the reason behind observed phenomenon.

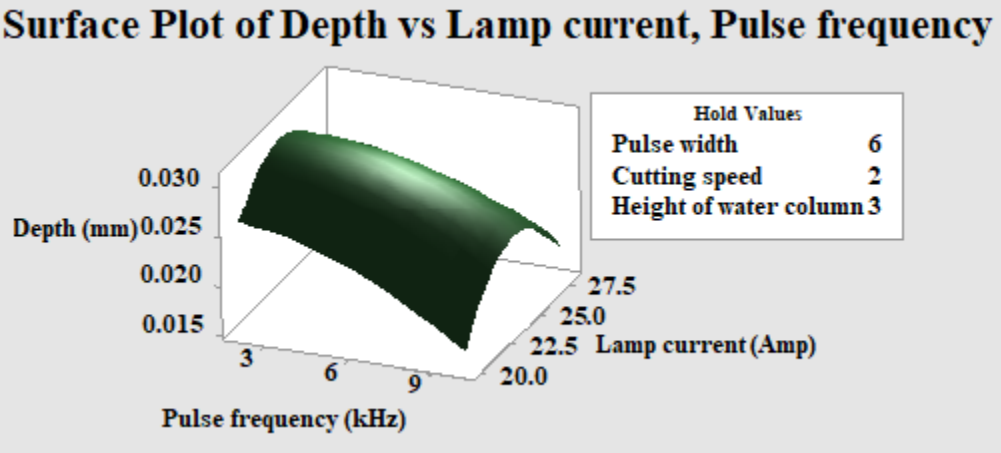

Fig. 6.44 surface plot of depth of cut vs pulse frequency vs lamp current

Figure 6.44 indicates that depth of cut linearly decreases with increase in pulse frequency whereas first increases with certain level of lamp current then decreases. The refraction and reflection of laser beam by the cut particles and bubbles in water are one of the reasons behind the loss of energy of laser beam during under water laser beam machining. At higher pulse frequency less energy beam is generated. For that reason laser beam cannot interact with the workpiece with moderate energy at higher pulse frequency during machining at submerged condition, results in low material removal and less amount of depth of cut is achieved. Whereas the reason behind the nature of depth of cut varies with lamp current may be with increase in lamp current laser power increases results in increase in material removal and depth of cut increases. When lamp current reaches at certain level water waves caused by vaporization of water and key hole formation at the laser–water intersection and air bubble suspending in water result in the unpredictable ablation behaviors, generates the non-uniform cut. For which depth of cut decreases with further increase in lamp current.

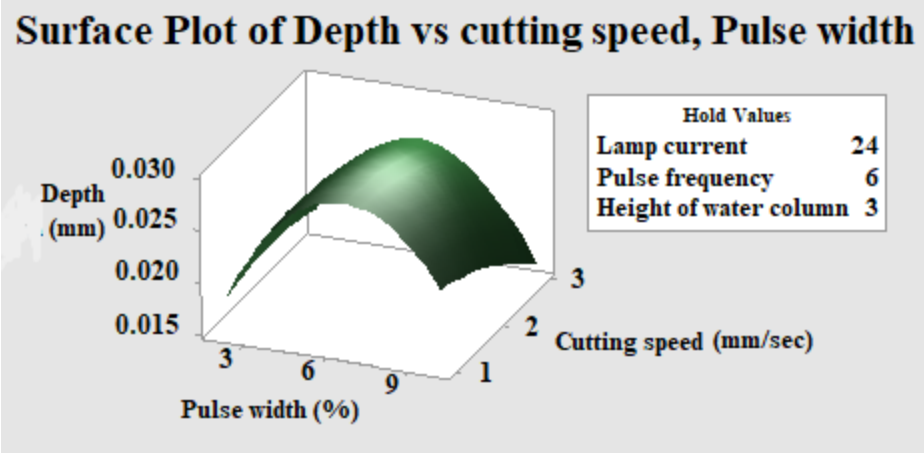

Fig. 6.45 Surface plot of depth of cut vs pulse width vs cutting speed

From the figure 6.45 it is observed that depth of cut decreases with increase in cutting speed and initially increases with certain level of pulse width then decreases. Here increase in pulse width means increase in percentage of duty cycle and results in increase in depth of cut upto certain level due to the increase in time of energy transfer. With further increase in pulse width results in decreased peak power. For that less depth of cut generates. Increase in cutting speed relates with decreased time of interaction of laser beam with workpiece material. Also increased cutting speed increases the water wave and bubble formation results in low depth of cut. Higher depth of cut is achieved around the mid level of pulse width with low level of cutting speed.

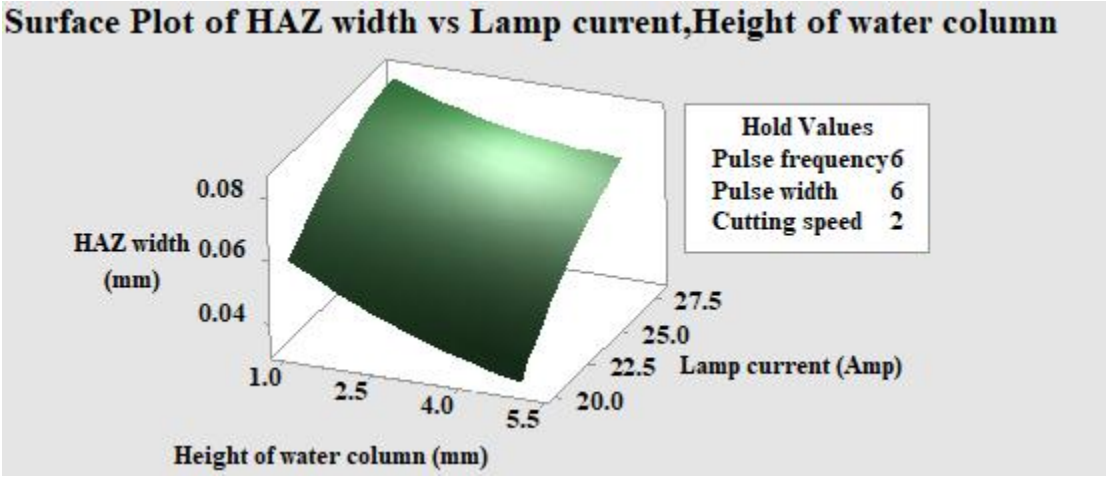

Fig. 6.46 Response surface of HAZ width vs height of water column vs lamp current

From fig.6.46 it is observed that, with increase in height of water column , the laser energy reaching the workpiece surface is reduced may be due to the absorption of laser energy by ionization of water and laser beam scattering by water vapour formed in the laser-material- water

interaction zone which results less amount of HAZ width along the kerf. Higher energy density of laser beam causes by increase in lamp current, results in increase in HAZ width.

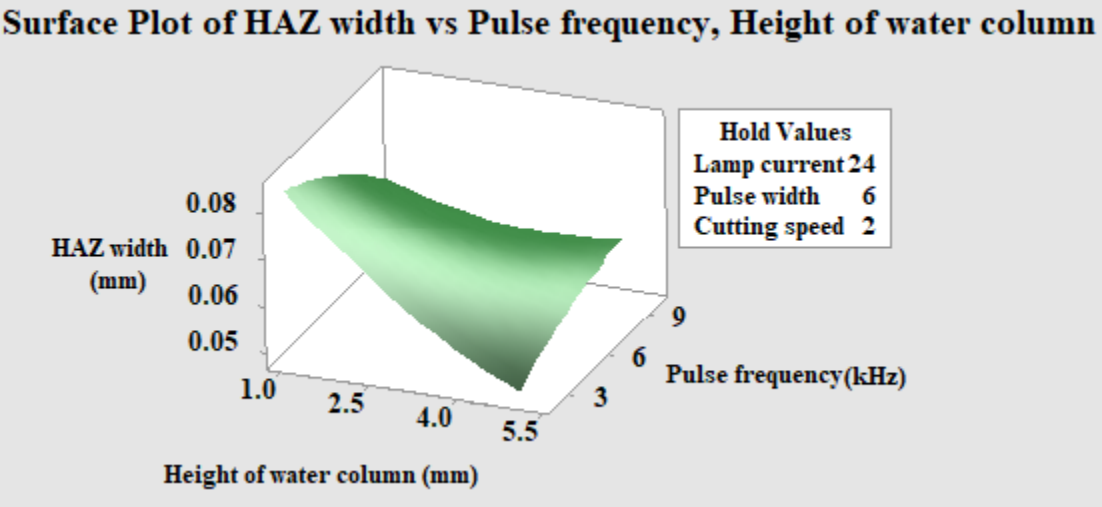

Fig. 6.47 Surface of HAZ width vs pulse frequency vs height of water column

During underwater laser beam machining settling time of the debris material removed from cut zone is much more for which the scattering and absorption of thermal energy of laser beam is more. At laser pulse frequency more laser power is generated for which amount of material removal is more at lower pulse frequency than higher pulse frequency. For that reasons during laser machining at submerged condition HAZ width is decreased with increase in pulse frequency. Whereas With change in height of water column the refractive index changes linearly results in less heat input to the top surface of the workpiece. For that reason HAZ width may be decreased with increase in height of water column.

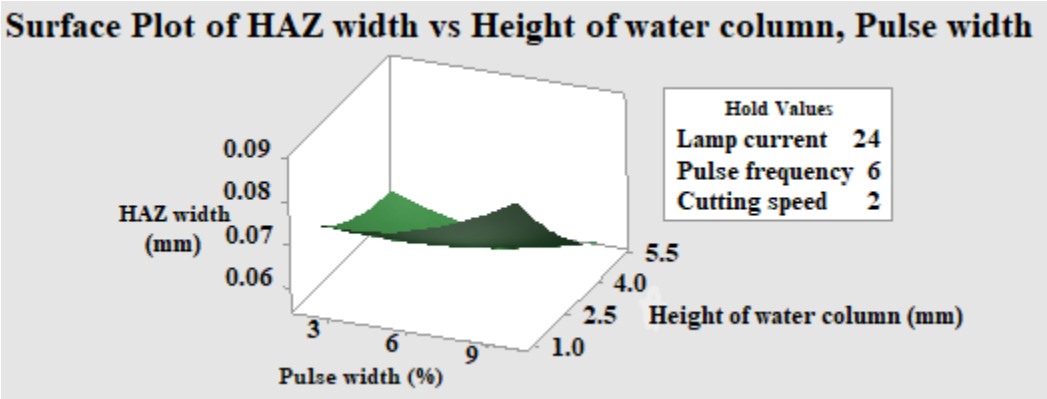

Fig. 6.48 Surface of HAZ width vs pulse width vs height of water column

From the figure 6.48 it is observed that HAZ width is increases with increase in pulse width whereas decreases with increase in height of water column for which minimum HAZ width can

be achieved at highest value of water column height with highest value of pulse width also. At the aforesaid parametric settings thermal energy incorporated into the process is not enough for that thermal effect is concentrated within the very narrow region adjacent to the path of laser beam movement, results in low HAZ formation.

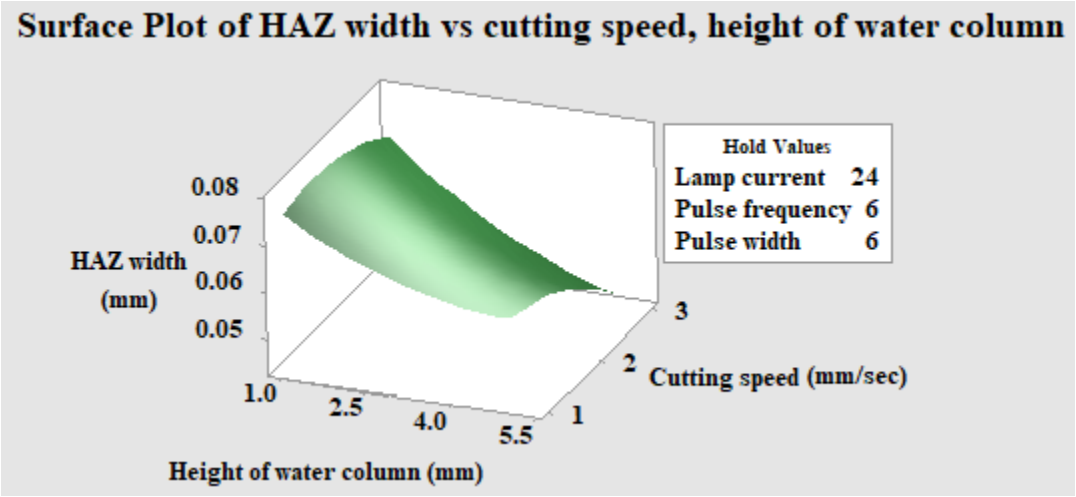

Fig. 6.49 Response surface of HAZ width vs height of water column vs cutting speed

Travel length of laser beam trough the water medium is gradually increased with increase in height of water column, results in more amount of heat loss due to heat absorption of water. This may be the reason behind decrease in HAZ width with increase in water column height. Decrease in interaction time between laser beam and workpiece material causes by increase in cutting speed. For that aforesaid reason less amount of thermal deformation may be take place around the machining zone, results in less HAZ.

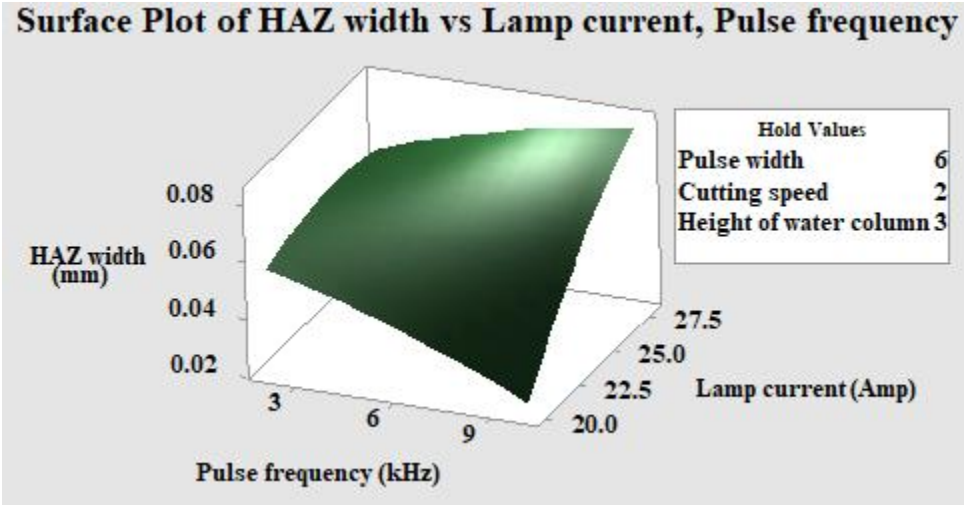

Fig. 6.50 surface plot of HAZ width vs pulse frequency vs lamp current

From figure 6.50 it is observed that HAZ width decreases with increase in pulse frequency whereas increases with increase in Lamp current. During under water laser beam machining heat input to the top surface of workpiece substrate is increased with increase in lamp current may be due to non linear optical effect of laser beam and higher laser energy density. Whereas laser energy is inversely proportional to pulse frequency results in decrease in HAZ width with increase in pulse frequency.

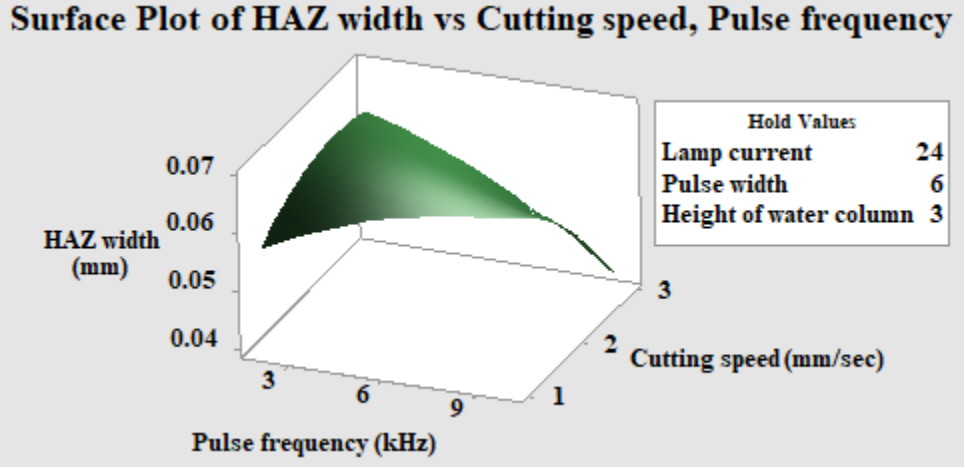

Fig. 6.51 surface plot of HAZ width vs cutting speed vs pulse frequency

It is found from the plot that combination of higher value of pulse frequency with lower value of cutting speed produces more HAZ width due to more energy per pulse beam interaction with work sample along with comparatively more interaction time and vice versa.

6.2.2.3 Sensitivity analysis

To obtained the sensitivity equation for machining responses, i.e. kerf width, depth of cut and HAZ width with respect to controllable variables, respective second order polynomial equations 6.21,6.22 & 6.23 are partially differentiated with respect to corresponding process parameters.

Partially derived equations for kerf width (KW)

$$\delta KW/\delta X_1=0.0605-0.00129*X_1-0.003672*X_2-0.000105*X_3-0.00152*X_4+0.001680*X_5 \quad (6.24)$$

$$\delta KW/\delta X_2=0.0862-0.000834*X_2-0.003672*X_1-0.000213*X_3+0.00106*X_4-0.003453*X_5 \quad (6.25)$$

$$\delta KW/\delta X_3 = 0.0082-0.000826*X_3-0.000105*X_1-0.000213*X_2+ 0.00037*X_4-0.000627*X_5 \quad (6.26)$$

$$\delta KW/\delta X_4=0.0031+0.00582*X_4-0.00152*X_1+0.00106*X_2+ 0.00037*X_3+0.00141*X_5 \quad (6.27)$$

$$\delta KW/\delta X_5= -0.0052-0.00224*X_5+0.001680*X_1-0.003453*X_2-0.000627*X_3+0.00141*X_4 \quad (6.28)$$

Partially derived equations for depth of cut

$$\delta D/\delta X_1 = 0.01547+0.000782\ X_1+0.000076\ X_2+0.000251\ X_3+0.000138\ X_4+0.000293\ X_5 \quad (6.29)$$

$\delta D/\delta X_2 = 0.00207-0.000214\ X_2+0.000076\ X_1-0.000054\ X_3-0.001755\ X_4+0.000109\ X_5$ (6.30)

$\delta D/\delta X_3 = 0.00202-0.00117\ X_3+0.000251\ X_1-0.000054\ X_2-0.000417\ X_4+0.000109\ X_5$ (6.31)

$\delta D/\delta X_4 = 0.01059-0.001794^*\ X_4+0.000138\ X_1-0.001755\ X_2-0.000417\ X_3+0.000404\ X_5$ (6.32)

$\delta D/\delta X_5 = -0.00984-0.000228\ X_5+0.000293\ X_1+0.000109\ X_2+0.000109\ X_3+0.000404\ X_4$ (6.33)

Partially derived equation for HAZ width

$\delta HW/\delta X_1=0.007893-0.002540X_1+0.003362X_2+0.000316X_3+0.000607X_4+0.000820X_5$ (6.34)

$\delta HW/\delta X_2= -0.001267- 0.001252X_2+ 0.003362X_1+0.000844X_3-0.002134X_4+0.001911X_5$ (6.35)

$\delta HW/\delta X_3= 0.001022+ 0.002122X_3+ 0.000316X_1+0.000844X_2+0.000410X_4-0.001027X_5$ (6.36)

$\delta HW/\delta X_4= -0.002791- 0.001758X_4+ 0.000607X_1-0.002134X_2+0.000410X_3-0.000711X_5$ (6.37)

$\delta HW/\delta X_5=-0.005027+0.001660X_5+0.000820X_1+0.001911X_2-0.001027X_3-0.000711X_4$ (6.38)

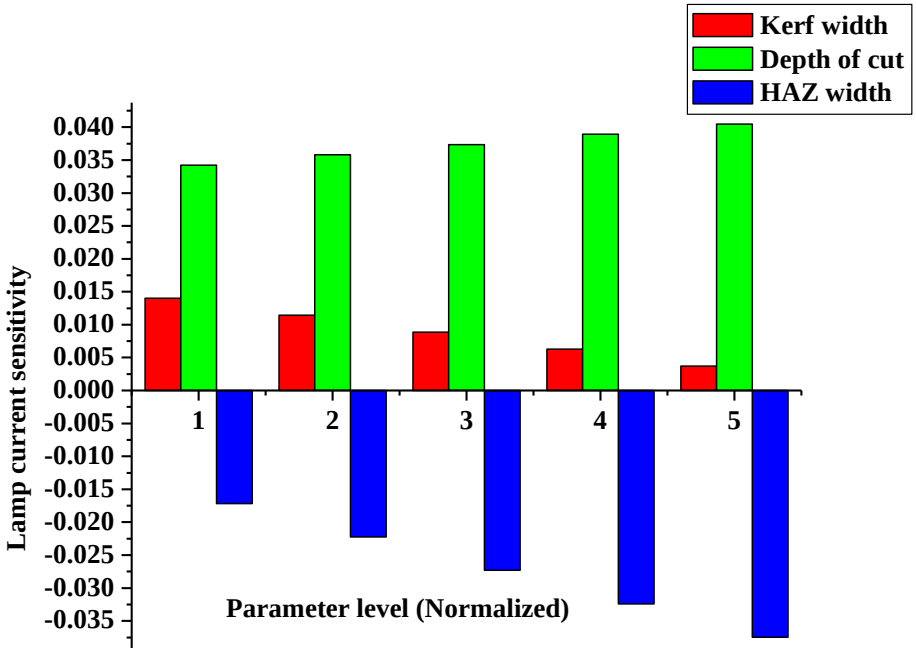

Fig. 6.52 Sensitivity of lamp current on machining responses

From the plot it is observed that sensitivity of lamp current on kerf width and depth of cut have a positive approach whereas negatively sensitive to HAZ width. It also observed that lamp current and HAZ width have a change in sensitivity but not much change in case of depth of cut. It is also find that increase in the level of lamp current shows a decreasing tendency of sensitivity to kerf width and HAZ width. From this plot it may conclude that thermal energy incorporate in the

process is much more to generate more amount of HAZ around the irradiate zone whereas low kerf width profile at higher value of lamp current is generate at submerged condition with a little effect on depth of cut. Comparatively higher turbulence is generated on the water column present at machining zone due to high energy density at higher value of lamp current which distracts the laser beam from precise irradiation. In addition, nonlinear absorption effect of water at higher laser intensity may be lead to lesser amount of heat accumulation adjacent to kerf. In submerged condition, initially the power density on the irradiate spot is not sufficient to melt and vaporize the material from the machining zone properly to produce clean kerf. A little change in lamp current add more power which enhance the material removal, results in better kerf width than previous condition. At the highest level of lamp current adequate amount of laser power is incorporated in the machining zone and a less wavy kerf width is visible, results in less sensitive at highest value of lamp current.

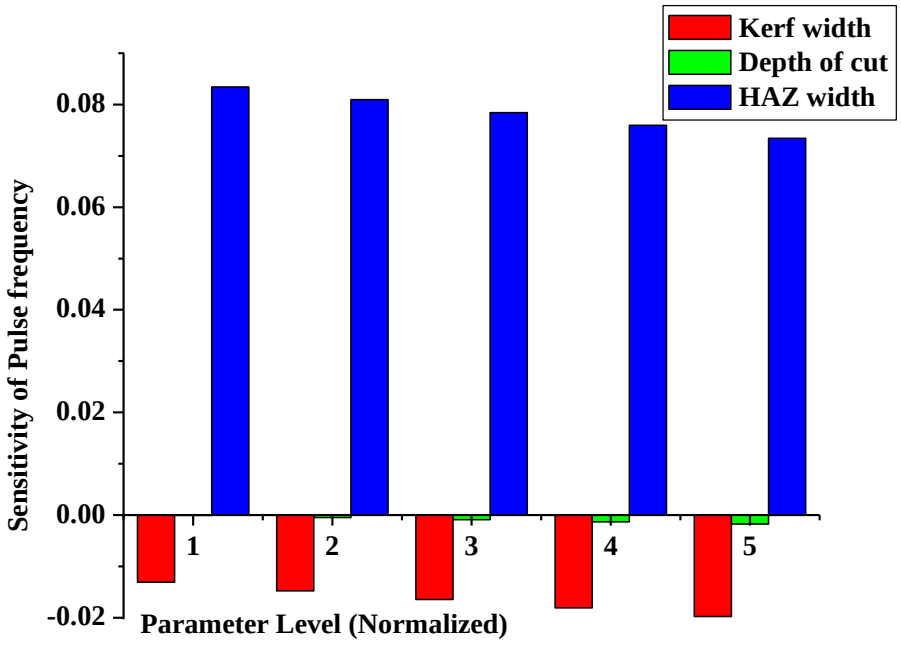

Fig. 6.53 Sensitivity of Pulse frequency on machining responses

It is observed from the plot that depth of cut is negligible sensitivity with pulse frequency whereas HAZ width and kerf width have sensitivity in positive and negative value respectively. It has been found from the plot that marginal decrement of sensitivity for both the HAZ width and kerf width with increase in pulse frequency. Energy density per pulse of the irradiate beam

decreases with increase in pulse frequency but the laser intensity remains almost same throughout the frequency from low to high. That may be the reason behind the relation between sensitivity of pulse frequency to HAZ width. In case of kerf width, less turbulence at machining zone due to comparatively less energy incorporation into submerged machining system leads to more uniform kerf generation, results in less sensitivity at higher level of pulse frequency.

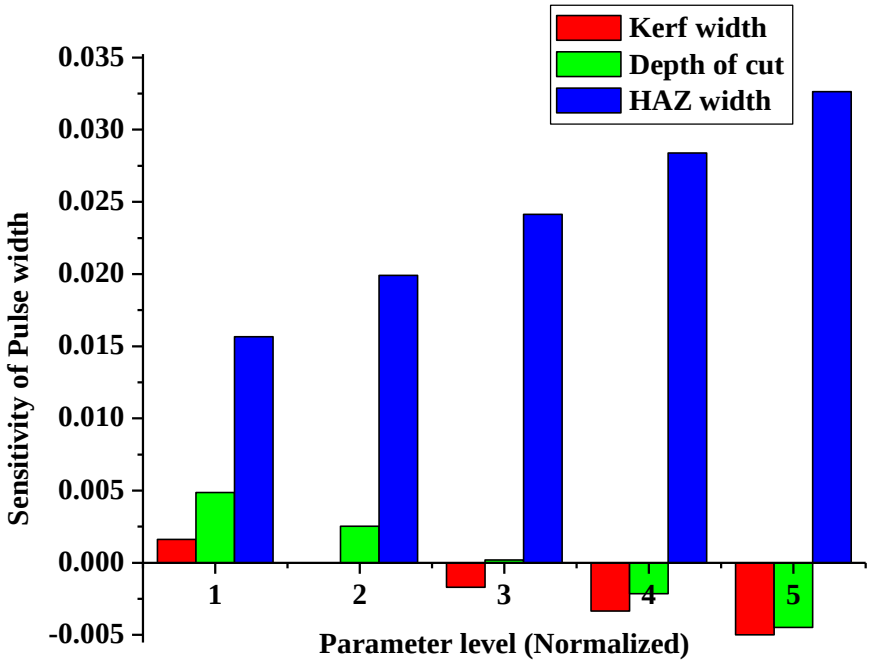

Fig. 6.54 Sensitivity of Pulse width on machining responses

It is observed from the plot that sensitivity of pulse width to HAZ width increases with increases with the value of pulse width, whereas sensitivity initially shows positive value with kerf width and depth of cut but gradually shows a negative tendency with increase in the value of pulse width. It is known that with increase in the value of pulse width depth of penetration decreases due to decrease in peak power which leads to increase in average power. For the above said reason diffusion on the work surface may be increased to generate more HAZ width and less depth of cut inspite of laser submerged machining. Due to this pulse on time factor at higher range of pulse width, sensitivity of pulse width is more with HAZ width. As material removal is more uniform at higher value of peak power for nano-second pulse laser beam machining system, kerf width is positively sensitive but at higher value within the chosen design space when average power dominates over peak power turbulence due to bubbles generation and burst

leads to move of debris in different form, from the machining zone, results in higher value of kerf width but less sensitivity.

From the graphical interpretation it can be said kerf width and HAZ width shows a negative sensitivity to cutting speed whereas depth of cut preliminary shows a positive sensitivity but later shows a negative sensitivity also. It is also observed that sensitivity of HAZ width and depth of cut decreases with increase in the value of cutting speed whereas sensitivity to kerf width increases. Change in interaction time with increment or decrement in cutting speed at submerged condition affects the machining characteristics due to change in thermal energy density at the laser irradiate zone and the wave produces on the water column due the vibration by movement of the CNC based axis system which affects the proper irradiation of laser beam on the work surface at submerged condition. Aforesaid phenomenon produces low HAZ , low depth of cut and non wavy uniform kerf.

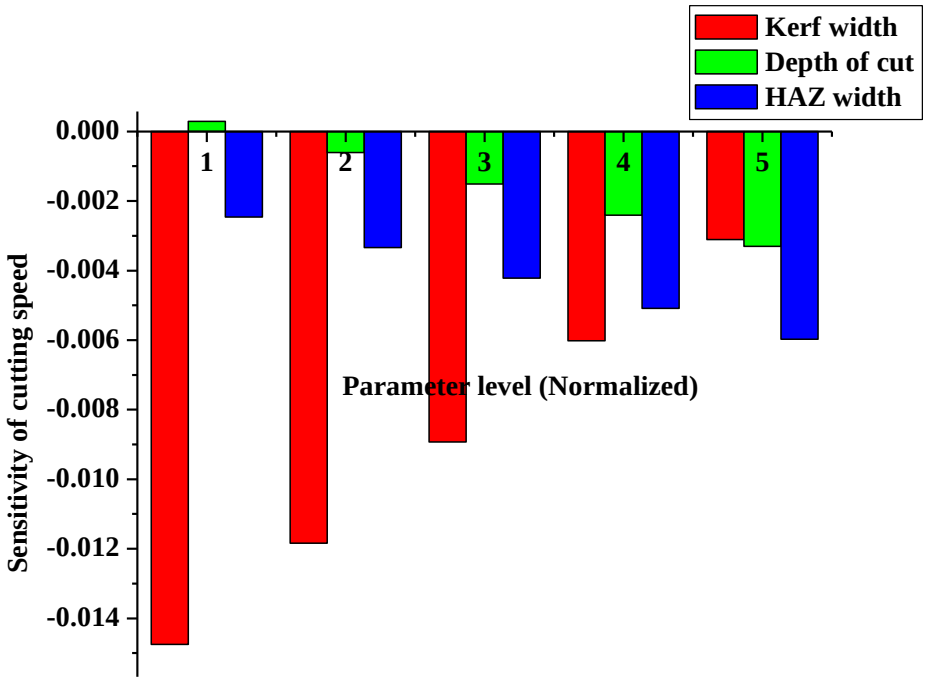

Fig. 6.55 Sensitivity of Cutting speed on machining responses

From the graphical interpretation it is evident that kerf width and HAZ width are positively sensitivity to height of water column whereas negatively to depth of cut. Sensitivity of height of water column shows an increasing tendency with HAZ width but decreasing tendency with kerf

width and depth of cut. In case of height of water column, at the lower level of water column turbulence at machining zone along with bubble burst in and around the irradiate spot and improper debris removal effects the kerf width mostly, results in waviness along the kerf. Whereas at the higher level, bubble burst is occurred at a distance from the machining zone which reduces the turbulence amount on the machining zone, and Increase in water volume by increase in water column results in more circulation water in & around the machining zone. Which along with bubbles expansion may helps uniform material removal from the machining zone. Thus creates a clean and uniform edge along the kerf. For the aforesaid reasons kerf width is more sensitive to water column height at lower level than higher range. Amount of laser energy absorption by water column is increased with increase in height of water column and circulation in water column due to marangoni effects, results in less laser power irradiation on the top surface of workpiece which leads to decrease in HAZ width. For these reasons sensitivity of HAZ width shows a increasing tendency.

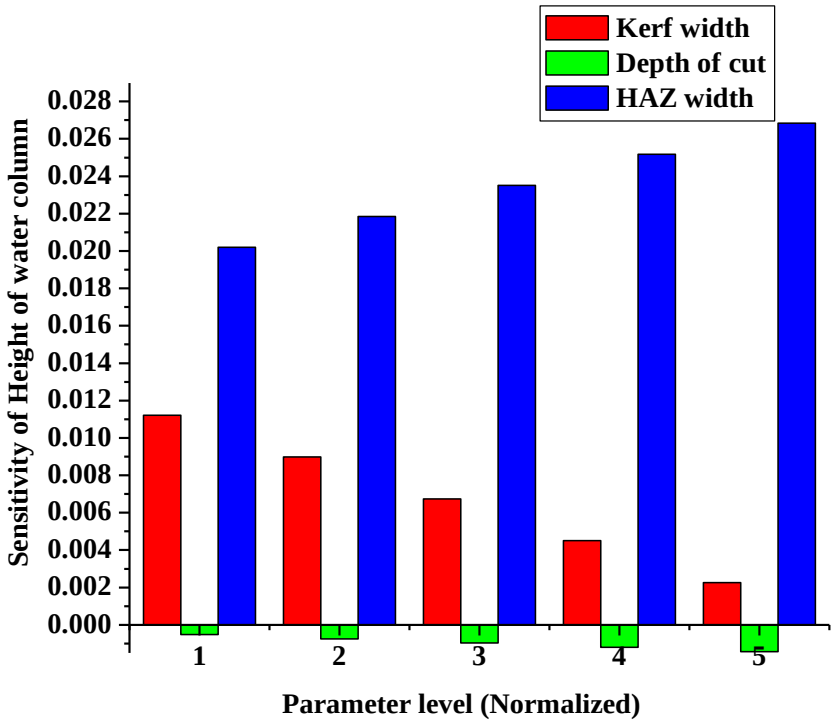

Fig.6.56 Sensitivity of Height of water column on machining responses

Fig. 6.57 exhibits the contour plot for investigating the influences of different combinations for all the process variables on kerf width at submerged condition. A large number of combinations are represented by each contour curve. Good interaction between the process variables and response is indicated by elliptical shape whereas circular shape indicates no interaction between the variables. From the plot it is observed that the most significant achievable region of kerf width within the chosen design space is 0.10 mm to 0.15 mm. fig.6.58 and 6.59 demonstrate the contour plots for depth of cut and HAZ width at submerged condition. From the plots it can be said that depth of cut of 0.25 mm to 0.35 mm is the mostly achievable during the experiments for all the statistically significant interactions whereas HAZ width of 0.07 mm to 0.03 mm can be achievable during the measurements. It is also observed that lamp current with pulse frequency, cutting speed and height of water column with lamp current, cutting speed are the most significant interactions.

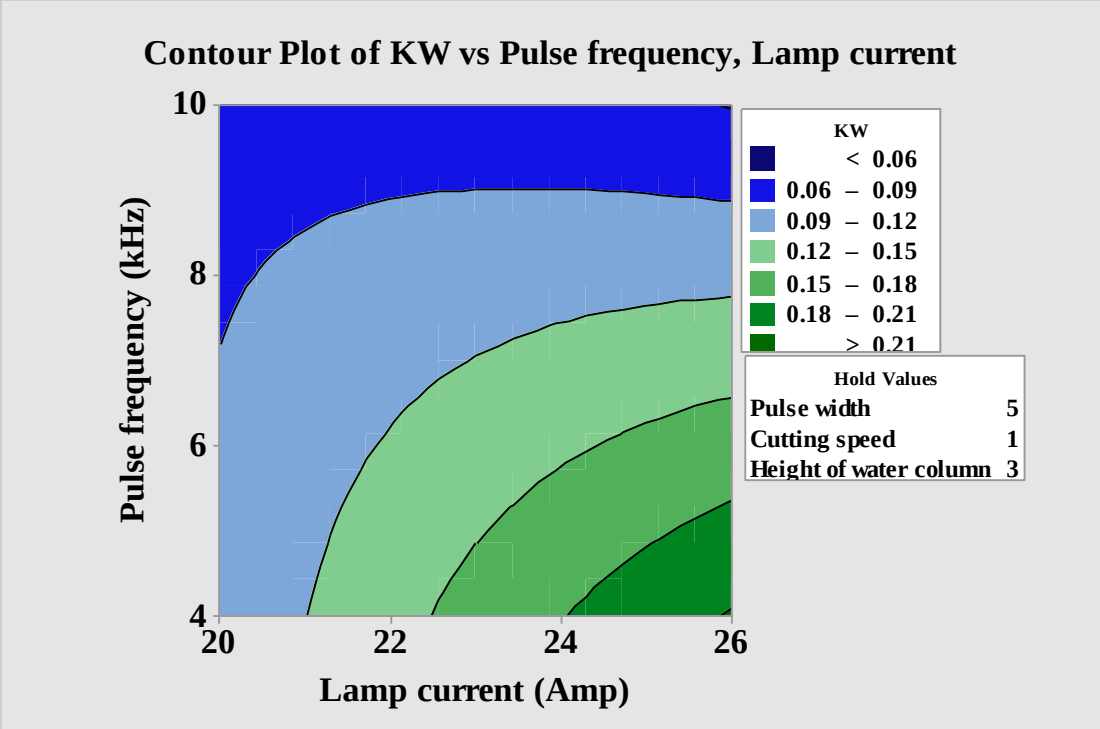

(a)

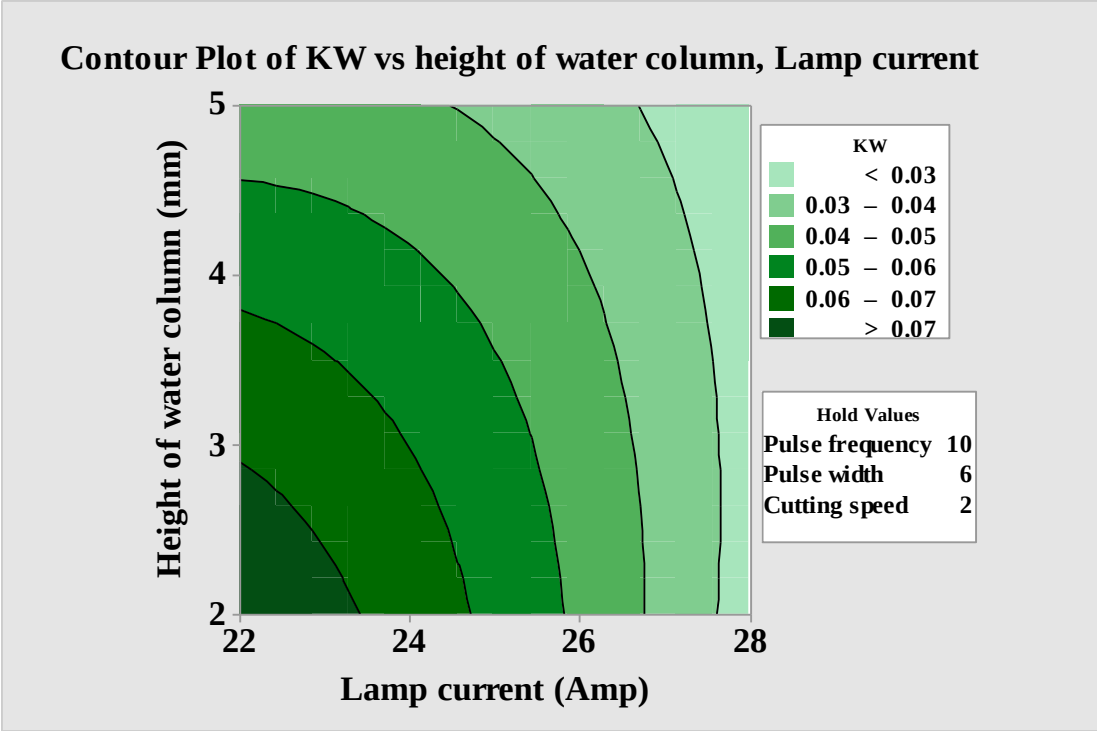
Contour Plot of KW vs height of water column, Lamp current
Height of water column (mm)
Lamp current (Amp)
5
4
3
2
22
24
26
28
KW
< 0.03
0.03 – 0.04
0.04 – 0.05
0.05 – 0.06
0.06 – 0.07
> 0.07
Hold Values
Pulse frequency 10
Pulse width 6
Cutting speed 2

(b)

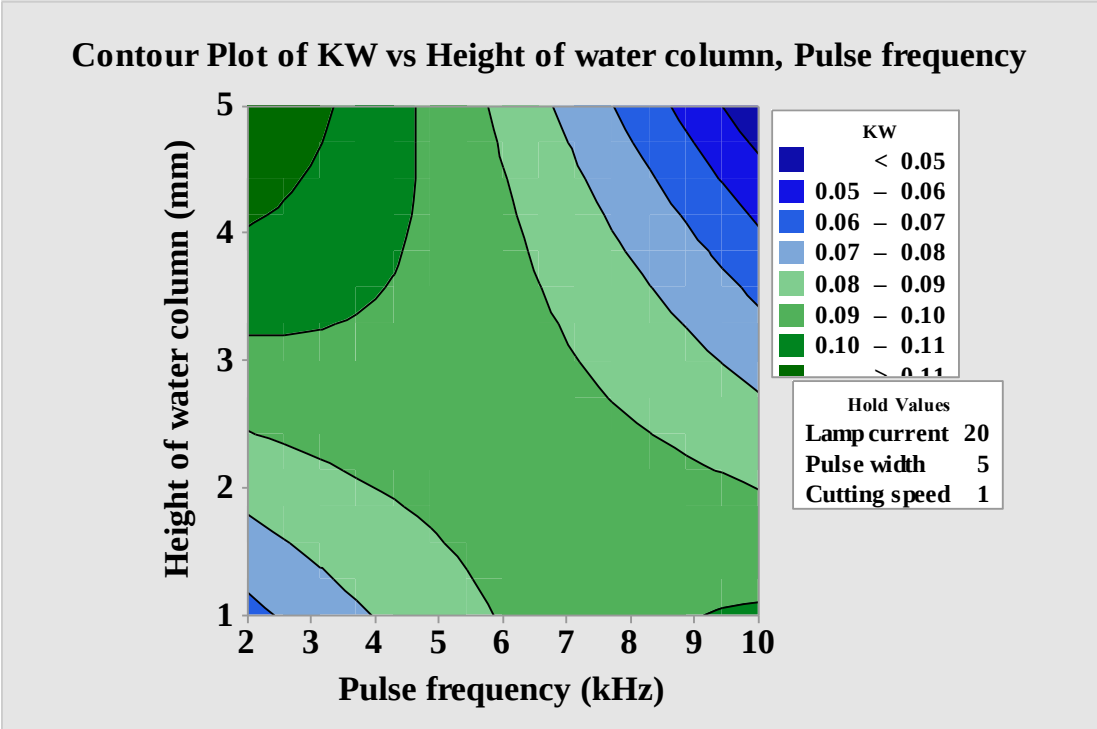
Contour Plot of KW vs Height of water column, Pulse frequency
Height of water column (mm)
Pulse frequency (kHz)
5
4
3
2
1
2
3
4
5
6
7
8
9
10
KW
< 0.05
0.05 – 0.06
0.06 – 0.07
0.07 – 0.08
0.08 – 0.09
0.09 – 0.10
0.10 – 0.11
Hold Values
Lamp current 20
Pulse width 5
Cutting speed 1

(c)

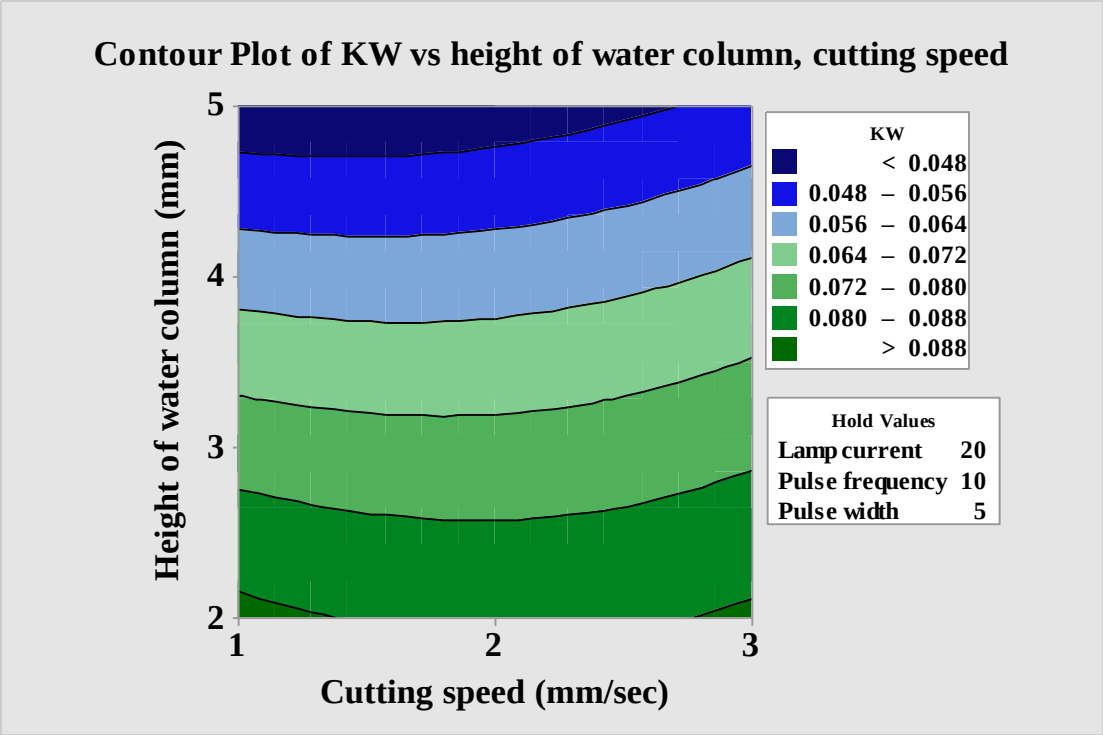

(d)

Fig. 6.57 (a,b,c,d) contour plots of kerf width with dominant process variables.

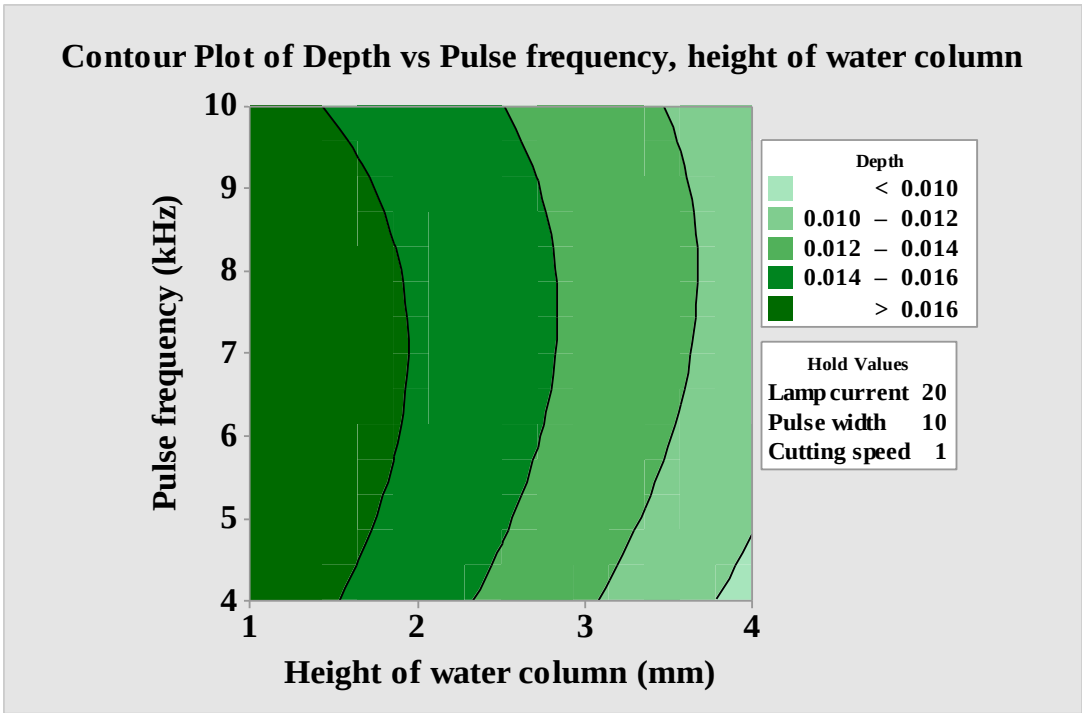

(a)

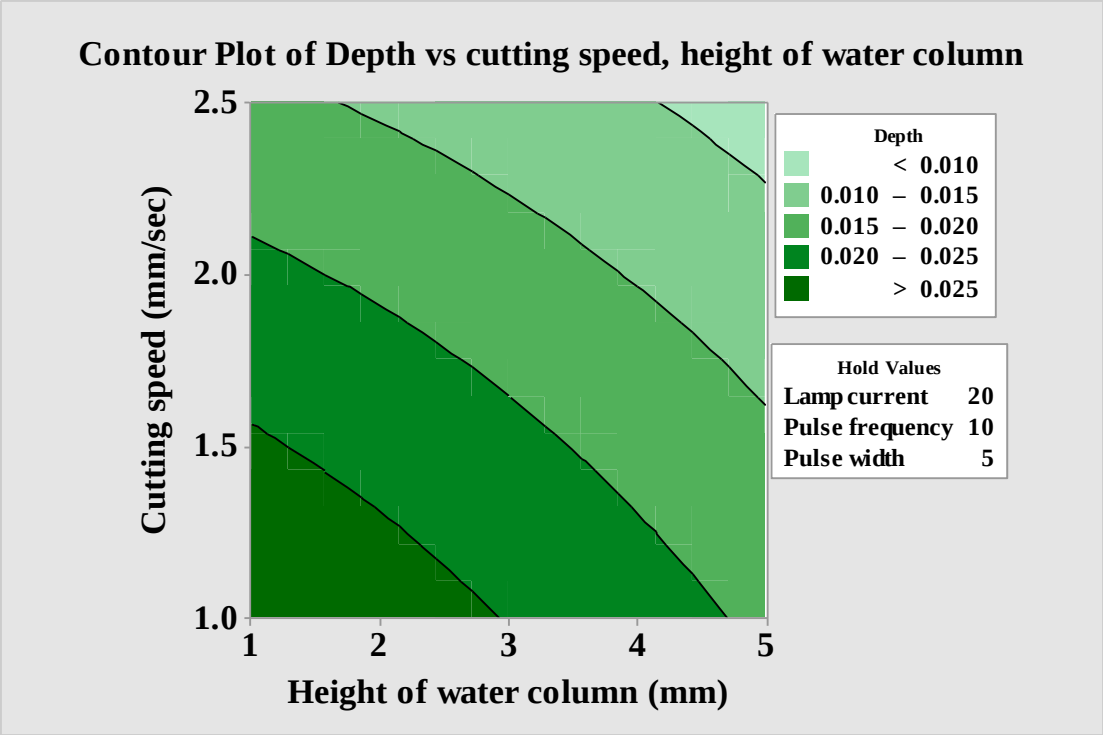
Contour Plot of Depth vs cutting speed, height of water column
Cutting speed (mm/sec)
2.5
2.0
1.5
1.0
1
2
3
4
5
Height of water column (mm)
Depth
< 0.010
0.010 – 0.015
0.015 – 0.020
0.020 – 0.025
> 0.025
Hold Values
Lamp current 20
Pulse frequency 10
Pulse width 5

(b)

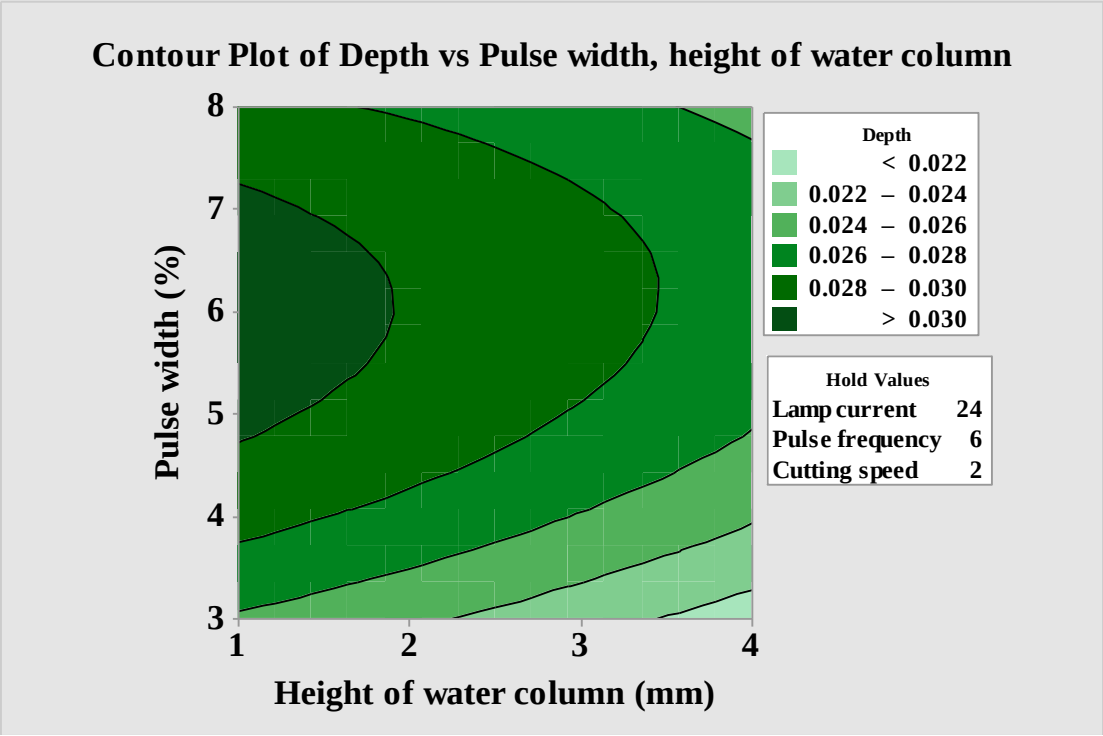
Contour Plot of Depth vs Pulse width, height of water column
Pulse width (%)
8
7
6
5
4
3
1
2
3
4
Height of water column (mm)
Depth
< 0.022
0.022 – 0.024
0.024 – 0.026
0.026 – 0.028
0.028 – 0.030
> 0.030
Hold Values
Lamp current 24
Pulse frequency 6
Cutting speed 2

(c)

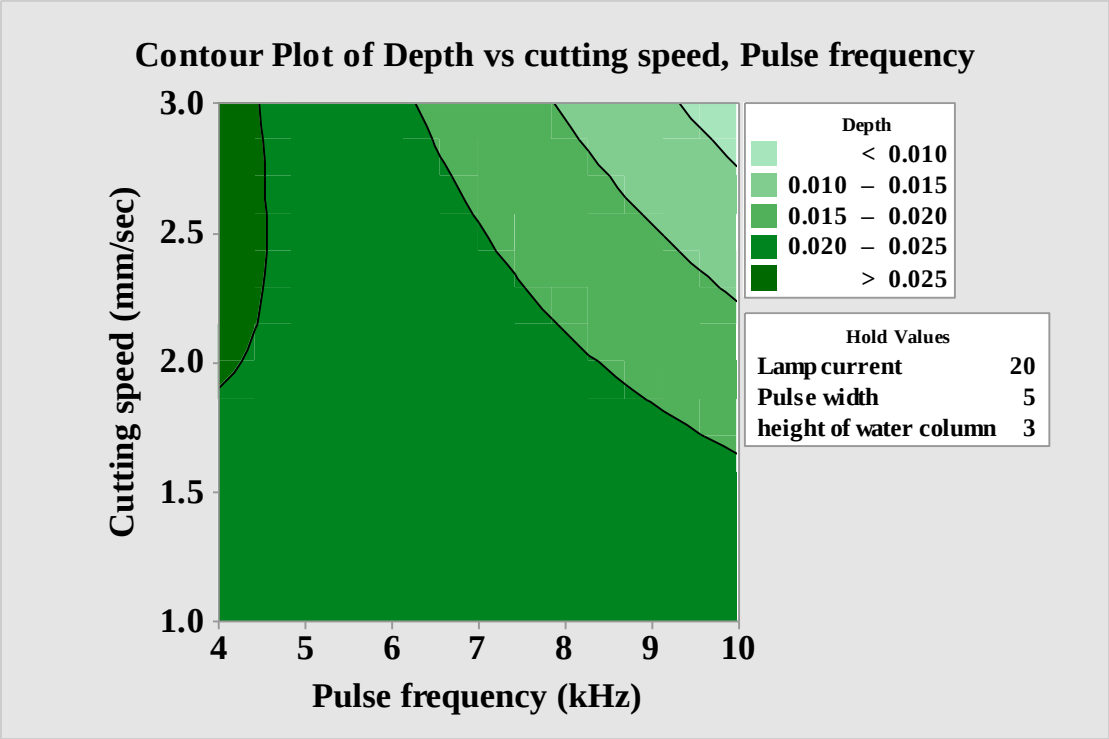

(d)

Fig. 6.58(a,b,c,d) Contour plots of depth of cut with dominant process variables.

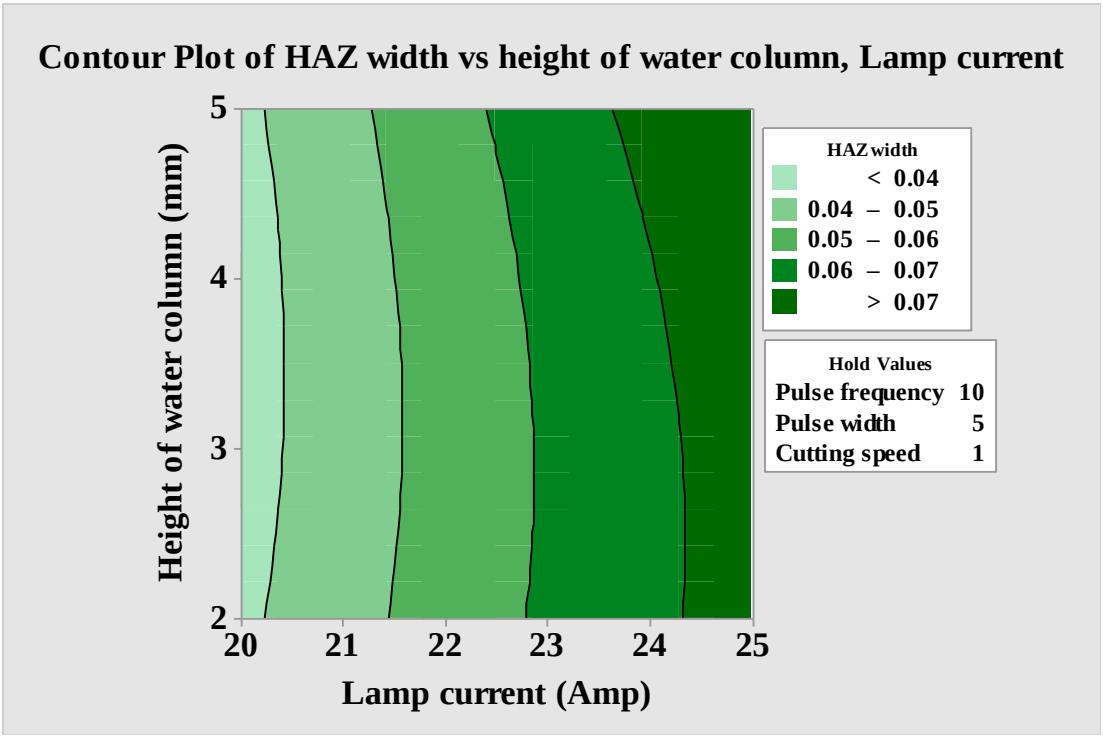

(a)

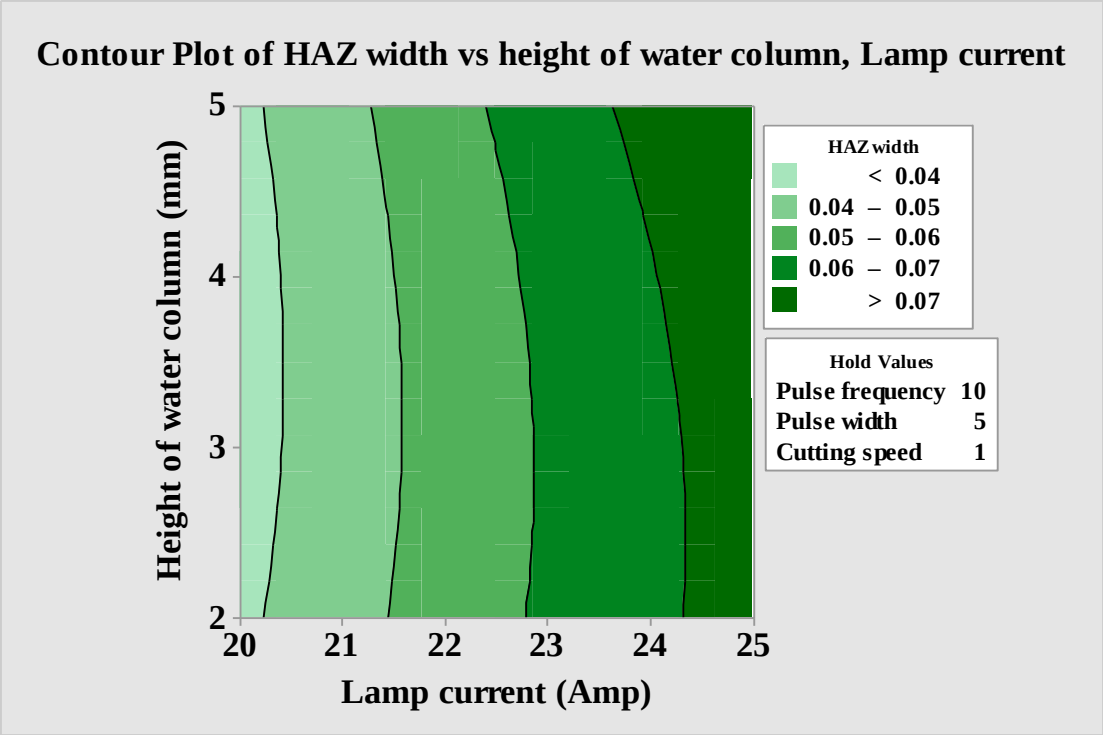
Contour Plot of HAZ width vs height of water column, Lamp current
Height of water column (mm)
Lamp current (Amp)
5
4
3
2
20
21
22
23
24
25
HAZ width
< 0.04
0.04 – 0.05
0.05 – 0.06
0.06 – 0.07
> 0.07
Hold Values
Pulse frequency 10
Pulse width 5
Cutting speed 1

(b)

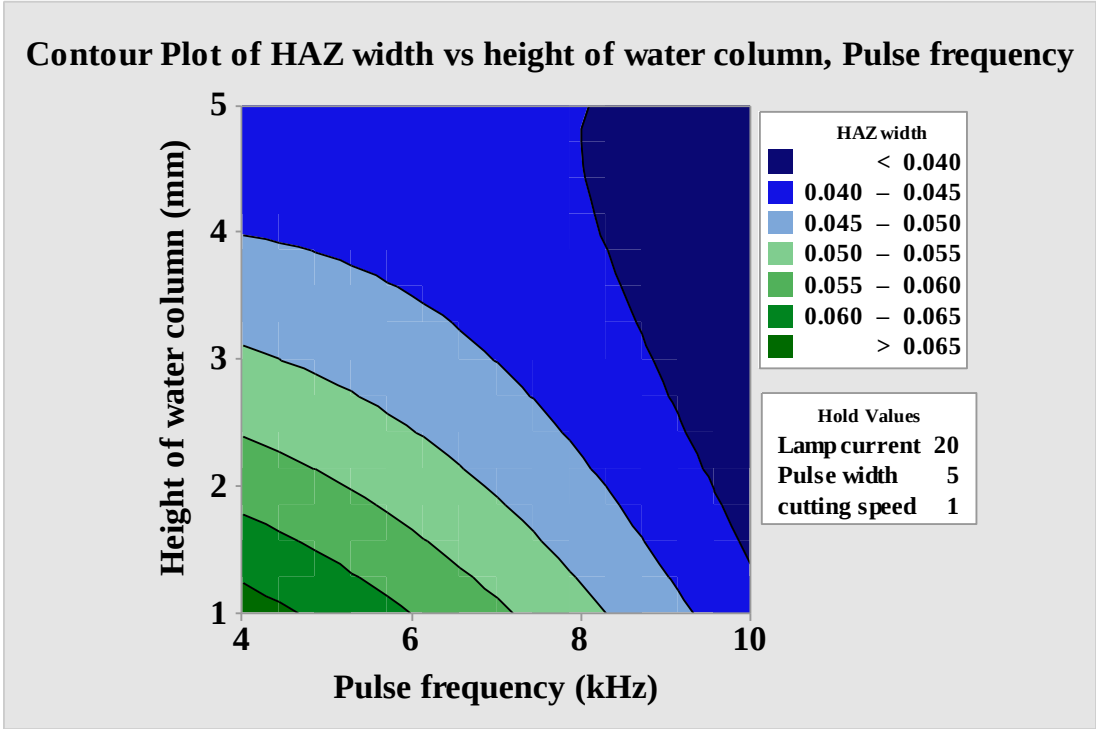
Contour Plot of HAZ width vs height of water column, Pulse frequency
Height of water column (mm)
Pulse frequency (kHz)
5
4
3
2
1
4
6
8
10
HAZ width
< 0.040
0.040 – 0.045
0.045 – 0.050
0.050 – 0.055
0.055 – 0.060
0.060 – 0.065
> 0.065
Hold Values
Lamp current 20
Pulse width 5
cutting speed 1

(c)

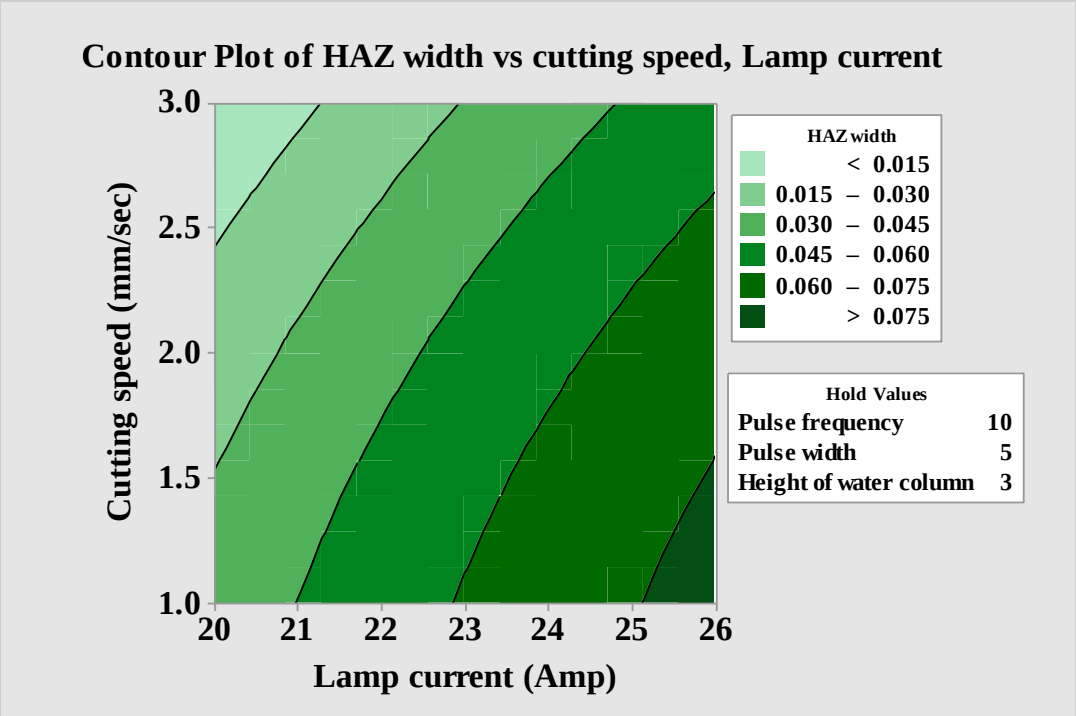

Fig. 6.59 (a,b,c,d) Contour plots of HAZ width with dominant process variables

6.2.2.4 Determination of optimal process parameter using Response surface methodology

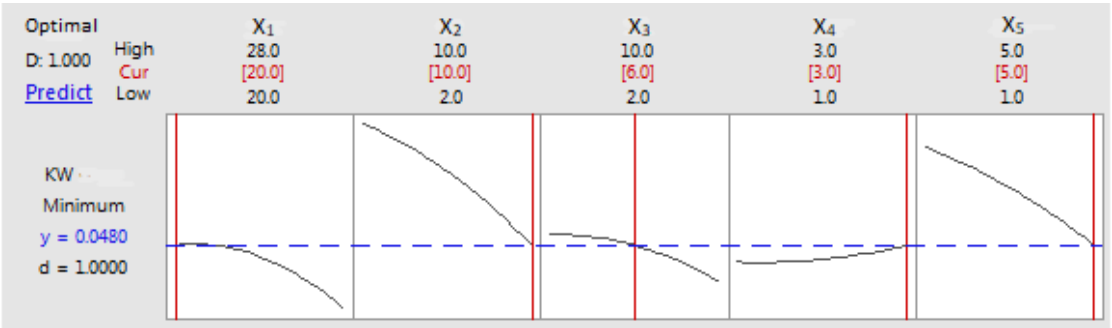

Fig. 6.60 Single objective optimization result of kerf width

Fig. 6.60 shows the optimization results for minimum KW based on the developed mathematical model using the equation of KW. The upper value and target value has been fixed at 0.1 mm and 0.05 mm respectively. The optimal parameter setting for minimum KW of 0.0480 mm are lamp current (X_1) at 20.0 Ampere, pulse frequency (X_2) at 10.0 kHz, pulse width (X_3) 6.0 %, cutting speed (X_4) 3.0 mm/sec and height of water level (X_5) of 5.0 mm. The desirability of optimization has been calculated as 1, i.e. all parameters are within their working range.

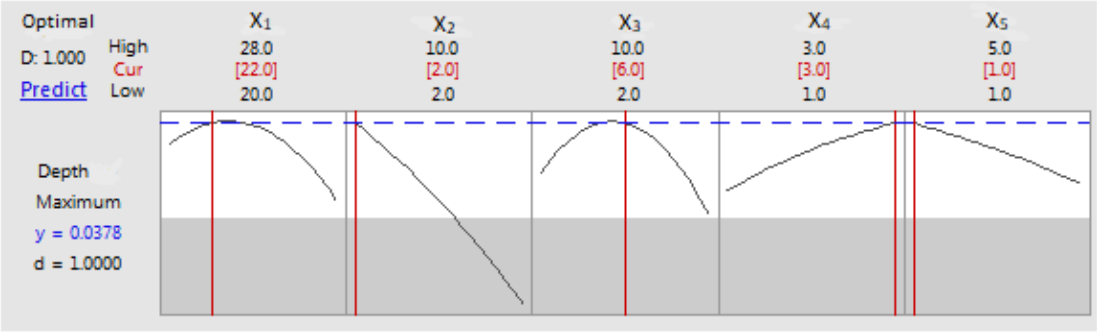

Fig. 6.61 **S**ingle objective optimization result of depth of cut

Fig.6.61 shows the optimization results for maximum depth of cut based on the developed mathematical model using the second- order polynomial equation for depth of cut. The lower value and target values are fixed at 0.02 mm and 0.03 mm respectively. The parameters setting for maximum depth of 0.0378 mm are lamp current (X_1) 22 Ampere, pulse frequency (X_2) 2.0 kHz, pulse width (X_3) 6.0 %, cutting speed (X_4) 3.0 mm/sec and height of water level (X_5) of 1.0 mm. The desirability of optimization has been calculated as 1, i.e. all parameters are within their working range.

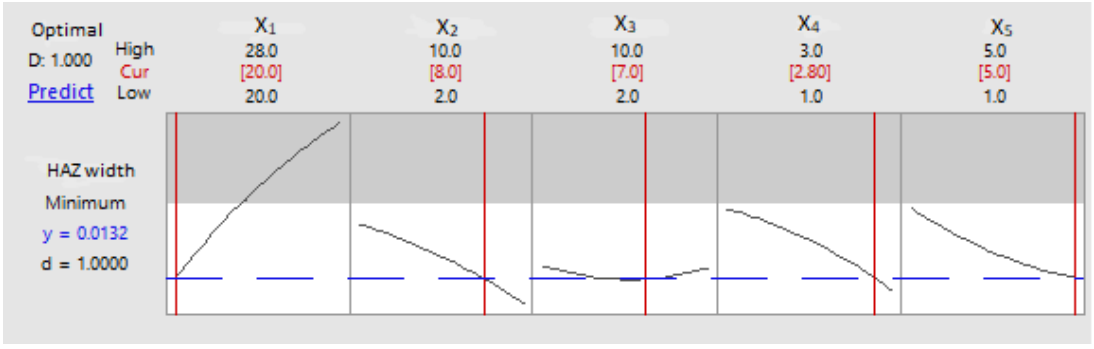

Fig. 6.62 **S**ingle objective optimization result of HAZ width

Fig. 6.62 shows the optimization results for the minimum HAZ width based on the mathematical model developed using Eq. (3). To get ideal machining response, the value of the weight for linear desirability function (d) is considered as 1. It is found from the figure that minimum HAZ width of 0.0132 mm dimension can be achieved at process parameter settings of 20 amp lamp current (X_1), 8 kHz pulse frequency (X_2), 7% pulse width (X_3), 3 mm/sec cutting speed (X_4) and 5mm height of water column(X_5).

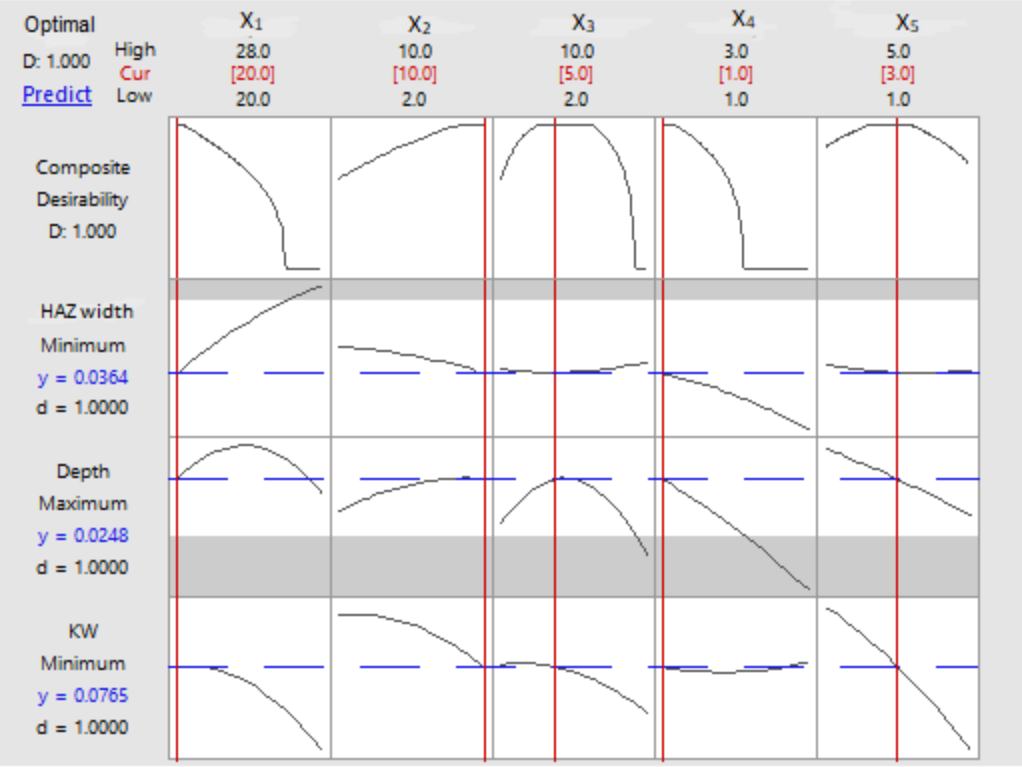

Fig. 6.63 Multi-objective optimization of machining responses in submerged condition

From the fig 6.63 it is observed that with aide of process parameter at optimal condition 20 amp lamp current (X_1), 10 kHz pulse frequency (X_2), 5% pulse width (X_3), 1 mm/sec cutting speed (X_4) and 3 mm height of water column (X_5), kerf width of 0.0765 mm, depth of 0.0248 mm and HAZ width of 0.0364 mm can be achieved.

6.2.2.4.1 Confirmation Test

Five additional experiments are carried as per optimal settings based on multiobjective optimization performed. Average of experimental results are taken into account for confirmation test and given below in table 6.21

Table 6.21 Confirmation test of laser microcutting at submerged condition

Machining responses	**Predicted value at Optimal parametric settings**	**Experimental value at Optimal parametric settings**	**% of error**
Kerf width (mm)	0.0765	0.0693	9.4
Depth of cut (mm)	0.0248	0.024	3.23
HAZ width (mm)	0.0364	0.0356	2.20

6.2.2.5 Outcome of the study

Nanosecond pulsed Nd:YAG laser with wavelength in NIR region is applied here successfully to carry out an experimental study on Inconel 65 superalloy. Single pass is used to create a blind cut on the top surface of the superalloy. Two different assist medium is selected to study the effects of those medium as well as other process variables on machining criteria. Dry (co-axially flown compressed air) and wet (work substrate submerged in water) are selected as two different environments. To avoid any chemical reaction on the machining zone de-ionised water at steady state and at room temperature is used instead of normal water. A specially designed workpiece holding device is designed and fabricated to hold the work substrate at submerged condition. Phenomenon observed during parametric study at different assist medium is discussed elaborately. ANOVA results indicate that lamp current is the most dominating controllable process variable for kerf width and HAZ width whereas pulse frequency is the most dominant variable for depth of cut during blind microcut operation performed at dry condition. On the other hand Pulse frequency is the most significant and contributing process variable for kerf width and depth of cut whereas average working power of laser in terms of lamp current is the key factor for HAZ width during laser microcutting operation is performed at wet environment. For both experiments, developed second-order polynomial model is used to perform sensitivity analysis of machining response on selected controllable process parameters within the design space. Results of multi objective optimization indicate that the responses are degraded when optimized simultaneously.

6.2.3 Comparative study of the effect of different assist medium on laser microcutting of Inconel 625

During comparative study of different assist medium on machining response, compressed air pressure as a function of dry environment and height of water column as a function of wet environment is taken into account. Design space for assist gas pressure is selected as 0.5 to 2.5 kg/cm^2 of compressed air whereas the range of wet environment is defined in between 1 mm to 5 mm height of de-ionized water column. Percentage contribution of the environments as per ANOVA results are given in a tabular form at below,

Table 6.22. Percentage contribution of different environments as per ANOVA

Machining Response	**Percentage contribution**	
	Dry (Compressed air pressure)	**Wet (Height of water column)**
Kerf width	1.83%	3.12%
Depth of cut	18.29%	32.14%
HAZ width	1.14%	25.78%

From the table it can be said that effect of wet environment on machining responses are much more than dry environment. Microscopic views of blind microcut at optimum parametric settings in both the dry and wet environment are given in fig. 6.64 and 6.65 which helps to comparative analysis at different assist medium on machining responses.

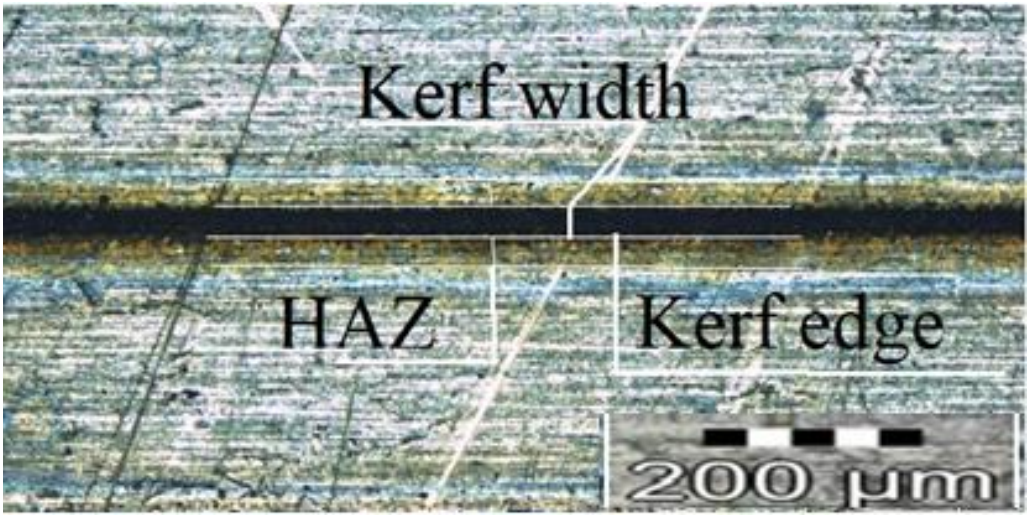

Fig. 6.64 Blind microcut at optimum parametric settings at dry environment

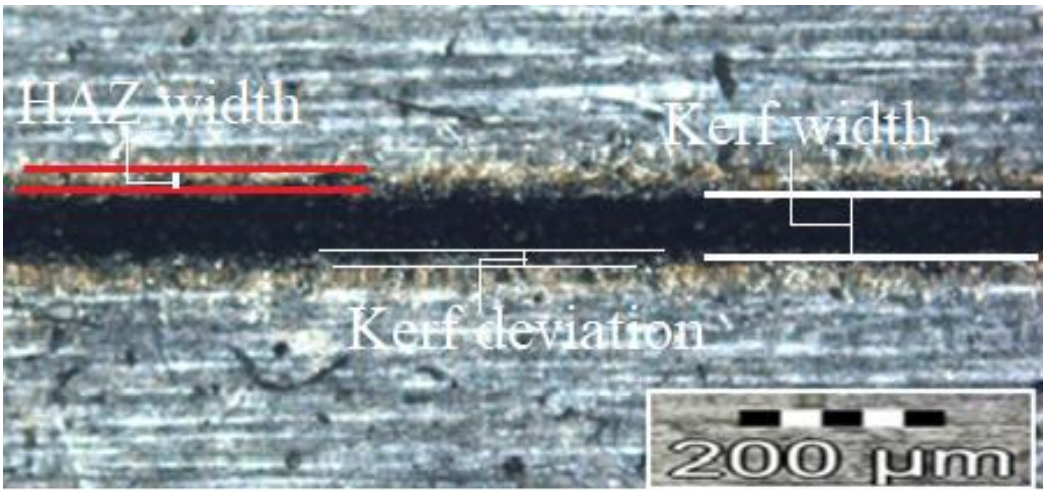

Fig. 6.65 Blind microcut at optimum parametric settings at wet environment

During parametric study it is observed that the material removal mechanism is quite different for wet condition than dry condition which affects the outcome of the machining process in micro domain. As the water is confined in the work substrate holding device, the circulation of water is happened by surface tension due to change in temperature and bubble burst which are formed by absorption of laser energy by water. This circulation of water is one of the governing factors which enhance material removal during laser microcutting operation performed at submerged condition. From the optical microscopic images it is observed that the kerf edge is smooth in case of laser microcutting performed with assist air pressure whereas kerf edge with a deviation is observed during the microcutting operation is performed at submerged in water condition. From experimental analysis it is found that kerf edge deviation in between the highest and lowest value of kerf width get is 0.0365 mm and 0.1336 mm for dry and wet assisted medium respectively. Similarly from HAZ width the value of deviation is 0.0423 mm for wet assisted medium and 0.0865 mm for dry environment. Depth deviation for dry and wet assisted medium is 0.0068 mm and 0.154 mm respectively. It is also observed that HAZ width is minimal during machining at submerged condition compared to machining with assist air.

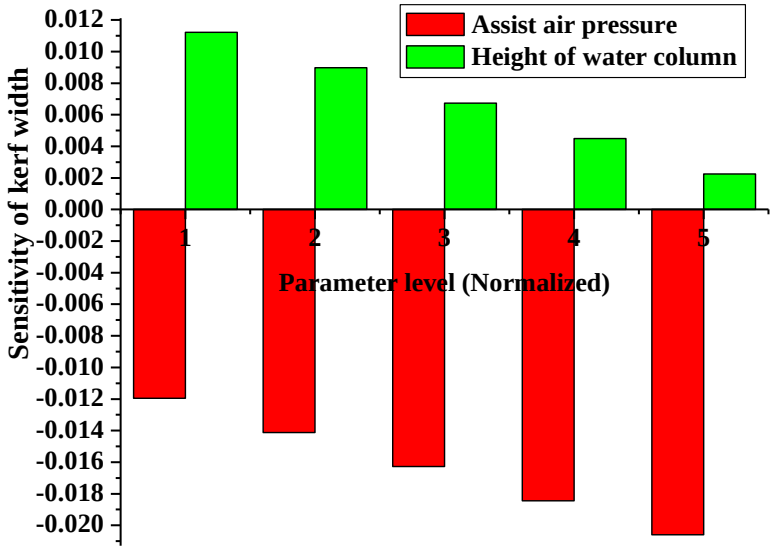

Fig.6.66 Comparative plot w.r.t. sensitivity of kerf width on different environment

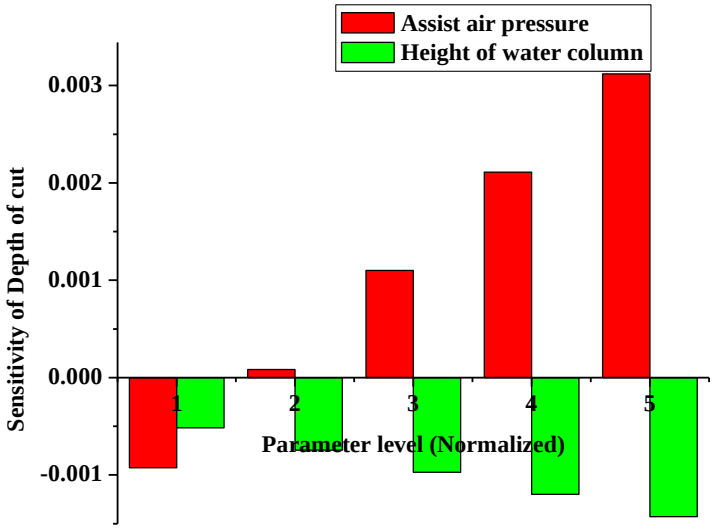

Fig.6.67 Comparative plot w.r.t. sensitivity of depth of cut on different environment

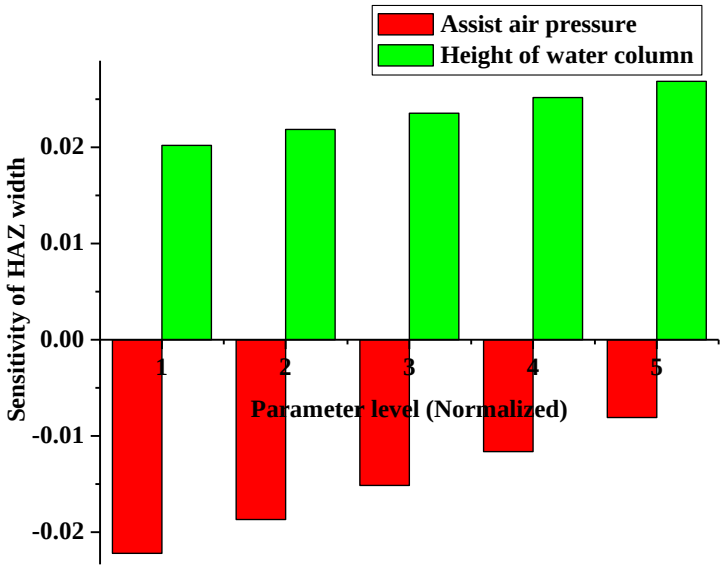

Fig.6.68 Comparative plot w.r.t. sensitivity of HAZ width on different environment

Comparative analysis of environmental effect plot, fig.6.66, 6.67 & 6.68 with respect to sensitivity of machining responses determines that HAZ width and kerf width have a positive sensitivity to height of water column whereas negatively sensitive to depth of cut. It is also observed from the plot that HAZ width is most sensitive machining response to environment.

Chapter 7

7.1 General Conclusion

Within the limitation, this dissertation demonstrates the feasibility and corresponding parametric analysis of laser micromachining with assisted medium. Nanosecond pulsed Nd:YAG laser drilling, cutting of various hard to machine materials, i.e., Aluminum 5052 alloy, SiC30BN nanocomposite, hydroxyapetite, Inconel 625 superalloy have been carried out in micro domain. The outcome of the scientific investigation indicates that low power (<50 watts) pulsed Nd:YAG laser can be successfully used to perform microdrilling operation on SiC30BN nanocomposite material. Microgrooving/ microcutting operations are also performed on hydroxyapetite, Inconel 625 respectively. Absence of proper technology guidance of laser beam micromachining of above mentioned three hard to machine engineering materials in their pure form with low power laser insist to do the present study with the help of different machining environment which reflects the novelty/ newness of the dissertation. Based on the findings the following conclusion can be drawn:

1. In-depth study of the performance characteristics of Q-switch based nanosecond pulsed Nd:YAG laser with wavelength in near infrared region reveals that application of assisted medium makes the said machine one of the most suitable tool to process various hard to machine materials in micro domain. It is observed that assist medium along with lamp current as a function of average working power of laser, pulse frequency, pulse width and cutting speed/feed rate are the most dominating and controllable factors to carry out microdrilling or microcutting operations.
2. To study the effect of different dominant process variables along with various assist mediums on machining characteristics, two different mediums in terms of dry (with aide of assist gas pressure) and wet environment (submerged in de-ionized water) are selected to perform the micromachining operations. A pressure regulator is attached to the assist gas supply unit to flow the pure argon gas into the system during machining operation with desired pressure. A rectangular shaped fixture is designed and fabricated with 3 mm thick transparent PMMA sheet to hold the workpiece in wet environment where de-ionized water

is used as wet medium. Water is confined in the device in static mode and this steady state is kept during each experimental run.

3. Aluminum alloy with high reflectivity (Al 5052), ceramic nanocomposite (silicon carbide 30% boron nitride) are selected as workpiece to carry out laser microdrilling operation whereas hydroxyapatite in it's pure form and nickel superalloy (Inconel 625) are chosen to perform blind microcut on them.
4. It is feasible to make a through micro hole on highly reflective aluminum alloy, hard to machine nanocomposite ceramic and blind micro cut on brittle hydroxyapetite and hard to machine Inconel 625 superalloy with nanosecond pulsed Nd:YAG laser having power less than 50 watts.
5. One factor at a time approach is applied for selection of design space for all the process variables, i.e., lamp current, pulse frequency, pulse width, focus distance, cutting speed, assist gas pressure and height of water column. After selection of design space for all controllable process variables, two different design of experiments method i.e., Taguchi method and central composite design based Response surface methodology is applied for carry out the micromachining operations.
6. From the experimental observations it may be concluded that all the process parameters including the assisted medium have some impact on machining responses, i.e., hole taper, hole circularity, kerf width, depth of cut and heat affected zone width. Pulse energy as a function of laser power and frequency along with the assist medium plays a vital role for HAZ width whereas laser power, pulse width and surrounding environment are the most dominant factors to get desired depth of cut or less tapered microhole.
7. Inspite of high brittleness and moderate reflectivity laser cutting operation is successfully performed on Hydroxyapetite (HAp) in its pure form though the machined surface is very rough and micro crack is also observed on the groove wall as well as on bed of machined surface. Uncontrolled crack propagation during laser irradiation leads to material removal by combination of ablation and very tiny chunk from crack regions. These are the main reasons behind achieved groove quality.
8. Developed second order polynomial model helps to establish a correlation between machining criteria with process parameters. This model further used for statistical analysis like, ANOVA and sensitivity analysis. Results of ANOVA help to check the feasibility of

the developed model along with calculation of percentage contribution. Sensitivity analysis helps to find out the sensitivity of machining responses to process variables which helps to enhance the machining characteristics by precise adjustment of process variables.

9. From the comparative study of laser beam microdrilling of silicon carbide 30% boron nitride, it may be concluded that argon as an assist gas is more suitable to perform laser microdrilling on SiC30BN nanocomposite to get desired microhole with low taper (0.0403 rad), less HAZ width (0.0728 mm) and moderate hole circularity at entry (0.918) over compressed air due to higher cooling efficiency of argon gas.
10. From the comparative study of laser beam microcutting of Inconel 625 superalloy, it may be concluded surface tension induced water flow helps to cool the machining zone which leads to generate lower value of HAZ width with higher value of depth of cut whereas bubble burst creates an adverse situation to produce kerf width with uniform kerf edge. That indicates that laser blind microcut of Inconel 625 superalloy may be good to reduce heat affected zone around the path of laser beam travel on work piece but not suitable to get uniform kerf when machine at submerged condition. Whereas laser blind microcut with aide of assist air pressure may helps to get uniform cut but comparatively higher heat affected zone along with lower value of depth of cut may not make this environment a suitable one over the wet environment.
11. Taguchi based Grey relation multiobjective optimization has been performed to optimize all the machining responses simultaneously for microdrilling of silicon carbide 30% boron nitride operation. On the other hand response surface methodology based single objective optimization is performed for microcutting of Inconel 625 to determine the optimal parameter settings which enhance to get best possible machining responses within the chosen design space.

7.2 Future scope of Work

During this research work some new ideas on laser beam micromachining have been grown up and in future, the following studies can be conducted.

1. To carry out laser microdrilling process on silicon carbide 30 % boron nitride and microcutting process on Inconel 625 superalloy with other assisted medium i.e., submerged in different kind of liquid or application of other neutral or reactive gas as assisted medium for understand the effect of different environment of laser micromachining operation on ceramic nanocomposite material or nickel based superalloys. Theoretical analysis of laser submerged machining when water kept at stagnant condition can be performed to study the feasibility of the laser machining process on other materials.
2. To carry out further study on different new and hard to machine advanced composites and superalloys for better understanding and generate technology guidance for laser processing of these kind of engineering materials.
3. To study the effect of water flow during laser micromachining of nickel based superalloy, new setup can be developed and a comparative study can be carried out between laser micromachining at submerged condition in confined steady state and under water flow condition.
4. Try to develop in-situ temperature and depth of melt pool measurement system to calculate the value of absorptivity experimentally and incorporate it in the experimental study.
5. To study the surface morphology of the machined surfaces as well as the adjacent area of irradiate zone of different materials either by destructive method or by nondestructive way (non-contact type measurement).

Bibliography

1. Masuzawa,T. (2000).State of the Art of Micromachining. CIRP Annals, **49 (2)**, pp. 473-488.

2. Johnstone R.W., Parameswaran M. (2004). Chapter 4, "Scaling Law", An Introduction to Surface-Micromachining. Kluwer Academic Publishers. ISBN 978-1-4020-8021-0 (eBook). DOI 10.1007/978-1-4020-8021-0.

3. Chavoshi,S.Z., Luo,X. (2015).Hybrid micro-machining processes: A review, Precision Engineering, **41,** pp. 1-23.

4. Küper, S., Stuke, M. (1992). Applied Physics Letters, **60**, 1633.

5. Davim, P. J. (2013). Nontraditional Machining Processes, Research Advances. ISBN 978-1-4471-5178-4, DOI 10.1007/978-1-4471-5179-1, Springer-Verlag London.

6. Ready, J.F. (1997). Industrial Applications of Lasers. Academic Press, San Diego.

7. Svelto, O. (1986). Principles of Lasers. Plenum Press, New York, pp. 1.

8. Hutchinson, M.H.R. (2003). Spectrochim. Acta (Part B) **58**, pp 1155–1161.

9. Nathan, M.I., Dumke, W.P., Burns, G., Dill F.H. Jr. (1962). Journal of Applied Physics Letters **1**, pp 62–64.

10. Patrick, G., ÕShea, O., Henry, P. (2001). Science **292**, pp 1853–1858.

11. Gower, M.(2000). Excimer laser microfabrication and micromachining. Proceedings of SPIE - The International Society 4088, DOI: 10.1117/12.405698.

12. Koç, M., Özel, T. (2011). Micro-manufacturing: Design and Manufacturing of Micro-Products. John Wiley & Sons, Inc.

13. Henyk M, Vogel N, Wolfframm D,Tempel A, Reif J. (1999), Femtosecond laser ablation from dielectric materials: Comparison to arc discharge erosion, Applied physics A **69**:1 pp: S355-S358.

14. Liu X, Du D, Mourou G. (1997) laser ablation and micromachining with ultrashort pulse, IEEE journal of electronics, **33**:10.

15. Rizvi, N.H., Apte, P. (2002). Developments in laser micro-machining techniques. Journal of Materials Processing Technology **127**, pp 206–210.

16. Samant A.N., Dahotre N.B. (2009). Laser machining of structural ceramics—A review. Journal of the European Ceramic Society. **29,** pp 969–993

17. Von, A. M. (1987). Laser-beam Interactions with Materials. Springer, Berlin.

18. Steen, W.M. (1991). Laser Materials Processing. Springer, London.

19. Welch, A.J., Gardner, C. (2002*).* Optical and thermal response of tissue to laser radiation. In: Waynant, R.W. (Ed.) Lasers in Medicine, CRC Press, Boca Raton, FL, pp 27–45.

20. Duley, W.W.(1983). Laser Processing and Analysis of Materials. Plenum Press, New York.

21. Allmen, M.F. (1983). Physical Processes in Laser-Materials Interactions. Bertolotti, M. (Ed.) Plenum, New York, chap. 2, pp 49–75.

22. Perry M.D., Pennington D., Stuart B.C., Tietbohl G., Britten J.A., Brown C., Herman S., Golick B., Kartz M., Miller J., Powell H.T., Vergino M., Yanovsky V. (1999), Optics Letter. **24**, pp 160–162.

23. French, P., Hand, D., Peters, C., Shannon, G., Byrd, P., Steen, W. (1998). Investigation of the Nd: YAG laser percussion drilling process using high speed filming, ICALEO'98 Proceedings LIA, Orlando, FL, pp 1–10.

24. Pangovski, K. (2014) Temporal Pulse Design and Analysis of Silicon Ablation Using Advanced Pulse Shaping and Digital Holography in the Nanosecond Domain. PhD Thesis. The University of Cambridge, Cambridge.

25. Collins G.W., Celliers P.M., DaSilva L.B., Cauble R., Gold D.M., Foord M.E., Holmes N.C., Hammel B.A., Wallace R.J., Ng A., (2001). Physics Review Letters. **87(16)**, art. no. 165504.

26. Bäuerle, D. (2000). Laser Processing and Chemistry. Springer, Heidelberg.

27. Dahotre N.B., Harimkar S.P. (2008). Laser Fabrication and Machining of Materials. Springer Science & Business Media, New York. USA,ISBN 9780387723433, DOI:10.1007/978-0-387-72344-0.

28. Kruusing, A. (2004b). Underwater and water-assisted laser processing: Part 2-Etching, cutting and rarely used methods. Optics and Lasers in Engineering **41**, pp 329–352.

29. Isselin J.C, Alloncle A.P, Autric M. (1998). On laser induced single bubble near a solid boundary: contribution to the understanding of erosion phenomena. Journal of Applied Physics **84(10)**, pp 5766–5771.

30. Datta, M., Romankiw, L.T., Vigliotti, D.R. (1987). Laser etching of metals in neutral salt solutions. Applied Physics Letters; **51(24),** pp 2040–2042.

31. Kim, D., Lee, H. (2001). Enhanced ablation and photoacoustic excitation in near-threshold laser ablation of liquid-coated surfaces. Journal of Applied Physics; **89(10)**, pp 5703–5706.

32. Roy, N., Kuar, A.S., Mitra, S. (2017).Underwater pulsed laser beam cutting with a case study, In Reviews: Mechanical Engineering Series, Microfabrication and Precision Engineering, Davim.J.P (Ed.),pp.189-212,Woodhead Publishing, ISBN 9780857094858.

33. Li, L., Achara, C. (2004). Chemical assisted laser machining for the minimization of recast and heat affected zone. Annals CIRP. **53(1)**, 175-178.

34. Jian. C.Y., Lau. W.S., Yue.T.M., Chiang.L. (1993). On maximum depth and profile of cut in pulsed Nd:YAG laser machining. Annals of the CIRP. **42(1)**,pp 223-226.

35. Ganesh R.K., Bowley W., Bellantone R.R., HahnY. (1996). A Model for Laser Hole Drilling in Metals. Journal of Computational Physics. **125,** 161–176.

36. Yilbas B.S. Parametric study to improve laser hole drilling process. (1997). Journal of Materials Processing Technology. **70**, pp-264273.

37. Tuersley I.P., Hoult T.P., Pashby I.R. (1998). Nd–YAG laser machining of SiC fibre/ borosilicate glass composites. Part I. Optimization of laser pulse parameters. Composites Part A. **29A,** pp- 947–954.

38. Sciti. D., Ballosi. A. (2001). Laser-induced surface drilling of silicon carbide. Applied surface science. **180**, pp. 92-101.

39. Tunna L., Kearns A., O'Neill W., (2001) Sutcliffe C.J. Micromachining of copper using Nd :YAGlaser radiation at 1064, 532, and 355 nm wavelengths, Optics & Laser Technology 33 135–143.

40. Ng G.K.L., Li. L. (2001). The effect of laser peak power and pulse width on the hole geometry repeatability in laser percussion drilling. Optics & Laser Technology. **33,** pp. 393–402.

41. Li L., Low D.K.Y., Ghoreshi M., Crookall J.R. (2002).Hole Taper Characterisation and Control in Laser Percussion Drilling. CIRP Annals. **51**(1), Pp 153-156.

42. Tsai, C.H., Chen. H.W.(2003). Laser cutting of thick ceramic substrates by controlled fracture technique. Journal of Materials Processing Technology. **136**. Pp.166–173.

43. Ho.C.Y., Lu. J.K. (2003). A closed form solution for laser drilling of silicon nitride and alumina ceramics. Journal of Materials Processing Technology **140**, pp. 260–263.

44. Quintero F., Pou J., Lusquinos F., Boutinguiza M., Soto R., Perez-Amor M. (2004).Quantitative evaluation of the quality of the cuts performed on mullite-alumina by Nd:YAG laser. Optics and Lasers in Engineering. **42**, pp- 327–340.

45. Tunna L., Neilla W. O., Khana A., Sutcliffe C. (2004). Analysis of laser micro drilled holes through aluminium for micro-manufacturing applications. Optics and Lasers in Engineering. **43**, pp-937–950.

46. Dumitru G., Lu¨scher B., Krack M., Bruneau S., Hermann J., Gerbig Y. (2005) Laser processing of hardmetals: Physical basics and applications, International Journal of Refractory Metals & Hard Materials **23**, pp 278–286.

47. Kuar A.S., Doloi B., Bhattacharyya B. (2006). Modelling and analysis of pulsed Nd:YAG laser machining characteristics during micro-drilling of zirconia (ZrO2). International Journal of Machine Tools & Manufacture. **46**, pp 1301–1310.

48. Ng G.K.L., Crouse P.L., Li L. (2006).An analytical model for laser drilling incorporating effects of exothermic reaction, pulse width and hole geometry. International Journal of Heat and Mass Transfer. **49**, pp 1358–1374

49. Huang J.X., Huang Y.X. (2007). Nd:YAG laser machining of bioceramics. Current Applied Physics. **7S1**, e45–e48.

50. Nakata K., Umehara M., Tsumura T. (2007). Excimer laser ablation of sintered hydroxyapatite. Surface & Coatings Technology. **201**, pp 4943–4947.

51. Paul C.P., Ganesha P., Mishra S.K., Bhargava P., Negi J., Nath A.K. (2007). Investigating laser rapid manufacturing for Inconel-625 components. Optics & Laser Technology. **39**, pp 800–805.

52. Das R.N., Egitto F.D., Lauffer J.M., Markovich V. R. (2007). Laser Micromachining of Nanocomposite-Based Flexible Embedded Capacitors. Proceedings of 57th Electronic Components and Technology Conference (ECTC 2007). DOI: 10.1109/ECTC.2007.373833 .

53. Gilbert. T., Kristic. V.D., Zak.G. (2007). Machining of aluminium nitride with ultra-violet and near-infrared Nd:YAG lasers. Journal of Materials Processing Technology. **189,** pp 409–417.

54. Salonitis.K., Stournaras.A., Tsoukantas.G., Stavropoulos.P., Chryssolouris.G. (2007). A theoretical and experimental investigation on limitations of pulsed laser drilling. Journal of Materials Processing Technology **183**, pp 96–103.

55. Kurita T., Komatsuzaki K., Hattor M. (2008). Advanced material processing with nano- and femto-second pulsed laser. International Journal of Machine Tools & Manufacture. **48**, pp 220–227.

56. Samanta A.N., Dahotre N.B. (2008). Computational predictions in single-dimensional laser machining of alumina. International Journal of Machine Tools & Manufacture. **48**, pp 1345– 1353.

57. Dubey A.K., Jadava V. (2008). Multi-objective optimisation of laser beam cutting process. Optics & Laser Technology. **40**, pp 562–570.

58. Theriault A., Xuea L., Dryden J.R. (2009). Fatigue behavior of laser consolidated IN-625 at room and elevated temperatures. Materials Science and Engineering A. **516**, pp 217–225.

59. Dinda G.P., Dasgupta A.K., Mazumder J. (2009). Laser aided direct metal deposition of Inconel 625 superalloy: Microstructural evolution and thermal stability. Materials Science and Engineering A. **509**, pp 98–104.

60. Samanta A.N., Dahotre N.B. (2009). Differences in physical phenomena governing laser machining of structural ceramics. Ceramics International. **35**, pp 2093–2097.

61. Kacar E., Mutlua M. , Akmana E., Demir A., Candana L., Canel T., Gunay V., Sınmazcelik T. (2009). Characterization of the drilling alumina ceramic using Nd:YAG pulsed laser. journal of materials processing technology. **209,** pp 2008–2014.

62. Samant.A.N., Daniel.C., Chand. R.H., Blue. C.A. Dahotre. N.B. (2009). Computational approach to photonic drilling of silicon carbide. International Journal of Advance Manufacturing Technology. **45**, pp 704-713.

63. Wee.L.M., Khoog.L.E., Tan.C.W., Lim.G.C. (2010). Solvent assisted laser drilling of Silicon Carbide. International journal of applied ceramic technology. Pp 1-14. DOI:10.1111/j.1744-7402.2010.02575.x.

64. Biswas R., Kuar A.S., Sarkar S., Mitra S. (2010). A parametric study of pulsed Nd:YAG laser micro-drilling of gamma-titanium aluminide. Optics & Laser Technology. **42**, pp 23–31.

65. Biswas R., Kuar A.S., Biswas S.K, Mitra S. (2010). Effects of Process Parameters on Hole Circularity and Taper in Pulsed Nd:YAG Laser Microdrilling of Tin-Al_2O_3 Composites. Materials and Manufacturing Processes. **25**, pp 503–514.

66. Sharma A., Yadava V., Rao R. (2010). Optimization of kerf quality characteristics during Nd: YAG laser cutting of nickel based superalloy sheet for straight and curved cut profiles. Optics and Lasers in Engineering. **48**, pp 915–925.

67. Ahn D.G., Byun K.W., Kang M.C. (2010) Thermal Characteristics in the Cutting of Inconel 718 Superalloy Using CW Nd:YAG Laser. J. Mater. Sci. Technol. **26(4),** pp 362-366.

68. Ahmed N., Voisey K.T., McCartney D.G. (2010). Investigation into the effect of beam shape on melt pool characteristics using analytical modeling. Optics and Lasers in Engineering. **48**, pp 548–554.

69. Ganesh, P. Kaul R., Paul C.P., Tiwari P., Rai S.K., Prasad R.C., Kukreja L.M. (2010). Fatigue and fracture toughness characteristics of laser rapid manufactured Inconel 625 structures. Materials Science and Engineering A. **527**, pp7490–7497.

70. Mahdieh M.H., Nikbakht M., Eghlimi Moghadam Z., Sobhani M. (2010). Crater geometry characterization of Al targets irradiated by single pulse and pulse trains of Nd:YAG laser in ambient air and water, Applied Surface Science **256**, pp 1778–1783.

71. Kuar A. S., Acherjee B., Ganguly D., Mitra S. (2011). Optimization of Nd:YAG Laser Parameters for Microdrilling of Alumina with Multiquality Characteristics via Grey–Taguchi Method. Materials and Manufacturing Processes. **27(3),** pp 329-336.

72. Yan Y., Ji L., Bao Y., JiangY.. (2012). An experimental and numerical study on laser percussion drilling of thick-section alumina. Journal of Materials Processing Technology. **212**, pp 1257– 1270.

73. Mishra S., Yadava V. (2013). Modeling and optimization of laser beam percussion drilling of thin aluminum sheet. Journal of Optics &Laser Technology. **48** pp.461–474.

74. Duangwas S., Tangwarodomnukun V., Dumkum C. (2014). Development of an Overflow-Assisted Underwater Laser Ablation. Materials and Manufacturing Processes. **29**, pp 1226–1231.

75. Alahmari A.M., Naveed Ahmed N., Darwish S. (2015). Laser beam micro-machining under water immersion. International Journal of Advance Manufacturing Technology. DOI 10.1007/s00170-015-7699-5.

76. Mullick S., Madhukar Y.K., Roy S., Nath A.K. (2015). An investigation of energy loss mechanisms in water-jet assisted underwater laser cutting process using an analytical model. International Journal of Machine Tools & Manufacture. **91**, pp 62–75.

77. Ross, P.J.(1996), Taguchi Techniques for Quality Engineering, 2nd edn. New Delhi (India): Tata McGraw-Hill Publishing Company Ltd.

78. Fung, C.P.(2003), Manufacturing process optimization for wear property of fiber-reinforced polybutylene terephthalate composites with grey relational analysis, Wear **254**, pp 298–306.

79. Acherjee, B., Kuar, A.S., Mitra, S. and Misra, D.(2010), Selection of process parameters for optimizing the weld strength in laser transmission welding of acrylic, Proc. IMechE Part B: Journal of Engineering Manufacture, **224 (B10)**, pp 1529–1536.

80. Pan, L K., Wang, C. C., Wei, Shien L., Sher, H F. (2007),Optimizing multiple quality characteristics via Taguchi method-based Grey analysis, Journal of Materials Processing Technology **182**, pp 107–116.

81. Montgomery D.C. Design and Analysis of Experiments. New York: Wiley. 2001.

82. Karaoglu, S., Secgin, A. 2008. Sensitivity analysis of submerged arc welding process parameters. Journal of Materials Processing Technology, **202(1–3),** pp 500–507.

83. Low D.K.Y., Li, L., Byrd, P.J. (2001b). The influence of temporal pulse train modulation during laser percussion drilling. Optics and Lasers in Engineering, **35**, pp 149–164.

84. Zhang Z, Yang X, Zhang J, Zhou G, Xu X, Zou B, (2011), Effect of welding parameters on microstructure and mechanical properties of friction stir spot welded 5052 aluminum alloy, Materials & Design, 32(8–9), pp. 4461-4470, ISSN 0261-3069, https://doi.org/10.1016/j.matdes.2011.03.058.

85. Ajayan, P.M., Schadler, L.S. and Braun, P.V. (2003). Nanocomposite science and technology, Wiley. ISBN 3527303596.

86. Li, Lin., Hong, Minghui., Schmidt, Michael., Zhong, Minlin., Malshe, Ajay., Veld, Bert, Huis. and Kovalenko, Volodymyr. (2011) Laser nano-manufacturing – State of the art and challenges, CIRP Annals - Manufacturing Technology, **60**, pp 735–755.

87. Xiangdong, W., Guanjun, Q., Zhihao J. **(**2004), Fabrication of Machinable Silicon Carbide-Boron Nitride Ceramic Nanocomposites. Journal of the American Ceramic Society, **87 (4)**, pp 565–570.

88. Shanjin Lv., Yang W. (2006), An investigation of pulsed laser cutting of titanium alloy sheet, Optics and Lasers in Engineering, **44(10)**, pp 1067-1077.

89. Kaplan A.F.H., J. (1996), An analytical model of metal cutting with a laser beam. Journal of Applied Physics, **79 (5)**, 2198.DOI: 10.1063/1.361098.

90. Riveiro A., Quintero F., Lusquiños F., Comesaña R., Pou J. (2010), Influence of assist gas nature on the surfaces obtained by laser cutting of Al–Cu alloys, Surface & Coatings Technology, **205**, pp 1878–1885.

91. Ji L, Yan Y, Bao Y, Jiang Y (2008) Crack-free cutting of thick and dense ceramics with CO_2 laser by single-pass process. Optics and Lasers in Engineering, **46(10)**, pp 785–90.

92. Halouani R., Bernache A D., Champion E, Ababou A (1994 Microstructure and related mechanical properties of hot pressed hydroxyapatite ceramics. Journal of Materials Science: Materials in Medicine, **5(8)**, pp 563-568, DOI: 10.1007/BF00124890.

93. Orlovskii VP, Komlev VS, Barinov SM (2002) Hydroxyapatite and Hydroxyapatite-Based Ceramics. Inorganic Materials, **38(10),** pp 1159-1172, DOI: 10.1023/A:1020585800572.

94. Kim, H. , Miyaji, F. , Kokubo, T. and Nakamura, T. (1996), Preparation of bioactive Ti and its alloys via simple chemical surface treatment. Journal of Biomedical Materials Research, vol 32, pp. 409-417, DOI:10.1002/(SICI)1097-4636(199611)32:3<409::AID-JBM14>3.0.CO;2-B.

95. Dorozhkin SV (2007) Bioceramics of calcium orthophosphates. Biomaterials, Vol. **31(7)**, pp.1465-1485, DOI: 10.1016/j.biomaterials.2009.11.050.

96. Berger J, Holthaus MG, Pistillo N, Roch T, Rezwan K, Lasagni AF (2011) Ultraviolet laser interference patterning of hydroxyapatite surfaces. Applied Surface Science, **257 (7)**, pp 3081-3087, DOI:10.1016/j.apsusc.2010.10.120.

97. Cheang P, Khor KA, Teoh LL, Tam SC (1996) Pulsed laser treatment of plasma-sprayed hydroxyapatite coatings. Biomaterials, **17 (19)**, pp 1901-1904, DOI: 10.1016/0142-9612(95)00146-8.

98. Ahn, D.G., Byun, K.W. Kang, M.C., (2010). Thermal Characteristics in the Cutting of Inconel 718 Superalloy Using CW Nd:YAG Laser, Journal of Material Science and Technology, **26(4),** pp 362-366.

99. Paul C.P., Ganesh P., Mishra S.K., Bhargava P., Negi J. and Nath A.K. (2007), Investigating laser rapid manufacturing for Inconel-625 components. Optics & Laser Technology **39(4)** pp 800–805.

100. Fujia Xu, Lv. Yaohui, Liu. Yuxin, Shu. Fengyuan, He. Peng, Xu. Binshi, (2013) Microstructural Evolution and Mechanical Properties of Inconel 625 Alloy during Pulsed Plasma Arc Deposition Process, Journal of Material Science and Technology, **29(5)**; pp 480-488.